II

THE GEOLOGY OF THE DRAGSMARK GRANITES, BOHUSLÄN, SOUTH WEST SWEDEN

with emphasis on the nature and origin of their alkali feldspar megacrysts

Submitted for the Degree of

Doctor of Philosophy

by

Peter Richard Gambles

1984

Contents

Abstract

The Dragsmark granites comprise a number of sub-concordant sheets within the Stora Le -Marstrand gneiss belt of south-west Sweden. Field evidence, fluid inclusion studies and geochemical restite-melt modelling indicate that they were intruded as wet near-eutectic magma, containing abundant crustally derived xenocrystic material (mainly plagioclase, garnet and sphene), at a depth of c.12 km. Their intrusion probably occurred between 1400 & 1200 Ma ago, a minimum age limit being provided by cross-cutting basic Orust dykes which form a regional chronostratigraphic marker separating the Svecofennian and Sveconorwegian orogenies. The most distinctive feature of the Dragsmark granites is the presence of abundant potassium feldspar megacrysts; such 'augen' granites are widespread in the Sveconorwegian Province.

Populations of megacrysts from the main, lowermost, sheet and the smaller overlying bodies show differences in composition, especially in Ba content. Crystals from the former have roughly constant K/Na, but varying Ba and Rb; samples from the latter show constant K/Ba and K/Sr ratios over a wide range in orthoclase content. Individual megacrysts from the main intrusion show an overall decrease in Ba content from core to rim, on which is superimposed a 100μ scale oscillatory zoning of the K/Ba ratio. The primary Al/Si distribution (structural state) of such megacrysts was more disordered than that of the groundmass; the reverse holds true for samples from the upper sheets.

These data favour an interpretation of dominant crystal-magma fractionation processes in the main body and bulk rock-fluid interaction in the overlying sheets. The conclusion is drawn that most megacrysts in the former originated as phenocrysts whilst those in the latter are mainly porphyroblasts.

Acknowledgements

This work was carried out during tenure of a NERC (CASE) studentship with Sveriges Geologiska Undersökelse.

I thank Professor G. Kelling for the provision of facilities in the Department of Geology at Keele, and also Professor P. Brown for the provision of facilities in the Department of Geology at Aberdeen.

I gratefully acknowledge the assistance and encouragement given by Dr. R.G. Park and Hr. L. Samuelsson in the course of their supervision of this research. Dr. A. Crane and Hr. K-I Ahåll are also thanked for their continued interest and advice.

I thank Drs. J.S. Daly, C.S. Exley, G. Rowbotham, I. Parsons and R.C.Standley for much helpful conversation, also D. Cronshaw and G.J. Lees for many fruitful discussions.

I am grateful to D. Emley and G.J. Lees for assistance with geochemical analysis and computing, and to the technical staffs of both Universities for their varied contributions, especially G. Taylor at Aberdeen.

J. Merefield and A. Palmer of the Department of Geology at Exeter are thanked for performing fluorine analyses.

Helge and Signe Turesson kindly provided excellent accomodation in Sweden, and Ingemar Gunnarsson of Skaftö assisted greatly in many ways.

Finally, my thanks go to my wife Ann, not least for typing this thesis.

Chapter 1

Introduction

a) Terminology and Definitions

The term megacryst is used throughout this work, with no genetic connotations, to indicate a crystal which is considerably larger than those of the surrounding matrix. The origin of megacrysts is discussed in terms of their being porphyroblasts or phenocrysts. The former is taken to imply growth in the solid state, usually in the presence of an aqueous phase. The latter are here defined as crystals which have grown from a silicate magma, but are not necessarily the (first) liquidus phase.

The lithological and structural nomenclatures of Park et al (1979) for western Orust are used with modifications where appropriate. The granitoid rocks are classified by modal analysis following Streckeisen (1975), whilst folds are described using the definitions of Fleuty (1964).

In Chapter 5, the structural state of the alkali feldspars is discussed, and the terminology for, and definitions of, end-members of structural series are taken from Wright and Stewart (1968).

All Rb/Sr ages quoted in this work have been recalculated, where necessary, to $\lambda^{87}\text{Rb} = 1.42 \times 10^{-11}\ \text{y}^{-1}$.

b) Regional Setting

The Dragsmark area lies within the Sveconorwegian Province of southern Scandinavia. This is defined by Magnusson (1960),and Magnusson et al (1960),as the region to the west of the "Schistosity Zone" or Sveconorwegian 'front' within which K-Ar dates fall in the range 1050 - 850 Ma. The area east of the Oslo Graben constitutes the Eastern Subprovince and is subdivided (Magnusson et al,1960; Gorbatschev,1975) into the Pregothian, Åmål or Gothian, Dal and Stora Le -Marstrand (Fig. 1.1). Terms such as group, series, belt, mega-unit have variously been used to describe these geological regions. An alternative subdivision can be made into roughly north-south trending 'segments', separated by a number of major linear features along which strain is thought to have occurred during the Sveconorwegian (Berthelsen,1980; Daly et al,1983). As can be seen from Fig. 1.1 , the boundaries of these various subdivisions of the Eastern Subprovince are not entirely coincident.

Considering the complexity of the geology of south-west Sweden, relatively few radiometric datings are available. Severe difficulties are encountered when trying to correlate these data with field observations in order to construct chronostratigraphic units. Table 1.1 lists the Rb/Sr ages (recalculated where necessary) presently available, together with a compilation of regional syntheses by Magnusson et al (1960), Gorbatschev (1975) and Samuelsson (1978).

Whilst it is clear that major problems still remain unresolved, some useful generalizations can be made. The Sveconorwegian orogeny (c. 1200 - 800 Ma) involved the intrusion of numerous granite bodies and the deformation and metamorphism of pre-existing rocks. The thermal maximum of Sveconorwegian metamorphism occurred at c. 1090 Ma (Daly et al,1983), this being a minimum age for the intrusion of the Orust-Koster dyke swarm.

b) Regional Setting

The Dragsmark area lies within the Sveconorwegian Province of southern Scandinavia. This is defined by Magnusson (1960),and Magnusson et al (1960),as the region to the west of the "Schistosity Zone" or Sveconorwegian 'front' within which K-Ar dates fall in the range 1050 - 850 Ma. The area east of the Oslo Graben constitutes the Eastern Subprovince and is subdivided (Magnusson et al,1960; Gorbatschev,1975) into the Pregothian, Åmål or Gothian, Dal and Stora Le -Marstrand (Fig. 1.1). Terms such as group, series, belt, mega-unit have variously been used to describe these geological regions. An alternative subdivision can be made into roughly north-south trending 'segments', separated by a number of major linear features along which strain is thought to have occurred during the Sveconorwegian (Berthelsen,1980; Daly et al,1983). As can be seen from Fig. 1.1 , the boundaries of these various subdivisions of the Eastern Subprovince are not entirely coincident.

Considering the complexity of the geology of south-west Sweden, relatively few radiometric datings are available. Severe difficulties are encountered when trying to correlate these data with field observations in order to construct chronostratigraphic units. Table 1.1 lists the Rb/Sr ages (recalculated where necessary) presently available, together with a compilation of regional syntheses by Magnusson et al (1960), Gorbatschev (1975) and Samuelsson (1978).

Whilst it is clear that major problems still remain unresolved, some useful generalizations can be made. The Sveconorwegian orogeny (c. 1200 - 800 Ma) involved the intrusion of numerous granite bodies and the deformation and metamorphism of pre-existing rocks. The thermal maximum of Sveconorwegian metamorphism occurred at c. 1090 Ma (Daly et al,1983), this being a minimum age for the intrusion of the Orust-Koster dyke swarm.

TABLE 1.1

Radiometric (Rb/Sr) Ages from the Sveconorwegian Province

Source	Age (Ma)	Location
(1)	891±34	Bohus granite
(2)	950±16	Pre-D4 pegmatites
(1)	1028±39	Dal supracrustals
(3)	1087±42	Orust dykes (D3 metamorphism)
(4)	1214±29	Håstefjorden granite
(5)	1224±49	Ursand granite
(6)	1376±46	Assmunderöd-Myckleby granite
(7)	1427±27	Lane granite
(6)	1432±92	Hållevіksstrand amphibolite
(8)	c.1654±152	Åmål I gneiss
(9)	c.1674±113	Tjörn tonalite gneiss
(10)	1684±88	Åmål I granite
(11)	1698±83	Western Pregothian gneiss
(12)	c.1900	Östfold migmatite

Event Chronology

800 Ma
Sveconorwegian = Dalslandian = (Grenvillian)
1200 Ma
Håstefjorden group
1250 Ma
1400 Ma
Gothian (~ Åmål II)
1450 Ma
1600 Ma
Pregothian (~ Åmål I)
1750 Ma
>1750 Ma
Svecofennian = Karelian = (Hudsonian)

TABLE 1.1 (cont.)

References

(1) Skiöld (1976)

(2) Daly et al. (1982)

(3) Daly et al. (1983)

(4) Welin and Gorbatschev (1976)a

(5) Gorbatschev and Welin (1975)

(6) Daly et al. (1979)

(7) Welin and Gorbatschev (1978)a

(8) Welin and Gorbatschev (1976)b

(9) Welin and Gorbatschev (1978)b

(10) Welin and Gorbatschev (1978)c

(11) Welin and Gorbatschev (1976)c

(12) Pederson in Hageskov (1978)

K-Ar systematics were reset and Rb-Sr systematics were disturbed (ibid). During the period from c. 1600 - 1200 Ma a large number of granitic bodies were intruded throughout the Eastern Subprovince, these forming the basis of the Åmål mega-unit of Gorbatschev (1975). The Stora Le -Marstrand and Pregothian gneisses probably predate all of these, though no reliable age data are available.

The rocks of the Stora Le -Marstrand belt and its northward continuation as the Östfold "Series" were first described as such by Larsson (1956) and Lundegårdh (1958). They are a thick polymetamorphic sequence of supracrustals, mainly quartzo-feldspathic gneisses (meta-greywackes) with subordinate metapelites, quartzites, metabasics and calc-silicates. The whole is more or less migmatized and intruded by several generations of granites (s.s) and granitoid to basic plutonic rocks.

Magnusson (1965) believed the belt to be older than the 'Gothian' supracrustals and granites to the east, but younger than the 'Pregothian' gneiss complex. This view is opposed by Gorbatschev (1971) who considered the Stora Le -Marstrand 'series' to be older than all but some of the earliest elements in the 'Pregothian'. This interpretation is partially supported by more recent radiometric dating (see Table 1.1).

The Dragsmark and Källviken augen granites were most probably intruded in the same time period as many other granites in southwestern Sweden i.e. between c. 1600 Ma and 1200 Ma . It can therefore be postulated that they are temporal equivalents of the granites of the 'Gothian' or Åmål II / Hästefjorden groups of the Åmål mega-unit (Gorbatschev,1975).

c) Previous Work

Lindström (1902), in his Description to accompany the 1 : 100,000 Uddevalla map sheet makes specific reference to "augen gneiss" in the Dragsmark area.

" Ögongneis förekommer såsom spridda och underordnade, ehuru ganska mäktiga lager i synnerhet inom västra delen af Dragsmarks socken, omkring Vägeröd och Efvensås inom nordliga delen af Skaftöland ... " (1)

He speculates as to whether the "augen gneiss" could be metamorphosed and 'schistosified' veins of old porphyritic granite, and notes that locally large xenoliths and pendants of the country gneisses are present in the granite, perhaps suggesting wall-rock assimilation. Mention is made of the pegmatite quarry at Munkeby.

Further details of pegmatites in the area are given by Sundius (1952). That at Munkeby was 100m long and 30m deep, comprising mainly alkali feldspar, quartz and plagioclase with minor muscovite and rare garnet and columbite. First opened in 1882 by Det Norske Grubekompagni, it produced commercial quantities of mica in 1926 and during the 2nd World War, when the price of Swedish muscovite reached a high of 2,247.7 kr/ton (from a pre-war price of 60 kr/ton).

Bergström (1963) describes the petrography of the Stora Le - Marstrand gneisses and a light red augen granite from the island of Tjörn, to the south of Orust (Fig. 1.1). This is augmented by the work of Berthelsen and Murthy (1970) on the petrography and structural evolution of the Assmunderöd-Myckleby augen granite and adjacent gneisses.

---

(1) Augen gneiss occurs, being widespread and minor, although probably fairly thick layers [occur] in the western part of Dragsmark parish, around Vägeröd and Evensås in the northern part of Skaftöland ...

Daly (1978) presents a detailed geochemical and geochronological investigation of this granite, the paragneisses and migmatites, various amphibolites, and the Orust dykes. The area sampled covers most of Orust, Skaftölandet and Dragsmark. The augen granite at Källviken is described in some detail, no distinction being made between it and the Dragsmark granites. B.S.P. Moorlock has made a reconnaissance map of these granites (pers. comm.) which was used as a starting point for this work.

Figs. 1.2 and 1.3A, B and C show respectively the gravity and various radioactivity maps of the relevant area. The Bohus-Iddefjord granite is clearly defined on all maps, but the granites of Skaftö and Dragsmark are only apparent on the gamma activity maps (Fig. 1.3). Whilst they are obviously not as rich in radionucleides as the Bohus laccolith, these bodies are readily distinguishable from the 'background' of Stora Le -Marstrand gneisses. This is confirmed by field measurements which show the granites to be 2 - 3 times as powerful gamma sources as the country rock.

The structure and geological history of a part of western Orust is presented by Park et al (1979), who also establish lithological and structural nomenclatures for the rocks of this section of the Stora Le - Marstrand belt. They recognize four major deformational episodes, with the Orust dykes forming a chronostratigraphic marker (Table 1.1) separating the earlier two pre-Sveconorwegian from the later Sveconorwegian events. D1 and D2 took place under amphibolite facies conditions and were accompanied by the intrusion of the older amphibolites, the Hålleviksstrand diorite-gabbro and various granites (the 'older granites'), and by the development of migmatitic leucosomes (Table 1.1). There then followed the intrusion of the 'younger granites' and the basic Orust dykes, the whole subsequently being deformed during the Sveconorwegian (D3, D4 and later events). The metamorphic grade at this time reached a maximum of lowest

amphibolite facies. See also Table 4.1 .

Daly et al (1979, 1982, 1983 (in press)) have dated a variety of lithologies from the Orust area by the Rb/Sr method. In particular, an age of emplacement of 1379 ± 46 Ma is reported for the Assmunderöd-Myckleby augen granite, a metamorphic (D3) date of 1087 Ma is obtained from Orust dykes, whilst the large pegmatites which are post-D3 but pre-D4 yield ages of c. 950 Ma .

d) Outline of the Project

The aims of the project were threefold: to produce and interpret a detailed geological map of the Dragsmark and north-east Skaftö, to investigate the origin of the granites, and to elucidate the nature and origin of the alkali feldspar megacrysts.

Following a reconnaissance study to delimit the area to be investigated, two field seasons were occupied in mapping at a scale of 1:10,000; the end-product is shown in Maps 1 and 2. The granite body as mapped by B.S.P. Moorlock and J.S. Daly and termed the Källviken augen granite by the latter (Daly, 1978), was found to encompass several augen granite sheets, of two different ages. The older, and more deformed, body which is best exposed at Källviken is here termed the Källviken granite, whilst the more extensive younger bodies are called the Dragsmark granites. For convenience in discussing various aspects of the nature and geological history of these intrusions, a subdivision of the Dragsmark granites into into two Areas is made. These are geographically distinct (Fig. 1.4) and can further be shown to differ in their chemistry, mineralogy, and alkali feldspar structure and composition.

The origin of the Dragsmark granites was investigated by petrographic and geochemical means. A limited number of whole rock analyses are interpreted in the light of the extensive field evidence for an origin by anatexis of Stora Le -Marstrand gneisses. The effects of the various metamorphic events on the region were investigated by use of the garnet/biotite geothermometer.

An extensive study of the alkali feldspar megacrysts and their relationship to the groundmass was carried out to ascertain their nature and origin. The structural state of the feldspars was determined by X-ray

diffractometry and their chemistry by atomic absorption spectrophotometry. These data are used to test the hypotheses of origin by porphyroblastesis or magmatic crystallization. An attempt is made to assign relative ages, within the framework of the deformational history, to the various intrusive and megacryst-forming episodes.

Figure 1.1

Geological map of southwest Sweden and eastern Norway showing the major subdivisions and the location of the area mapped. After Berthelsen (1980); Daly et al (1983); Gorbatschev (1975); Magnusson et al (1960).

OG - Oslo graben

BI - Bohus- Iddefjord granite

D - Dal group

SLM - Stora Le -Marstrand belt

Å - Åmål mega-unit

EPG, WPG - Eastern, Western Pregothian

ÖS - Östfold slab

MS - median segment

ES - eastern segment

MZ - Mylonite zone

SZ - Schistosity zone or Sveconorwegian front

Localities : D - Dragsmark

S - Skaftö

O - Orust

T - Tjörn

1.1

and eastern Norway showing the

n of the area mapped. After

); Gorbatschev (1975); Magnusson et al

ian

gian front

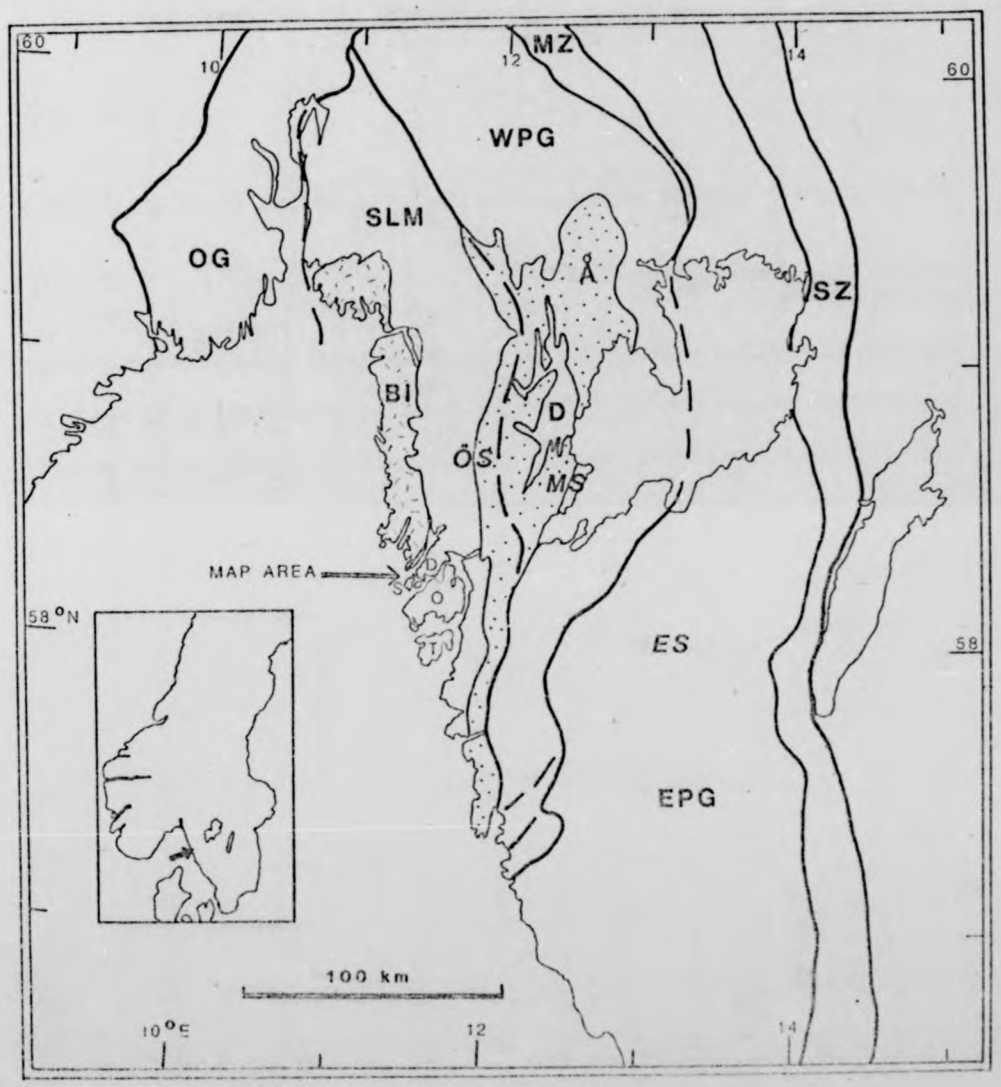

Figure 1.2

Bouger gravity anomaly map covering the area mapped (from Lind, 1982).

Contours at 2 mgal intervals.

The large negative anomaly due to the Bohus granite is readily apparent (top) and extends across Skaftö. There is a slight perturbation in the main northeast-southwest trend over Dragsmark which may be due to the presence of the Dragsmark granites (see Fig. 1.4).

S : Skaftö

D : Dragsmark

1.2

ng the area mapped (from Lind, 1982).

he Bohus granite is readily apparent (top)
is a slight perturbation in the
Dragsmark which may be due to the
(see Fig. 1.4).

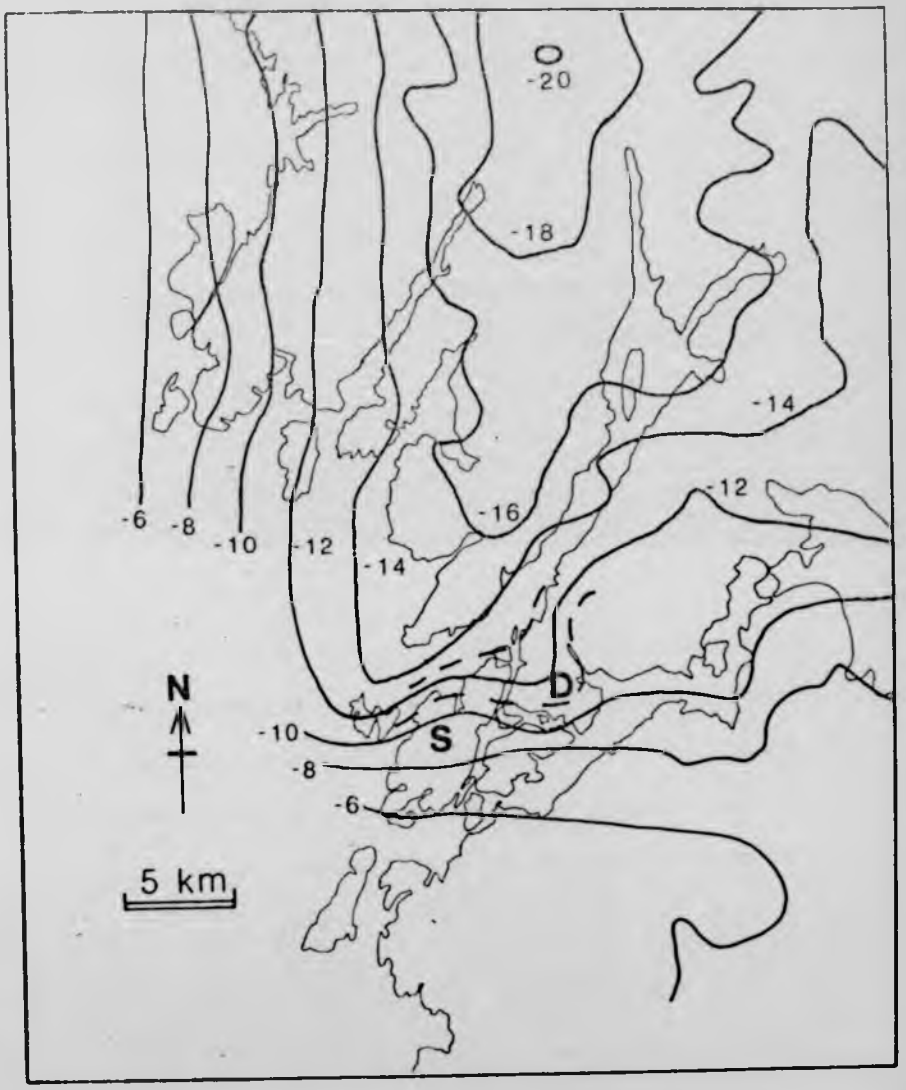

Figure 1.3

Three-component radioactivity maps of the Skaftö region of coastal southwest Sweden.

Left : K

Middle : U

Right : Th

The Bohus-Iddefjord granite (top, left; see Fig. 1.1) is clearly much richer in these elements than the surrounding Stora Le -Marstrand gneisses. The outcrop boundaries of the Dragsmark granites (heavy lines; see Fig. 1.4) are superimposed, and they can be seen to exhibit slightly greater activity than the country rocks.

ure 1.3

aps of the Skaftö region of coastal

, left; see Fig. 1.1) is clearly much
e surrounding Stora Le -Marstrand
s of the Dragsmark granites (heavy lines;
and they can be seen to exhibit slightly
y rocks.

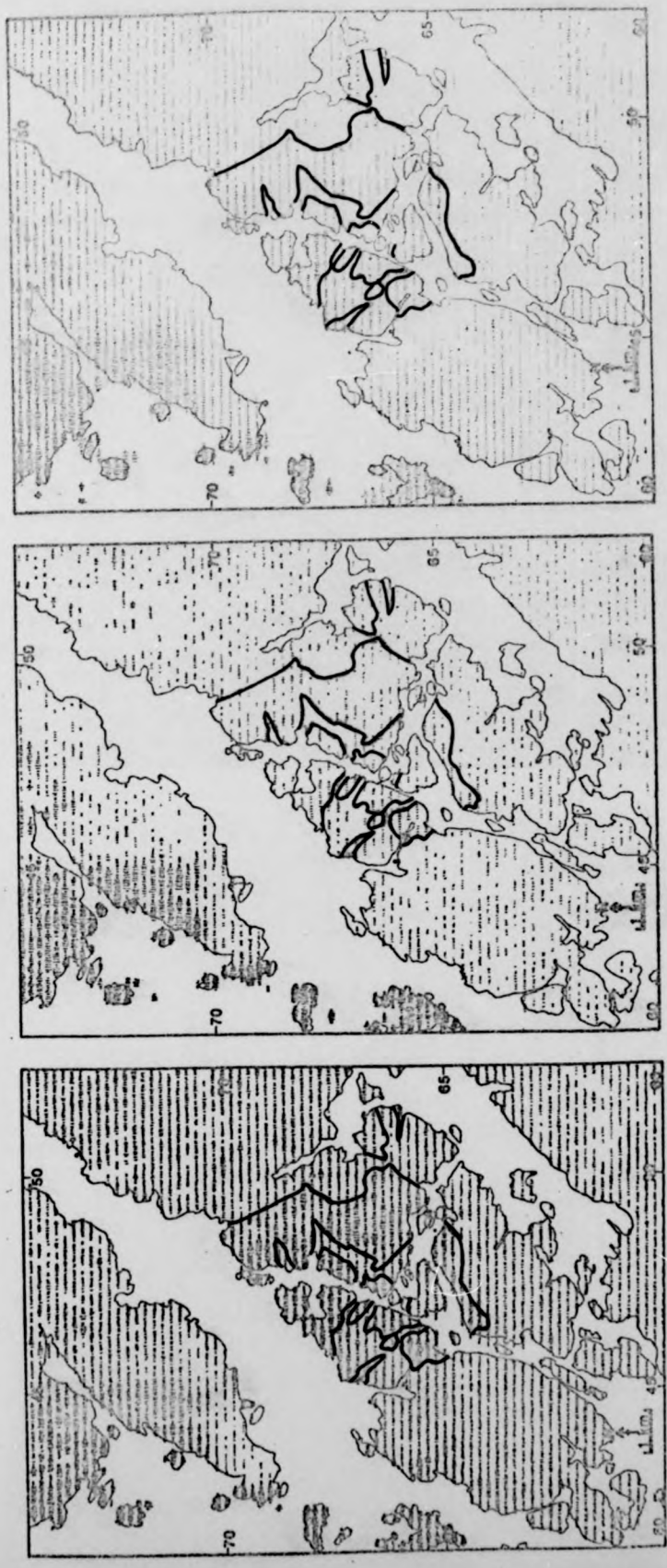

Figure 1.4

Outline geological map of the Dragsmark area showing the various augen granites.

-- Dragsmark granite Area 2

-- Dragsmark granite Area 1

-- Kallviken granite

1.4

mark area showing the various

2

1

1

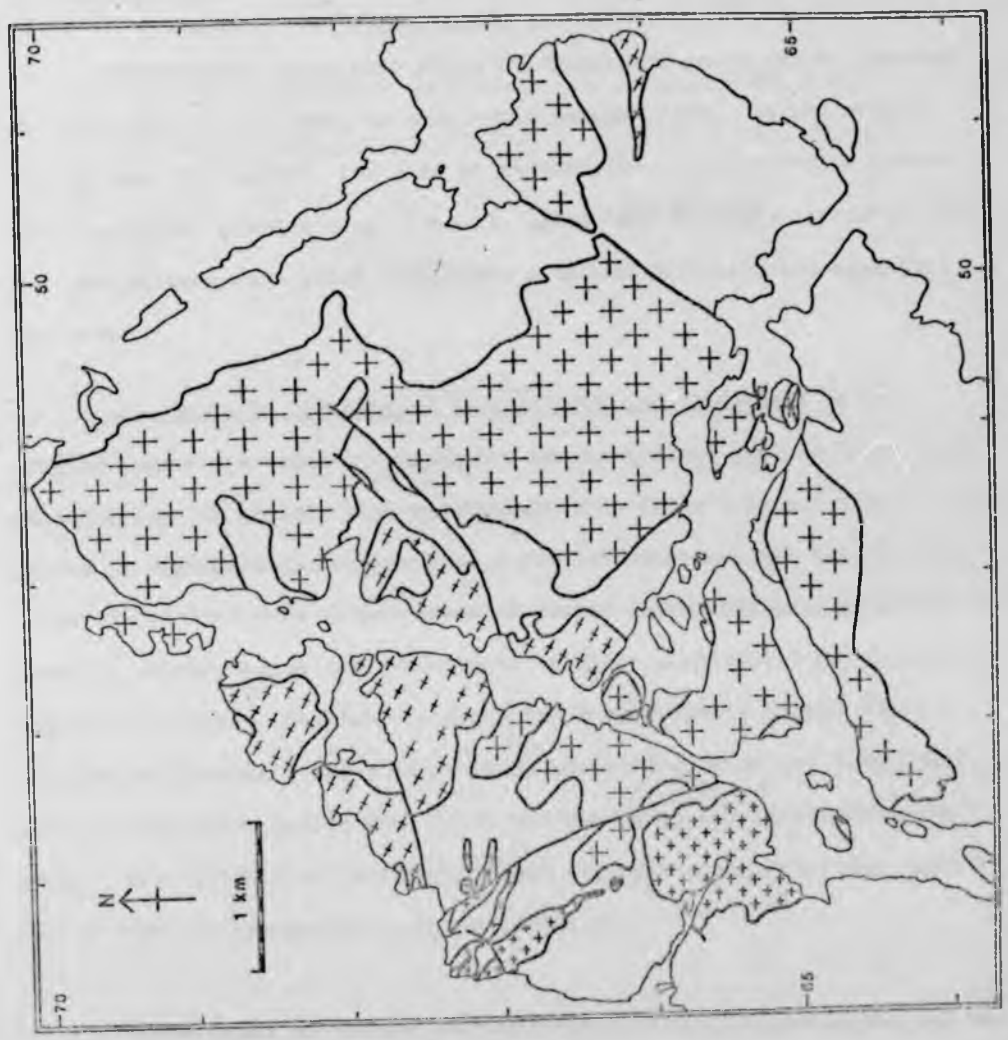

Chapter 2

Lithological Description

a) Country Rocks

The country rocks into which the Dragsmark granites are intruded are dominated by the Stora Le -Marstrand paragneisses. In the central part of the area mapped, and also at Klostergård, a granodiorite gneiss and a gneissose granite occur (Map 1). These are probably intrusive into the paragneisses with which they share a common foliation and migmatite leucosome.

The Stora Le - Marstrand paragneisses and migmatites in the Dragsmark area are variably migmatized medium-grained grey to light pink mica-gneisses of broadly semi-pelitic affinity (Figs 2.1A and 2.1B). The degree of migmatization ranges from a few leucosome strings through pods a few metres across to larger areas of coarse white gneissose granitic neosome, without augen, with autoliths of older amphibolite and psammitic gneiss (loc. 868). Abundant evidence for a sedimentary origin exists; alternating psammitic and pelitic bands up to 50cm thick are common and rare calc-silicate lenses (loc. 429) and dark grey quartzites (loc. 905) occur. Daly (1978) has carried out more extensive investigations, particularly into the geochemistry of the migmatites.

Three types of gneiss, with differing mineral assemblages, can be recognized, the petrographic differences depending ultimately on their potassium content. The commonest has the assemblage:

	Quartz	plagioclase	muscovite	biotite/chlorite	K-feldspar
av.%	46	14	15	13	11
range	30-60	5-23	10-20	10-17	0-25

with accessory epidote, garnet, opaque and zircon. These are medium grey

schistose gneisses banded on a 1 - 2mm scale with average grain size 0.6mm, although both muscovite and potassium feldspar tend to be larger. Plagioclase is typically heavily sericitized and diffuse segregations of quartz and feldspar 1 - 2mm thick are common (Fig. 2.1A).

Essentially similar gneisses occur which seem to have suffered less metamorphic segregation, perhaps on account of their lower potassium content, with the sub-assemblage:

	Quartz	plagioclase	biotite ± muscovite ± K-feldspar + accessories
av.%	41	37	22
range	20-50	30-60	10-50

The plagioclase is oligoclase and occurs with quartz in diffuse bands 2 - 5mm wide. These gneisses are more equigranular, lacking muscovite or K-feldspar blasts.

The third type of gneiss (in the Stora Le -Marstrand) in this area occurs mainly within 100m of contacts with the Dragsmark granites, especially at Rödberget (loc. 12) and Koskär (loc. 390). It is pink with potassium feldspars upto 1.5cm across cutting a compositional banding which is 1 - 3cm thick and discontinuous (Fig. 2.1B). The average grain size is 0.7mm. The assemblage is:

	K-feldspar	quartz	plagioclase	biotite/chlorite
av.%	37	31	25	5
range	30-50	20-40	20-30	0-10

with accessory epidote, sphene, garnet, zircon, topaz and opaque. The plagioclase is albite-oligoclase and is partially replaced by potassium feldspar (as patch antiperthite), often with biotite or myrmekite rims. These textures, the presence of topaz, the increased amount of alkali feldspar (and hence K_2O) and the spatial association with the granites all suggest an origin by granitization. It is possible however that the potassium was derived by breakdown of muscovite, which is absent from these

rocks. Locally (loc. 804) potassium feldspar megacrysts are found in Stora Le -Marstrand gneisses immediately overlying the Dragsmark granite. These only occur in layers of suitable composition, with biotite-rich layers being virtually unaffected.

The granodiorite gneiss is typically a pink or grey migmatitic banded gneiss with many mafic layers varying in composition from tonalite to amphibolite on a scale of a few millimetres to a decimetre or more (Fig. 2.2A). Locally (loc. 107) it is a more homogeneous leucogranite (Fig. 2.2B). Rare supracrustal remnants occur as micaceous schleiren or bands upto 5m across (loc. 1039).

Petrographically two types are discernible, although there is a continuous gradation and the two may occur as bands in the same hand-specimen. The gneissosity and compositional variation are probably metamorphic effects rather than primary features. The mafic-poor, alkali feldspar-rich variety is a biotite-monzogranite (Fig. 2.3), with the assemblage:

	Quartz	plagioclase	K-feldspar	biotite/chlorite
av.%	32	30	26	7
range	23-37	25-36	23-32	4-10

with accessory muscovite, epidote, sphene, garnet, topaz and opaque. The other is a mafic-rich and alkali feldspar- poor biotite-granodiorite (Fig. 2.3) having the assemblage:

	Quartz	plagioclase	biotite/chlorite	K-feldspar	epidote - allanite - topaz
av.%	32	32	19	11	
range	17-38	24-38	8-38	1-18	

with accessory muscovite, sphene, hornblende and opaque. In both types, the plagioclase is variably altered, the most calcic composition found being oligoclase (An_{12-16}). The more leucocratic varieties tend to be

more homogeneous and coarser grained (av. 1.2mm cf. 0.7mm).

The gneissose granite is medium-grained (average grain size 1mm), leucocratic and pinkish-grey in colour. It is more homogeneous at outcrop than the granodiorite gneiss and often homegeneous in hand-specimen, although a poorly developed gneissosity on a 1 - 10mm scale, sometimes with a degree of migmatitic segregation, is commonly present (Fig. 2.4). It has a common foliation with the Stora Le -Marstrand paragneisses and the granodiorite gneiss and is cut by the Källviken and Dragsmark granites, occurring as large xenoliths in the former (loc. 624). Field relations are uncertain, but at loc. 724 the gneissose granite carries mafic xenoliths possibly derived from the nearby granodiorite gneiss. It thus appears to be younger than the paragneisses and granodiorite gneiss, but to have undergone at least one migmatization.

Petrographically the granite is fairly uniform although the potassium feldspar content is rather variable - this however may partly be due to errors in modal analysis of individual thin sections arising from the relatively coarse grain size (average 1.7mm). The assemblage is:

	Plagioclase	quartz	K-feldspar	biotite/chlorite
av.%	31	30	28	8
range	22-41	23-36	18-47	3-14

with accessory epidote, allanite, muscovite, sphene, garnet, opaque and topaz. Mineralogically this is a biotite-monzogranite (Fig. 2.3) and is indistinguishable from the more alkali feldspar-rich samples of the granodiorite gneiss. The plagioclase is variably sericitized: less altered grains are oligoclase. Feldspar grains tend to be rather larger than quartz and the micas. Zones of fine grained material are quite common at the margins of potassium feldspars which predate the fabric. Such zones are parallel to the fabric, which is defined by aligned micas, the feldspars often being elongate in the same direction. Epidote occurs

more homogeneous and coarser grained (av. 1.2mm cf. 0.7mm).

The gneissose granite is medium-grained (average grain size 1mm), leucocratic and pinkish-grey in colour. It is more homogeneous at outcrop than the granodiorite gneiss and often homegeneous in hand-specimen, although a poorly developed gneissosity on a 1 - 10mm scale, sometimes with a degree of migmatitic segregation, is commonly present (Fig. 2.4). It has a common foliation with the Stora Le -Marstrand paragneisses and the granodiorite gneiss and is cut by the Källviken and Dragsmark granites, occurring as large xenoliths in the former (loc. 624). Field relations are uncertain, but at loc. 724 the gneissose granite carries mafic xenoliths possibly derived from the nearby granodiorite gneiss. It thus appears to be younger than the paragneisses and granodiorite gneiss, but to have undergone at least one migmatization.

Petrographically the granite is fairly uniform although the potassium feldspar content is rather variable - this however may partly be due to errors in modal analysis of individual thin sections arising from the relatively coarse grain size (average 1.7mm). The assemblage is:

	Plagioclase	quartz	K-feldspar	biotite/chlorite
av.%	31	30	28	8
range	22-41	23-36	18-47	3-14

with accessory epidote, allanite, muscovite, sphene, garnet, opaque and topaz. Mineralogically this is a biotite-monzogranite (Fig. 2.3) and is indistinguishable from the more alkali feldspar-rich samples of the granodiorite gneiss. The plagioclase is variably sericitized: less altered grains are oligoclase. Feldspar grains tend to be rather larger than quartz and the micas. Zones of fine grained material are quite common at the margins of potassium feldspars which predate the fabric. Such zones are parallel to the fabric, which is defined by aligned micas, the feldspars often being elongate in the same direction. Epidote occurs

extensively as syntaxial overgrowths on euhedral allanite. Garnet, where present, is deformed and may be embayed by alkali feldspar. Topaz carries two-phase (fluid plus vapour) fluid inclusions.

b) Amphibolite Bodies

Various amphibolites occur throughout the area (see Map 1), mainly of demonstrably igneous origin. Three suites can be distinguished, separated by episodes of metamorphism and deformation -: the older amphibolites, the Koskär dykes and the Orust dykes.

The older amphibolites are a diverse group of basic rocks, characterized by the presence of banding and/or two generations of migmatite leucosome (Fig. 2.5A). Locally small homogeneous bodies may lack one leucosome, making distinction between them and the Koskär dykes difficult (see below). Outcrops vary in size and shape from pods and bands a few centimetres to metres across to large sheet-like bodies several hundred metres in extent. Some bodies are clearly intrusive into the paragneisses, but others are concordant and may be volcanigenic in origin as suggested by Daly (1978).

The amphibolites are generally light to dark green and medium grained (average grain size 1mm) with a moderately well-developed foliation due to aligned hornblende and biotite. Where present, compositional banding from tonalite to (garnet)-amphibolite is on a centimetre to decimetre scale. Typical assemblages are:

	Hornblende - plagioclase ± quartz ± biotite ± garnet		
av.%	60	30	10

and

	Plagioclase - quartz ± hornblende ± biotite/chlorite		
av.%	60	30	10

with accessory sphene, zircon, potassium feldspar, epidote (s.l.) and opaques. Relict augitic clinopyroxene occurs in one sample (154). The plagioclase is very heavily sericitized and its composition could not be determined; a range of An_{30}- An_{50} is given by Park et al. (1979). The hornblende has α light brown, β mid-greenish brown, γ bluish green and

from two micro-probe analyses (Table B2.1) is a tshermakitic ferro-hastingsite.

The first migmatite leucosome forms thin (less than 1cm) discontinuous veins parallel to the banding and foliation and locally has been folded prior to the development of the second granitic leucosome, which is white or light pink, leucocratic and coarse grained (Fig. 2.5A). The second leucosome occurs as veins or more diffuse patches up to several decimetres wide and locally gives rise to agmatites (Fig. 2.5B).

Koskär dykes are uncommon, occurring at Koskär (loc. 1) where they cut the Källviken granite and at Rödberget (loc. 10). Their diagnostic feature is the presence of only the second migmatite leucosome (Fig. 2.6A); where this is absent positive identification is not possible. The garnet-amphibolite at loc.119 may belong to this suite as may other narrow basic dykes provisionally classified with the older amphibolites.

The Koskär dykes are medium to dark green, medium-grained (1mm) schistose biotite-amphibolites up to 1m wide and 10m long intruded into the Stora Le -Marstrand gneisses and the Källviken augen granite, but not the Dragsmark granites. Rarely, chilled margins have been preserved. The dykes have the assemblage:

	Hornblende	plagioclase	biotite	quartz ± sphene ± garnet
av.%	38	31	20	8
range	15-70	15-40	10-50	0-20

with accessory epidote, apatite, zircon, topaz and opaques. The plagioclase is oligoclase (An_{26}) and the hornblende α straw, β very dark green, γ bluish green. Topaz occurs at contacts of Koskär dykes with the Källviken granite (Fig. 2.7A) and presumably indicates the presence of fluorine in the fluid phase associated with either the second migmatization or the intrusion of the Dragsmark granite (see Ch. 8d).

Only a few representatives of the Orust dyke suite, which occur throughout Orust and Skaftölandet, are present in the area studied, and description is limited to these. For more detailed descriptions together with geochemical and geochonological studies, see Daly (1978) and Park et al. (1979). They constitute an important chronological marker in coastal South West Sweden.

The dykes are dark green, medium-grained (1mm), homogeneous amphibolites. They occur both strongly deformed (Fig. 2.8A) and undeformed, the latter having chilled margins and relict sub-ophitic textures (Figs. 2.7B and 2.8B); none are migmatized. Examples occur in the country gneisses (loc. 12), the Källviken granite (at Krämarevik) and the Dragsmark granites (loc. 421). Assemblages are rather variable, depending on the degree of metamorphism, for example:

Plagioclase - hornblende - chlorite ± clinopyroxene ± quartz ± biotite

with accessory sphene, garnet, apatite, muscovite, tremolite, potassium feldspar, epidote (s.l.) and opaques. The hornblende has α dark straw, β dark olive green, γ bluish green and the pyroxene is augitic (Fig. 2.7B). The plagioclase is more calcic than that of the Koskår dykes, being andesine (An_{47}).

c) Megacryst-bearing Granites

In addition to numerous small bands and pods of augen-bearing granitoid of uncertain age and origin, two major intrusive megacryst-bearing granites can be distinguished in the Dragsmark area (Map 1) -: the Källviken and Dragsmark granites.

The Källviken granite is a red, coarse-grained, highly deformed and migmatized augen granite outcropping in the central part of the area mapped, and structurally below the main sheet of the Dragsmark granite (see Map 1 and Ch.4). It is distinguished from the latter by its generally more deformed nature and by the widespread occurrence of a migmatite leucosome. The potassium feldspar megacrysts are variably preserved from virtually undeformed at the contacts with some xenoliths through true augen up to 5cm long to narrow polycrystalline strings. These feldspars define a gneissosity with a discontinuous banding on a scale of 1 - 3cm (Fig. 2.9A). The micas in the intervening mafic layers are elongate in this plane, as are some garnets, which form up to 10% of individual layers. Elsewhere a stictolithic texture is exhibited by hornblende and small (2mm) garnets. Patches and veins of a coarse, light-pink leucosome cutting the banding are common and locally can be seen to be axial planar to upright tight to isoclinal folds (Fig. 2.9B). In many instances the original banding is transposed parallel to this neosome.

The upper 50m or so of the Källviken granite at Skaftö (e.g. loc. 620) is less deformed and has a weaker fabric. This fabric is parallel to the contact with the Stora Le -Marstrand gneisses but truncates the banding in the granite immediately below, which is roughly perpendicular to the contact. Within this upper zone, the alkali feldspar megacrysts are euhedral and tend to occur in clusters. Migmatite leucosome is absent. A similar zone, but less deformed and more augeniferous forms the top to

a small sheet at Klostergård, also capped by Stora Le -Marstrand gneisses. The megacryst granite shows sharply discordant intrusive contacts to the gneisses (Fig. 2.10), and on these grounds this sheet is also assigned to the Källviken granite. These features are interpreted as the result of remobilization in the roof zone, probably associated with the intrusion of the Dragsmark granites.

The Källviken granite is a (mela)-monzogranite (Fig. 2.11) with the assemblage:

	Quartz	K-feldspar	plagioclase	biotite/chlorite	accessories
av.%	33	27	23	9	8
range	28-41	17-33	18-29	4-14	2-19

The accessory minerals are garnet, epidote, magnetite/haematite and topaz ± sphene, zircon, hornblende and allanite. The plagioclase is variably altered, with albite (An_{0-4}) being common whilst more heavily altered grains are andesine-labradorite (An_{37-54}); some of these are zoned. Inclusions of quartz, biotite, garnet and sphene occur in plagioclase; the alkali feldspar, which is a perthitic microcline, also has plagioclase inclusions. Many larger grains of plagioclase are patch antiperthite. Both feldspars tend to be larger than the average grain size of 1.2mm. The fabric is defined by aligned micas and is deformed around or overgrows the garnets, which thus predate the foliation. Biotite, sphene and topaz occur as clots a few millimetres across, sometimes partially included in a hastingsitic hornblende.

The numerous outcrops of megacryst-bearing granite in the Dragsmark area that are neither highly deformed (except locally) nor migmatized and are thus not part of the Källviken granite are termed the Dragsmark granites. The main body extends in a belt roughly two kilometres wide from Hultås to Munkeby, a distance of about five kilometres

(Map 1). The smaller bodies at Klostergård and Flatön, Bassholmen and many smaller islands, together with those extending from Skaftö to Evensås on eastern Skaftölandet (Map 3) are interpreted as being part of this main body (see Ch.4) which therefore forms a single sheet about 6km by 6km. This main sheet of Dragsmark granite is termed Area 1 throughout this work. The remaining minor granites are restricted to the region Vågerö̈d - Östersidan - Rödberget (Map 1) and are termed Area 2. As will be demonstrated in later chapters, this subdivision of the Dragsmark granite on the grounds of structural interpretation and spatial distribution is supported by differences in the nature of the alkali feldspar megacrysts from the two areas. The megacrysts range in size from less than 1cm to 10cm in length, those from Area 2 generally being somewhat smaller and less abundant than those from Area 1 (Fig. 2.12). Details of the macroscopic and microscopic features associated with the alkali feldspar megacrysts are described and discussed in Chapter 3.

The Dragsmark granite is a pink, medium-grained (0.5 - 1mm) variably foliated, megacryst-bearing monzogranite (Fig. 2.12). Locally the alkali feldspars are white, causing the rock to be light grey; elsewhere, especially where the granite has been mylonitized and recrystallized, they are dark red. This reddening of the granite is most notable at Rödberget, but occurs throughout the area. The brittle deformation which causes the above effects is probably D4 in age (see Chs.1 and 4), and is associated with veining by chlorite, epidote and pyrite.

The groundmass grain size is very variable, but on average samples from Area 2 (the minor bodies) are slightly finer-grained (0.6mm cf. 0.9mm) than those from Area 1. The extent to which the foliation is developed is largely dependent on the degree of deformation of those megacrysts which predate the fabric and on the density of those which postdate it. The main sheet (Area 1) tends to have a better schistosity

due to its higher mica content (Fig. 2.12).

Partially assimilated xenoliths of amphibolite and, more commonly, psammitic or granitic gneiss are abundant in the Area 2 granites, especially at the margins, but uncommon in Area 1. They range from a few centimetres to 20m across, usually with a foliation discordant to that in the granite. Autoliths of country-rock gneisses 1m wide and 100m long are abundant at Rödberget, where the Stora Le -Marstrand gneisses show evidence of granitization (p.). In contrast, clots and streaks of deformed garnets, with or without biotite, occur frequently in the main sheet, but garnet is rare in all bodies in Area 2.

The granite margins are generally poorly exposed and in many places are slightly sheared and apparently concordant (Fig. 2.13A). The northeastern boundary of the main sheet in particular is highly deformed, with extensive development of a mylonite 1 - 5m thick (see Ch.4). On a regional scale, the sheets of granite are concordant or subconcordant, as might be expected from the intrusion of a magma into well-foliated gneisses. At individual outcrops however, sharp and discordant contacts can be observed (Fig. 2.13B, see also Fig. 2.10).

Petrographically the Dragsmark granites are monzogranites (Fig. 2.11), those from Area 1 being slightly poorer in alkali feldspar and richer in mafic minerals than those from Area 2. The assemblages are, for Area 1:

	Quartz	K-feldspar	plagioclase	biotite/chlorite
av.%	31	27	29	10
range	26-45	15-40	19-40	2-18

with accessory epidote (1.5%), garnet (1%), sphene (0.2%), topaz (0.2%) and magnetite/haematite (0.1%) ± zircon, allanite, muscovite and ilmenite.

The granites of Area 2 have the assemblage:

	Quartz	K-feldspar	plagioclase	biotite/chlorite
av.%	31	32	28	7
range	16-42	21-54	17-40	4-11

with accessory epidote, sphene, topaz and zircon ± garnet and hornblende.

The texture in the groundmass varies from granoblastic-polygonal to decussate-diablastic with the larger feldspars in particular having strongly embayed margins. Most of the megacrysts are subhedral single crystals of film-perthitic, cross-hatched microcline, although more deformed augen tend to be polycrystalline. A few megacrysts are plagioclase and these are invariably highly altered and pre-date the fabric of aligned biotites. Microcline can occur in the pressure shadows, strongly suggesting a degree of mobility of alkali feldspar after solidification of the granite (Fig. 2.14A). These larger plagioclases are more calcic than the smaller grains, which are less altered or clear and range in composition from An_{13} to An_{0}. The larger grains are andesine-oligoclase with compositions varying from An_{45} to An_{17}, with an average of roughly An_{30}. A few zoned crystals are present with oligoclase cores and albitic rims. Many plagioclase grains, especially the larger ones, are patch antiperthites and a complete range in feldspar textures is seen from patch antiperthite to patch perthite. Such features again indicate movement of alkali feldspar in the post-magmatic stage.

Both feldspars contain inclusions of quartz, biotite, sphene and garnet, the alkali feldspar also containing inclusions of plagioclase. Garnet is commonly broken (Fig. 9.2B), or included in, the feldspars which may be undeformed (Fig. 2.14B), suggesting a pre-magmatic origin. Biotite is frequently chloritized, and it is possible that two types are present, one (the commoner) with α light brown, $\beta = \gamma$ dark reddish brown, the other with α greeny-straw, $\beta = \gamma$ light brown. Biotite, sphene and

topaz, sometimes with garnet, often occurs as mafic clots, although only in samples from Area 1.

Electron microprobe analyses of a number of plagioclase grains, and of both the host potassic phase and albitic lamellae in microcline crystals are given in Table B2.1 . Because of the coarseness of the exsolution lamellae, bulk compositions of the perthite can only be obtained by X-ray diffraction or wet chemical methods (see Chs. 5 and 6).

d) Veins

A variety of veins or narrow dykes (none wider than 15cm) are found in the Dragsmark area. They are unfoliated or only weakly foliated and cut the fabric of their host rocks. Most are quartz veins, some containing up to 20% xenocrystic plagioclase set in a matrix of euhedral quartz crystals. Many of these fill or are oriented parallel to post-D4 fractures (see Ch.4).

At loc.30, a number of hornblende-bearing, pink, granitic veins cut the Kållviken augen granite. They are coarse grained (av. 3mm) and leucocratic, bearing only a few percent of hornblende, biotite, sphene and topaz as the sole mafic constituents. These predate F4 folds and may be associated with the intrusion of the Dragsmark granite.

Cutting the Dragsmark granite at loc.447 and also occurring in the Kållviken granite and country rocks are a number of veins which are distinguishable by their very low alkali feldspar content. They are light grey and moderately coarse-grained (av. 1.5mm) with a weak fabric, sometimes slightly cataclastic. They have the assemblage:

	Plagioclase	quartz	biotite/chlorite	K-feldspar
av.%	49	28	10	9
range	42-58	9-38	3-18	3-12

with accessory sphene and topaz. Plagioclase grains are often larger than other minerals and are strongly antiperthitic (Fig. 2.15), implying that they were once anorthoclase. Potassium feldspar occurs only as antiperthite lamellae or interstitially between plagioclase grains, suggesting that these veins were originally one-feldspar granodiorites (Fig. 2.11). This implies that they crystallized rapidly at $P_{H_2O} <$ ca. 2.2kb or were superheated and that any subsequent metamorphic reheating was not sufficient to cause complete exsolution. The relative age of these veins is not

known other than that they are younger than the Dragsmark granites: they may be part of the younger granite suite of Park et al. (1979).

Figure 2.1

Photographs of typical Stora Le -Marstrand paragneisses.
Hammer is 40 cm. long.

A : Medium-grey quartz- two feldspar- two mica pelitic gneisses showing an average degree of migmatization and well-developed S1 foliation (loc. 42).

B : Pink-white alkali feldspar rich quartz- two feldspar- biotite gneisses showing very well developed banding. This is probably primary variation enhanced by relatively intense migmatization and local granitization (loc. 12).

Figure 2.1

Photographs of typical Stora Le -Marstrand paragneisses.
Hammer is 40 cm. long.

A : Medium-grey quartz- two feldspar- two mica pelitic gneisses showing an average degree of migmatization and well-developed S1 foliation (loc. 42).

B : Pink-white alkali feldspar rich quartz- two feldspar- biotite gneisses showing very well developed banding. This is probably primary variation enhanced by relatively intense migmatization and local granitization (loc. 12).

.1

e -Marstrand paragneisses.

eldspar- two mica pelitic gneisses
of migmatization and well-developed

rich quartz- two feldspar- biotite
developed banding. This is probably
by relatively intense migmatization and
2).

A

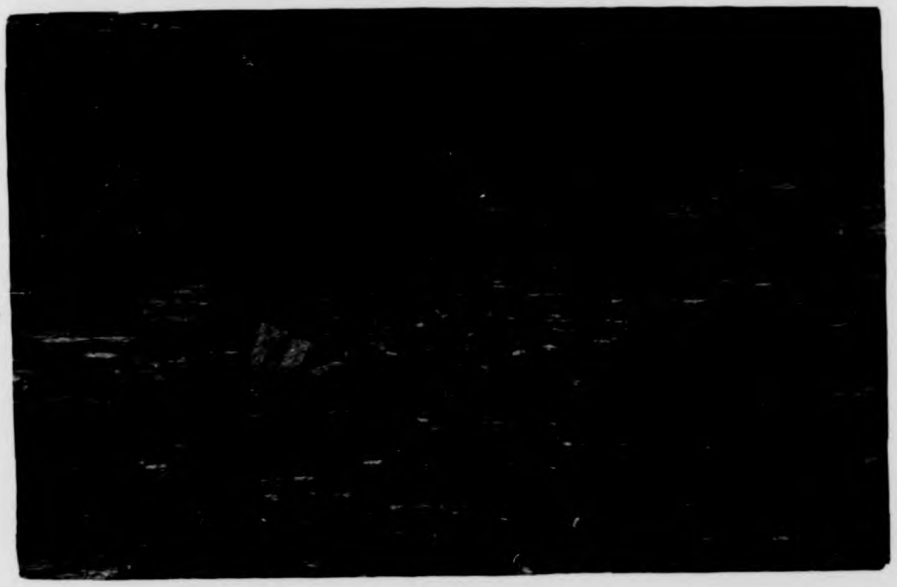

B

.1

Le -Marstrand paragneisses.

eldspar- two mica pelitic gneisses
of migmatization and well-developed

rich quartz- two feldspar- biotite
developed banding. This is probably
by relatively intense migmatization and
2).

A

B

Figure 2.2

Photographs of the granodiorite gneiss showing the variation in the degree of development of banding.
Hammer is 40 cm. long, lenscap is 5 cm. across.

A : Intensely banded and migmatized grey gneisses showing compositional variation from amphibolite to tonalite (loc. 49). Note fine, concordant first generation leucosome (centre).

B : More homogeneous leucogranitic gneiss with moderate degree of migmatization (loc. 930).

igure 2.2

te gneiss showing the variation in the
ing.
p is 5 cm. across.

matized grey gneisses showing compositional
te to tonalite (loc. 49). Note fine,
ion leucosome (centre).

anitic gneiss with moderate degree of

A

B

ure 2.2

gneiss showing the variation in the

g.

is 5 cm. across.

tized grey gneisses showing compositional

to tonalite (loc. 49). Note fine,

leucosome (centre).

tic gneiss with moderate degree of

A

B

ure 2.2

gneiss showing the variation in the

s 5 cm. across.

ized grey gneisses showing compositional

to tonalite (loc. 49). Note fine,

leucosome (centre).

tic gneiss with moderate degree of

A

B

Figure 2.3

Modal analyses of country rock gneisses from the Dragsmark area plotted on the quartz (Q)- alkali feldspar (AF)- plagioclase (PF) triangle. Field boundaries and nomenclature after Streckeisen (1975).

o - granodiorite gneiss, low K_2O

• - granodiorite gneiss, high K_2O

Δ - gneissose granite

3a - syenogranite

3b - monzogranite

4 - granodiorite

5 - tonalite

ure 2.3

gneisses from the Dragsmark area

ali feldspar (AF)- plagioclase (PF)

d nomenclature after Streckeisen (1975).

K_2O

K_2O

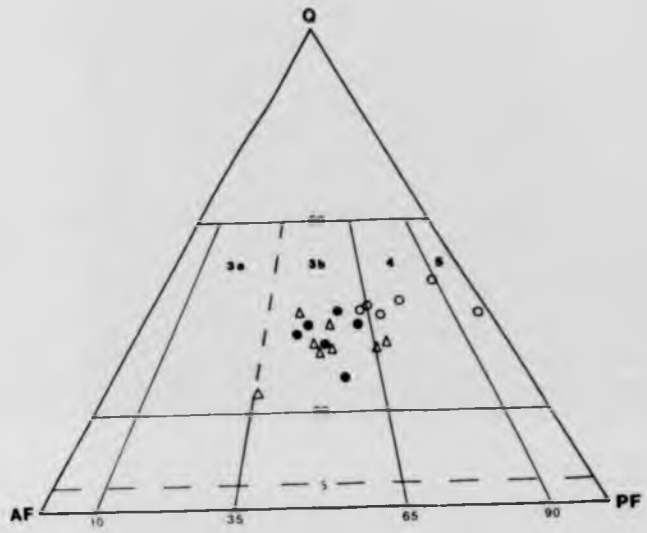

Figure 2.4

Outcrop of the gneissose granite (loc. 844).

This degree of banding is rather atypical (but contrast with Fig. 2.2A of the granodiorite gneiss).

Hammer is 40 cm. long.

Figure 2.4

Outcrop of the gneissose granite (loc. 844).

This degree of banding is rather atypical (but contrast with Fig. 2.2A of the granodiorite gneiss).

Hammer is 40 cm. long.

re 2.4

(loc. 844).

atypical (but contrast with Fig. 2.2A

ure 2.4

e (loc. 844).

r atypical (but contrast with Fig. 2.2A

Figure 2.5

Photographs of the older amphibolite.

A : Moderately homogeneous outcrop showing the first generation leucosome (veinlets, centre) folded prior to the development of the coarser, more diffuse second generation leucosome (loc. 629). Compass base is 10 cm. long.

B : Agmatitic variety of older amphibolite (loc. 753). The thin first generation neosome is again seen to be truncated by the coarser second generation leucosome forming the matrix. Hammer is 40 cm. long.

B

re 2.5

olite.

crop showing the first generation
e) folded prior to the development of
second generation leucosome (loc. 629).
g.

amphibolite (loc. 753). The thin
s again seen to be truncated by the
leucosome forming the matrix.

A

B

ure 2.5

olite.

crop showing the first generation
e) folded prior to the development of
second generation leucosome (loc. 629).
g.

amphibolite (loc. 753). The thin
s again seen to be truncated by the
leucosome forming the matrix.

A

B

Figure 2.6

Photographs of the Koskår dykes.

A : At loc. 10, one of the larger dykes is set in Stora Le -Marstrand gneisses. Note the presence of minor migmatitic leucosome (second generation- see text p.15) at the right-hand margin. A faint S3 foliation is discernible in the dyke (trending from upper left to lower right).

B : Intensely folded Koskår dykes (loc. 2) in the Kållviken granite. The folding is probably D4 in age.

Figure 2.6

A

B

Photographs of the Koskår dykes.

A : At loc. 10, one of the larger dykes is set in Stora Le -Marstrand gneisses. Note the presence of minor migmatitic leucosome (second generation- see text p.15) at the right-hand margin. A faint S3 foliation is discernible in the dyke (trending from upper left to lower right).

B : Intensely folded Koskår dykes (loc. 2) in the Kållviken granite. The folding is probably D4 in age.

re 2.6

er dykes is set in Stora Le -Marstrand

e of minor migmatitic leucosome

t p.15) at the right-hand margin.

scernible in the dyke (trending from

kes (loc. 2) in the Kållviken

robably D4 in age.

A

B

re 2.6

er dykes is set in Stora Le -Marstrand

e of minor migmatitic leucosome

t p.15) at the right-hand margin.

scernible in the dyke (trending from

.

kes (loc. 2) in the Kållviken

robably D4 in age.

A

B

Figure 2.7

A : Photomicrograph showing development of Topaz (T) at the contact between a Koskår dyke (lower half of picture) and the Kållviken granite (upper half of picture) at loc. 1.
Crossed polars.

B : Photomicrograph of sample no. 421 of the large Orust dyke at Vågerød showing preservation of sub-ophitic texture. The mafic phase is heavily altered, but relict clinopyroxene cores are locally present (CPX).
Plain polarized light.

gure 2.7

evelopment of Topaz (T) at the contact
wer half of picture) and the Kållviken
cture) at loc. 1.

no. 421 of the large Orust dyke at
ion of sub-ophitic texture. The mafic
but relict clinopyroxene cores are

A

B

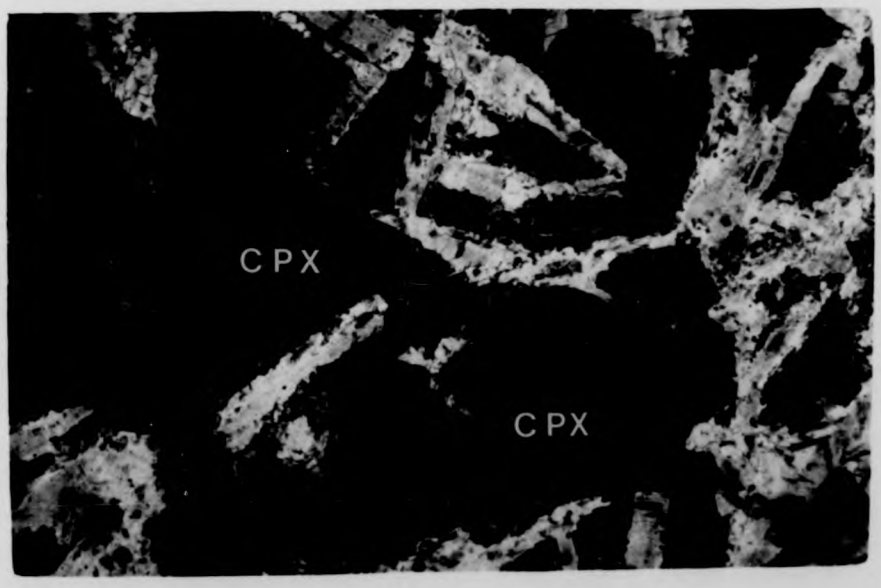

igure 2.7

development of Topaz (T) at the contact
ower half of picture) and the Kållviken
icture) at loc. 1.

e no. 421 of the large Orust dyke at
tion of sub-ophitic texture. The mafic
but relict clinopyroxene cores are

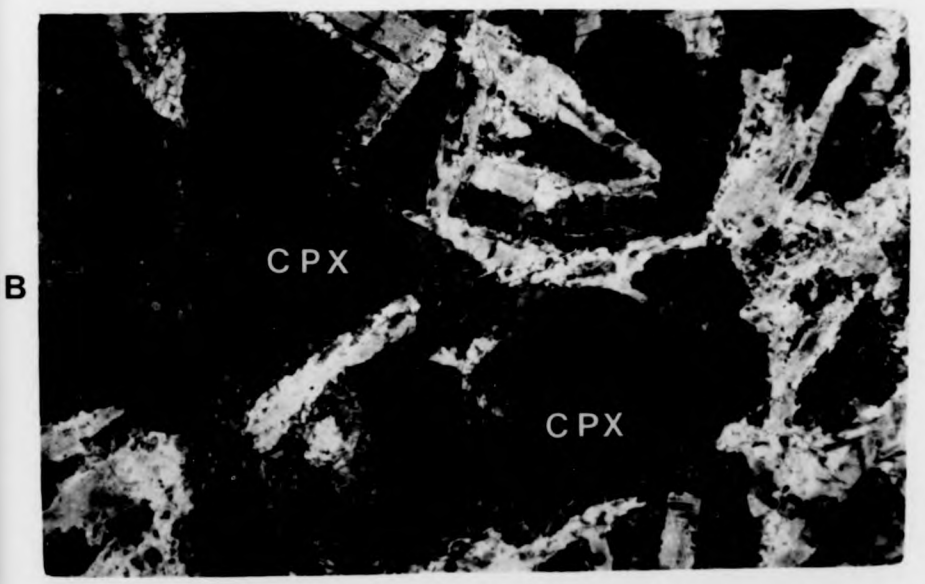

Figure 2.8

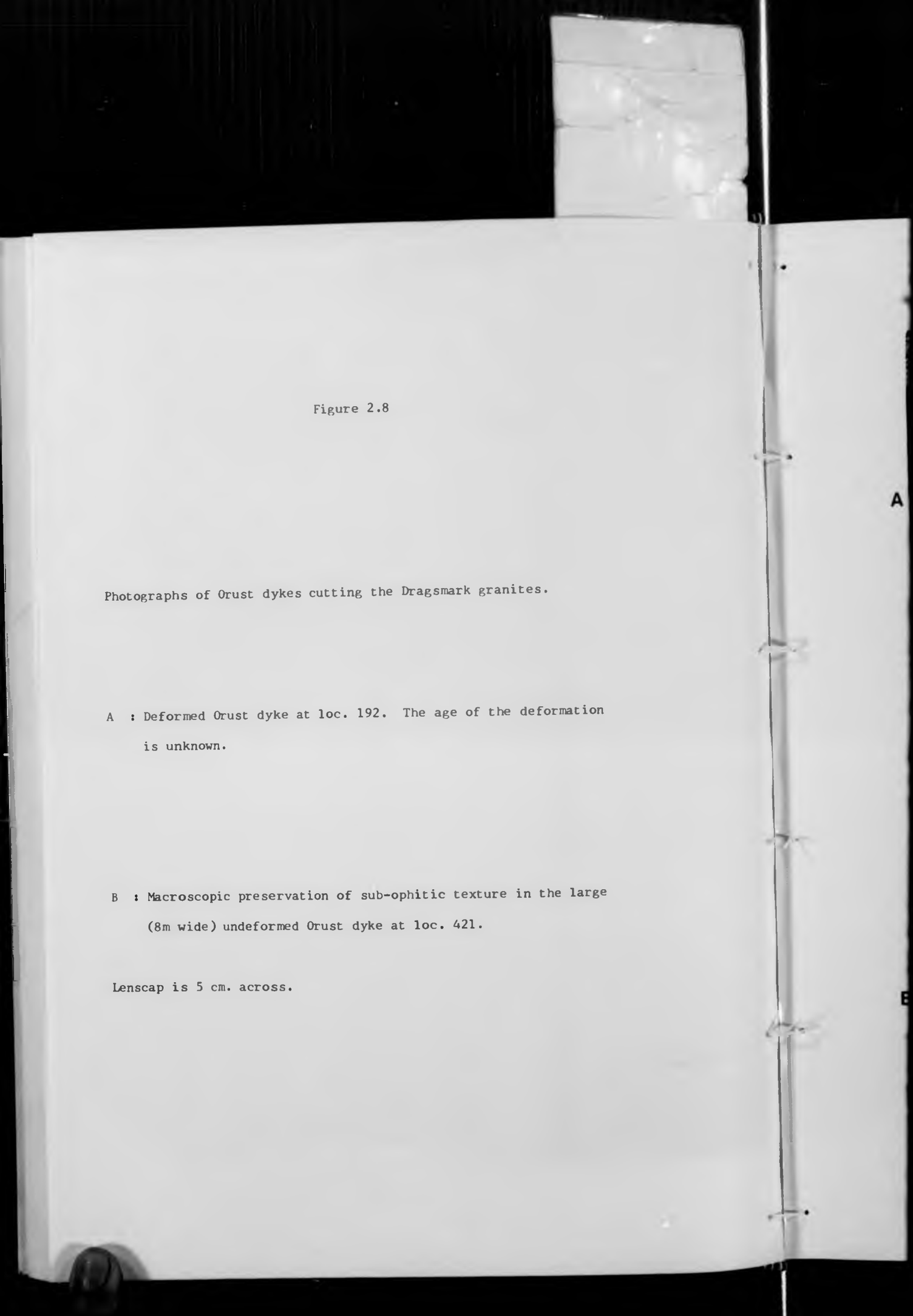

Photographs of Orust dykes cutting the Dragsmark granites.

A : Deformed Orust dyke at loc. 192. The age of the deformation is unknown.

B : Macroscopic preservation of sub-ophitic texture in the large (8m wide) undeformed Orust dyke at loc. 421.

Lenscap is 5 cm. across.

mark granites.

ge of the deformation

texture in the large

421.

A

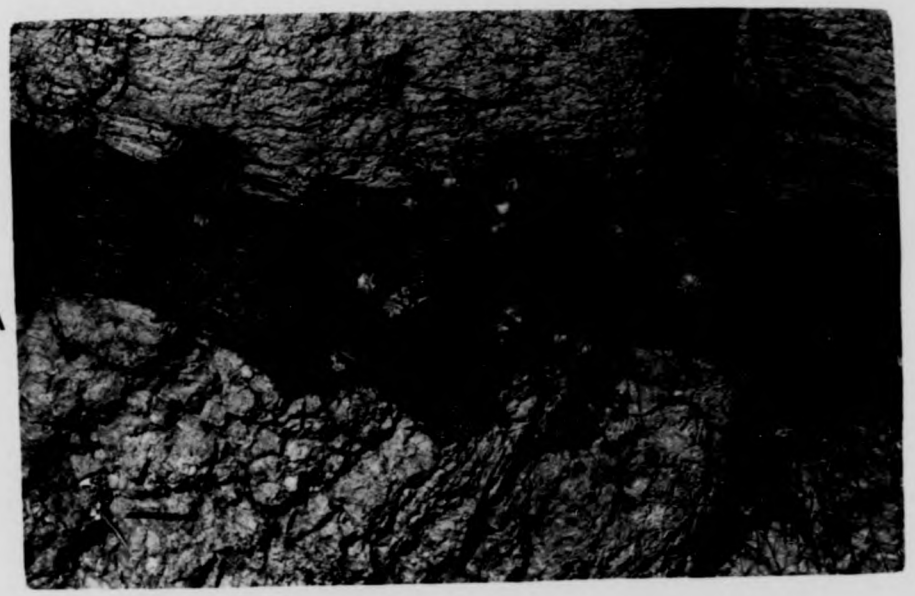

B

mark granites.

ge of the deformation

texture in the large

421.

A

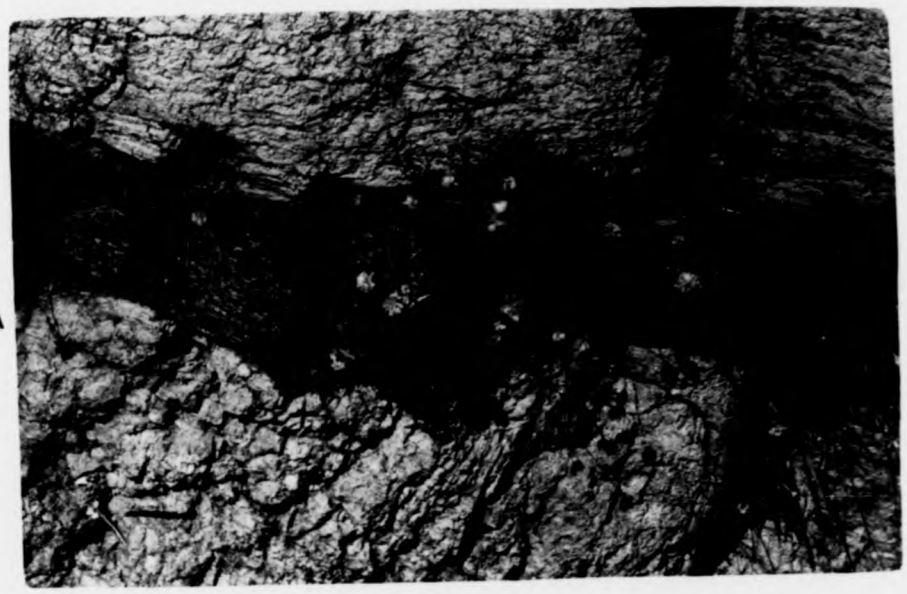

B

Figure 2.9

Photographs of the Kållviken granite.

Hammer is 40 cm. long, lenscap is 5 cm. across.

A : Loc. 372. Moderately well preserved alkali feldspar augen define a gneissosity which is folded by open to close folds, probably D1 in age. Locally an incipient axial planar fabric is detectable.

B : Highly deformed granite at the type locality at Kållviken showing almost total recrystallization of the augen and development of a coarse stictolithic migmatite leucosome. This is parallel to a schistosity which is roughly axial planar to close to isoclinal folds. The leucosome is probably second generation. Loc. 30.

ss.

kali feldspar augen

open to close folds,

nt axial planar fabric

cality at Kållviken

of the augen and

igmatite leucosome. This is

ghly axial planar to close to

bably second generation.

A

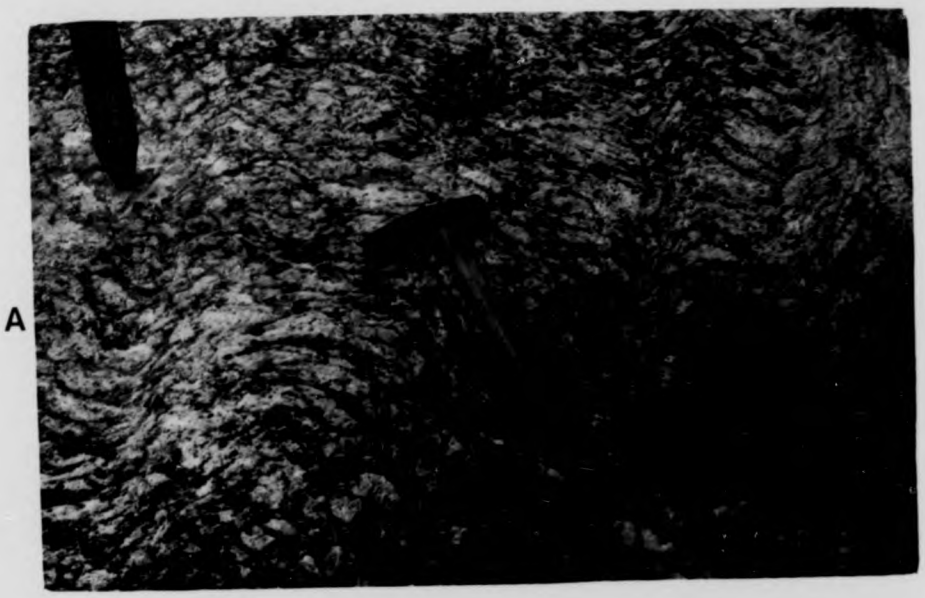

B

ss.

kali feldspar augen

open to close folds,

nt axial planar fabric

cality at Kållviken

of the augen and

igmatite leucosome. This is

ghly axial planar to close to

bably second generation.

A

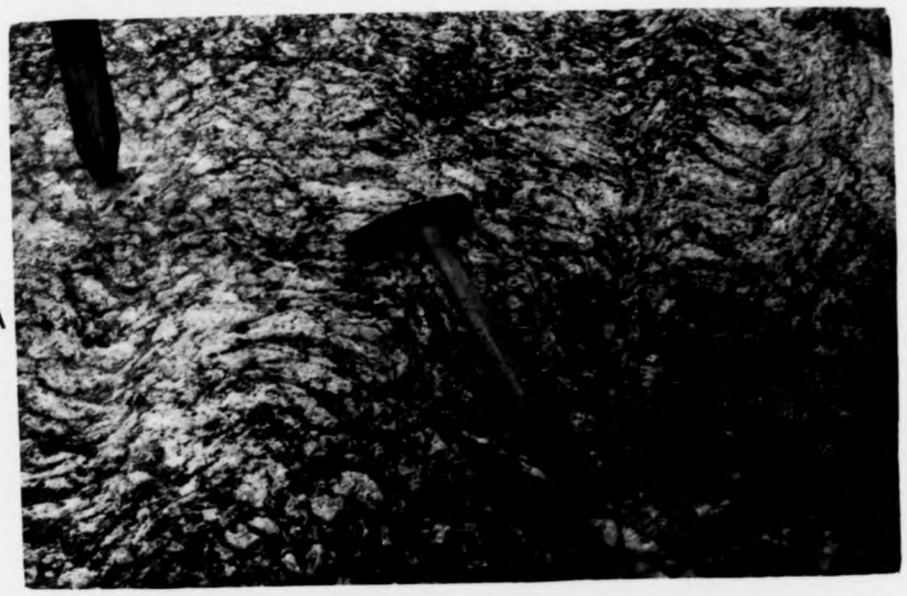

B

Figure 2.10

Sharp, discordant contact between the minor augen granite sheet (left) at Klostergård (assigned to the Kållviken granite) and Stora Le -Marstrand gneisses (loc. 470).

Hammer measures 40 cm.

augen granite sheet (left)

granite) and Stora Le -Marstrand

t augen granite sheet (left)

granite) and Stora Le -Marstrand

r augen granite sheet (left)

granite) and Stora Le -Marstrand

r augen granite sheet (left)

granite) and Stora Le -Marstrand

Figure 2.11

Modal compositions of granites and veins from the Dragsmark area plotted on the quartz (Q)- alkali feldspar (AF)- plagioclase (PF) triangle. Field boundaries and nomenclature after Streckeisen (1975).

o - Dragsmark granite Area 1

● - Dragsmark granite Area 2

▲ - Kållviken granite

▽ - veins

1 - quartz-rich granitoids

3a - syenogranite

3b - monzogranite

4 - granodiorite

7* - quartz syenite

10* - quartz diorite

om the Dragsmark area

(AF)- plagioclase (PF)

e after Streckeisen (1975).

Figure 2.12

A : Cut surface of sample no. 818 from Area 1 of the Dragsmark granite. Note well-developed schistosity (defined by biotite) and large alkali feldspar megacryst (euhedral).

B : Cut and stained surface of sample no. 72 from Area 2 of the Dragsmark granite. Contrast the smaller alkali feldspar megacrysts and weaker fabric with the above. Note also the finer grain size.

rea 1 of the Dragsmark granite.

fined by biotite) and large

.

. 72 from Area 2 of the

aller alkali feldspar megacrysts

Note also the finer grain size.

A

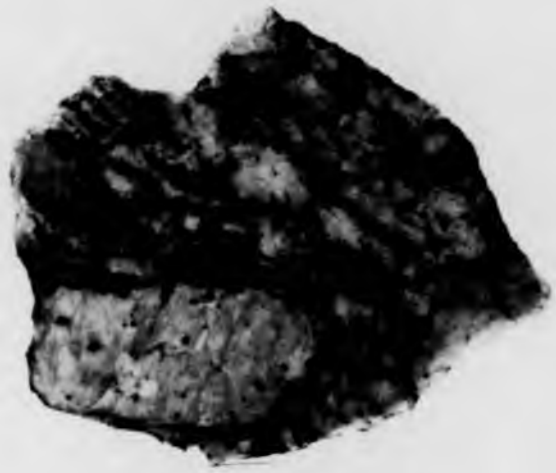

0 5 CM.

B

rea 1 of the Dragsmark granite.

fined by biotite) and large

).

o. 72 from Area 2 of the

aller alkali feldspar megacrysts

Note also the finer grain size.

A

B

rea 1 of the Dragsmark granite.

ined by biotite) and large

).

A

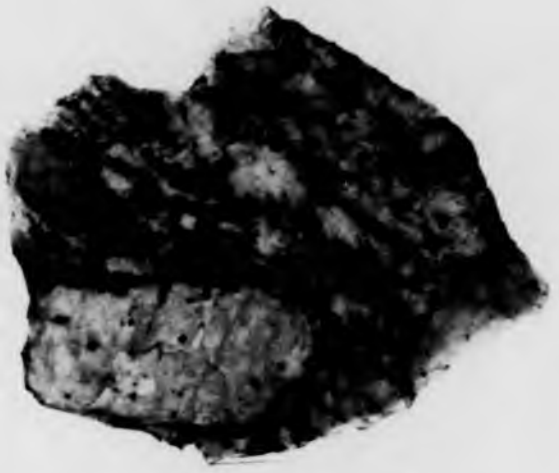

0 5 CM.

. 72 from Area 2 of the

aller alkali feldspar megacrysts

Note also the finer grain size.

B

Figure 2.13

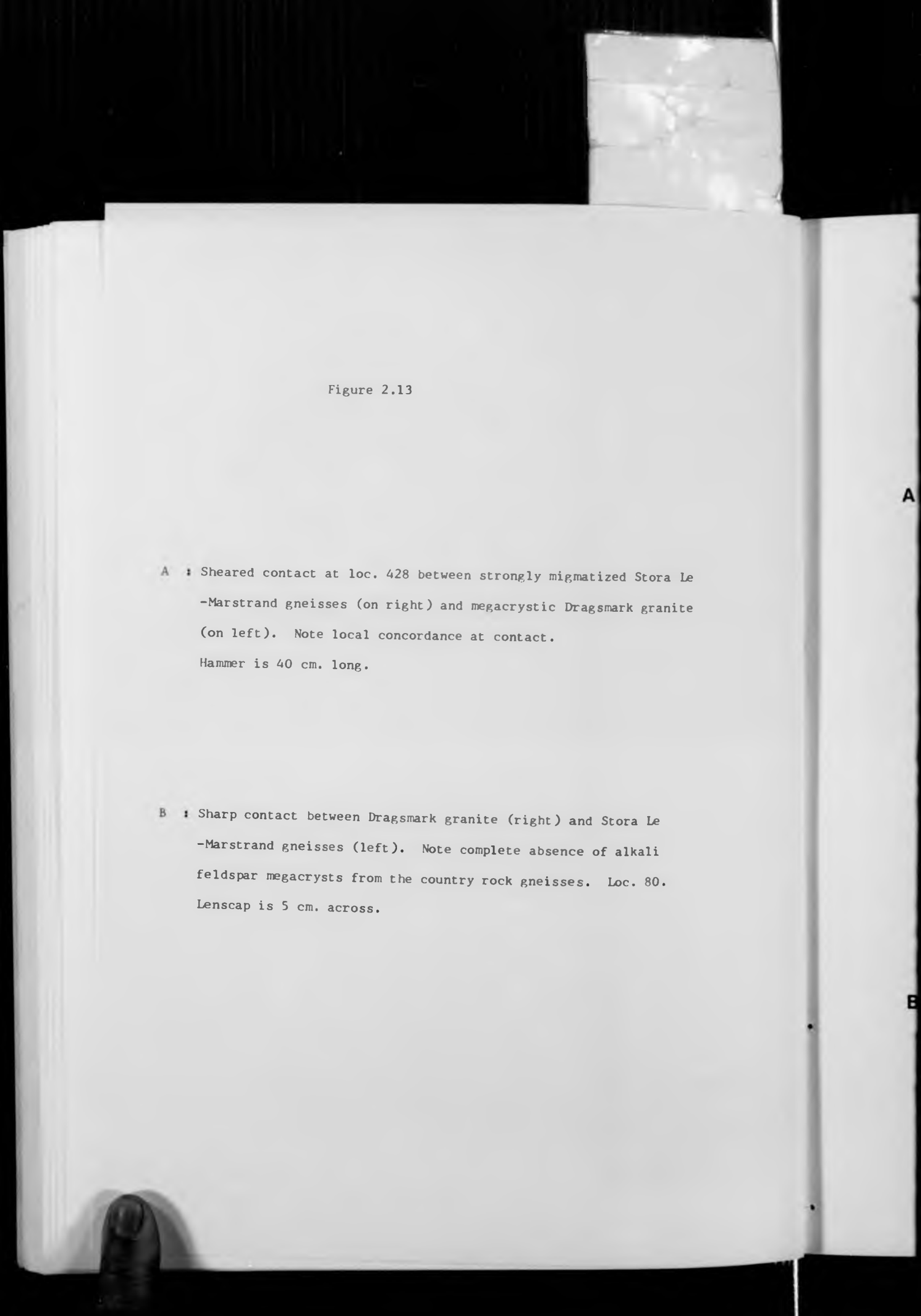

A : Sheared contact at loc. 428 between strongly migmatized Stora Le -Marstrand gneisses (on right) and megacrystic Dragsmark granite (on left). Note local concordance at contact. Hammer is 40 cm. long.

B : Sharp contact between Dragsmark granite (right) and Stora Le -Marstrand gneisses (left). Note complete absence of alkali feldspar megacrysts from the country rock gneisses. Loc. 80. Lenscap is 5 cm. across.

en strongly migmatized Stora Le

d megacrystic Dragsmark granite

e at contact.

anite (right) and Stora Le

complete absence of alkali

ry rock gneisses. Loc. 80.

A

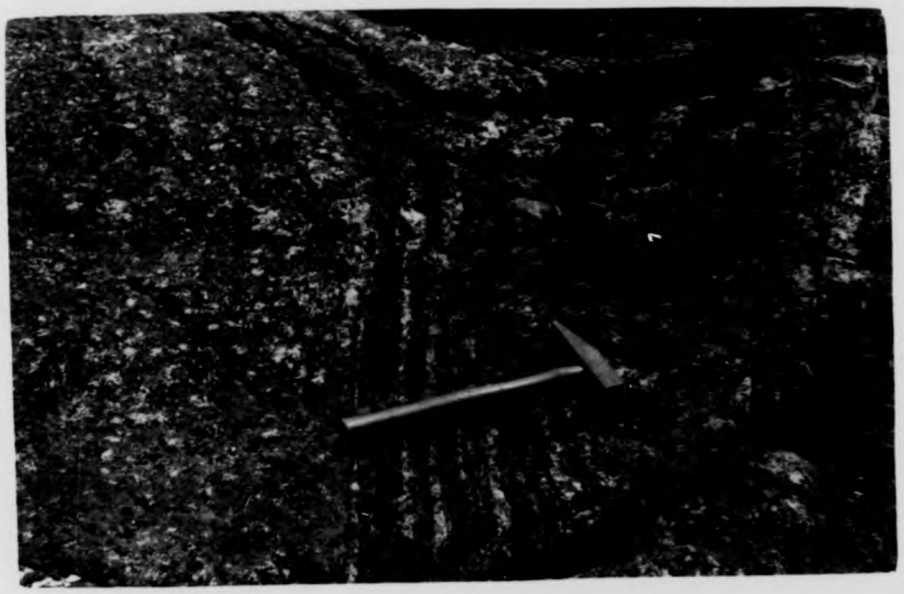

B

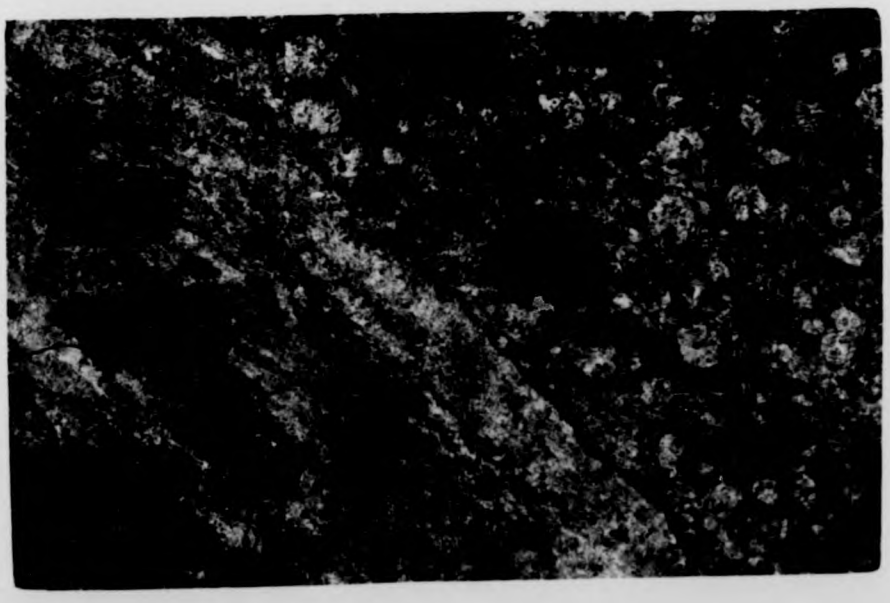

en strongly migmatized Stora Le

d megacrystic Dragsmark granite

e at contact.

anite (right) and Stora Le

complete absence of alkali

ry rock gneisses. Loc. 80.

A

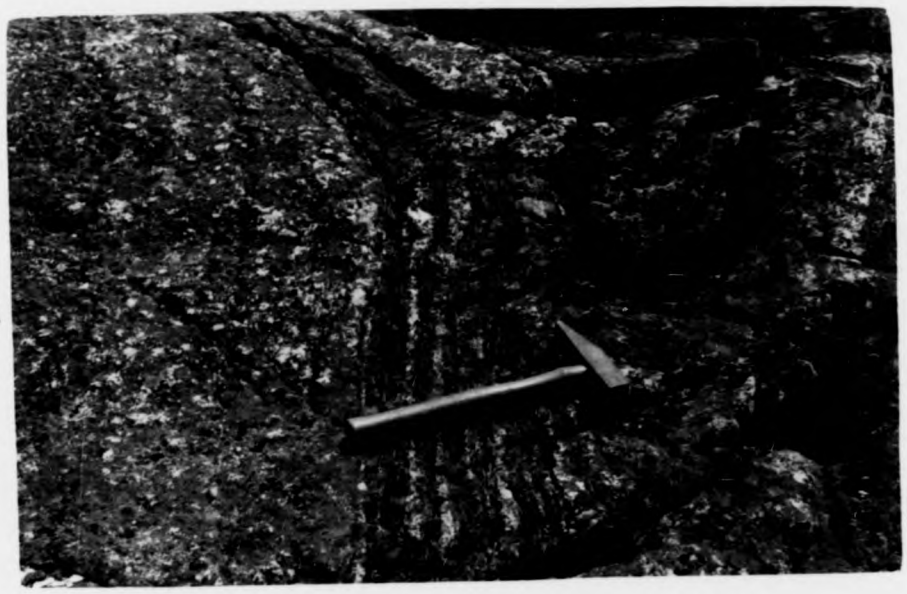

B

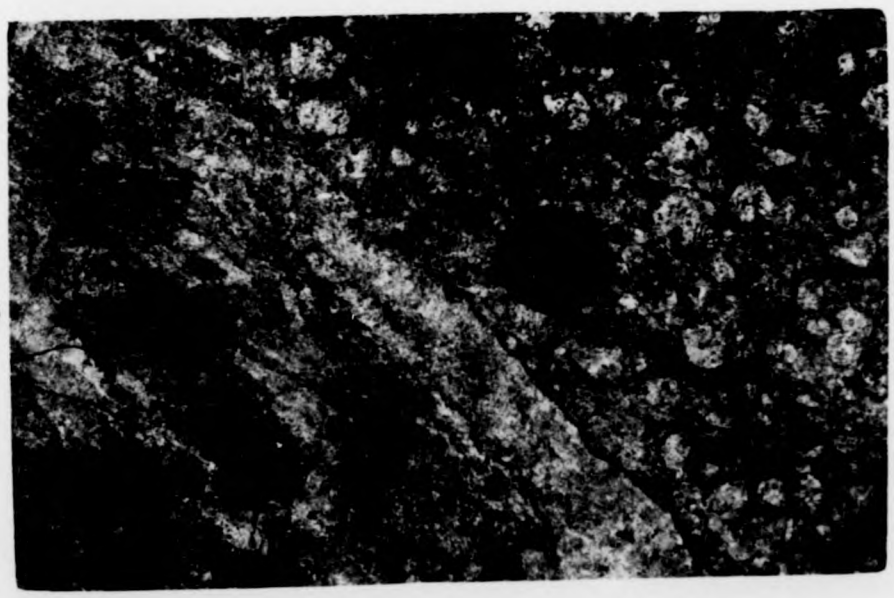

Figure 2.14

Photomicrographs of the Dragsmark granite.

A : A highly altered plagioclase megacryst (P), with microcline (M) in the pressure shadows. The main foliation is defined by biotite (B). It is apparent that there was a degree of mobility of alkali feldspar after solidification of the magma.
Sample no. 248.
Plain polarized light.

B : An angular fragment of garnet (G) included in a plagioclase crystal (P). Sample no. 187.
Plain polarized light.

st (P), with microcline (M)
oliation is defined by biotite
a degree of mobility of
of the magma.

cluded in a plagioclase

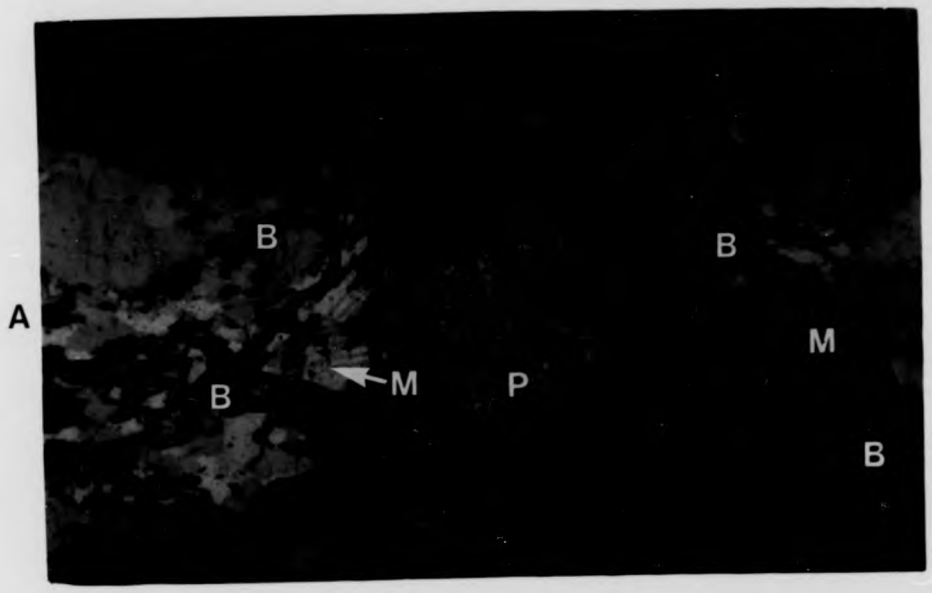

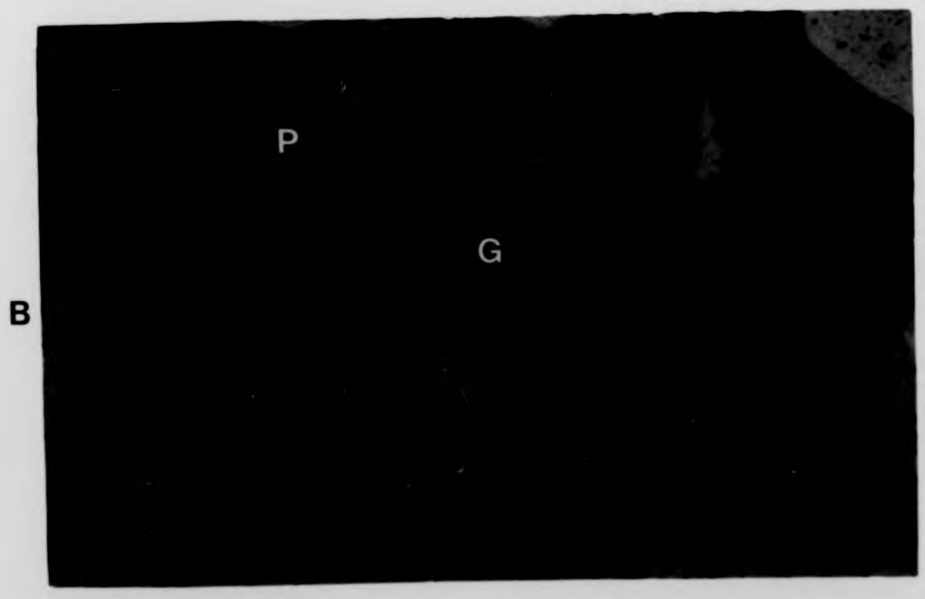

st (P), with microcline (M)

oliation is defined by biotite

a degree of mobility of

of the magma.

cluded in a plagioclase

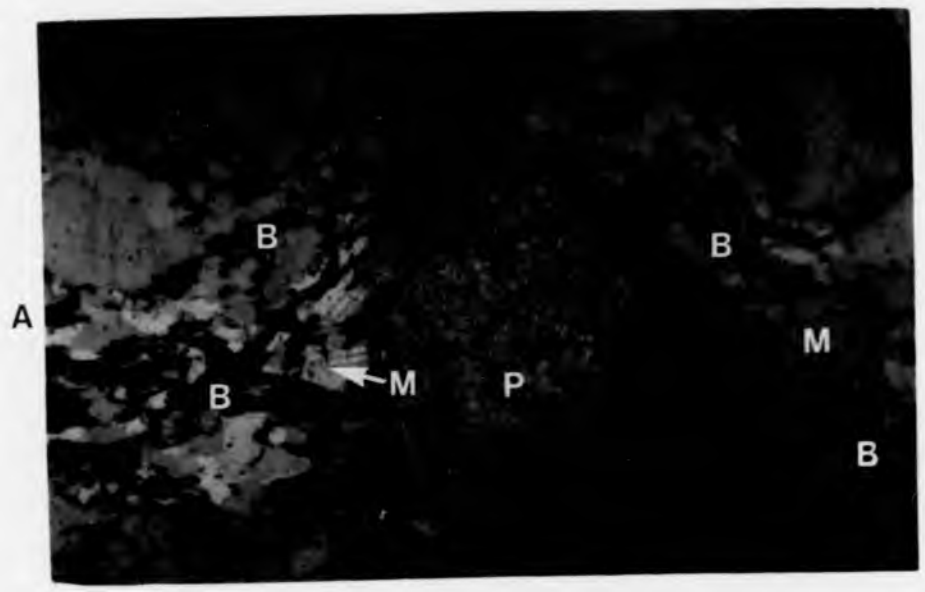

Figure 2.15

Photomicrograph of a one-feldspar vein cutting the Dragsmark granite at loc. 447 showing a large alkali feldspar with two generations of exsolved lamellae.

2.15

ein cutting the Dragsmark granite

feldspar with two generations of

2.15

ein cutting the Dragsmark granite

feldspar with two generations of

Chapter 3

Physical Characteristics of the Alkali Feldspar Megacrysts

a) Macroscopic Features

The most distinctive feature of the Dragsmark granites is the presence of alkali feldspar megacrysts (Fig. 3.1A, B; see also Figs. 2.12 and 2.13). These are commonly pink-red, although locally they may be white (loc.249) or brick-red. The most intense colouration is found in the most deformed rocks, for example at Rödberget (Map 3) and is due to the presence of submicroscopic flakes of haematite in both alkali feldspar and plagioclase. It is not known what significance the colour of the feldspar has, but the correlation between colouration and deformation suggests that iron became mobile under stress. Daly (1978) notes that larger, single-crystal, lineated or sheared augen from the Assmunderöd - Myckleby body tend to be darker red than normal.

Undeformed megacrysts up to 15cm long occur in the Dragsmark granite, but most are between 2cm and 4cm and approximately equidimensional. Berthelsen and Murthy (1970) state that augen from the Assmunderöd granite are generally rounded or flattened and 3 - 5cm long whereas those from the Myckleby granite tend to be smaller (2cm). They range in colour from light grey to brick-red, being mainly pink-red. In contrast, Stone and Austin (1961) describe white potash feldspar megacrysts from the Carmenellis granite (S.W. England) as being 2 - 3cm long and subhedral to euhedral, whilst Booth (1968) finds the magmatic megacrysts of the Land's End granite also to be white and tabular euhedral, but with an average length of 6cm.

The Assmunderöd granite is strongly lineated and commonly foliated, these fabrics being defined by the augen (Berthelsen and Murthy, 1970).

Neither the Myckleby nor Dragsmark granites are lineated, except locally in D4 shear zones (loc.953). The main foliation (S2; see Ch.4) in the Dragsmark granites is variably developed but nowhere very intense and often absent (Fig. 3.1). Where well defined, this fabric is a true augen structure, but is frequently overgrown by potassium feldspar megacrysts. This suggests that megacryst growth in at least the main sheet of the Dragsmark granite occurred both during and after the D2 deformation.

Those crystals lying in the plane of the fabric cannot automatically be assumed to be pre- or syndeformational, as post-tectonic blasts would tend to crystallize with their two long axes in the S-plane, this orientation offering the least resistance to growth (Harry, 1951). Nevertheless, the presence in the same hand-specimen of highly deformed augen and undeformed euhedral alkali feldspars probably indicates two phases of megacryst growth. That some of the megacrysts grew by blastesis in the solid rock is evidenced by several examples of crystals growing across contacts to the country gneisses (Fig. 3.2). Such phenomena are much more common in the minor sheets of Area 2, but the presence of potash feldspar megacrysts in xenoliths of older amphibolite at loc.158 (Map 3) indicates that some blastesis also occurred in the main sheet.

It is notoriously difficult to obtain estimates of the three-dimensional shape of crystals from measurements made in two dimensions, and no quantitative investigation has been attempted of any variation in megacryst morphology. Comparison of the breadth/length ratios (axial ratios) of megacrysts from different areas as measured in hand-specimens and on randomly oriented sections cut perpendicular to the foliation does however yield useful information. Such data have been collected for samples from Areas 1 and 2 of the Dragsmark granite and from the Källviken granite, and for undeformed euhedral megacrysts (often showing Carlsbad twinning); the results are presented in Fig. 3.3. It can be seen from

Fig. 3.3A that the mean axial ratio of undeformed crystals is 1 : 1.5 which is markedly different from a mean value of 1: 3.5 for alkali feldspars from the Carmenellis granite (Austin, 1960). Mean axial ratios for megacrysts from Areas 1 and 2 and the Källviken granite are 1: 3.0 , 1: 1.9 and 1: 4.1 respectively (Fig 3.3B, C, D). There is no overlap between the ranges in values for undeformed crystals and the Källviken granite (Fig. 3.3D), supporting the field observation that nearly all megacrysts in this granite are deformed (p.15). The highly variable degree of deformation of augen from Area 1 of the Dragsmark granite is reflected in the wide range of axial ratios (Fig. 3.3B), which is in fact greater than that for the Källviken granite. This contrasts with the virtually undeformed (neglecting localized D4 deformation, see Ch.4) nature of the Area 2 bodies, which is indicated by the similarity in axial ratios between megacrysts from this Area and in the undeformed state (Fig. 3.3C).

Modal analysis of thin-sections of the Dragsmark granites yields averages of 27% potassium feldspar in Area 1 and 32% in Area 2 (Ch. 2c). In order to determine what proportion of this feldspar was present as megacrysts, the % area of megacrysts of alkali feldspar was measured on slabs of granite averaging 100cm^2 using an Apple Graphics Tablet. The alkali feldspar was stained yellow by a standard HF/sodium cobaltinitrite treatment. Eight slabs of granite from Area 1 yielded values of 11 - 28% megacryst with an average of 21%. Those samples from the southern parts of the main sheet (Flatön and Evensås, Map 3) had fractionally higher megacryst contents whilst two samples from Area 2 yielded values of 13.5% and 37.5%. Taking 21% megacrysts and 27% total alkali feldspar, it can be seen that approximately 80% of the total alkali feldspar in the main sheet of the Dragsmark granite is contained in the megacrysts. In contrast, Booth (1966) finds that even in the most porphyritic type of the main coarse grained Land's End granite, the megacrysts account for only 60% of the total potash feldspar although they constitute 24% of the rock. In

the moderately porphyritic type, they account for only 15% of the total.

In a few samples only about $^{2}/_{3}$ of the augen are pure alkali feldspar, the remainder being glomeroblasts containing quartz and plagioclase in addition. Berthelsen and Murthy (1970) and Daly (1978) note that such aggregates are much more abundant than large single crystals in the Assmunderöd-Myckleby augen granite.

At localities from which megacrysts were taken for chemical analysis (see Map 3), their areal density was measured to investigate the possibility of systematic variation. The number of megacrysts (with a minimum length of 1cm) visible in an area of 200cm^2 was counted on ten randomly chosen surfaces and the average value multiplied by fifty to yield the number of megacrysts per square meter. There is a slight tendency for megacryst density to increase upwards in the northern part of Area 1 (traverse B) ; results are given in Table 3.1 . It can further be seen from the Table that the small bodies in Area 2 (loc. X1 etc.) show by far the greatest variation in megacryst density (range 170 - 855/m^2) and that the southern part of the main sheet (traverses E and F) shows a greater density that the northern part. The possible significance of these observations is discussed in Ch. 10 . Comparable values for the Land's End granites (Booth, 1966) are 400 megacrysts per square meter for the Highly porphyritic type and 100/m^2 for the Moderately porphyritic type. The Dragsmark granites may thus be described as extremely megacrystic.

Table 3.1

Megacryst density (per square meter) in the Dragsmark granites

	Locality	Density
AREA 1 (North)		
Top	B2	520
	B3	465
	B4	410
	B5	415
	B6	335
	B7	270
	B8	310
	B9	320
	B10	360
Base	B11	375
	B av.	360 ± 75
	B range	270 - 520

	Locality	Density
AREA 1 (Central)		
Base	C12	545
	C11	565
	C10	555
	C9	535
	C8	480
	C7	470
Top	C6	480
	C5	530
	C4	590
	C3	450
	C2	375
Base	C1	345
	C av.	495 ± 75
	C range	345 - 590

	Locality	Density
AREA 1 (South)		
Top	E5	550
	E4'	625
	E4	675
	E3	760
	E2	620
Base	E1	655
	E av.	650 ± 70
	E range	550 - 760

	Locality	Density
AREA 1 (South)		
Top	F6	645
	F5	560
	F4	700
	F3	665
	F2	690
Base	F1	540
	F av.	635 ± 70
	F range	540 - 700

Table 3.1 (cont.)

Megacryst density (per square meter) in the Dragsmark granites

Locality	Density
AREA 2 (minor sheets)	
X1	415
X2	340
X3	210
X4	500
X6	640
X7	440
X7'	540
X8	610
X9	170
X10	855
X av.	430 ± 165
X range	170 - 855

Locality		Density
AREA 2 (largest sheet)		
Top	D7	740
	D6	595
	D5	615
	D4	615
	D3	535
	D2	720
Base	D1	485
	D av.	615 ± 90
	D range	485 - 740

av. = average

b) Microscopic Features

The commonest megacrysts in Area 1 (the main sheet of Dragsmark granite) are film ± bead perthites with microcline cross-hatched twinning usually coarser at the margins of crystals (Fig. 3.4A). Inclusions of quartz and plagioclase are ubiquitous. A summary of the microscopic features of Dragsmark granite megacrysts is given in Table 3.2 . Roughly one-third of those from Area 1 show one (or more) of the following features: i) Carlsbad twinning with the twin plane stepped and commonly deformed at the margins (Fig. 3.4A), ii) either incomplete myrmekite rims or albite rims to groundmass plagioclase, iii) inclusions of biotite ± sphene ± zircon, iv) oriented plagioclase inclusions and/or zonal arrangement of inclusions, v) string perthite (Fig. 3.4B). Swapped rims to groundmass alkali feldspar are rare.

Those samples with Carlsbad twinning have more uniform cross-hatched twinning and never exhibit untwinned cores or string perthite. Relative to samples not showing Carlsbad twinning, they more commonly have biotite inclusions, biotite or quartz within plagioclase inclusions and show orientation and zonal arrangement of inclusions. The biotites in plagioclase are often very acicular, perhaps indicating a primary igneous origin. Quartz septa straddling the twin plane in the core (Fig. 3.4A) occasionally suggest relict outlines of 'seed' crystals (Mehnert and Büsch, 1981).

The string perthites are distinguished by rarely showing uniform cross-hatched twinning (Fig. 3.4B) and by having coarser perthite at the margins. They do not have albite rims to either groundmass or included plagioclase and rarely show orientation or zonation of inclusions.

Megacrysts showing evidence implying or suggesting some growth in

b) Microscopic Features

The commonest megacrysts in Area 1 (the main sheet of Dragsmark granite) are film ± bead perthites with microcline cross-hatched twinning usually coarser at the margins of crystals (Fig. 3.4A). Inclusions of quartz and plagioclase are ubiquitous. A summary of the microscopic features of Dragsmark granite megacrysts is given in Table 3.2 . Roughly one-third of those from Area 1 show one (or more) of the following features: i) Carlsbad twinning with the twin plane stepped and commonly deformed at the margins (Fig. 3.4A), ii) either incomplete myrmekite rims or albite rims to groundmass plagioclase, iii) inclusions of biotite ± sphene ± zircon, iv) oriented plagioclase inclusions and/or zonal arrangement of inclusions, v) string perthite (Fig. 3.4B). Swapped rims to groundmass alkali feldspar are rare.

Those samples with Carlsbad twinning have more uniform cross-hatched twinning and never exhibit untwinned cores or string perthite. Relative to samples not showing Carlsbad twinning, they more commonly have biotite inclusions, biotite or quartz within plagioclase inclusions and show orientation and zonal arrangement of inclusions. The biotites in plagioclase are often very acicular, perhaps indicating a primary igneous origin. Quartz septa straddling the twin plane in the core (Fig. 3.4A) occasionally suggest relict outlines of 'seed' crystals (Mehnert and Büsch, 1981).

The string perthites are distinguished by rarely showing uniform cross-hatched twinning (Fig. 3.4B) and by having coarser perthite at the margins. They do not have albite rims to either groundmass or included plagioclase and rarely show orientation or zonation of inclusions.

Megacrysts showing evidence implying or suggesting some growth in

Table 3.2

Microscopic features of megacrysts from the Dragsmark granites

Feature	Area 1 (n=22) (%)		Area 2 (n=21) (%)	
Carlsbad twinning	32 (stepped)		10 (straight)	
'Microcline' twinning, uniform	36		57	
'Microcline', coarser at rim	59		24	
Untwinned core	14		24	
Film perthite	77		67	
String / crypto perthite	32		38	
Bead / patch perthite	50		5	
Myrmekite at rim	32		57	
Perthite coarser at rim	23		10	
Swapped rim to K-feldspar	18		52	
Albite rim to plagioclase	32		43	
'Pseudopods'	9		48	
Assimilation of plagioclase	18	27	24	62
K-feldspar inclusions	18		14	
Quartz / plagioclase inclusions	95		100	
Biotite inclusions	32		67	
Sphene / zircon / etc. inclusions	27		38	
Oriented plagioclase inclusions	27		0	
Concentric zones of inclusions	32		10	
Albite rim to plag. inclusions	27		38	
Solid state growth / string perthite	50		86	

the solid state are moderately common (27%, Table 3.2). Features taken to indicate blastic growth are assimilation/replacement of groundmass plagioclase (Fig. 3.4C), inclusions of microcline, potash-rich patch antiperthites, and 'pseudopods'. The last term is used to describe crystallographically continuous, sinuous extensions of a subhedral crystal into, and often partially including, the groundmass (Fig. 3.5A). These range in size from 0.1 to 0.7mm long and clearly imply solid state growth of at least the outermost part of the megacryst. They are a relatively common feature of porphyroblastic alkali feldspar, but those found in specimens from the Dragsmark granite appear to represent the final stage of the main blastesis, in contrast to the chemically distinct hydrothermally deposited 'feelers' of Mehnert and Büsch (1981). The samples from Area 1 exhibiting such features are further distinguished by usually having albite rims to both groundmass and included plagioclase, again suggesting mobility of sodium and calcium. Otherwise they are no different from the 'typical' megacrysts, suggesting growth in the late magmatic stage rather than during a separate metasomatic event.

The commonest megacrysts from Area 2 (the minor sheets of Dragsmark granite) are film perthites with uniform cross-hatched twinning, incomplete myrmekite rims and inclusions of quartz, plagioclase and biotite (Fig. 3.5B). Roughly two-thirds show evidence of solid state growth, with 'pseudopods' being especially abundant (Table 3.2 and Fig. 3.5A). As was the case with samples from Area 1, these are otherwise indistinguishable from the 'typical' megacrysts. Other common features of Area 2 megacrysts, shown by approximately one-third of the samples (Table 3.2) are: i) string perthite (Fig. 3.5C), ii) swapped rims to groundmass alkali feldspar, iii) albite rims to plagioclase in both the groundmass and as inclusions, iv) inclusions of accessory minerals (sphene, zircon, hornblende, opaques, topaz).

Several megacrysts exhibit a difference in the nature of the quartz inclusions across the crystal. Those in the core tend to be anhedral and less than 0.1mm across whereas those in the outer parts are generally larger (0.3mm) and sub- to euhedral dihexahedra (Fig. 3.5B). Stone and Austin (1961) and Mehnert and Büsch (1981) interpret this phenomenon as indicative of growth by solid state replacement. The common occurrence of topaz either concentrated in the vicinity of megacrysts or actually included in them further supports the hypothesis of a porphyroblastic origin for many megacrysts from Area 2. 86% of the megacrysts from Area 2 are either string perthite or show other evidence of solid state growth, as compared with 50% from Area 1.

The string perthites are usually non-uniformly cross-hatched, never Carlsbad twinned and commonly have an untwinned core, occassionally with an optically distinguishable rim (Fig. 3.5C). They rarely carry inclusions other than quartz or plagioclase, or exhibit film perthite. Typically, they have very irregular outlines with no preferred elongation direction.

No megacrysts from Area 2 show oriented inclusions and only a few have zonal arrangement of inclusions. Only two examples of Carlsbad twinning were observed, and in both cases the twin plane was straight (cf the stepped planes characteristic of Area 1 megacrysts). Otherwise these crystals have no distinguishing features. Tertsch (1936) and Köhler (1948) both note that stepped or interpenetrant Carlsbad twinning is characteristic of magmatic alkali feldspars, whilst straight sharp (010) twin planes are associated with pegmatitic feldspars i.e. those formed from aqueous fluids.

Comparison of the characteristics of megacrysts from the two parts of the Dragsmark granite reveal (Table 3.2) that evidence of solid

state growth is more abundant in Area 2, but that crystals exhibiting such features from the two Areas show little else in common. In contrast, the string perthites are essentially identical, the main difference being that those from Area 1 more commonly show slight coarsening effects such as development of fine scale cross-hatched twinning in the core and coarse (film) perthite near the margins. Parsons (1978a) has suggested that there is a relationship between the formation and growth of microcline twinning and the coarsening of exsolution lamellae. Heier (1957) reports that metasomatic alkali feldspars are commonly perthitic 'orthoclase', that is they are optically monoclinic but triclinic to X-rays, suggesting ordering with small (sub-microscopic) triclinic domains. It seems likely therefore that the string perthite megacrysts represent a late-stage growth of potassium feldspar distributed fairly evenly throughout the Dragsmark granites.

Turning to those megacrysts not showing string perthite, the differences between the two Areas are marked. Area 1 megacrysts show the following features much more commonly: Carlsbad twinning, orientation and zonation of inclusions, bead perthite, coarsening of microcline twinning at the rim. Area 2 megacrysts more commonly show 'pseudopods', assimilation of groundmass plagioclase, incomplete myrmekite rimes, inclusions of biotite and accessory minerals and very irregular outlines. These differences are consistent with a magmatic origin for typical Area 1 megacrysts, with superimposed disequilibrium features, and a porphyroblastic origin for typical Area 2 megacrysts.

Figure 3.1

A : Typical exposure of undeformed Dragsmark granite illustrating its extremely megacrystic nature. Loc. C7 -: near the top of the main sheet.
Hammer is 40 cm. long.

B : Cut slab of Dragsmark granite (sample no. 891) showing a moderate degree of deformation. Most of the augen are elongate in the S2A plane, the foliation being further defined by aligned biotite. This sample is from Area 2, and the megacrysts are generally smaller than in the main sheet (above; see also Fig. 2.12).

ragsmark granite illustrating its

oc. C7 – near the top of the

mple no. 891) showing a moderate

the augen are elongate in the S2A

r defined by aligned biotite.

the megacrysts are generally

bove; see also Fig. 2.12).

A

B

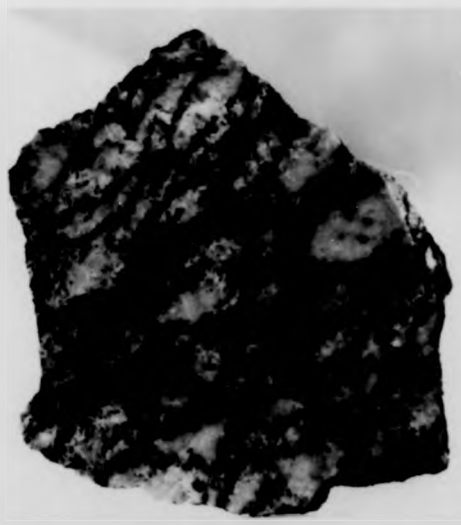

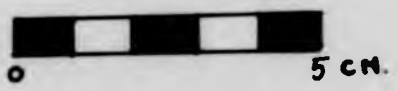

ragsmark granite illustrating its

oc. C7 -: near the top of the

ample no. 891) showing a moderate

the augen are elongate in the S2A

er defined by aligned biotite.

the megacrysts are generally

above; see also Fig. 2.12).

A

B

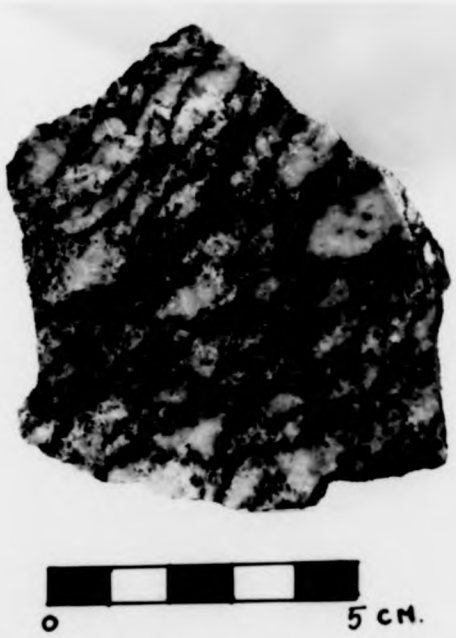

Figure 3.2

Alkali feldspar megacrysts (1,2) cutting the sharp contact between Dragsmark granite (left) and Stora Le -Marstrand paragneisses at loc. 79. Note the total absence of megacrysts from the latter. Compass is 6 cm. wide.

.2

ting the sharp contact between

e -Marstrand paragneisses at

megacrysts from the latter.

.2

tting the sharp contact between

Le -Marstrand paragneisses at

megacrysts from the latter.

Figure 3.3

Plots of length versus breadth for suites of alkali feldspar megacrysts from the various augen granites in the Dragsmark area. The mean B:L ratio (axial ratio) is given, together with the range for undeformed crystals.

A : Undeformed crystals from the Dragsmark granites.

B : Megacrysts from Area 1 of the Dragsmark granite.

C : Megacrysts from Area 2 of the Dragsmark granite.

D : Megacrysts from the Kållviken granite.

...tes of alkali feldspar megacrysts
... Dragsmark area. The mean B:L
... with the range for undeformed

...gsmark granites.

...agsmark granite.

...agsmark granite.

...anite.

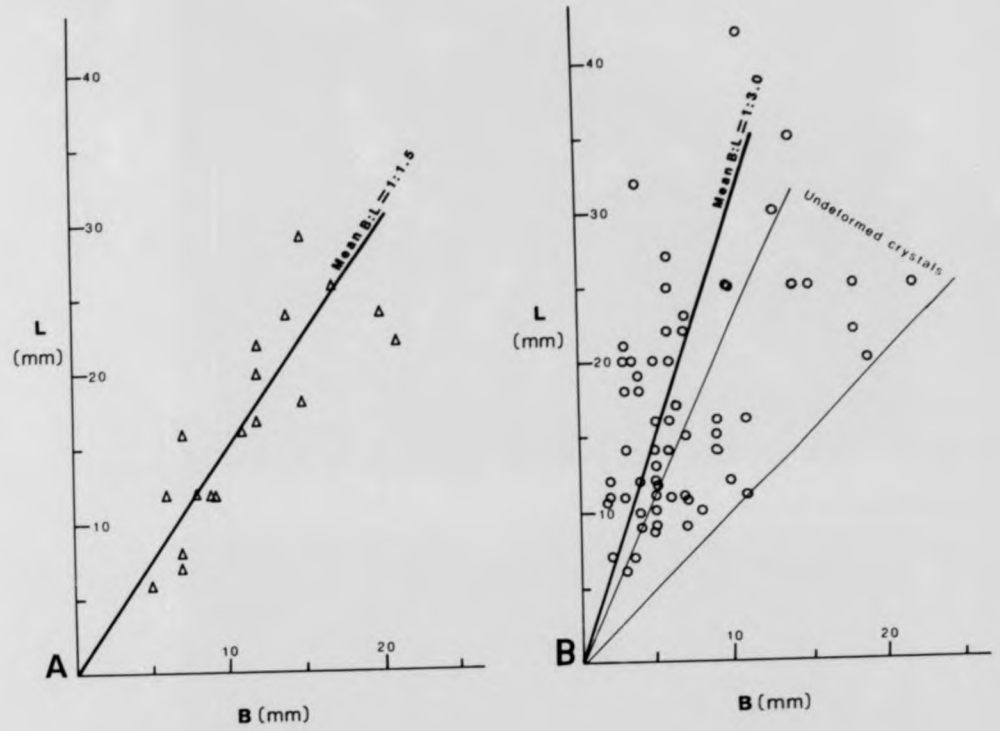

Figure 3.4

Photomicrographs of alkali feldspar megacrysts from Area 1 of the Dragsmark granite.
All under crossed polars.

A : Sample no. 145. Showing typical development of cross-hatched microcline twinning and film perthite. This sample also exhibits a stepped Carlsbad twin plane, with quartz inclusions straddling the twin plane and possibly outlining ghost seed crystals (Mehnert and Büsch, 1981).

B : Sample no. 524. The grainy texture is characteristic of string perthites, those of the Dragsmark granite often having non-uniform microcline twinning. This can be seen to become coarser locally at the margins of crystals (bottom left).

C : Sample no. 504. An alkali feldspar megacryst (AF, on the left) is in contact with an altered plagioclase (PF). The microcline partially encloses part of the plagioclase (at X), within which are a number of quartz blebs (Q).

egacrysts from Area 1 of the

development of cross-hatched
thite. This sample also exhibits
ith quartz inclusions straddling
ining ghost seed crystals

ure is characteristic of string
k granite often having non-uniform
e seen to become coarser locally
om left).

par megacryst (AF, on the left) is
oclase (PF). The microcline
lagioclase (at X), within which
).

A

B

C

.4

megacrysts from Area 1 of the

l development of cross-hatched
rthite. This sample also exhibits
with quartz inclusions straddling
lining ghost seed crystals

ture is characteristic of string
rk granite often having non-uniform
be seen to become coarser locally
tom left).

spar megacryst (AF, on the left) is
ioclase (PF). The microcline
plagioclase (at X), within which
).

A

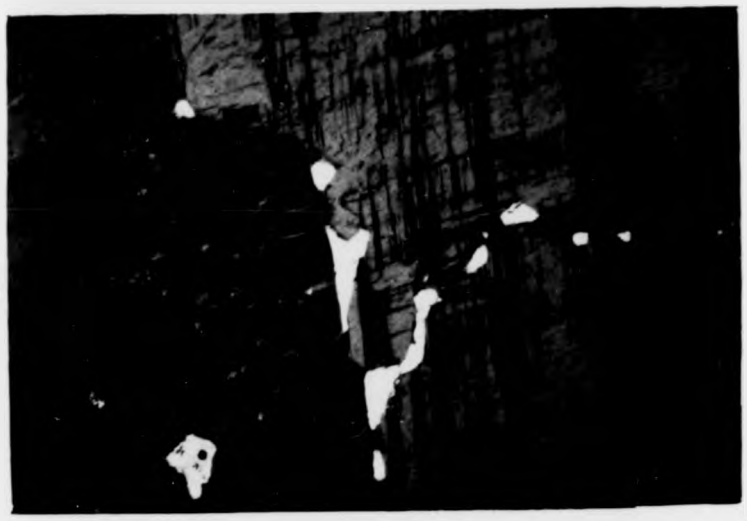

B

C

Figure 3.5

Photomicrographs of alkali feldspar megacrysts from Area 2 of the Dragsmark granite.

Crossed polars.

A : Sample no. 408. A well-developed 'pseudopod' extending out from a megacryst (top left) and partially enclosing heavily altered groundmass plagioclase.

B : Sample no. 72. Uniformly microcline-twinned megacryst with inclusions of quartz (black, grey), plagioclase (bottom centre) and microcline. Those quartz inclusions near the margin are larger than those in the core, and also exhibit sub- to euhedral dihexahedral outlines (see text p. 31).

C : Sample no. 11. String perthite. Note the absence of cross-hatched twinning except at the extreme margins, which are also optically distinguishable.

3.5

megacrysts from Area 2 of the

ped 'pseudopod' extending out
d partially enclosing heavily
e.

rocline-twinned megacryst with
rey), plagioclase (bottom centre)
inclusions near the margin are
, and also exhibit sub- to euhedral
xt p. 31).

te. Note the absence of cross-
extreme margins, which are also

A

B

C

3.3

megacrysts from Area 2 of the

oped 'pseudopod' extending out
nd partially enclosing heavily
e.

rocline-twinned megacryst with
grey), plagioclase (bottom centre)
inclusions near the margin are
, and also exhibit sub- to euhedral
xt p. 31).

ite. Note the absence of cross-
e extreme margins, which are also

A

B

C

Chapter 4

Structure and Geochronology

a) Summary of the Regional Framework

In order to facilitate comparison with adjacent areas and to avoid an unnecessary profusion of structural terminologies, the structure of the Dragsmark area will be described in terms of the sequence of events established by Park et al.(1979) for Western Orust. Thus, for example, folds which have the characteristics of F4 folds (ibid) will be described as such, although they may not necessarily be the fourth deformation observed in Dragsmark.

The main foliation (S1) in the Stora Le- Marstrand country rock gneisses is a schistose gneissosity and/or compositional banding, with the first generation of migmatitic leucosome often forming thin, sub-concordant veinlets. Locally pre-D1 banding (possible primary bedding) and folds occur. S1 is cut by the second generation leucosome, the intrusion of Hällevikstrand amphibolite and Assmunderöd-Myckleby augen granites separating the two migmatitic episodes (Daly, 1978). The second deformational event on Orust resulted in numerous folds (F2) with wavelengths from 1cm to hundreds of metres. These are generally tight to isoclinal and asymmetric, with long limbs dipping moderately east. A penetrative axial planar fabric is only locally developed.

The Orust dyke suite constitutes an important regional stratigraphic marker, separating these pre-Sveconorwegian features from the post-dyke Sveconorwegian (Daly et al, 1982). A mean Rb-Sr age of c.1090Ma has been obtained from members of the suite and is interpreted as the age of D3, the first post-dyke deformation (Daly et al, 1983). D3 structures are only rarely detectable outside the dykes and are rather heterogeneous

and variable in their development. Many dykes carry a moderate planar mineral fabric, S3 (consisting of aligned biotite and hornblende), which is often sigmoidal or oblique to the margins.

The major post-dyke deformation (D4) is characterized by the development of open to tight folds (F4) with wavelengths from a few millimetres to several tens of metres and with axial planes which are horizontal or dip moderately south to south-east. A crenulation cleavage is common in more schistose lithologies, this S4 fabric being created by both rotation and recrystallization of micas. Later folds occur but are geographically restricted and difficult to interpret.

A summary of the structural sequence in Orust as presented by Park et al (1979) is given in Table 4.1 .

TABLE 4.1

Structural Sequence in Western Orust

(after Park et al, 1979)

Deformation		Lithological Features
		Older amphibolites
		1st. generation migmatite leucosome
D1	Intense regional folding; penetrative foliation	
		Hälleviksstrand amphibolite;
		older granites,
		2nd. generation migmatite leucosome
D2	N-S tight asymmetric folds, facing west; shears and faults	
		Younger granites;
		Orust dykes
D3	Foliation in dykes and shears	
		Late pegmatites
D4	Chevron folding, shallow axial planes	

b) Observed Structural Features in the Dragsmark Area

The main fabric in the country rock gneisses is a compositional banding which in the metasediments can be seen to be a composite of a metamorphic gneissosity and primary sedimentary variations (Fig. 2.1B). As already described (Ch.2), it is formed by aligned micas, hornblende and diffuse quartzofeldspathic segregations 1 - 2mm thick. This first-generation migmatitic leucosome is generally parallel to the foliation which is designated S1. Locally it is seen to be axial planar to isoclinal folds of an earlier banding.

The coarse, pink second generation migmatitic leucosome occurs both as concordant pods and as cross-cutting veins up to 20cm wide. Frequently it is axial planar to folds affecting both S1 and the first leucosome; elsewhere it forms the 'matrix' of agmatitic or nebulitic amphibolite migmatites (Figs. 2.5A and B). A biotite selvedge is common in micaceous gneisses.

This leucosome is found in both the Källviken granite and the Koskär dykes (Ch.2) and is axial planar to folds affecting the foliation in the former. The margins of the granite are however discordant to the S1 foliation in the surrounding gneisses. An amphibolitic xenolith at loc.384 within the Källviken granite shows two foliations, the later and more intense being parallel to, and continuous with, that in the surrounding granite. It thus appears that there was a (local) fabric-forming event after the intrusion of the Källviken granite but prior to the intrusion of the Koskär dykes, the development of the second leucosome, and the intrusion of the Dragsmark granites. Daly (1978) states that the Assmunderöd-Myckleby augen granite, which cuts the migmatitic banding in the country gneisses, carries an augen foliation which in turn is cut by the second leucosome. No pre-D2 foliation is recorded for the Hälleviks-

strand amphibolite.

The Dragsmark granites cut S1 and both migmatitic leucosomes and are clearly post-D1. As they are intruded by undeformed Orust dykes (loc.421), it follows that the S- fabric in the granites must result from the D2 deformation of Park et al. (1979). This S2 foliation is defined by aligned biotite and (locally) well-developed potassium feldspar augen, but is commonly folded with further, undeformed, alkali feldspar megacrysts cutting the folds (Fig. 4.1). It is thus apparent that D2 was both more intense and more complex in the Dragsmark area than in Western Orust.

The first D2 event that can be recognized in Dragsmark is the formation of this S2 foliation. Stereograms of π-poles to the foliation in various sub-areas of the Dragsmark granites are presented in Fig. 4.2 . Most show folding about an axis which plunges gently south to south-east; this is the result of D4 deformation and is discussed below. Despite this folding, several show a well-defined maximum of π-poles. This is interpreted as the pole to the S2 fabric, which thus dips gently to moderately south-south-east.

Examination of Map 2 shows a number of folds affecting the Dragsmark granite. Some of these are aligned approximately parallel to the S2 foliation, but others (e.g. the large synform in the main sheet) are strongly discordant to, and fold, this fabric. Although there is some variation in axial planar trend, two dominant orientations are evident: one set trending north-west / south-east, the other east-north-east / west-south-west (Map 2). The latter are restricted to the southern part of the area (south Bassholmen and Flatön), where they trend parallel to the foliation, with which they are thought to be synchronous. These earlier folds are thus termed F2A, and the above-mentioned S-fabric is consequently S2A. The later, north-west / south-east trending folds which

affect S2A are termed F2B, although it should be noted that all that can be said with certainty is that they are post-S2A and pre-D4. It is in fact possible that they may have suffered further deformation during D4.

Because there was no pre-existing fabric in the granites, little can be determined as to the nature of the F2A folds, except that they have wavelengths of several hundred metres. The S2A fabric is commonly folded by open to tight upright folds with wavelengths of 10 - 50cm and rounded hinges. These are frequently virtually obliterated by later megacrysts. If these are regarded as F2B folds, it suggests that this deformation occurred prior to an episode of K-feldspar porphyroblastesis. Elsewhere however, F2B folds seems to deform all megacrysts.

The regionally more significant F2B folds are commonly tight and asymmetric with long limbs dipping moderately south-west. They are often overturned to the north-east, with axial planes dipping moderately south-west and sub-rounded hinges. It should be noted that this sense of asymmetry and overturning is the opposite of that found by Park et al (1979) for F2 folds in western Orust and by Berthelsen and Murthy (1970) for folds affecting the Assmunderöd - Myckleby augen granites. A π-pole stereogram of the contacts between the Dragsmark granites and the country rock gneisses indicates an axis of folding plunging gently south-east, presumably associated with F2B (Fig. 4.2). A three-dimensional representation of an F2B fold, based on the well-exposed folding of the granite margin at Evensås (Map 3) is given in Fig. 4.3 (see also Fig. 4.11).

Examination of Map 2 and Fig. 4.2 shows that fabrics striking north-west / south-east, that is parallel to the F2B axial planar trend, are geographically restricted. They are particularly common at Evensås and Rödberget (sub-areas 3 and 2) and near the sheared margins of

the main body of granite e.g. at Hultås and Kättorp (Map 3). It should be noted that no undeformed, cross-cutting megacrysts are found in these margins.

The simplest interpretation that takes account of all these features is that the Dragsmark granites were deformed during and after the growth of most of the megacrysts, with the formation of a foliation dipping moderately south-south-east. This fabric (S2A) is defined by feldspar augen and a schistosity. It is variably developed, but nowhere intense and often apparently absent although this may result from subsequent overgrowth by K-feldspar megacrysts. Examples of syn-tectonic megacryst growth (with respect to S2A) are abundant. In the south of the area mapped, anumber of F2A folds were formed. There was then a second episode of folding (F2B), this time with north-west / south-east axial planar trends. This locally caused realignment of the S2A fabric.

The only structure that can with certainty be ascribed to D3 is a weak biotite S-fabric with aligned garnets oblique to the margins of some Koskår dykes (Fig. 4.4). Some of the deformation of Orust dykes in the Dragsmark granites (Fig. 2.8A) may also be D3 age, but this cannot be proved.

The main D4 structures observed in the Dragsmark area are a well-developed lineation which is parallel to the axes of F4 folds, and a number of shears. These folds are tight with angular hinges and sub-horizontal axial planes (Fig. 4.5A). They are typically asymmetric (Figs. 4.5B and 2.6B). A new penetrative axial planar fabric of aligned biotite and new muscovite is occasionally developed and there are some instances of a minor new leucosome (Fig. 2.9B). Transposition of pre-existing fabrics is however rather more common. Wavelengths are usually between 10cm and 50cm, although larger folds with wavelengths of several metres

also occur (e.g. west Flatön, Map 2) and a crenulation is common in the pelitic gneisses. An illustration of a 'typical' F4 fold is given in Fig. 4.6 (contrast with Fig. 4.3 of an F2B fold).

In addition to the crenulation, a mineral lineation parallel to the fold axes is common in areas of D4 deformation. π-pole plots of the composite foliations in the Stora Le- Marstrand gneisses and the Kållviken granite demonstrate folding about F4 axes (Fig. 4.7, see also Fig. 4.2 and p.36). These can be seen to vary from south-east to south with gentle to moderate plunges. There is some systematic variation in trend (map, Fig. 4.7), but it is not possible to say whether this is due to later refolding or to regional variation in the D4 stress field.

Other linear features are abundant, such as rodding of quartz veins and migmatitic leucosomes, elongation of augen in the granites and of garnets and hornblendes in amphibolites, and development of slickensides, usually with epidote, on shears and joint surfaces (Fig. 4.8). A stereographic plot of linear features from the whole area is given in Fig. 4.9A and shows a maximum with a gentle south-south-east plunge. At Sundsandsvik, approximately 20km east of Dragsmark, augen in similar granitic sheets are strongly elongate in the same direction.

Fig. 4.9B shows π-poles to axial planes of folds from the whole area. As F4 folds are the most readily measured in the field, the maxima from Figs. 4.9A and B are interpreted as being associated with the D4 deformation. F4 folds are particularly abundant in the Stora Le- Marstrand gneisses at Östersidan and Grönskult (Map 3); axes and axial planes determined from these are shown in Fig. 4.9C .

A summary of the structural features of the Dragsmark area is

given in Fig. 4.9D . The similarity in orientation of F2B and F4 suggests that it is impracticable to definitively attribute all the deformation involved in the major folds to any one fold phase. Thus whilst the shearing of the Dragsmark granite on the north-eastern margin (Hultås to Kättorp, Map 3) is ascribed to F2B, the local mylonitization of the basal granite and/or underlying gneiss is probably of D4 age. At loc.38 this cataclastic fabric can be seen to be at a slight angle to both the sheared foliation in the basal granite and the fabric in the underlying gneisses.

This mylonite attains a maximum thickness of 1½m, but that under the augen granite at Klostergård (Map 3) is up to 5m thick. All degrees of cataclasis from brittle fracturing of augen through to cataclasites (s.s.) or mylonites (Higgins, 1971) are found. Evidence of brittle deformation, often with some epidote veining, is also to be found on the faults running from Berg to Kållviken (and its westward continuation on north Skaftö) and from Klostergård to Munkeby (Map 3). The former further shows clear evidence of shearing (loc.588) with rotation of the foliation in the gneisses parallel to the 'fault'.

In the Stora Le- Marstrand paragneisses south of Östersidan, several sinistral shears running roughly north-south displace minor older amphibolite bands (Map 2) by 50 - 200m. The most easterly of these shears is laterally the most extensive, causing deformation of the margin of the large Area 2 granite at Östersidan (e.g. loc.428). The north-eastern contact of this sheet is similarly sheared, with a local sub-vertical cataclastic fabric. At loc.951 the southern extension of this main shear (here trending east - west) has a very intense D4 linear fabric, and all these shears are thus thought to be D4 in age.

A fracture cleavage can locally be observed to be axial planar to,

or parallel to the long limbs of, F4 folds, although this perhaps coincidence. Minor quartz veining and rare pegmatites may also be apparent in the same orientation, presumably filling fractures (Fig. 4.10A). Fractures, often forming conjugate sets and cutting and displacing augen, are most abundant in the Dragsmark granites, although observable elsewhere. A rose diagram of the orientations of these fractures is given in Fig. 4.10B, and it is apparent that there are two dominant directions at an angle of c.80° with the acute bisector on 165°. This inter-fracture angle is rather larger than predicted by theory and experimental data (c.60°; Hobbs et al,1976), but this may be due to sampling bias. Individual conjugate sets (only 10 measured) form an angle of c.65° with the acute bisector again trending 165° (Fig. 4.10C). Following Park et al. (1979), the mean 'apparent shortening axis' Zap is thus interpreted as having an azimuth of 165° during the post-D4 deformation in the Dragsmark area. In western Orust, the D4 Zap plunges steeply north with an azimuth of 170°, whilst the D5 Zap is sub-horizontal on 160° (ibid.).

During the intrusion of granitic sheets, it is clear that the local stress pattern will not only have influenced the nature of the intrusion, but will also be influenced by the presence of a crystallizing magma. It might be expected that deformation would be concentrated at the margins of a cooling body and this effect is indeed apparent on the north-eastern margin of the main Dragsmark sheet and on the base of the Area 1 granite on Bassholmen. Re-activation and further strain along these lithological boundaries would very probably take place during a later deformational event.

c) Macroscopic Structure of the Dragsmark Granites

Map 1 shows the distribution of lithological types, whilst structural data are to be found on Map 2, with only the important boundaries shown. A block diagram, to scale, in Orthographic projection (McIntyre and Weiss, 1956) is presented in Fig. 4.11, giving the interpreted structure at depth along a number of cross-sections through the area. The various points to be discussed below, such as the throw on faults, the primary variation in thickness of the granite bodies and the spatial relationships between them, and the effects of the major F2 folds on the distribution of the granites are all illustrated in this Figure.

The present day outcrop pattern of the Dragsmark granites is the result of the interaction of topography, deformation and the primary (intrusive) shape of the sheets. The granite has proved more resistant to weathering than the Stora Le- Marstrand paragneisses and has a marked effect on the subdued topography of the area. The various faults running through the area also form topographic features e.g. the narrow seachannel between Skaftö and Dragsmark. In most cases it has proved possible to estimate the amount of movement involved and the throws and directions of strike-slip where appropriate are given on Map 1.

The main strike slip fault between Skaftö and Dragsmark trends 025° and has a dextral slip of c.500m, whilst the possibly conjugate sinistral fault running from Vågeröd to Rödberget (Map 3) has a slip of c.250m. Both show increasing vertical displacement to the north. Park et al. (1979) indicate a dextral slip of the order of 1km on 010° between Hårmanö and Stocken in western Orust (their Fig. 11). The above mentioned faults displace and are therefore younger than that running from Berg to Källviken, which may perhaps be D4. All affect F2 folds.

Of the various fold generations, F2B has the greatest effect on the outcrop pattern except in the extreme southern part of the area (south Bassholmen and Flatön), where F2A is dominant (Fig. 4.11). These folds also, of course, control the distribution of the Kållviken granite and various of the larger older amphibolites. The folds affecting the amphibolite at Kållviken (Maps 1 and 2) do not affect the Dragsmark granite and are therefore pre-D2. The same may be true of the minor folds trending roughly east-west which affect the granodiorite gneiss and gneissose granite on the islands between Bassholmen and Kårlingesund.

Because of the amount of deformation the area has undergone, it is not possible to reconstruct accurately the original shape of the various sheets of Dragsmark granite. From Map 1 and Fig. 4.11 it is apparent however that the main sheet is thickest in the north and was intruded as a sub-concordant sill, transgressing slightly upwards to the west. Thus at Stora Gassholmen (Map 3), the base of the granite rests on the granodiorite gneiss, whilst at Evensås it directly overlies Stora Le-Marstrand paragneiss. The transgression is particularly evident near the north of Bassholmen (Map 1).

This main sheet is in fact split into two wedges, one lying under the Kållviken granite, the other over. The junction of these two 'fingers' is in the vicinity of Kållehed (Map 3) and from the narrowness of the outcrop of Dragsmark granite here it is evident that the intrusion nearly formed two discrete sheets.

The Area 2 body at Vågerød clearly overlies the south-western termination of the main sheet, as does the 'fingering out' of the smaller sheet at Östersidan (loc.74). The interdigitation of the granite with Stora Le- Marstrand gneisses is especially fine-scaled and complex at

loc.72 just to the south. As indicated in Fig. 4.11 and Map 2, several of theapparently discrete bodies of Area 2 granite near Rödberget are in fact the result of nearly isoclinal F2B folding of a single sheet with a thickness of c.50m. At Rödberget itself there are many minor sheets varying from 1m to 50m thick.

Using estimates of the thicknesses of the various parts of the granite intrusion obtained from internally consistent cross-sections, it is possible to construct a very approximate isopach map for the Dragsmark granite (Fig. 4.12). The Area 2 body at Vågeröd can be seen to be roughly circular in outline with an ellipsoidal cross-section and a maximun thickness of greater than 200m. The two overlapping 'fingers' of the main Area 1 sheet both thin to the south and west and attain maximum thicknesses of over 600m in the north-east.

In summary, the Dragsmark granites take the form of a number of overlapping sheets interfingered with the country rocks and thinning as they transgress upwards to the south and west. It is reasonable to assume that they were intruded from the north-east and that the presence of the Kållviken granite caused the main sheet to divide into two wedges, one passing under this body, the other (and more extensive) over.

d) Geochronology

It has been demonstrated earlier in this Chapter that the Dragsmark granites are younger than both generations of migmatitic leucosome and are older than D2 and the Orust dyke suite. The Källviken granite and Koskär dykes were emplaced between the two migmatizations. No new geochronological work has been undertaken (and the pervasiveness of D4 epidote probably precludes accurate isotopic studies), but some relevant information is available in the literature. All published Rb/Sr data have been recalculated, where necessary, to $\lambda = 1.42 \times 10^{-11} y^{-1}$.

The Assmunderöd-Myckleby augen granites and the Hållevikssstrand amphibolite, both of which cut S1 but carry the second leucosome, have been dated at 1379 ± 46Ma and 1432 ± 92Ma respectively (Daly,1978; Daly et al,1979). These ages are interpreted as respesenting the time of emplacement. A short crustal history of c.150Ma is proposed for the precursor to the augen granites on the basis of their relatively high initial $^{87}Sr/^{86}Sr$ ratio of 0.713 ± 3 (Daly,1978). In the absence of any evidence to the contrary, it is suggested that the Källviken granite and Koskär amphibolitic dykes were also intruded at roughly 1400Ma, although no direct correlation between the two regions can be proposed. This further provides an older age limit for the formation of the Dragsmark granites.

A younger limit is imposed by the dates obtained from Orust dykes. Daly et al (1983) have examined three dykes deformed by D3 which yield a weighted mean Rb/Sr of 1087 ± 42Ma. This is interpreted as the date of the metamorphic peak which accompanied the D3 deformation. In the continuation of the Stora Le- Marstrand series north into Østfold, basic dykes correlated with the Orust swarm cut the Røyken quartz - feldspar porphyry (Hageskov and Pedersen, 1980). This latter has been

dated (Rb/Sr) at 1225Ma, representing a maximum age for the dykes, which were thus intruded between c.1225 and c.1090Ma. The Dragsmark granites may therefore be concluded to have been intruded between c.1400Ma and the time of intrusion of the Orust dykes. A chronology of events in the Dragsmark area is presented in Table 4.2 .

TABLE 4.2

Chronology of Events in the Dragsmark Area

Deformation		Radiometric Data
D1	1st. generation migmatite leucosome, regional S1 foliation, intrusion of the Kållviken granite, (local) fabric-forming event, pre-D2 folds, intrusion of the Koskår dykes, 2nd. generation migmatite leucosome	c.1400 Ma
D2	Intrusion of the Dragsmark granites, S2A augen fabric, locally axial planar to F2A, syndeformational megacryst growth, F2B, possible syndeformational porphyroblastic megacryst growth	
D3	Intrusion of the Orust dykes, S3 (in Koskår dykes)	<c.1225 Ma c.1090 Ma
D4	L4 lineation, axial to F4, shears, local mylonitization, Berg-Kållviken fault	
	Conjugate fractures cleavage, strike-slip faulting	

Figure 4.1

Photograph of the Dragsmark granite at loc. 577 showing close round-hinged folds affecting the S2A augen fabric, with some overgrowth by alkali feldspar megacrysts (bottom centre). The folds may be related to D2B.

Compass base is 10 cm. long.

Figure 4.1

Photograph of the Dragsmark granite at loc. 577 showing close round-hinged folds affecting the S2A augen fabric, with some overgrowth by alkali feldspar megacrysts (bottom centre). The folds may be related to D2B.

Compass base is 10 cm. long.

t loc. 577 showing close round-
fabric, with some overgrowth by
ntre). The folds may be related

.1

t loc. 577 showing close round-

fabric, with some overgrowth by

ntre). The folds may be related

Figure 4.2

Stereograms of π-poles to the foliation in structural sub-areas of the Dragsmark granite, together with a map showing those sub-areas. Stereograms of π-poles to the foliation in the sheared north-east margin of the main sheet and of contacts between the Dragsmark granites and the country rock gneisses are also shown (X and Y respectively).

Sub-areas :	1	Vågeröd	N = 25
	2	Rödberget	N = 21
	3	Evensås	N = 26
	4	Bassholmen	N = 47
	5	Berg	N = 68
	6	Hultås	N = 66
	7	Klostergård	N = 19
	X -: N = 17 ; Y -: N = 37		

Contours at 1, 10, 15, 20, 25, 30 % points per 1% unit area.

2

ion in structural sub-areas of the

p showing those sub-areas.

ion in the sheared north-east

cts between the Dragsmark granites

o shown (X and Y respectively).

N = 25

N = 21

N = 26

N = 47

N = 68

N = 66

N = 19

37

oints per 1% unit area.

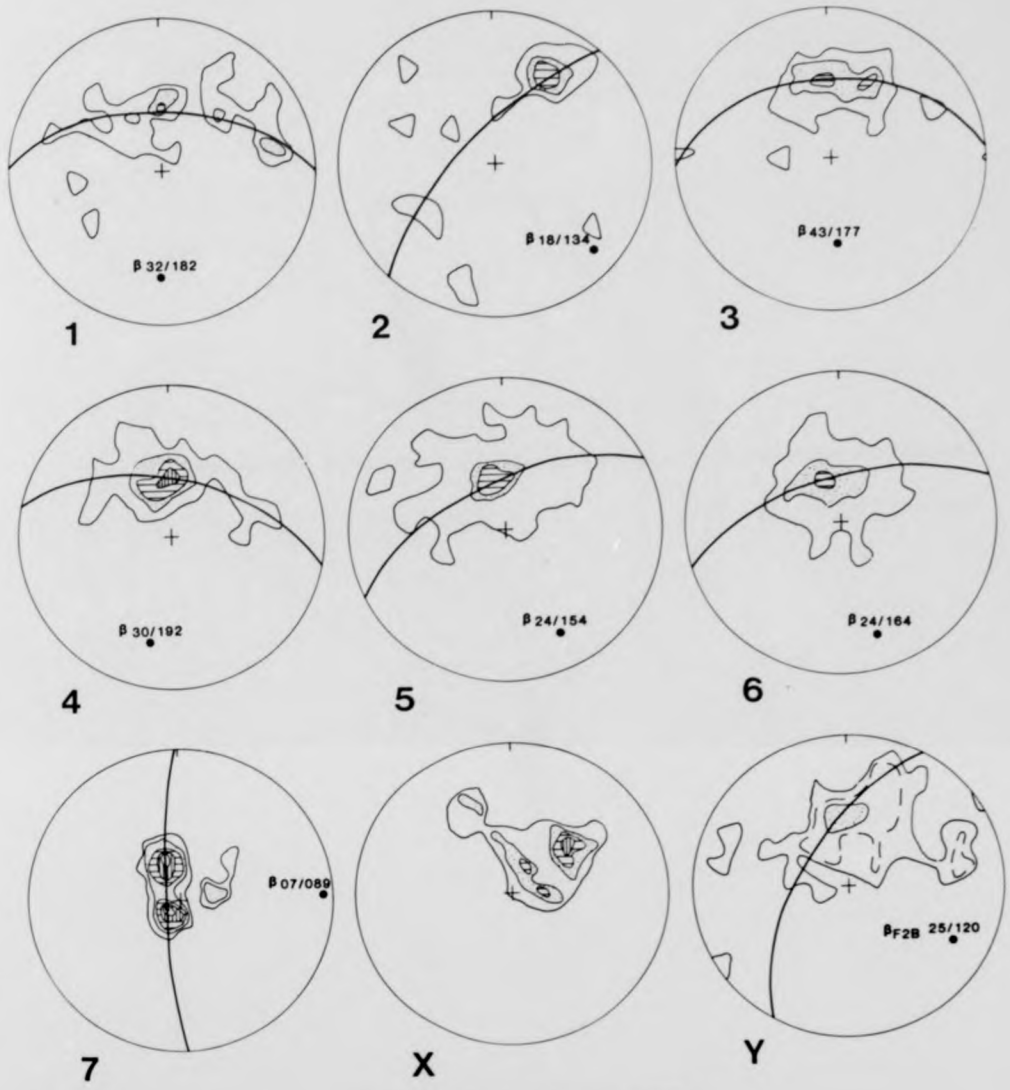

Figure 4.3

Isometric orthographic projection of an idealized F2B fold.

Contrast with Fig. 4.6.

n idealized F2B fold.

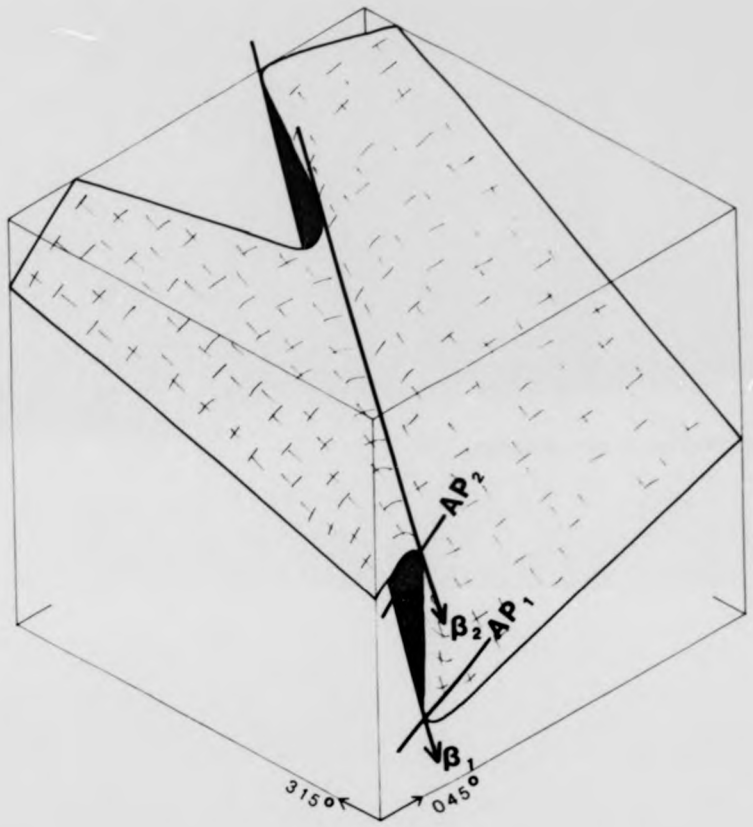

Figure 4.4

Photograph of a Koskår dyke at loc. 1 showing (in the shaded upper part of the dyke) a very weak oblique S3 fabric picked out by trails of garnet.

Lenscap measures 5 cm. across.

showing (in the shaded upper

S3 fabric picked out by trails

showing (in the shaded upper

S3 fabric picked out by trail

Figure 4.5

A : F4 folds in the granodiorite gneiss at loc. 607. Note the angular hinges and tight interlimb angle.
Compass base is 10 cm. long; light end of needle points south.

B : Strongly asymmetric F4 folds affecting an older amphibolite layer in Stora Le -Marstrand gneisses (loc. 946). The hammer is 40 cm. long and lies on the contact between the amphibolite and the paragneisses (right). Note the thin concordant leucosome in the amphibolite (probably first generation).
Taken facing east (i.e. North is to the left).

4.5

gneiss at loc. 607. Note the
rlimb angle.
light end of needle points south.

A

affecting an older amphibolite
gneisses (loc. 946). The hammer is
ontact between the amphibolite and
e the thin concordant leucosome in
t generation).
is to the left).

B

4.3

gneiss at loc. 607. Note the

r limb angle.

light end of needle points south.

affecting an older amphibolite

gneisses (loc. 946). The hammer is

ontact between the amphibolite and

te the thin concordant leucosome in

st generation).

is to the left).

A

B

Figure 4.6

Isometric orthographic projection of an idealized F4 fold. Contrast with Fig. 4.3 of an F2B fold.

an idealized F4 fold. Contrast

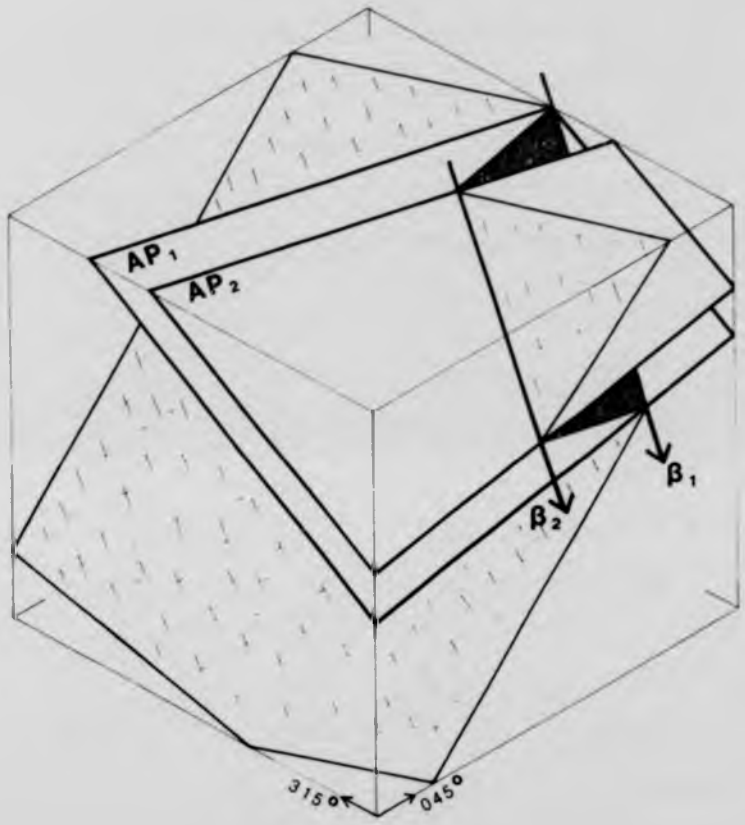

Figure 4.7

Stereographic plots of π-poles to foliations in various structural sub-areas of the country rocks in the Dragsmark area; that is, all lithologies older than the Dragsmark granites. All show clear indications of folding about F4 axes, and the directions of plunge of these are shown in the accompanying map.

Sub-areas :	1 Östersidan	N = 144
	2 Skaftö	N = 46
	3 Lindholmen (gneiss only)	N = 21
	4 Flatön	N = 47
	5 Kårlingesund	N = 94
	6 Källviken (gneiss only)	N = 48
	7 Berg	N = 35
	8 Hultås	N = 74
	9 Munkeby	N = 40
Källviken granite		
	10 N.E. Skaftö	N = 14
	11 N.W. Skaftö & Lindholmen	N = 18
	12 Strömberget	N = 13
	13 Källviken	N = 14

Contours at 1, 10, 15, 20, 25, 30 % points per 1% unit area.

oliations in various structural
e Dragsmark area; that is, all
granites. All show clear
, and the directions of plunge of
map.

N = 144
N = 46
nly) N = 21
N = 47
N = 94
ly) N = 48
N = 35
N = 74
N = 40

N = 14
men N = 18
N = 13
N = 14

oints per 1% unit area.

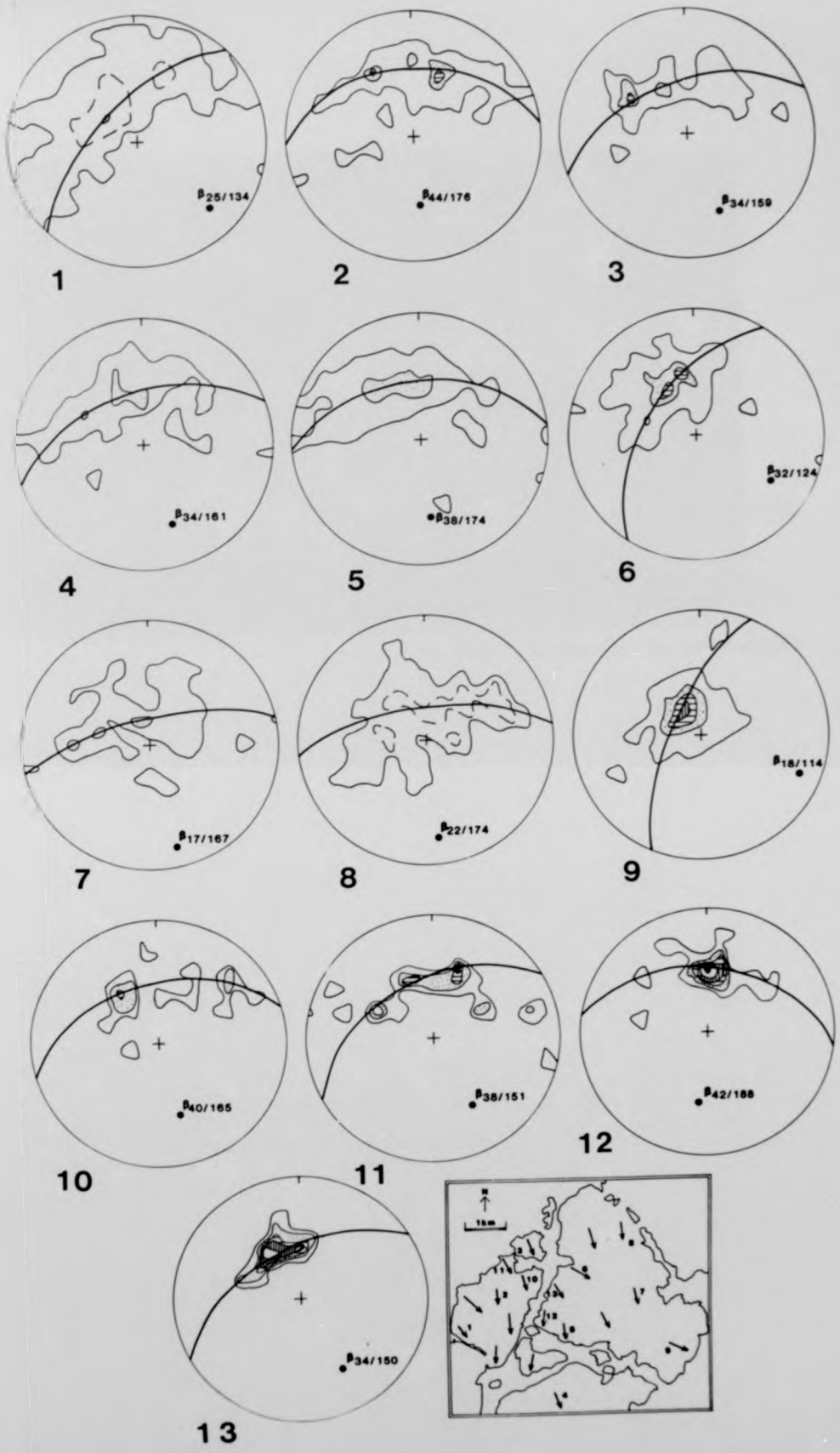

Figure 4.8

Epidote veining showing slickensides on a D4 joint surface (loc. 951). Compass base is 10 cm. long; light end of needle points south. The direction of lineation is consistent with the F4 β -axes constructed for foliations in the country rocks (Fig. 4.7).

4.8

s on a D4 joint surface (loc. 951).
end of needle points south. The
t with the F4 β -axes constructed for
g. 4.7).

s on a D4 joint surface (loc. 951).
end of needle points south. The
t with the F4 β -axes constructed for
g. 4.7).

Figure 4.9

Stereographic plots of various structural features in the Dragsmark area.

A : Mineral lineations, fold axes, quartz rodding etc. from the whole area mapped. N = 58. The maximum is coincident with F4 β -axes (Fig. 4.7).

B : π -poles to axial planes of folds from the whole area. N = 20. Also shown is the cyclographic trace of the plane corresponding to the π-pole maximum. See text p.39 for further discussion.

C : Axial planes and axes of F4 folds in the Stora Le -Marstrand gneisses at Ostersidan and Gronskult.

o - Axes

-●- - Axes with associated axial planes (cyclographic trace)

x - π -pole to axial planes

D : Summary of the orientations in stereographic projection of the main structural elements in the Dragsmark area.

Contours at 1, 10, 15, 20 % points per 1% unit area.

tural features in the Dragsmark area.

quartz rodding etc. from the

maximum is coincident with F4

lds from the whole area. N = 20.

trace of the plane corresponding

ext p.39 for further discussion.

ls in the Stora Le -Marstrand

skult.

l planes (cyclographic trace)

stereographic projection of the

Dragsmark area.

er 1% unit area.

A

B

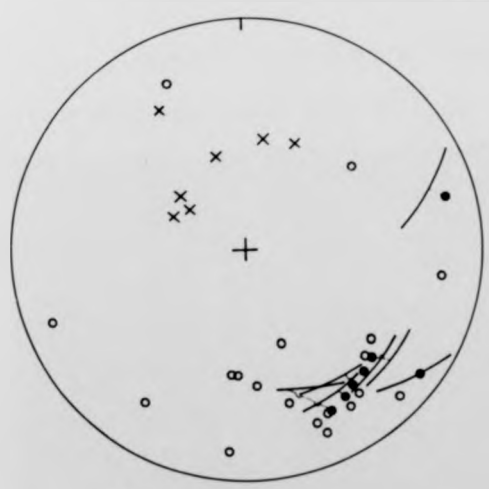

C

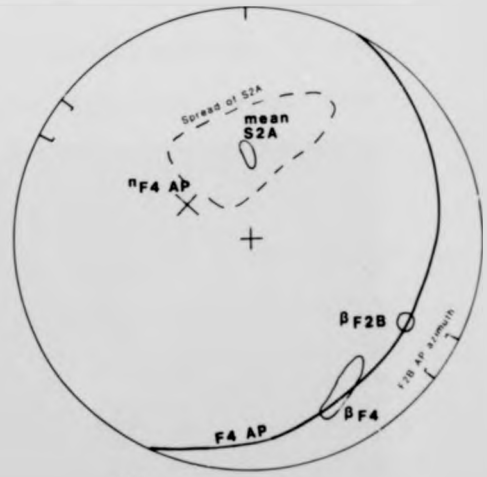

D

Figure 4.10

Brittle deformation in the Dragsmark area.

A : Rose diagram of the trends of fracture cleavage sets (white) and quartz veins and rare pegmatites (stippled). N = 34.

B : Rose diagram of discrete fractures (mainly in the Dragsmark granite). N = 95.
Sets of conjugate fractures shown in black. The inferred mean apparent shortening axis (Z_{ap}) is also given; see text p.41.

C : Photograph of a conjugate fracture set in the Dragsmark granite at loc. 442.
Compass base is 10 cm. long; light end of needle points south.

.10

area.

fracture cleavage sets (white)

tites (stippled). N = 34.

ures (mainly in the Dragsmark granite).

wn in black. The inferred

(Z_{ap}) is also given; see text p.41.

ure set in the Dragsmark granite

ght end of needle points south.

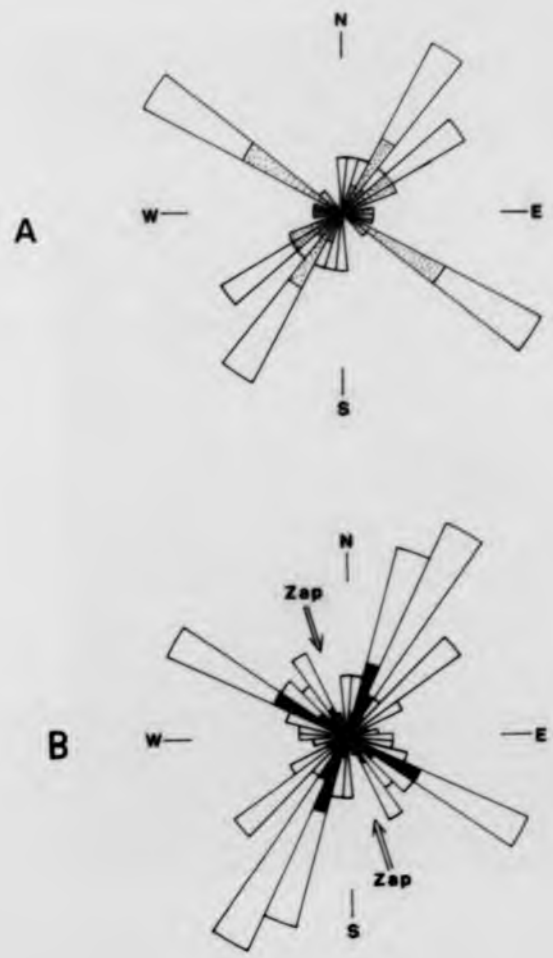

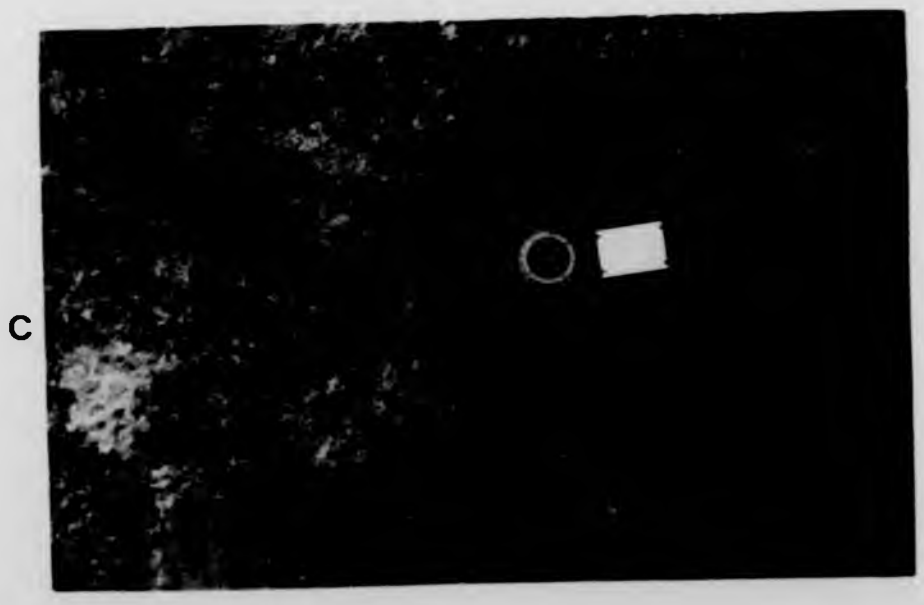

4.10

k area.

fracture cleavage sets (white)

atites (stippled). N = 34.

ures (mainly in the Dragsmark granite).

own in black. The inferred

(Z_{ap}) is also given; see text p.41.

ture set in the Dragsmark granite

ght end of needle points south.

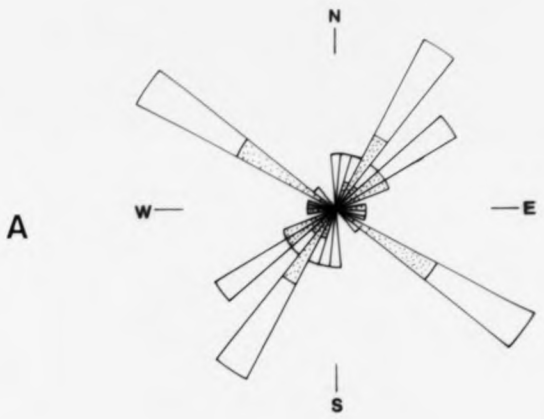

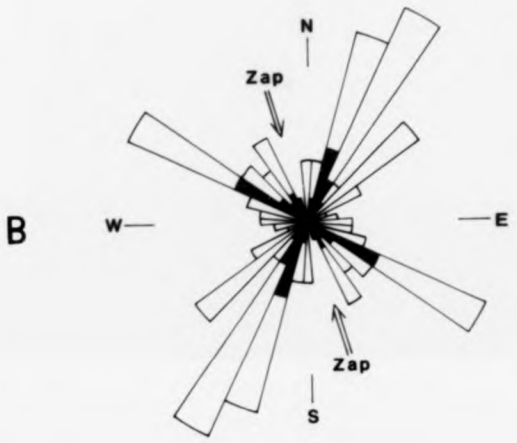

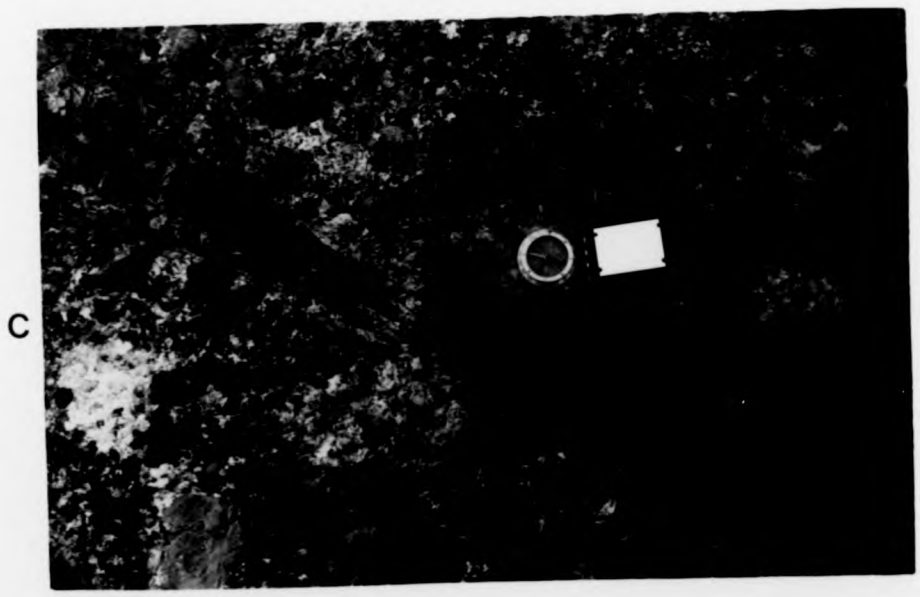

Figure 4.11

Orthographic projection (to scale) showing the major inferred geological features of the Dragsmark area. Four cross-sections on 030° through the area are presented, together with a cross-section on 300°.

- Dragsmark granite Area 1
- Dragsmark granite Area 2
- Kållviken granite
- older amphibolite
- gneissose granite
- granodiorite gneiss
- Stora Le -Marstrand paragneisses
- Fault
- Antiform; synform

Note: Interpretation of gravity data indicates that the Bohus granite underlies the Dragsmark area with its upper surface only about 0.5 km. below the present land surface. It would truncate the folds shown here, but may be offset by the strike-slip faults; for the sake of clarity it is omitted from the diagram.

howing the major inferred
area. Four cross-sections on
together with a cross-section

gneisses

indicates that the Bohus granite
ith its upper surface only about
surface. It would truncate the
ffset by the strike-slip faults;
omitted from the diagram.

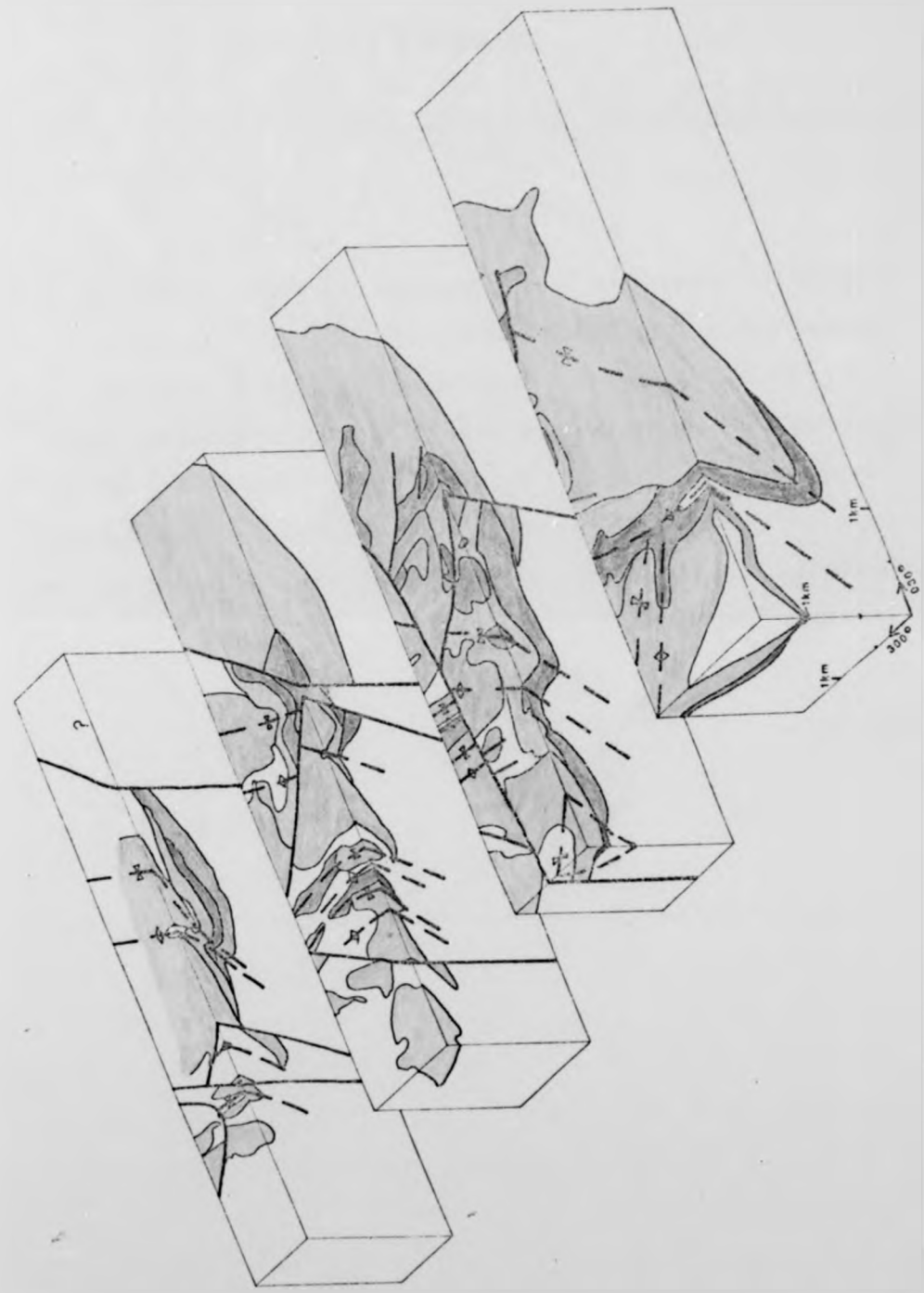

.11

lowing the major inferred
area. Four cross-sections on
together with a cross-section

gneisses

indicates that the Bohus granite
with its upper surface only about
surface. It would truncate the
offset by the strike-slip faults;
omitted from the diagram.

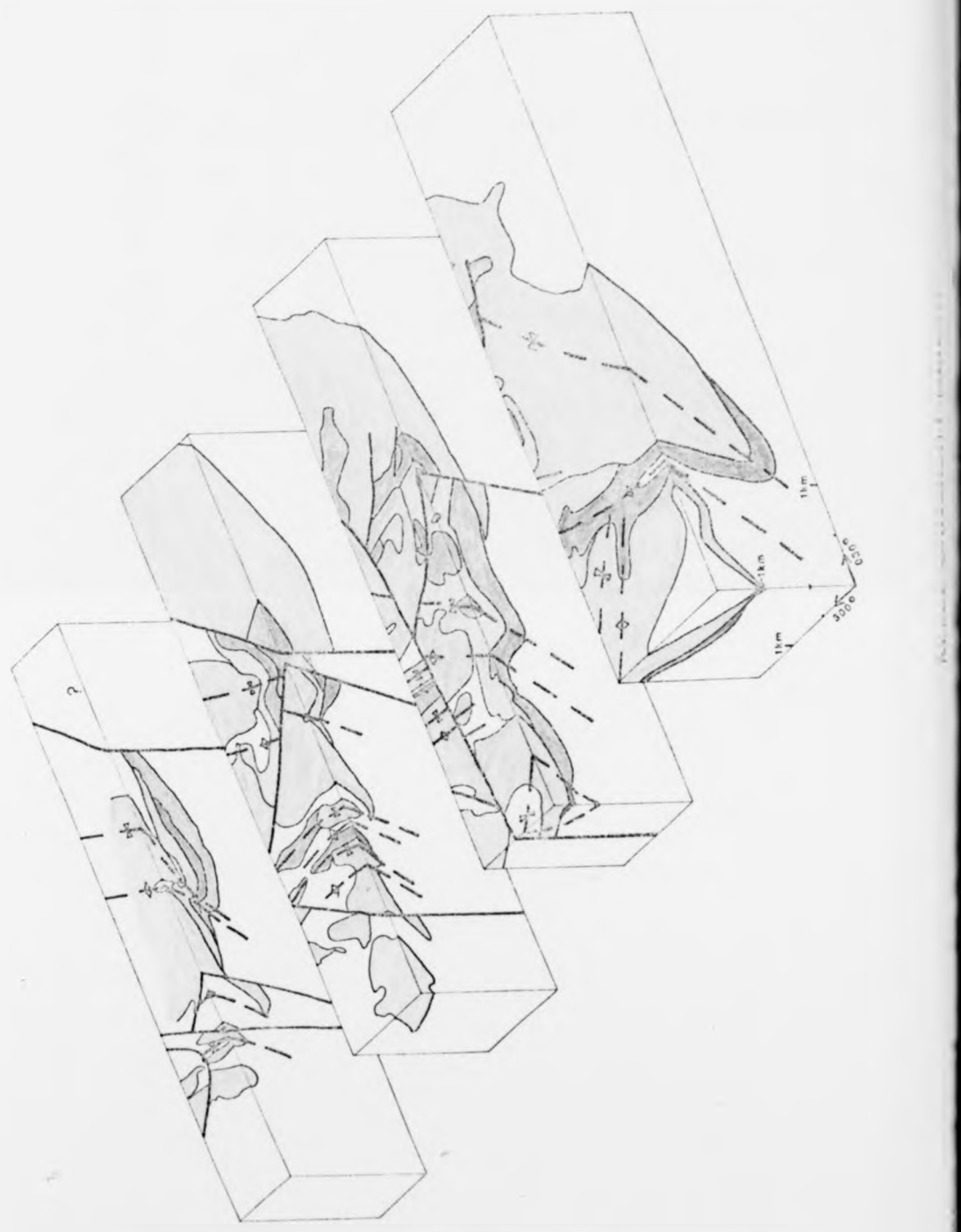

Figure 4.12

Approximate isopach map for the Dragsmark granites.

Contours are at 200m intervals.

The thickest lines indicate major strike-slip faults; continuous thinner lines are contours for Area 1, dot-dash lines for the Area 2 body at Vågeröd.

Note that the northern 'finger' of the main sheet (Area 1) locally underlies the southern 'finger' (indicated by a broken line) and that the Area 2 body overlies the main sheet.

smark granites.

rike-slip faults; continuous

1, dot-dash lines for the Area 2

he main sheet (Area 1) locally

icated by a broken line) and that

eet.

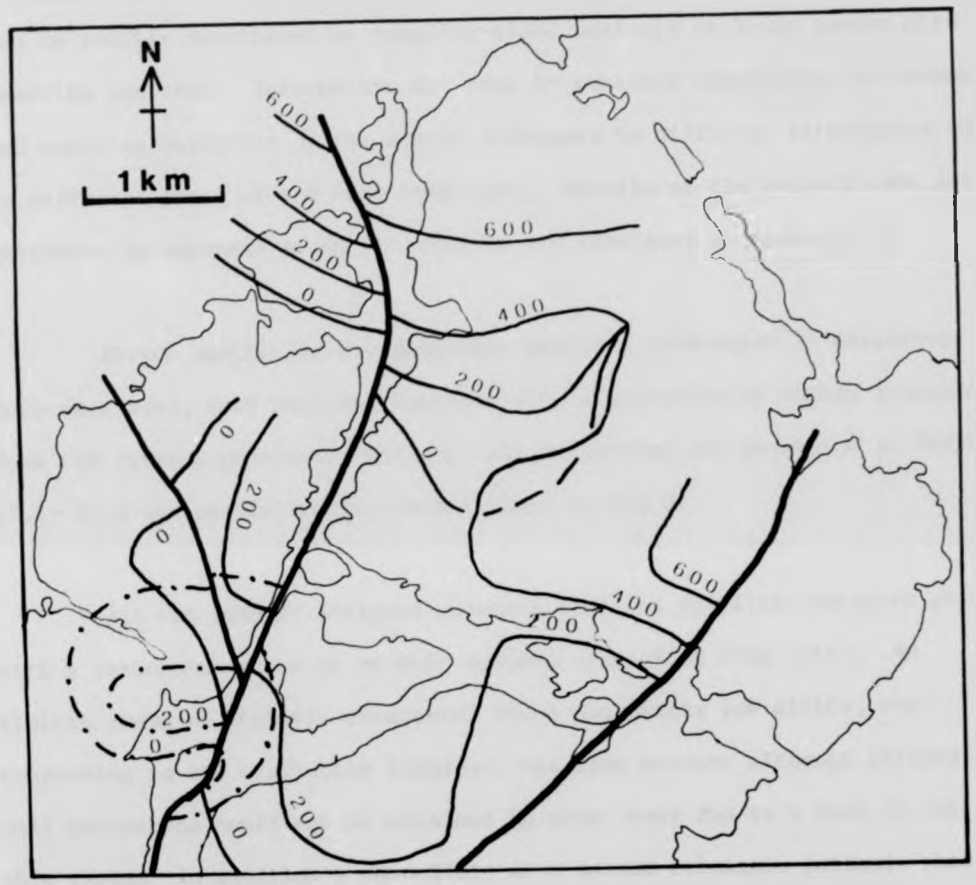

ngsmark granites.

strike-slip faults; continuous

a 1, dot-dash lines for the Area 2

the main sheet (Area 1) locally

ndicated by a broken line) and that

sheet.

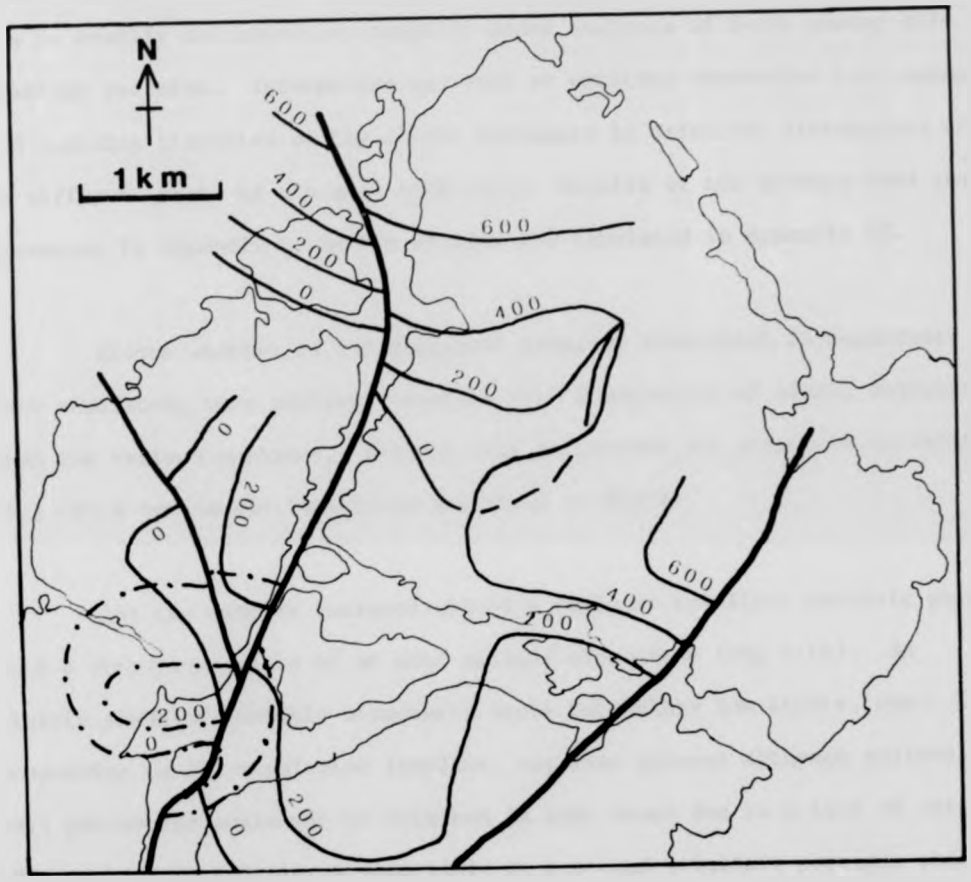

Chapter 5

X-ray Diffraction Analysis of the Alkali Feldspars

a) Introduction

The unit cell parameters of alkali feldspars are affected by both composition and Al/Si distribution within the lattice. These parameters can be readily determined by computer-aided analysis of X-ray powder diffraction patterns. Information may thus be obtained concerning the thermal and unmixing histories of the alkali feldspars in different lithologies and in different parts of the same rock unit. Details of the methods used are presented in Appendix A and the results are tabulated in Appendix B5.

Eleven samples of the Dragsmark granite, from which 25 megacrysts were separated, were analysed together with a selection of alkali feldspars from the various gneisses. Refined cell parameters are presented in Tables B5.1 - B5.4 and sample localities are shown on Map 3.

All the samples analysed showed a dominant triclinic potassic phase with a structural state of or near maximum microcline (Fig 5.1A). An albitic phase of variable structural state but mainly low albite, corresponding to the exsolution lamellae, was also present although refined cell parameters could not be obtained in some cases due to a lack of suitable peaks. In addition a monoclinic or a second triclinic potassic phase occurred but was refinable in only about two-thirds of the samples.

Although uncommon, cases of two co-existing potassic phases of different structural state within alkali feldspar crystals are documented e.g. Tilling (1968), Rayland (1969). Comparison of the powder diffraction patterns with those obtained by Steiger and Hart (1967) for synthetic orthoclase-microcline admixes indicates that the majority of samples have less than 10% monoclinic feldspar but about a fifth show

between 20% and 40% (Fig. 5.1B). One of the latter shows 'patchy' cross-hatched twinning indicating that the development of twins on the albite and pericline laws is incomplete within the crystal, perhaps due to incomplete inversion to the triclinic state, but others are apparently 'completely' twinned. This suggests that the monoclinic phase is present as sub-microscopic domains distributed throughout the crystal whereas in other cases microscopic areas of orthoclase are present. No connection is found between the inferred size of these domains and composition, strain or geological setting.

b) Structural State

The term structural state is defined by Wright and Stewart (1968) as "any one particular polymorphic modification of the feldspar structure". Any given composition may exist in a number of structural states and conversely, any given structural state may be found in a range of compositions, which may not be isostructural. The structural state is dependant principally on the Al/Si distribution, that is the probability of finding Al at any tetrahedral site.

Following Wright and Stewart (op.cit.) and Stewart and Wright (1974) cell parameter data, which reflects both structural state and composition, is presented as plots of b against c and α^* against γ^* (Figs. 5.2 & 5.3). Such plots yield two types of information. Firstly they yield theoretical values for a, which can be compared with the 'observed' values as a measure of strain within the lattice, and secondly they allow calculation of the Al/Si distribution. From these diagrams it is clear that the structural state of the dominant potassic phase (Fig. 5.2A) does not depart greatly from maximum microcline, the variation shown being mainly parallel to the maximum microcline-low albite tieline. Such variation can be caused by either or both of composition and strain. In contrast the orthoclases (Fig. 5.2B and C) vary greatly in degree of order as is to be expected considering their metastable state (monoclinic phases plot at $\alpha^* = 90^o$, $\gamma^* = 90^o$ by definition).

There is a consensus that sodic feldspar orders more rapidly than potassic feldspar and no natural coexisting feldspar pairs are known with the sodic feldspar less ordered than the potassic. The albitic exsolution lamellae from the Dragsmark granite appear to contradict this statement, many showing apparently lower degrees of order than their host triclinic potassic phases. However, they exhibit low b values,

causing the majority to plot outside the b - c quadrilateral (Fig. 5.2A), and anomalously low cell volumes which generate negative Or contents using the equation of Stewart and Wright (1974) relating cell volume and composition. This phenomenon is noted by them as being typical of perthite lamellae and the suggestion is made that Al/Si ordering data by their methods on such feldspars may not be reliable.

An alternative explanation is that if exsolution occurred mainly prior to inversion, the albite lamellae should be compared with the monoclinic potassic phase. If this is done, the number showing a greater degree of disorder than their host is greatly reduced and none show less ordering than the initial crystallization structural state (see p.52 and ff.). Some support for this theory is supplied by the association of those albites plotting furthest from the theoretical ordering line with diffraction patterns indicating large amounts of relict orthoclase eg. 145GM,73/1. If the above explanation is correct, it implies some mechanism whereby the host potassic phase can partially invert and order without affecting the sodic exsolution lamellae.

It is possible that symmetry inversion, which affects only the potassic phase, has a catalytic effect on Al/Si ordering. The b - c plot is contoured for a values of homogeneous feldspars, allowing comparison of the actual a dimension (a observed) with an 'ideal' value (a estimated) derived from the plot. Δa (defined as a observed - a estimated) is generally regarded as an index of strain, with feldspars being termed strained when $\Delta a > 0.05\text{Å}$ (Stewart and Wright,1974). Table 5.1 presents values of Δa for the phases present in the samples, together with compositional data from cell volumes, bulk compositions from homogenized feldspars (see p.55) and brief textural descriptions.

Strain arises as a result of exsolution and/or symmetry inversion

TABLE 5.1

Strain and Composition from XRD data i) Dragsmark granite Area 1

Sample	Δa Tricl	Δa Monoc	Δa Sodic	% Or Tricl	% Or Monoc	% Or Bulk	Twinning, Perthite
32/1	+0.11	-	+0.02	84	-	78	P,Fm
32/2	+0.09	-0.03	-0.01	85	92	84	F,Fm
32GM	+0.10	+0.01	-	81	88	-	F,Fm
53/1	-0.04	+0.22	-	93	95	-	F,N-P
53/3	+0.15	+0.28(T)	-0.03	84	82	75 *	U,Fm
53/4	+0.09	-	+0.02	95	-	-	F,N-Fm
53GM	+0.24	+0.22	-0.01	92	81	- *	F,(N)
79WR	0.00	+0.25	0.00	95	93	86 *	F,(N)
145/1	0.06	-	+0.01	90	-	80	F,B
145/2	-0.04	-	-0.01	94	-	76	F,B
145/3	+0.17	+0.31	-	85	86	- *	U,Fm
145/4	+0.09	-	-	86	-	-	F,N-Fm
145/5	-0.04	+0.19(T)	-0.06	93	83	83 *	P,Fm
145GM	+0.19	-0.13	+0.02	96	90	-	F,Fm
187/1	+0.05	-	-0.04	87	-	77	P,S
187/2	+0.11	+0.14	-	93	92	-	F,N
187GM	+0.08	-	-0.08	84	-	-	F,Fm
241/1	-0.10	+0.16	-	91	88	74	F,N-S
241/2	+0.09	-0.06	-0.02	86	100	-	F,N-S
241/3	+0.05	+0.31	0.00	92	87	- *	F,B
249/1	+0.25	+0.05	-	88	92	55 *	F,N
249/2	-0.06	+0.25	-	100	85	55 *	P,S
299WR	+0.19	-0.01(T)	0.00	88	49	-	P,Fm
364/1	+0.09	-0.26	-0.02	100	66	73 *	F,N-Fm-B

Tricl = Triclinic, Monoc = Monoclinic, (T) = minor triclinic phase,
P = Patchy, F = Full, U = Untwinned, S = String, N = Nonperthitic, B = Bead,
Fm = Film, * - see text p.52.

TABLE 5.1 (cont.)

Strain and Composition from XRD data ii) Dragsmark granite Area 2

Sample	Δa Tricl	Δa Monoc	Δa Sodic	% Or Tricl	% Or Monoc	% Or Bulk	Twinning, Perthite
65/1	-0.15	+0.08	-0.02	91	87	77 *	F,N-Fm
65/2	-0.01	-	-0.02	91	-	-	F,N-Fm
65GM	+0.12	+0.36(T)	-0.03	100	80	- *	F,Fm
70/1	-0.02	+0.24	+0.01	88	93	84 *	F,N-S-B
70GM	+0.02	+0.11	-	92	91	-	F,Fm
73/1	+0.05	+0.33	+0.01	100	90	75 *	F,B
73/2	+0.16	+0.16	-0.03	93	92	-	F,N
73GM	-0.01	+0.32	-	92	90	66 *	F,N
205/1	-0.05	-	0.00	97	-	-	F,N-S-P
205/2	+0.05	-	-	82	-	-	P,S
205GM	+0.14	-	0.00	88	-	-	F,Fm

TABLE 5.1 (cont.)

Strain and Composition from XRD data iii) Other Lithologies

Sample	Δa Tricl	Δa Monoc	Δa Sodic	% Or Tricl	% Or Monoc	% Or Bulk	Twinning, Perthite
Stora Le -Marstrand gneisses							
39WR	=0.19	-0.18	-	91	97	-	F, Fm
197/1	+0.07	+0.36	0.00	83	86	77 *	P,S
197/2	+0.12	-0.13	-0.06	83	91	72 *	F,N-Fm
leucosome							
286/1	-0.02	-	+0.01	96	-	83	F,B
granodiorite gneiss							
103WR	+0.02	-	-	89	-	-	F, Fm
105WR	+0.14	-0.12	+0.03	89	92	-	F, Fm
107WR	+0.08	+0.12	-0.01	87	98	-	F,N
110WR	-0.03	+0.22	+0.01	92	100	48	F, Fm
Kållviken granite							
18WR	+0.05	-	-	89	-	84	F,N
Standard errors				±1.6	±4.1	±2.3	

and is related to the degree of coherency between the exsolved phases (Robin,1974). Cryptoperthites show the highest strains, reflecting the highly coherent bonding across the phase interface (Fig. 5.4). Coherency affects the temperature of the onset of exsolution by lowering the isobaric solvus temperature at any given composition by 50° - 70°C; if the perthite is coherently bonded i.e. strained, then the coherent solvus should be used and not the hydrostatic solvus (ibid.). From Table 5.1 it can be seen that nearly all the sodic exsolution lamellae are unstrained whereas the potassic phases are commonly strained. The former implies that the perthite is noncoherent in those samples for which refined cell parameters were obtainable for the sodic phase, and consequently the hydrostatic solvus should be used. Note that many optically nonperthitic samples did not yield measurable albite reflections.

If the perthite is noncoherent, it follows that the strain detected in the host potassic phase must result form symmetry inversion. This, together with the sharpness of the diffraction patterns (Fig. 5.1A), supports the view of Stewart and Wright (1974) that the strained volume is homogeneously distributed throughout the crystal and is not confined to regions near the exsolution interfaces. It is further possible that the strain may be externally imposed e.g. by regional stress, with the higher kinetic rates associated with sodic feldspars over potassic compositions allowing dispersal of this strain from the exsolution lamellae only. This question could perhaps be resolved by single-crystal diffraction and transmission electron microscopy but is outside the scope of the present work.

In Fig. 5.5 Δa is plotted against bulk composition and it can be seen that in general the monoclinic and disordered triclinic phases are more strained than the highly ordered triclinic phases. All of the latter fall below or very near the boundary separating microperthite from

and is related to the degree of coherency between the exsolved phases (Robin,1974). Cryptoperthites show the highest strains, reflecting the highly coherent bonding across the phase interface (Fig. 5.4). Coherency affects the temperature of the onset of exsolution by lowering the isobaric solvus temperature at any given composition by $50^{o} - 70^{o}C$; if the perthite is coherently bonded i.e. strained, then the coherent solvus should be used and not the hydrostatic solvus (ibid.). From Table 5.1 it can be seen that nearly all the sodic exsolution lamellae are unstrained whereas the potassic phases are commonly strained. The former implies that the perthite is noncoherent in those samples for which refined cell parameters were obtainable for the sodic phase, and consequently the hydrostatic solvus should be used. Note that many optically nonperthitic samples did not yield measurable albite reflections.

If the perthite is noncoherent, it follows that the strain detected in the host potassic phase must result form symmetry inversion. This, together with the sharpness of the diffraction patterns (Fig. 5.1A), supports the view of Stewart and Wright (1974) that the strained volume is homogeneously distributed throughout the crystal and is not confined to regions near the exsolution interfaces. It is further possible that the strain may be externally imposed e.g. by regional stress, with the higher kinetic rates associated with sodic feldspars over potassic compositions allowing dispersal of this strain from the exsolution lamellae only. This question could perhaps be resolved by single-crystal diffraction and transmission electron microscopy but is outside the scope of the present work.

In Fig. 5.5 Δa is plotted against bulk composition and it can be seen that in general the monoclinic and disordered triclinic phases are more strained than the highly ordered triclinic phases. All of the latter fall below or very near the boundary separating microperthite from

cryptoperthite. Those samples with monoclinic phases plotting in the cryptoperthite field are marked thus * in Table 5.1 and most show microscopically nonperthitic areas, or else are untwinned or only patchily twinned. These latter support the idea of strain being due to failure to invert.

Stewart and Ribbe (1969) state

> "relative position on the b - c plot gives total Al in T_1o and T_1m ... ; total Al in the T_2 sites, where $T_1o = T_1m$, is obtained by difference. Relative position on the $\alpha^* - \gamma^*$ plot gives the difference in Al content between T_1o and T_1m"

This relationship has been widely tested and the revised plots of Stewart and Wright (1974) are used in this work to obtain Al site occupancies, which are presented on their halved triangular plot.

This plot (Fig. 5.6) has t_1o, t_1m and $t_2o + t_2m$ as its apices where notation is after Kroll (1971) with t_1o, t_1m etc. denoting the probability of finding Al in the T_1o, T_1m etc. sites. As t_2 is never greater than 0.50 and t_1m never greater than t_1o, only the bottom left part of the triangle is accessible to feldspars. Monoclinic feldspars, with $t_1o = t_1m$, plot on the median line and maximum microcline together with low albite, with $t_1o = 1.0$, plot at the t_1o apex. Analbite (high albite) is co-incident with sanidine, lying on the median line at $t_2 = 0.5$; the theoretical and empirical one step ordering path for albites involving transfer of Al to T_1o equally from T_1m, T_2o and T_2m joins analbite (high albite) and low albite (see Fig. 5.7).

Two conclusions can be drawn from the data for the Dragsmark granite alkali feldspars. Firstly, considering Area 1, despite a very considerable range in degree of order for both megacryst and groundmass

orthoclase, the megacrysts tend to have higher t_2 values i.e. the megacrysts are more disordered than the groundmass. For Area 2 feldspars this tendency is more marked, but is reversed, the megacrysts being more ordered (lower t_2) than the groundmass. Within limits of error, the most disordered representatives from Area 1 megacrysts, Area 1 groundmass and Area 2 groundmass are coincident, with $t_2 = 0.43$. The corresponding maximum for Area 2 megacrysts is $t_2 = 0.20$. Although the t_2 value for any one sample represents merely the degree of order attained when Al/Si ordering became blocked (in a manner analogous to that of isotopic fractionation), the maximum value for a given suite should reflect the degree of order at the time of crystallization. It thus appears that Area 2 megacrysts crystallized in a considerably more ordered state than did the other groups; the implications of this are discussed later (Ch. 5d).

Secondly, many albite exsolution lamellae plot well away from the theoretical ordering line (Fig. 5.7). It is important to realize that this line represents the path taken by a free crystal ordering from analbite. Clearly an exsolution product cannot start to order until it is formed, and if the parent crystal has already ordered to some degree e.g. an orthoclase with $t_2 = 0.3$ then this must represent the starting structural state of the exsolution product. This initial crystal will presumably be metastable and tend to order in such a manner as to attempt to attain the structure of a free crystal. If equilibrium is attained under constant conditions, the albite lamellae will come to plot on the theoretical ordering line at a structural state thermodynamically equivalent to that of the host potassic phase. But in a natural system, where the temperature and thus the equilibrium t_2 values are falling, the path taken by the albite will be a concave downward curve and moreover, Al/Si diffusion may become blocked before reaching the 'ideal' state.

Although there are insufficient data points for any quantitative

assessment, two ordering curves for perthitic albite can be drawn through those data points not falling near the theoretical ordering path A (Fig. 5.7), in accordance with the above observations. Most such points from Area 2 lie nearer to the lower curve (Line 2, Fig. 5.7), which originates at $t_2 = 0.15 - 0.10$. The remaining albites, from Area 1, define the upper curve (Line 1, Fig. 5.7), originating at $t_2 = 0.35 - 0.30$, although some plot nearer the lower curve. In both cases, these degrees of ordering at the onset of exsolution are higher (lower t_2) than the presumed initial crystallization order, implying a temperature interval between crystallization and intersection of the solvus.

c) Composition

The compositions of the exsolved phases can be calculated from their cell volumes; the equation used here is that presented in Stewart and Wright (1974)

$$\text{Or (mole \%)} = \frac{0.2962 - \sqrt{0.953131 - 0.0013V}}{0.0018062}$$

(cell volume V in Å^3)

For potassic compositions, error due to variation in volume with structural state are minimal and outweighed in the present study by the errors associated with the cell volume (see Tables B5.1 - B5.3). As previously stated, the anomalously low cell volumes calculated for the albitic perthite lamellae generate negative Or contents and consequently only data for the potassic phases are presented together with bulk compositions derived by homogenization (Table 5.1).

Heating a microperthite for about 48 hours at 1050°C homogenizes the grains; precise measurement of the position of the $\bar{2}01$ peak then allows calculation of the bulk composition of the feldspar (Orville,1967). The method used is essentially that of Jones et al. (1969) : see Appendix A. Differences in values obtained by use of their equation and that of Wright (1968) were less than 1% Or which is within the estimated errors of both equations.

The compositions of the two exsolved potassic phases are approximately the same for many samples; of those where the compositions differ, no more show the triclinic phase to be more potassic than the monoclinic than show the reverse. These values reflect the degree of exsolution achieved and it might have been expected that the relict monoclinic phases would show less exsolution and hence lower Or contents; this is obviously not always the case. The factors governing exsolution on a local scale are clearly very complex and no fruitful conclusions can be

drawn from this data. With the exception of the relict phases of two samples (299WR and 364/1); the exsolved compositions plot off published solvi i.e. below 300°C, indicating as expected that exsolution over the crystal as a whole proceeded to very low temperatures. These two exceptions are also the only samples for which % Or monoclinic > % Or bulk which throws doubt on their validity. Discussion of the significance of the bulk compositions is deferred to Chapter 7.

d) Crystallization History

The alkali feldspars of the Dragsmark granite are remarkable but not unique in showing two structural states of the potassic phase, maximum microcline with subordinate orthoclase. The few cases with a highly disordered triclinic phase instead of orthoclase represent complete inversion but incomplete ordering. Steiger and Hart (1967) document the transformation of the microcline in Precambrian granites and gneisses into orthoclase in the contact aureole of a Laramide (55ma.) quartz monzonite. In the Dragsmark region however no younger intrusions are found, and moreover Parsons and Boyd (1971) record the preservation of orthoclase xenocrysts in microcline-bearing syenite, indicating that reheating need not cause the microcline - orthoclase transformation. The disordered phases detected are therefore interpreted as relicts of a primary monoclinic state. Their preservation despite later deformation and metamorphism is noteworthy but compatible with the suggestion by Stewart and Wright (1974) of exceedingly slow Al/Si diffusion in alkali feldspars at temperatures below 600^{o}C. Parsons and Boyd (1971) hypothesize that fine details of the initial crystal growth, perhaps controlled by volatile components of the system, may be important in determining the ease and rate with which a crystal will invert on cooling.

The likely significance of factors such as the presence of volatiles, cooling rate and crystal growth rate on both the equilibrium degree of Al/Si order and the rate of ordering render the use of structural state as a geothermometer almost impossible. Stewart and Wright (1974) present a graph of equilibrium Al content in T_1 against temperature but admit (p.369, ibid.);

> "If, by either low temperature or rapid growth, diffusion is unable to achieve an equilibrium Al/Si configuration, disordered states can form and be

preserved. These states may not differ from those found at equilibrium at higher temperatures or different growth rates."

Using their graph yields initial crystallization temperatures of 790^{o} - 870^{o}C for the alkali feldspars from the Dragsmark granite. Such temperatures are geologically acceptable only for a dry granitic magma intruded at very shallow levels at P_{H_2O} of a few bars. Considering the regional setting (Ch. 1 b) this is so unreasonable that the above explanation of metastable formation of disordered states, probably due to rapid growth, is accepted. Only in the case of the Area 2 megacrysts, with a maximum temperature of 610^{o}C on their scale, is it likely that true Al/Si equilibrium pertained at the time of crystallization. A modified version of their graph, without absolute temperatures, is therefore used here (Fig. 5.8). The relative temperature scale is retained unaltered, with $dT/dt_2 \approx 100^{o}C/0.1Al$ in the central portion, as it is felt that this may be approximately valid for a set of samples crystallizing under the same conditions.

From Fig. 5.8A it can be seen that the megacrysts and groundmass from Area 1 commenced crystallization at approximately the same temperature, although the groundmass continued to equilibrate, or was later reset, to lower temperatures than the megacrysts. This relationship is explicable by a simple magmatic model, the megacrysts being phenocrysts with rapid growth accounting for their highly disordered structural states. The same holds true for the groundmass, only their smaller size has rendered the attainment of near equilibrium structural states by diffusion more feasible both during crystallization and by later metamorphic reheating.

The bodies of granite comprising Area 2 being much smaller than the main Area 1 body, classic igneous modelling allows for them to have

cooled more rapidly and thus to be lacking high temperature phenocrysts and to consist solely of a 'quenched' groundmass. In the admittedly few samples available, the groundmass does indeed show Al/Si ordering implying a similar crystallization temperature to that of the main body (Fig.5.8B). Area 2 megacrysts show much lower maximum t_2 perhaps suggesting lower, subsolidus, temperatures (although see above) and textural evidence indicates that they are postmagmatic, i.e. porphyroblasts, due to metamorphism or metasomatism.

Taking the aforementioned value of $dT/dt_2 \approx 100^{\circ}C/0.1Al$, temperature intervals between crystallization and onset of exsolution of $100^{\circ} - 150^{\circ}C$ for Area 1 and $50^{\circ} - 100^{\circ}C$ for Area 2 megacrysts can be derived. For a bulk feldspar composition of Or 75 (see Table 5.1) and a pressure of 2 - 5 kb, the temperature gap between the granite solidus and feldspar hydrostatic solvus is $200^{\circ} - 130^{\circ}C$ (Fig. 5.9). Bearing in mind the considerable errors generated by uncertainties in the graphs, the data, and the extrapolations, the agreement between these estimates is quite good. This further supports a magmatic origin for all but the Area 2 megacrysts, for which a sub-solidus origin is indicated.

Figure 5.1

A : X-ray powder diffraction patterns of alkali feldspar from two samples (nos. 70GM, 145GM) of the Dragsmark granites.

131 - microcline peak

131A - albite peak

131M - orthoclase peak (monoclinic)

Qz - quartz peak

B : Comparison of the 131 regions (28 - 32° 2θ) of powder diffraction patterns for seven alkali feldspars (nos. 70GM, 197/2, 53/4, 187/2, 73/1, 73/2 and 145GM) from the Dragsmark granites with those of synthetic admixes of orthoclase and maximum microcline (after Steiger and Hart, 1967). The samples are listed in order of increasing monoclinic feldspar content, and show a range from 100% microcline (70GM) to ca.60% microcline (145GM).

Mi_{80} - admix of 80% microcline, 20% orthoclase, etc.

Figure 5.1

A : X-ray powder diffraction patterns of alkali feldspar from two samples (nos. 70GM, 145GM) of the Dragsmark granites.

131 - microcline peak

131A - albite peak

131M - orthoclase peak (monoclinic)

Qz - quartz peak

B : Comparison of the 131 regions (28 - 32° 2θ) of powder diffraction patterns for seven alkali feldspars (nos. 70GM, 197/2, 53/4, 187/2, 73/1, 73/2 and 145GM) from the Dragsmark granites with those of synthetic admixes of orthoclase and maximum microcline (after Steiger and Hart, 1967). The samples are listed in order of increasing monoclinic feldspar content, and show a range from 100% microcline (70GM) to ca.60% microcline (145GM).

Mi_{80} - admix of 80% microcline, 20% orthoclase, etc.

.1

ns of alkali feldspar from two

agsmark granites.

nic)

(28 - 32° 2θ) of powder diffraction
pars (nos. 70GM, 197/2, 53/4,
om the Dragsmark granites with
rthoclase and maximum microcline
. The samples are listed in order
ar content, and show a range from
% microcline (145GM).

20% orthoclase, etc.

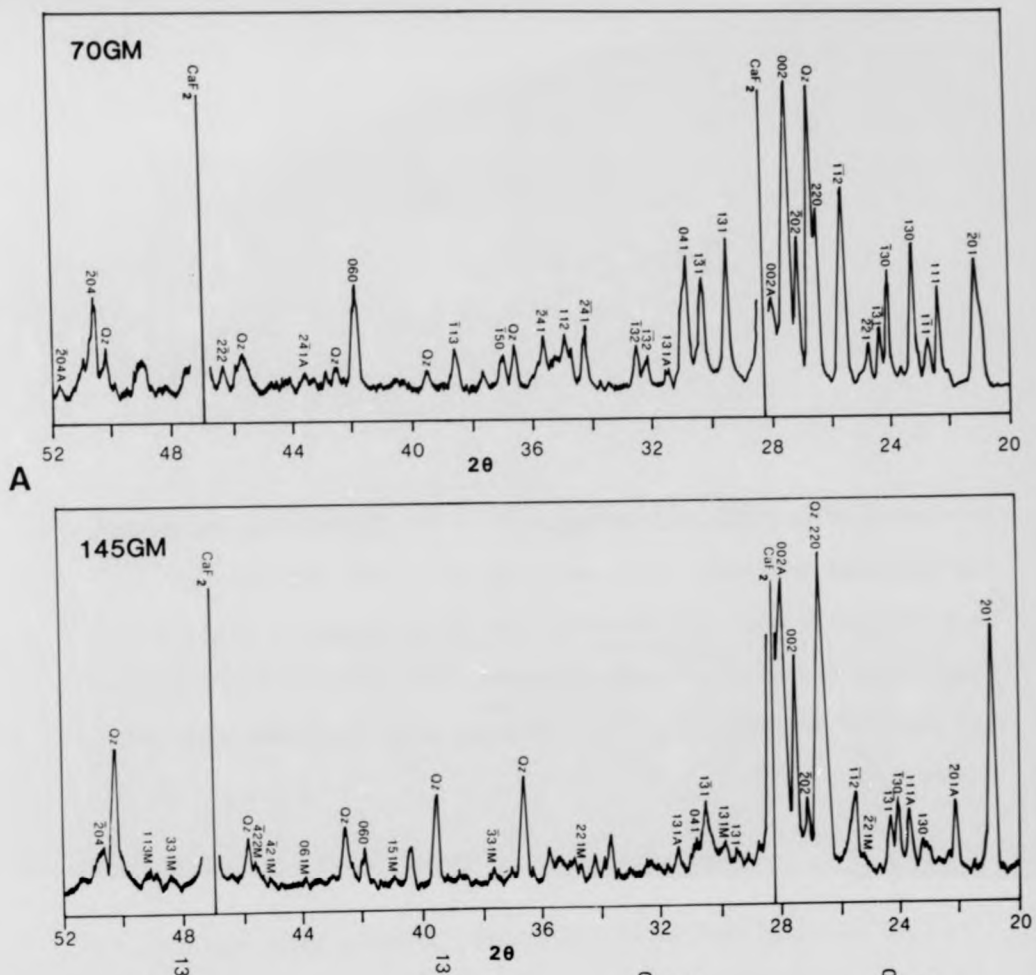

A

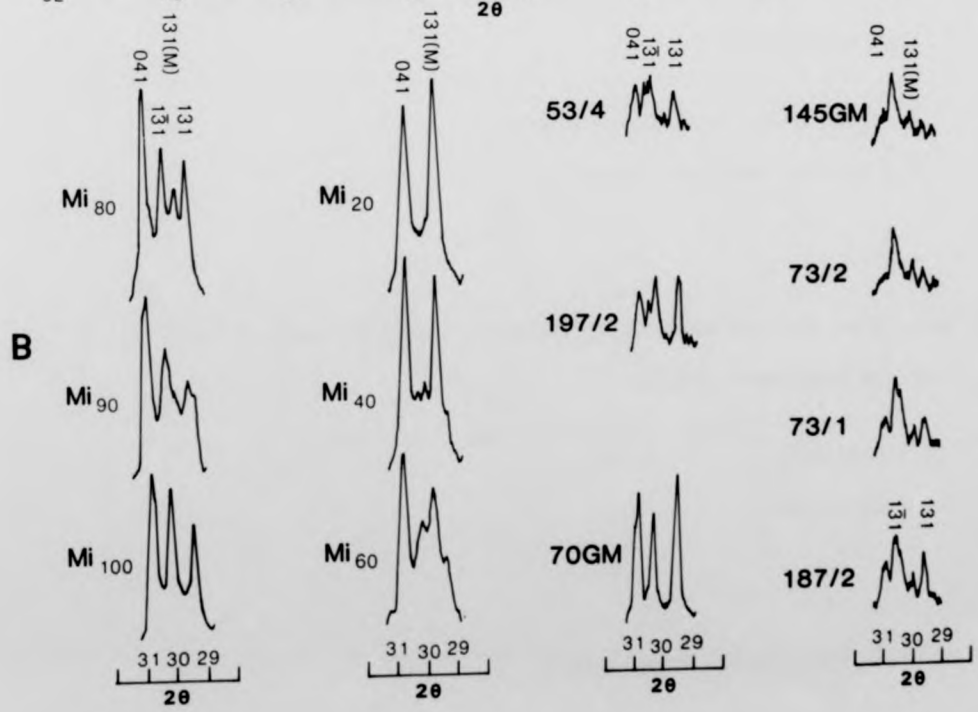

B

Figure 5.2

b - c plots of refined cell parameter data for alkali feldspars from the Dragsmark granites. a, b and c are unit cell parameters, $t_1o + t_1m$ is a measure of the Al/Si ordering. Maximum microcline plots at the upper right corner of the quadrilateral, low albite at the upper left and sanidine and high albite at the lower right and lower left apices respectively.

A : b - c plot for the dominant triclinic potassic phase and the albite lamellae

∇ - microcline (triclinic phase)

+ - albitic perthite lamellae

B : b - c plot for the monoclinic potassic phase in samples from Area 1 of the Dragsmark granite

o - megacrysts

● - groundmass

C : As B, for samples from Area 2

5.2

t data for alkali feldspars from

are unit cell parameters, $t_1o + t_1m$

Maximum microcline plots at the

eral, low albite at the upper left

lower right and lower left apices

clinic potassic phase and the

)

ssic phase in samples from Area 1

A

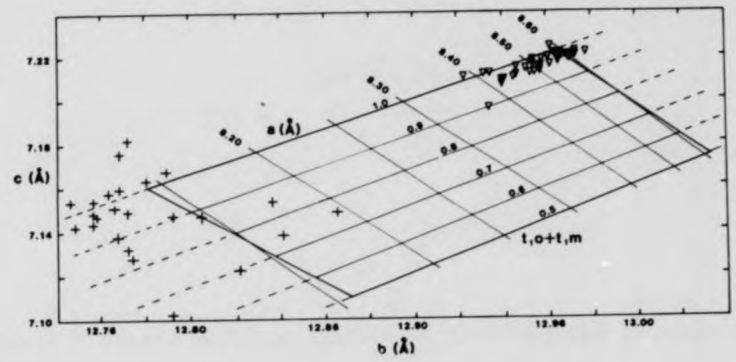

B

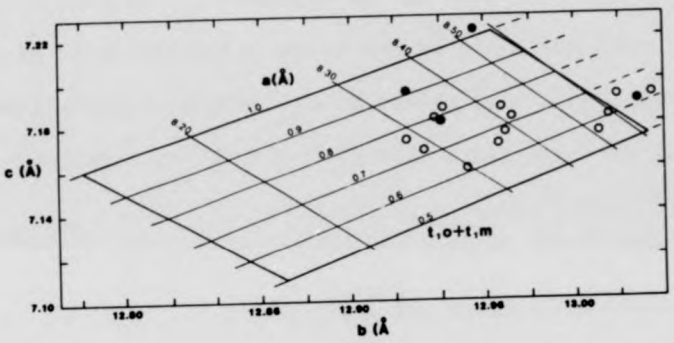

C

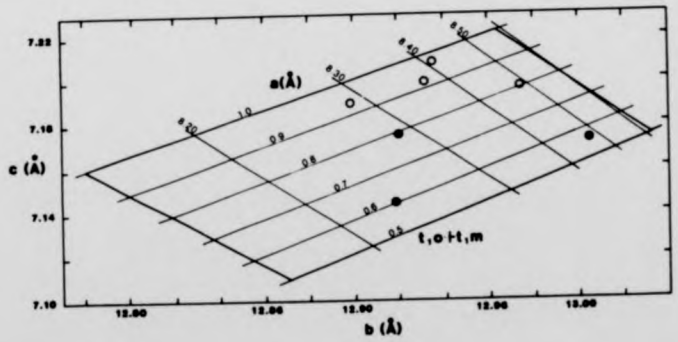

Figure 5.3

α^* - γ^* plot of refined cell parameter data for alkali feldspars from the Dragsmark granite. α^* and γ^* are reciprocal unit cell parameters, t_1o - t_1m is a measure of the Al/Si ordering. Maximum microcline plots at the upper right corner of the quadrilateral, low albite at the upper left, high albite at the lower left and all monoclinic phases at the lower right apex ($\alpha^* = \gamma^* = 90^o$ by definition for monoclinic substances).

▽ - microcline (dominant triclinic phase)

\+ - albitic perthite lamellae

• - minor triclinic phase

Figure 5.3

α^* - γ^* plot of refined cell parameter data for alkali feldspars from the Dragsmark granite. α^* and γ^* are reciprocal unit cell parameters, $t_1o - t_1m$ is a measure of the Al/Si ordering. Maximum microcline plots at the upper right corner of the quadrilateral, low albite at the upper left, high albite at the lower left and all monoclinic phases at the lower right apex ($\alpha^* = \gamma^* = 90^o$ by definition for monoclinic substances).

∇ - microcline (dominant triclinic phase)

\+ - albitic perthite lamellae

• - minor triclinic phase

ata for alkali feldspars from
ciprocal unit cell parameters,
ring. Maximum microcline
uadrilateral, low albite
wer left and all monoclinic
= 90° by definition for

se)

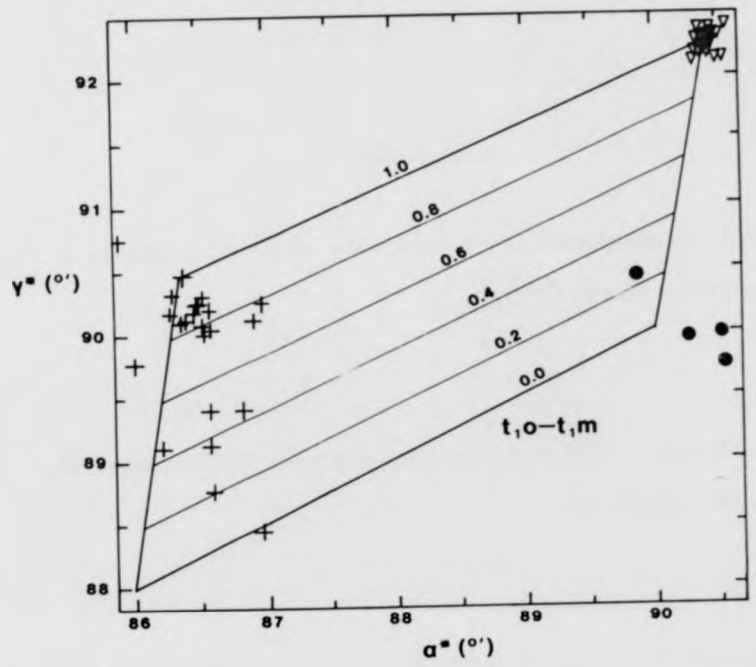

Figure 5.4

Diagrammatic representation of coherency of bonding across a phase interface (after Yund, 1975).

A : Noncoherent. Different lattice spacings across interface e.g. microperthite

B : Semicoherent. Edge dislocations with bending of other planes across interface e.g. strained perthite. Inhomogeneous strain.

C : Perfectly coherent. Elastic strain due to adjustment of lattice spacings e.g. cryptoperthite. Homogeneous strain.

of bonding across a phase

cings across interface

th bending of other planes

hite. Inhomogeneous strain.

n due to adjustment of lattice

ogeneous strain.

A

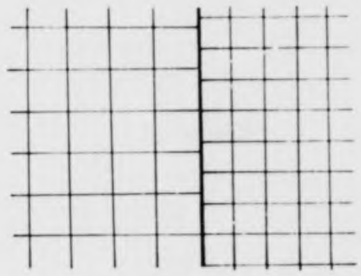

NONCOHERENT

B

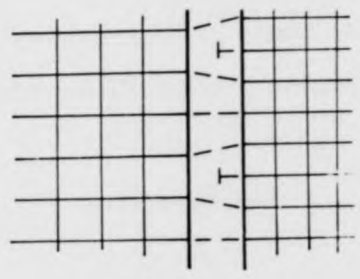

SEMICOHERENT

C

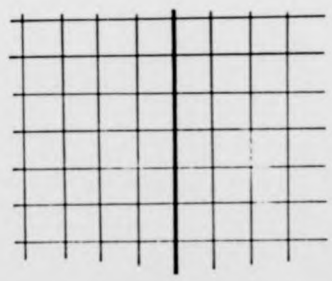

PERFECTLY COHERENT

Figure 5.5

Plot of $\Delta a(a_{observed} - a_{estimated})$ against bulk composition for the potassic phases in alkali feldspars from the Dragsmark granites. Boundary between cryptoperthite and microperthite from Stewart and Wright (1974).

∇ - triclinic phase

o - microclinic and minor triclinic phases

inst bulk composition for

from the Dragsmark granites.

roperthite from Stewart and

ses

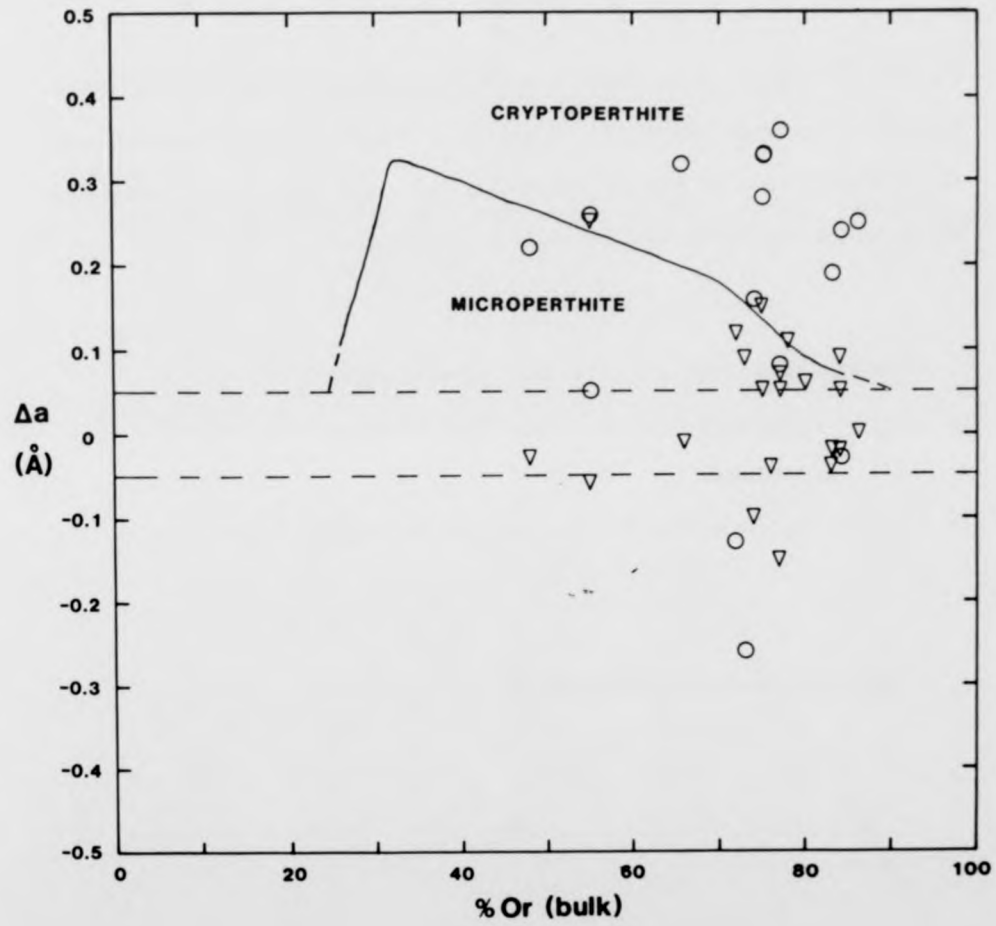

Figure 5.6

Al-site occupancy plots for the monoclinic phase in alkali feldspars from the Dragsmark granites. t_1o, t_1m and $t_2o + t_2m$ are, respectively, the probabilities of finding Al in the T_1o, T_1m and two T_2 tetrahedral sites in the feldspar lattice (see text, p.52).

A : Samples from Area 1 of the Dragsmark granite

o - megacrysts

• - groundmass

M - field occupied by the dominant triclinic phase

B : As A, for samples from Area 2

Figure 5.6

Al-site occupancy plots for the monoclinic phase in alkali feldspars from the Dragsmark granites. t_1o, t_1m and $t_2o + t_2m$ are, respectively, the probabilities of finding Al in the T_1o, T_1m and two T_2 tetrahedral sites in the feldspar lattice (see text, p.52).

A : Samples from Area 1 of the Dragsmark granite

o - megacrysts

• - groundmass

M - field occupied by the dominant triclinic phase

B : As A, for samples from Area 2

nic phase in alkali feldspars

and $t_2o + t_2m$ are, respectively,

T_1o, T_1m and two T_2 tetrahedral

, p.52).

k granite

nt triclinic phase

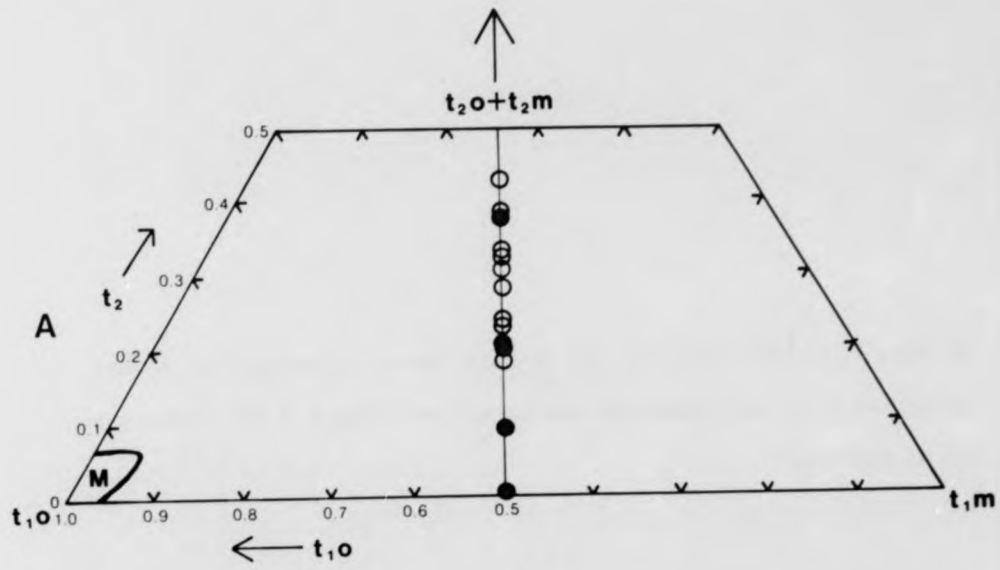

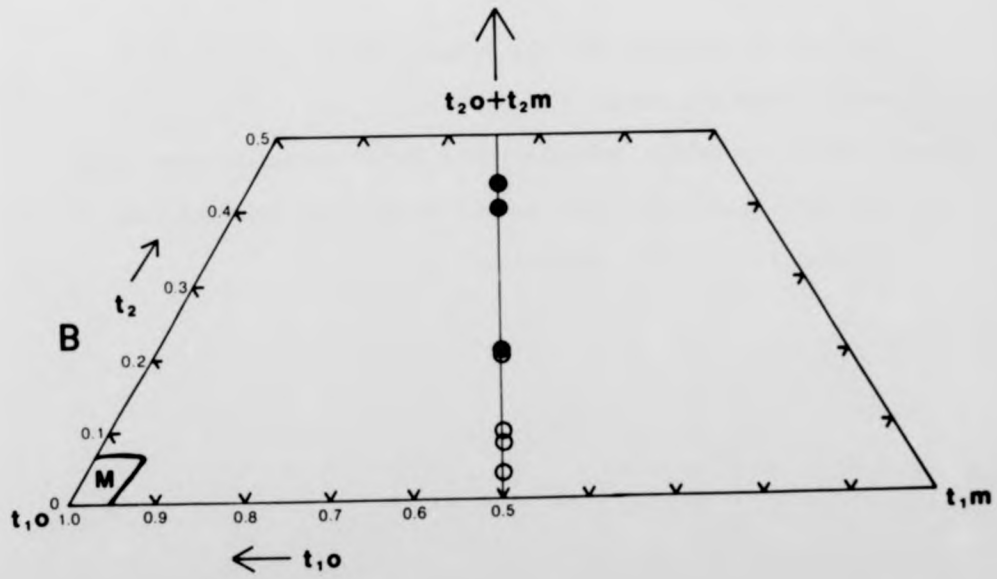

Figure 5.6

Al-site occupancy plots for the monoclinic phase in alkali feldspars from the Dragsmark granites. t_1o, t_1m and $t_2o + t_2m$ are, respectively, the probabilities of finding Al in the T_1o, T_1m and two T_2 tetrahedral sites in the feldspar lattice (see text, p.52).

A : Samples from Area 1 of the Dragsmark granite

o - megacrysts

● - groundmass

M - field occupied by the dominant triclinic phase

B : As A, for samples from Area 2

nic phase in alkali feldspars

and $t_2o + t_2m$ are, respectively,

T_1o, T_1m and two T_2 tetrahedral

, p.52).

k granite

t triclinic phase

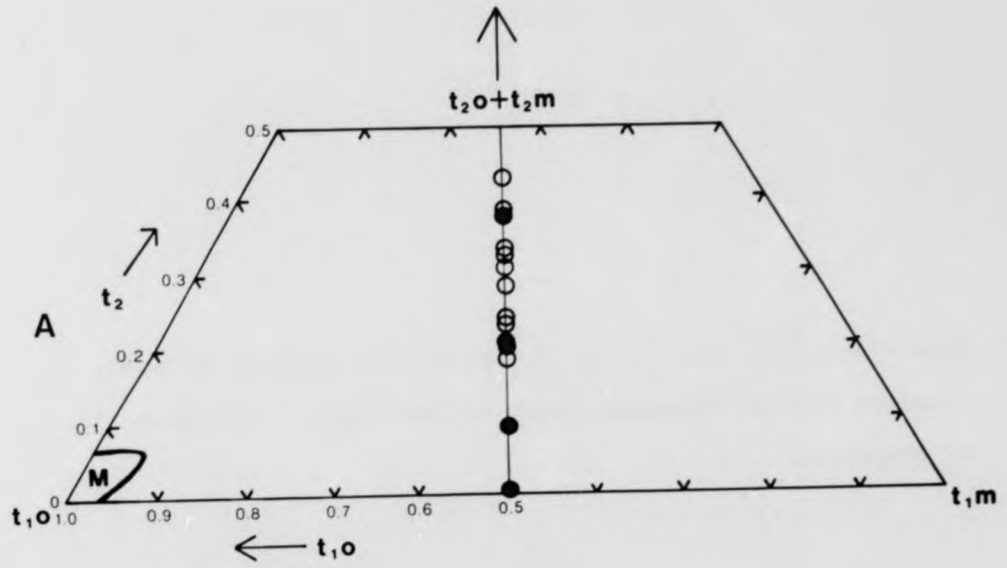

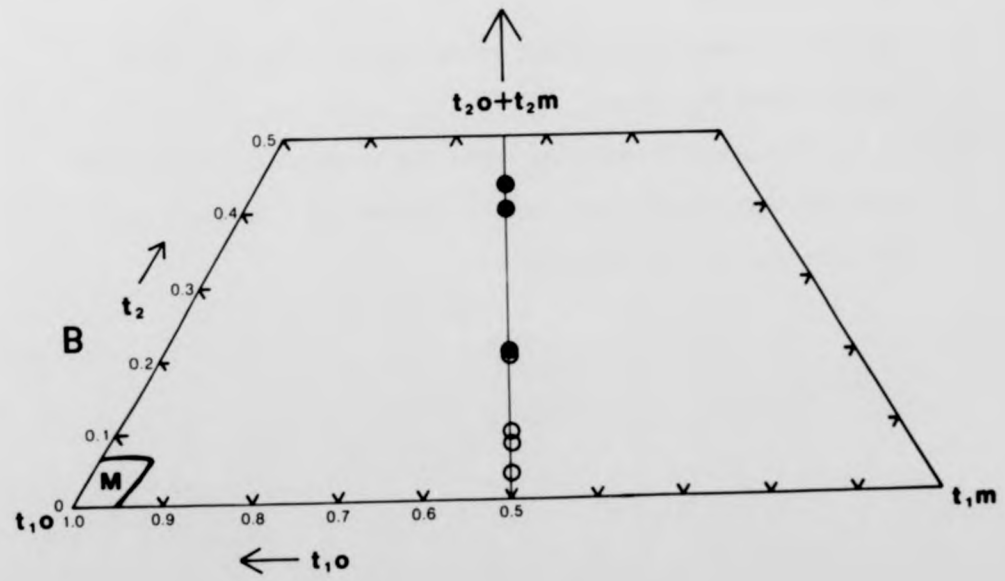

Figure 5.7

Al-site occupancy plot for the albitic perthite lamellae in alkali feldspars from the Dragsmark granites. See Fig. 5.6 for explanation of parameters.

+ - samples from Area 1

□ - samples from Area 2

A - theoretical ordering path for albite of Al to T_1o from T_1m, T_2o and T_2m equally

B - theoretical ordering path for orthoclase of Al to $2T_1$ sites equally from $2T_2$ sites

Lines 1 and 2 - possible ordering paths for those albite exsolution lamellae which do not plot on the theoretical ordering line, A. See text (p.53) for discussion.

c perthite lamellae in alkali

. See Fig. 5.6 for explanation

bite of Al to T_1o from T_1m, T_2o

thoclase of Al to $2T_1$ sites

hs for those albite exsolution

e theoretical ordering line, A.

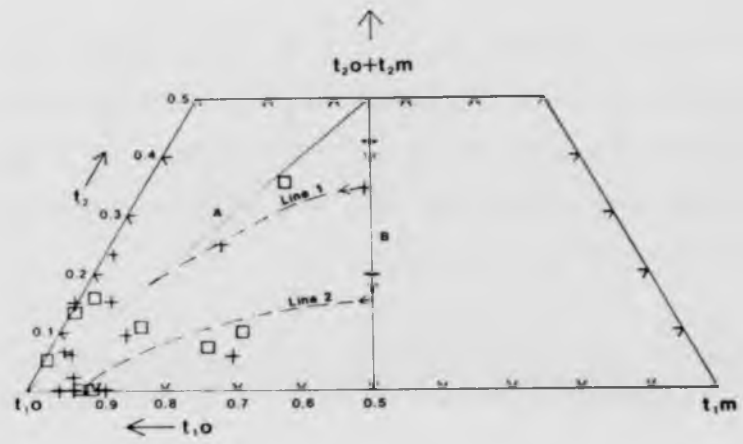

Figure 5.8

Plots of Al-site occupancy ($t_1o + t_1m$) of the monoclinic phase in alkali feldspars from the Dragsmark granites on the temperature v site occupancy curve of Stewart and Wright (1974). The temperature axis is marked in divisions of 100°C, but no absolute values are indicated (see text for discussion).

A : Plot for samples from Area 1 of the Dragsmark granite.

o - megacrysts

• - groundmass

B : As A, for samples from Area 2.

) of the monoclinic phase in
ranites on the temperature v
right (1974). The temperature
but no absolute values are

the Dragsmark granite.

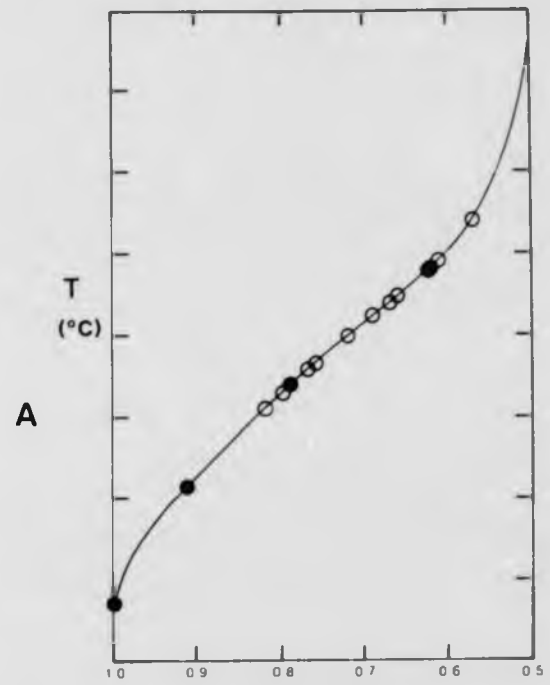

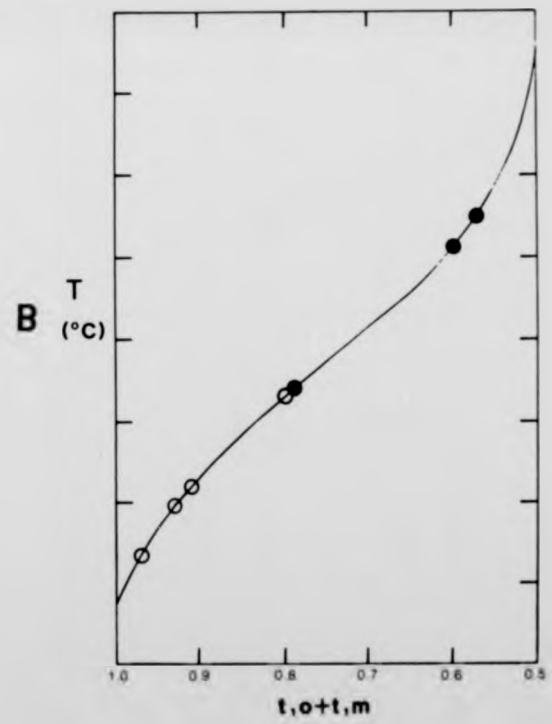

Figure 5.9

Temperature versus P_{H_2O} plot of the wet granite solidus (Tuttle and Bowen, 1958) and the limb of the alkali feldspar solvus (hydrostatic) for a feldspar with bulk composition Or 75% (Smith and Parsons, 1974).

The P_{H_2O} range within which the Dragsmark granite probably crystallized is also shown. The temperature interval between crystallization of an alkali feldspar and the onset of exsolution can be seen to be 130- 200°C.

ranite solidus (Tuttle and

eldspar solvus (hydrostatic)

5% (Smith and Parsons, 1974).

granite probably crystallized

between crystallization of

ution can be seen to be

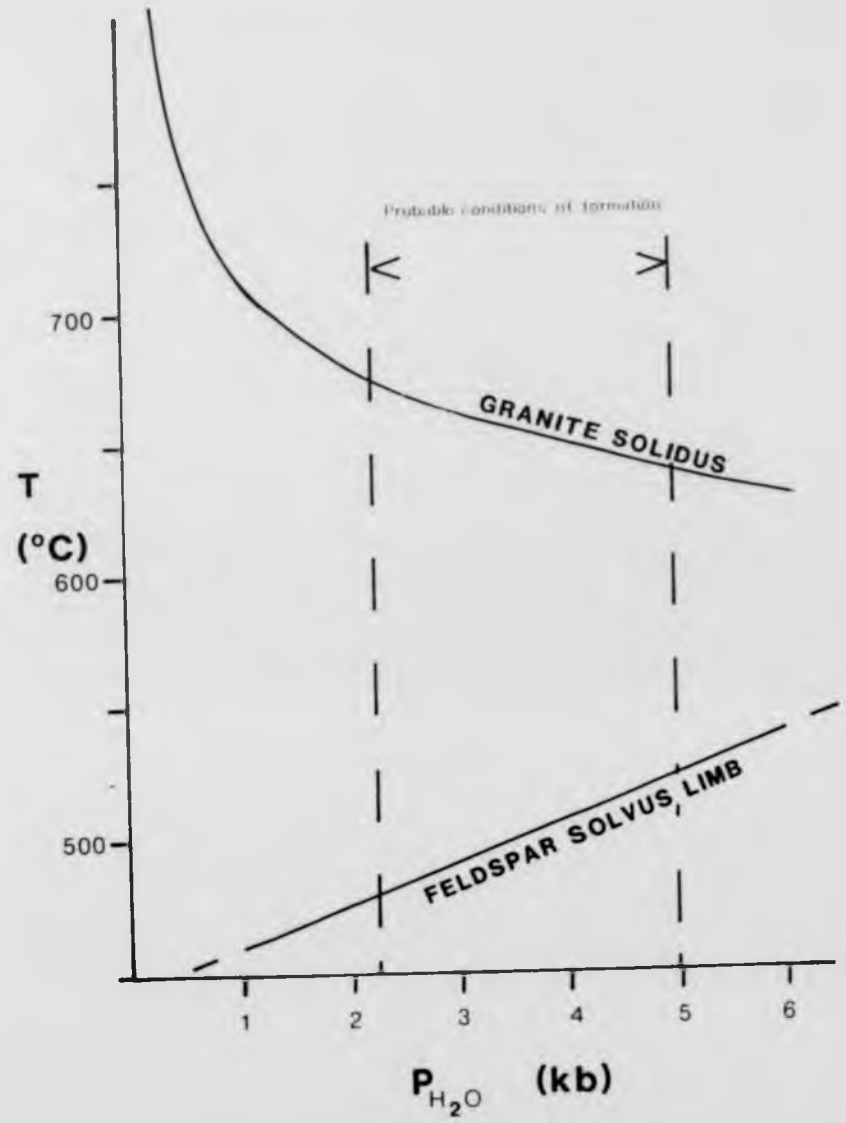

Chapter 6

Chemical Analysis of the Alkali Feldspars

a) Compositional Variation

Approximately eighty samples of alkali feldspar from the Dragsmark area have been analysed for K_2O, Na_2O, CaO, MgO, Ba, Rb and Sr. These included megacrysts from traverses across the various bodies constituting the Dragsmark granites, bulk rock K-feldspar extracted from these granites, and multiple samples of a pegmatitic feldspar from Östersidan. All the localities are marked on Map 3. In addition, a number of megacrysts have been examined from similar granitic sheets at Sundsandvik (about 20km east of Dragsmark) and from the Assmunderöd augen granite; these are denoted BS and OR respectively. Tabulated chemical analyses are presented in Table B6.1 with details of analytical techniques in Appendix A. Table B6.2 shows the results of the replicate sampling of the Östersidan pegmatite; the standard deviations and co-efficients of variation from this study are used to indicate the likely errors associated with other analyses.

As is explained in Appendix A, the presence of minor amounts of quartz causes the analyses to total less than 100%, but introduces virtually no chemical contamination. Therefore, compositions normalized to 100% are used in the various diagrams in this work.

The orthoclase content ranges from 18% to 87%, with an average of 82% for Area 1 megacrysts (Table 6.1). CaO varies from less than 70ppm to more than 7000ppm (equivalent to c. 4% An). Rb, Sr and MgO are all of the order of 100 - 500ppm, whilst there is approximately ten times as much Ba (Table B6.1). Feldspars from Area 2 (traverses D and X) are distinguished by lower Ba and Sr contents (c. 1200ppm and c. 100ppm respectively

Table 6.1

Compositions of megacrysts from traverses across the Dragsmark granites.

Sample		mol % Or	mol % Ab	mol % An	Rb/K $\times 10^3$
AREA 1					
Top	B1	81.1	17.9	1.0	3.9
	B2	81.5	18.5	0.0	3.7
	B3	83.2	16.2	0.6	3.4
	B4	83.0	16.2	0.8	3.7
	B5	79.7	20.0	0.3	4.3
	B6	81.6	18.2	0.2	3.8
	B7	83.2	16.3	0.5	3.8
	B8	83.1	16.4	0.5	2.9
	B9	83.0	16.7	0.3	2.9
	B10	82.1	16.7	1.2	3.4
Base	B11	78.9	20.9	0.2	3.9
					av. 3.6
Base	C1	75.5	23.7	0.8	3.7
	C2	81.9	17.9	0.2	3.4
	C3	83.4	16.6	0.0	3.9
	C4	81.8	17.9	0.3	4.1
	C5	83.6	16.4	0.0	3.0
	C6	79.8	19.2	1.0	2.6
Top	C7	83.4	16.4	0.2	2.7
	C8	80.1	19.6	0.3	3.6
	C9	82.6	17.4	0.0	3.3
	C10	81.3	18.7	0.0	3.8
	C11	80.2	19.1	0.7	3.3
Base	C12	81.6	17.4	1.0	3.7
					av. 3.4
Base	E1	81.5	18.0	0.5	3.4
	E2	80.8	19.0	0.2	3.2
	E3	84.8	14.9	0.3	2.9
	E4	81.2	18.1	0.7	2.8
Top	E5	78.8	19.9	1.3	2.9

Table 6.1 (cont.)

Compositions of megacrysts from traverses across the Dragsmark granites.

Sample	mol % Or	mol % Ab	mol % An	Rb/K $\times 10^3$
AREA 1				
Base F1	84.6	14.6	0.8	3.5
F2	80.0	18.7	1.3	2.9
F3	76.8	22.9	0.3	3.0
F4	78.9	20.6	0.5	2.8
xF5	77.4	30.3	2.3	3.6
Top xF6	76.6	22.4	1.0	4.2
				av. 3.3
AREA 2				
D1	85.1	14.9	0.0	3.1
D2	74.3	25.2	0.5	5.2
D3	73.6	26.4	0.0	5.4
D4	74.2	25.1	0.7	5.7
D5	81.6	18.4	0.0	4.4
D6	78.3	20.7	1.0	5.6
D7	82.6	17.1	0.3	4.5
D8	18.7	77.5	3.8	6.1
D9	86.6	13.1	0.3	5.0
				av. 5.0
X1	82.1	16.6	1.3	4.0
X2	72.4	26.3	1.3	3.6
X3	76.8	23.2	0.0	5.0
X4	54.7	43.5	1.8	4.7
X5	36.0	59.9	4.1	2.8
X6	77.9	21.3	0.8	3.1
X7	81.6	17.9	0.5	4.4
X8	81.1	18.4	0.5	4.5
X9	71.3	27.8	0.9	3.8
X10	83.5	16.5	1.0	4.2

x - much xenolithic material

cf. 2500ppm and 200ppm for Area 1). The samples from Sundsandvik and Orust are chemically indistinguishable form those from Dragsmark, except that they are slightly more calcic.

Heier (1962) presents a review of the principles governing the chemistry of alkali feldspars and of the empirical data then available. In natural systems, the composition of potassium feldspar is dominated by K and Na, although substantial substitution by Rb can occur, especially in pegmatites, and celsian, the Ba-feldspar, is not unknown. All these elements, together with Ca and Sr, substitute exclusively into the 'alkali' position in the lattice. The structural position of Mg is uncertain: it may behave like Ca, or be associated with Fe in the tetrahedral site.

Taylor and Heier (1960) demonstrate that a plot of Rb v Ba can be used to discriminate between feldspars from large pegmatites and from other 'granitoid' rocks, as a result of the effects of the fractionation processes involved in the former. All the feldspars from Dragsmark fall outside the 'large pegmatite' field (Fig. 6.1).

A more complete survey of chemical variation in alkali feldspars from 'granites' is given by Smith (1974). Fig. 6.2 shows a number of variation diagrams comparing data for the two Areas of Dragsmark granite with this 'granite' field. All the plots show some separation between feldspars from Areas 1 and 2, with the latter tending to fall outside the 'granite' field (Fig. 6.2B, C and F). Examination of these diagrams suggests that the megacrysts from Area 2 are characterized by lower than 'normal' Ba and Sr content. The three feldspars with abnormally low Or content are nos. X4, X5 and D8 (Table 6.1) and are discussed further in Ch.7c.

Rubidium behaves very coherently with respect to potassium, and

consequently the Rb/K ratio can be changed only by considerable fractionation. This is the cause of the marked Rb enrichment observed in late-stage alkali feldspars (Taylor and Heier, 1960). Rb/K ratios for the samples from Dragsmark are given in Table 6.1 .

Using experimentally determined distribution coefficients between potassium feldspar and silicate melts, Gordienko and Krivovichev (1978) derive graphical relationships between the Rb/K and Ba/K ratios in feldspars and the 'degree of crystallization' (раскристаллизации) of the system. Shmakin and Makagon (1979), in a critical reply to the above, refute these findings, claiming instead that the trace element geochemistry is controlled largely by pressure, inasmuch as the Ba/Rb ratio in the outermost zones of pegmatites varies with 'specialization' and hence depth of formation. Changes in pressure of the order of several kilobars during the course of crystallization of a pegmatite are envisaged.

In the case of the Dragsmark granites, it is difficult to conceive of there being any great difference in the pressure or temperature prevailing at the times of formation of the alkali feldspar megacrysts from the two Areas (see also Ch.7). It is therefore suggested that the theories of Gordienko and Krivovichev (1978) can be applied in at least a qualitative manner to the Dragsmark granites. This is illustrated in Fig. 6.3 .

It can be seen from the Figure that the Rb/K data (Table 6.1) indicate an average 'degree of crystallization' of c.50% for Area 1 megacrysts and c.75% for Area 2 (Fig. 6.3A). The Ba/K ratios (Fig. 6.3B) seem to imply much lower 'degrees of crystallization', but it should be noted that there is considerable uncertainty as to the precise position of the 'fractionation trend', and furthermore that the shape of the curves renders this ratio unsuitable for use in the later stages of crystallization.

Despite all these difficulties it can reasonably stated that the geochemical evidence implies that the Dragsmark granites were more crystalline at the time of growth of the megacrysts from Area 2 than of those from Area 1. This supports the hypothesis advanced in Chapters 3 and 5 of a magmatic origin for typical Area 1 megacrysts and a porphyroblastic origin for typical Area 2 megacrysts.

Examination of Table 6.1 shows that traverses C and E exhibit lower Rb/K ratios at the top of the relavant portion of the Area 1 granite than at the base (2.6 - 30 cf 3.2 - 4.1). Note that traverse C is across an overfold (see Ch.4, Fig. 4.11) and that samples C5, C6 and C7 are nearest to the top. This implies that the magmatic alkali feldspars in the upper parts of the main sheet of Dragsmark granite are less differentiated than those lower down, which suggests that the body crystallized from the roof downwards. This would be expected if the intrusion were emplaced at a relatively high level in the crust, as most heat loss would then take place through the upper surface of the sheet. The same argument accounts for the less differentiated nature of the south-western termination of this sheet: average Rb/K values for traverses E and F are 3.0 and 3.3 respectively, cf 3.6 and 3.4 for traverses B and C (Table 6.1, see also Map 3).

The variation in alkali feldspar chemistry is conveniently demonstrated by the use of triangular plots. Such representations are particularly suitable where it is the ratios between pairs of elements that is of interest, rather than the absolute contents. For example, the actual Rb content is largely a function of the % Orthoclase and is of no great value, but the Rb/K ratio is of importance. With analyses for seven elements, there are clearly dozens of possible triangular plots; many of these however are subject to excessively large analytical errors which render them useless. Those plots which are considered of interest are given in Figs. 6.4 and 6.5 . Data from traverse A (the minor body at

Klostergård assigned to the Källviken granite) are coincident with data from Area 1 and are omitted from the diagrams for clarity.

It is apparent from the above Figures that megacrysts from the two Areas of Dragsmark granite form two distinct populations, although there is some overlap. This is to be expected, as it is not proposed that the two modes of formation of megacrysts suggested for the two Areas are mutually exclusive. In particular, most specimens from Area 2 (the overlying sheets) can be seen to be enriched in Rb and depleted in Ba and Sr with respect to those from Area 1 (Fig. 6.4A and B). They also exhibit slightly higher Rb/K ratios (Table 6.1 and Fig. 6.4B), but the Ba/Sr ratio is approximately constant (Fig. 6.4A). On the K/100 - Na/10 - Ba plot (Fig. 6.5A) and the equivalent Sr plot (Fig. 6.5B), two trends are discernible. Megacrysts from Area 1 appear to have constant K/Na ratios (i.e. orthoclase content), whilst those from Area 2 have roughly constant K/Ba and K/Sr ratios. The two trends intersect at the low-Ba (and low-Sr) end of the 'Area 1 trend' (Fig. 6.6).

The megacrysts of Area 1 of the granite can thus be seen to show a progressive depletion in Ba and Sr with a concomitant enrichment in Rb, which phenomena can readily be interpreted as the result of trace element fractionation. As these crystals are believed to be magmatic in origin, their K_2O content would be expected to be buffered by the silicate melt causing there to be little variation in orthoclase content. This is indeed the case.

Assuming the hypothesis of a porphyroblastic origin for most Area 2 megacrysts to be correct, the absolute quantities of both the relevant elements and of the total energy of the system would be several orders of magnitude less than in a silicate magma. There would thus be no chemical buffering of mineral compositions or mineral assemblage, nor

could the temperature be expected to be constant. It is not known why this should result in constant K/Ba, K/Sr and K/Rb ratios; it may perhaps be that the availability of Na was the limiting parameter in determining mineral chemistry. Furthermore, in the granite system, lowering the temperature does result in more sodic alkali feldspars (Tuttle and Bowen, 1958).

The envisaged crystallization history for the megacrysts is summarized below and in Fig. 6.6 . The earliest magmatic alkali feldspars were potassic and relatively barium (and strontium) rich and rubidium poor. With continued fractionation, the orthoclase content remained roughly constant, Ba and Sr decreased markedly and there was a slight increase in the Rb/K ratio. The 'Area 2 trend' commences at the most evolved end of this 'magmatic trend' (with some overlap), but the direction of chemical change is markedly different. It is now the orthoclase content that varies greatly, the crystals becoming more sodic, presumably in response to falling temperature, whereas the significant trace elements behave coherently with respect to potassium.

b) Megacryst - Groundmass Relationships

It is obviously not possible to extract all the megacrysts from a hand-specimen in order to analyse the groundmass. The bulk rock alkali feldspar, that is the total feldspar in a sample, will however be a composite of the megacrysts and groundmass. Granted that the compositional range of the megacrysts is known, it is thus possible to obtain information concerning the groundmass. Analyses of 24 bulk rock feldspars are given in the Appendix (Table B6.1). One of these (no.30) is from the Kållviken granite, four (nos. 72, 418, 888 and 891) are from Area 2 of the Dragsmark granite; the remainder are from Area 1 (Map 3). Figs. 6.7 and 6.8 show these data on triangular plots together with the fields occupied by megacrysts from the two Areas.

The majority of bulk rock feldspars fall within the compositional range of Area 1 megacrysts, but a number of points representing samples from Area 1 plot some distance further along the 'magmatic evolution' trend. This implies that the groundmass alkali feldspar is more fractionated than the megacrysts, as would be expected if the latter are phenocrysts. There is also overlap between the least fractionated Area 2 megacrysts and the bulk rock feldspar (Figs. 6.7 and 6.8). This could be interpreted as supporting the hypothesis put forward in Ch.3b for as origin of the porphyroblasts by recrystallization of the groundmass.

c) Electron Microprobe Analysis

The possibility of fine-scale chemical variation was investigated using electron microprobe line-scanning traverses across megacrysts. The study was carried out on the Cambridge Microscan II operating in wavelength-dispersive mode at the University of Aberdeen. Elements were analysed in pairs, three runs being required for Si-Al, K-Na and Ba-Ca. The sample scan speed was 30μ/min and consequently traverses of over 1000μ were impracticable. Analyses integrated over the whole traverse, together with scan lengths, are given in Table 6.2 . Because the feldspars are so coarsely perthitic a sampling bias is introduced, the relatively short lengths resulting in under-representation of the sodic lamellae and hence higher orthoclase contents than those indicated by wet chemical methods (compare Table 6.1 with Table 6.2). This discrepancy has been noted by Higgins and Kawachi (1977) and Brown et al (1983), and makes direct comparison between the two techniques difficult. The same problems apply to barium, as it behaves coherently with respect to potassium.

Typical traverses across megacrysts from Areas 1 and 2 of the Dragsmark granite are shown in Fig. 6.9 . From these it can be seen that, in general, K-Ba and Na-Ca behave as coherent pairs of elements, with an antipathetic relationship to each other. The samples from Area 2 (nos. 888/2, 891) are string/crypto perthites, and this is reflected in their very homogeneous nature (Fig. 6.9) as contrasted with the coarse microcline perthites of Area 1. From Table 6.2 it can be seen that the former have lower Ba contents (2500ppm cf 4000ppm).

Although continuous profiles across complete megacrysts were precluded by their size (except for no.53/2), changes in composition from core to rim were searched for in three samples using several scans averaging 500μ in length spaced across the crystals. Fig. 6.10 shows the positions of these scans within megacrysts whilst the analyses are given

Table 6.2

Electron Microprobe Analyses of Alkali Feldspar Megacrysts

Sample	wt.% K_2O	wt.% Na_2O	Ca (ppm)	Ba (ppm)	% Or	length (μ)
AREA 1						
53/1	14.63	1.21	621	4261	89	414
53/2	14.42	1.28	926	4129	89	1038
Core 818/4	14.02	1.47	792	4383	87	456
818/3	14.20	1.23	1414	5269	89	510
818/2	14.28	1.36	761	5219	88	516
818/5	14.55	1.09	428	4646	90	435
Rim 818/1	13.57	1.22	447	4377	89	492
Core 821/6	15.16	1.14	395	4023	90	444
821/5	14.91	1.25	554	2185	89	795
821/4	12.95	1.86	640	2458	83	621
821/1	14.31	1.57	359	2107	87	525
821/2	15.01	0.93	572	1659	92	378
Rim 821/3	14.26	1.30	524	1230	88	561
Core 823/3	14.87	0.91	478	4536	92	237
823/2	12.66	1.64	398	4627	84	279
Rim 823/1	13.28	2.06	965	3276	82	975
AREA 2						
888/1	14.90	1.30	549	2644	89	312
888/2	15.64	1.37	416	2429	89	870
891	13.32	0.98	384	2551	90	879

in Table 6.2 , in sequence from core to rim.

Only in no.823 is zoning of the orthoclase content observable, with the rim being 10% more sodic than the core. All three however exhibit zonation of the barium content which decreases from the centre to the rim (with some variation). This is illustrated in Fig. 6.11 , from which it is apparent that individual megacrysts from Area 1 show the same fractionation pattern on a microscopic scale as does the whole sheet. This provides conclusive evidence for the occurrence of trace element fractionation within the granitic magma during the growth of the alkali feldspar megacrysts.

Zonation of barium content in megacrysts, with Ba decreasing from core to rim, is noted by Dickson and Sabine (1967) and Higgins and Kawachi (1977). Those studied by the latter are very similar to some of the Dragsmark feldspars, having aligned inclusions of plagioclase and biotite and being apparently euhedral but with very irregular margins (see p.29). Boettcher et al (1967) and Mehnert and Büsch (1981) have published electron microprobe line scans across megacrysts which reveal a fine-scale oscillatory zoning superimposed on this coarse variation in barium content. The crystals used in the former study were non-perthitic low-triclinicity microclines, whilst the latter authors claim that perthitic lamellae had no detectable effect on the Ba content recorded, although they were observable on the K and Na traces.

Such fine zoning is also to be found in alkali feldspars from the Dragsmark granites, but its detection is complicated by their coarsely perthitic nature. Any primary variation in barium content is clearly likely to be obscured by the presence of virtually Ba-free albitic lamellae (Fig. 6.9). The approach was therefore adopted of investigating the Ba/K ratio, as this should not be drastically affected by exsolution processes.

This was performed in a semi-quantitative manner by visual comparison of the K and Ba traces on profiles such as those shown in Fig. 6.9 . A more accurate method would have been to integrate the analyses every few seconds during line scanning. The results of this investigation are shown in Fig. 6.12. The term 'positive Ba anomaly' is used to indicate a region where the Ba/K ratio is higher than the average.

Two important points arise in connection with Fig. 6.12 . Firstly, the symmetrical distribution of positive and negative Ba anomalies about the core of no.53/2 demonstrates that the anomalies are real, and not an artifact of the method. Secondly, the complete lack of correlation between the Ba anomaly patterns and the positions of perthitic lamellae shows that the anomalies are not the result of exsolution. It may therefore safely be concluded that the oscillatory zonation of the Ba/K ratio indicated in Fig. 6.12 is a primary feature of the alkali feldspar megacrysts of the Dragsmark granite.

Examination of Fig. 6.12 shows that this phenomenon is restricted to megacrysts from Area 1, that is to megacrysts believed to be of magmatic origin. The zones appear to be present throughout those crystals within which several traverses have been made (nos. 818, 821, 823) and to have thicknesses of between 40 μ and 250 μ. The zones in the celsian-rich feldspars studied by Boettcher et al (1967) are 100 - 200 μ thick (their Fig.2).

Mehnert and Busch (1981) described a three-fold structure of alkali feldspar megacrysts from granites from the Black Forest, corresponding to three stages of formation. These are:

i) Core; relatively uniform and high Ba; early magmatic

ii) Shell; variable Ba, pronounced maxima; late magmatic

iii) Rim; low Ba; pegmatitic/hydrothermal.

The core is interpreted (ibid) as representing small (typically 1mm) early

phenocrysts which have been later recrystallized. Thin septa of quartz may mark the relict crystal boundaries (see Fig. 3.4A). The rim is typically a couple of millimetres wide, but xenomorphic, penetrating 'very "far" into the already crystallized matrix' (ibid, p.247). No distinct rims were detected on Dragsmark samples during line scanning (but see Fig. 3.5C); this stage may be represented by the abundant 'pseudopods' (p.30). The shells of Black Forest megacrysts are characterized by strongly asymmetric Ba-rich zones which vary between 200μ and 600μ thick. The sense of asymmetry is constant, with the Ba-content increasing sharply then waning slowly (from core to rim). Concentrically distributed aligned inclusions of plagioclase are very common.

Mehnert and Büsch (1981) tentatively propose that these shells may be formed in an analogous manner to zoning in plagioclase i.e. as a result of disequilibrium crystallization. Despite the differences between their specimens and megacrysts from Dragsmark, there seems no reason to reject this hypothesis.

Figure 6.1

Plot of Rb versus Ba for alkali feldspar megacrysts from the Dragsmark granite. The field occupied by large pegmatite feldspars (Taylor and Heier, 1960) is also shown.

o - Area 1 megacrysts

• - Area 2 megacrysts

6.1

ldspar megacrysts from the

pied by large pegmatite feldspars

hown.

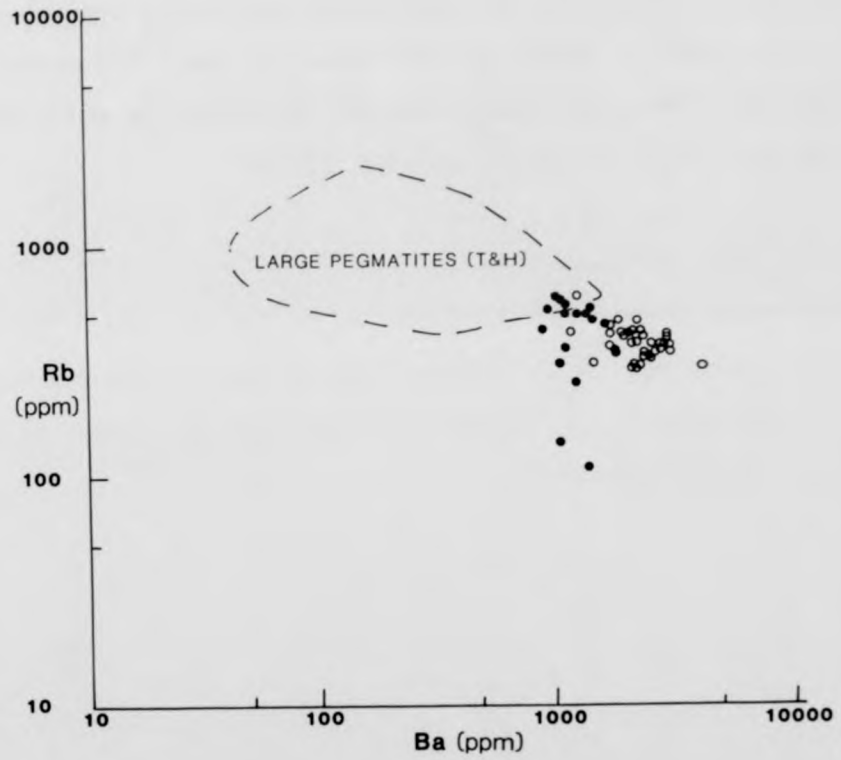

Figure 6.2

Plots of Rb, Sr, Ba, Mg contents and K/Rb and K/Ba ratios against wt% Orthoclase for alkali feldspar megacrysts from the Dragsmark granites. Also shown (dashed line) are the fields for alkali feldspars from granites (s.l.) taken from Smith (1974).

o - Area 1 megacrysts

• - Area 2 megacrysts (including sample nos. X4, X5 and D8)

⊢ - Error bars for the feldspar analyses derived from replicate analyses of the Östersidan pegmatite feldspar (shown in the correct position)

.2

K/Rb and K/Ba ratios against
egacrysts from the Dragsmark
are the fields for alkali feldspars
h (1974).

sample nos. X4, X5 and D8)
analyses derived from replicate
gmatite feldspar (shown in the

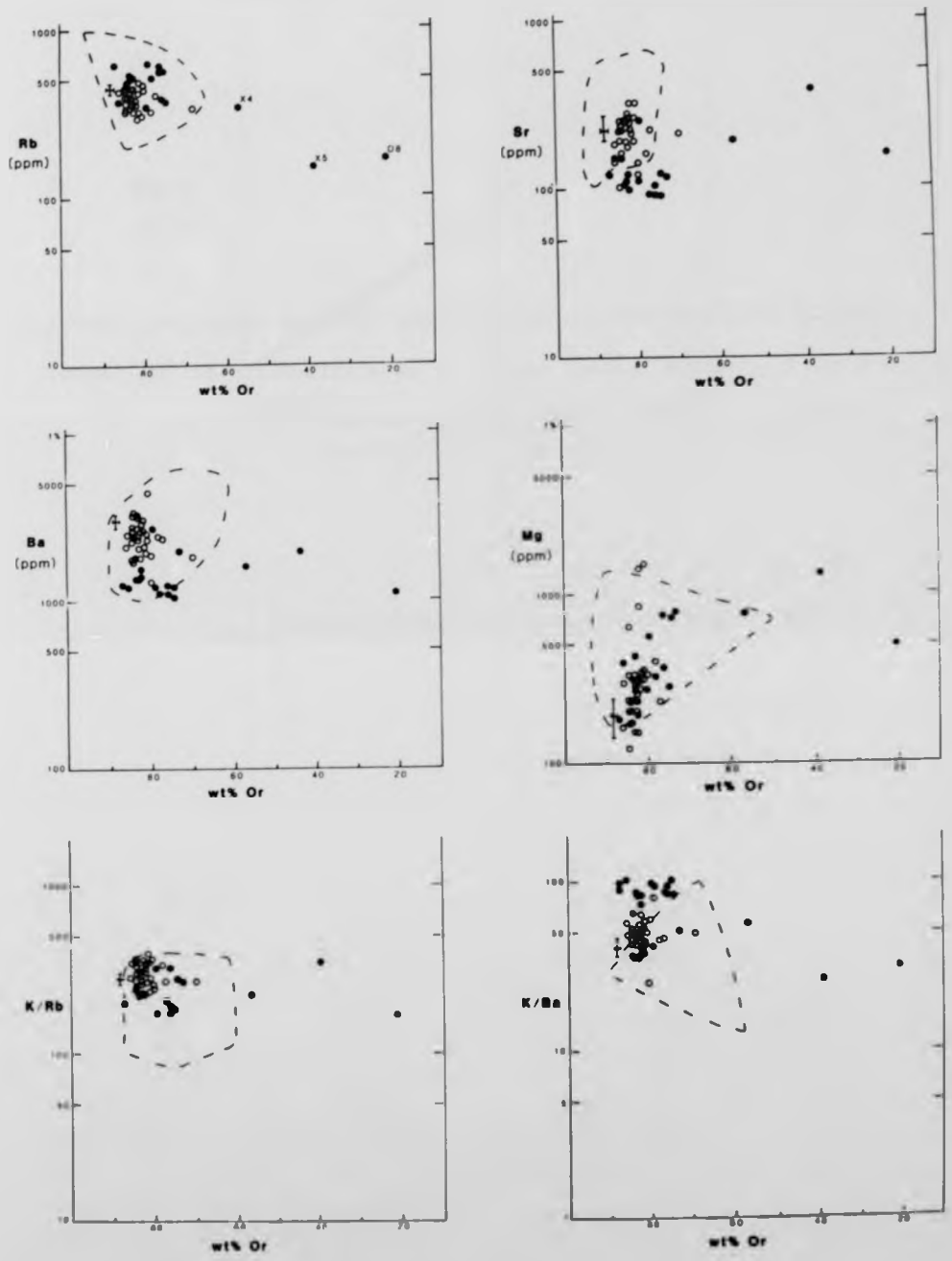

Figure 6.3

Plots of Rb/K and Ba/K ratios of alkali feldspar megacrysts from the Dragsmark granites against degree of crystallization of the magma. Curves from Gordienko and Krivovichev (1978).

A : $Rb/K \times 10^3$ versus Degree of crystallization

o - Area 1 megacrysts

• - Area 2 megacrysts

B : $Ba/K \times 10^3$ versus Degree of crystallization

Symbols as for A.

Dashed lines indicate degree of uncertainty in the position of the curve.

6.3

lkali feldspar megacrysts from the

of crystallization of the magma.

hev (1978).

rystallization

rystallization

of uncertainty in the position

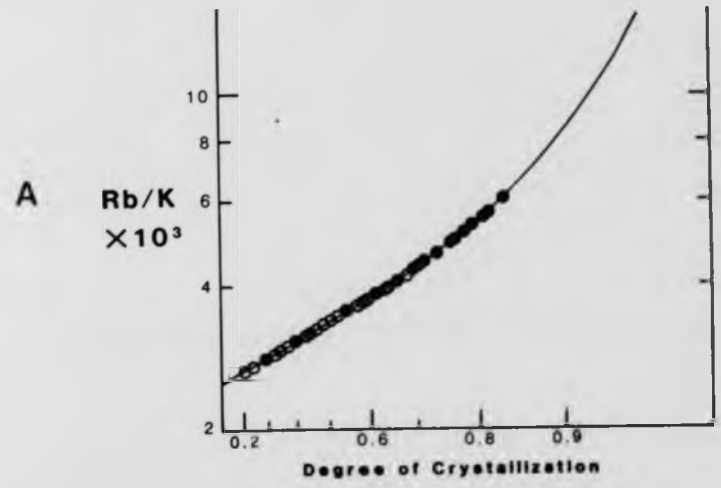

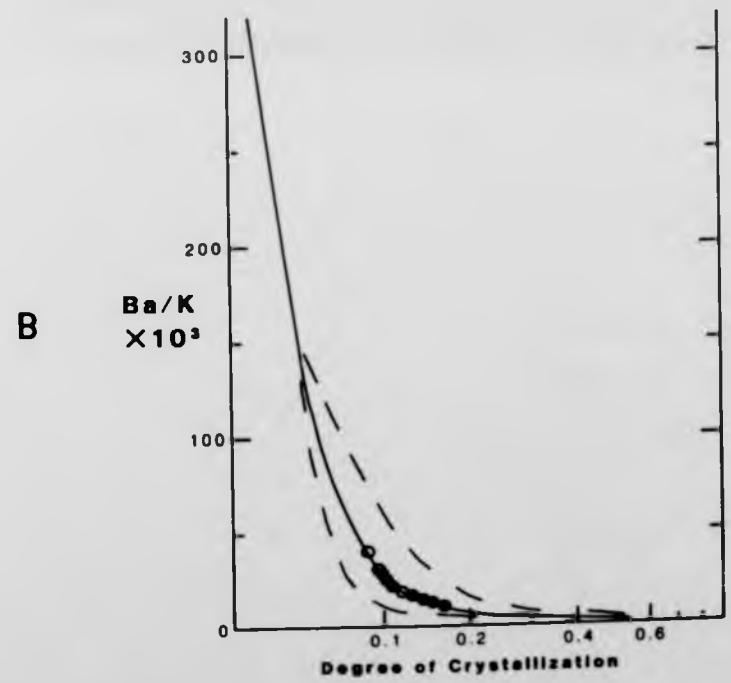

Figure 6.4

Triangular compositional plots for alkali feldspar megacrysts from the Dragsmark granites.

Data are plotted by normalization to 100 wt% of the species indicated at the apices.

The area of error of replicate analyses of the Ostersidan pegmatite is indicated thus : ⟨P⟩ . This is displaced from its true position for clarity.

A : Ba - Rb - Sr

o - Area 1 megacrysts

● - Area 2 megacrysts

B : K/100 - Rb - Sr x 10

Symbols as for A.

6.4

alkali feldspar megacrysts

to 100 wt% of the species indicated

lyses of the Ostersidan pegmatite

is displaced from its true

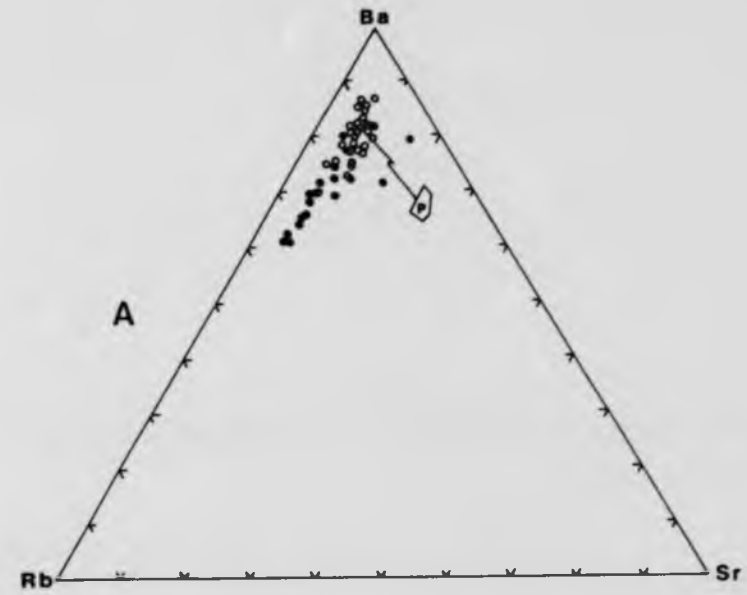

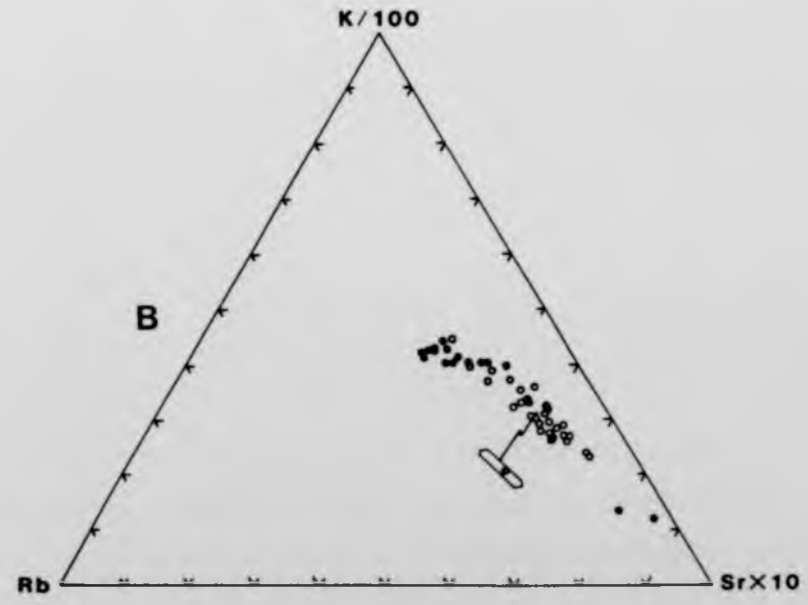

Figure 6.5

Triangular compositional plots for alkali feldspar megacrysts from the Dragsmark granites.

Derivation as for Fig. 6.4

o - Area 1 megacrysts

• - Area 2 megacrysts

A : K/100 - Na/10 - Ba

B : K/100 - Na/10 - Sr x 10

The bulk composition in wt% Or is indicated on the left-hand side. Note that the nature of the plot is such as to spread out the more potassic compositions relative to the sodic feldspars.

6.5

alkali feldspar megacrysts from

indicated on the left-hand side.

is such as to spread out the more

the sodic feldspars.

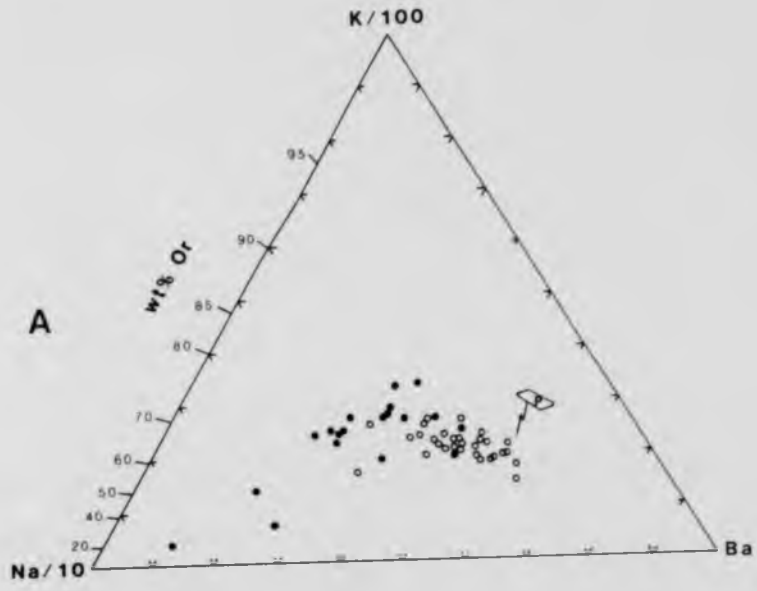

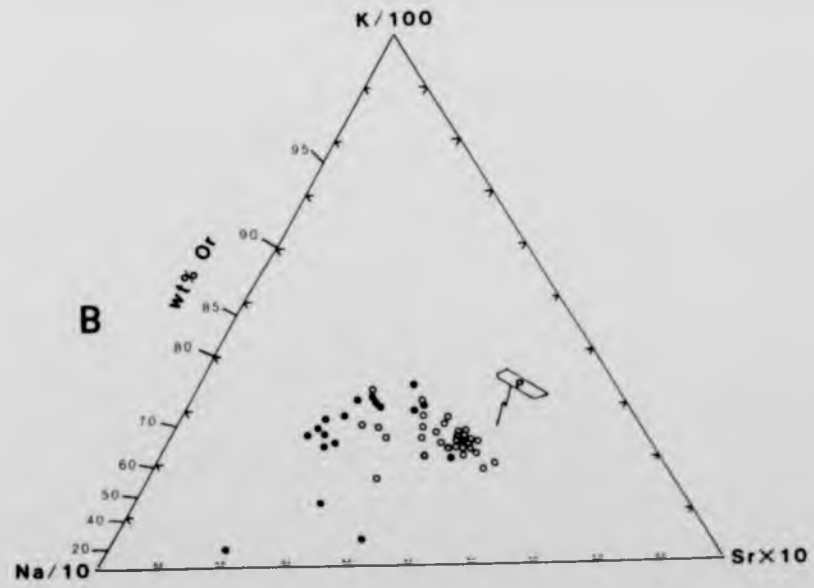

Figure 6.6

K/100 - Na/10 - Ba triangular plot showing the distinct fractionation trends exhibited by alkali feldspar megacrysts from the two Areas of the Dragsmark granite. The Rb characteristics associated with the two populations of megacrysts are also given. The trends intersect at the low-Ba end of the magmatic Area 1 trend.

e 6.6

t showing the distinct fractionation
ar megacrysts from the two Areas of
aracteristics associated with the two
o given. The trends intersect at the
trend.

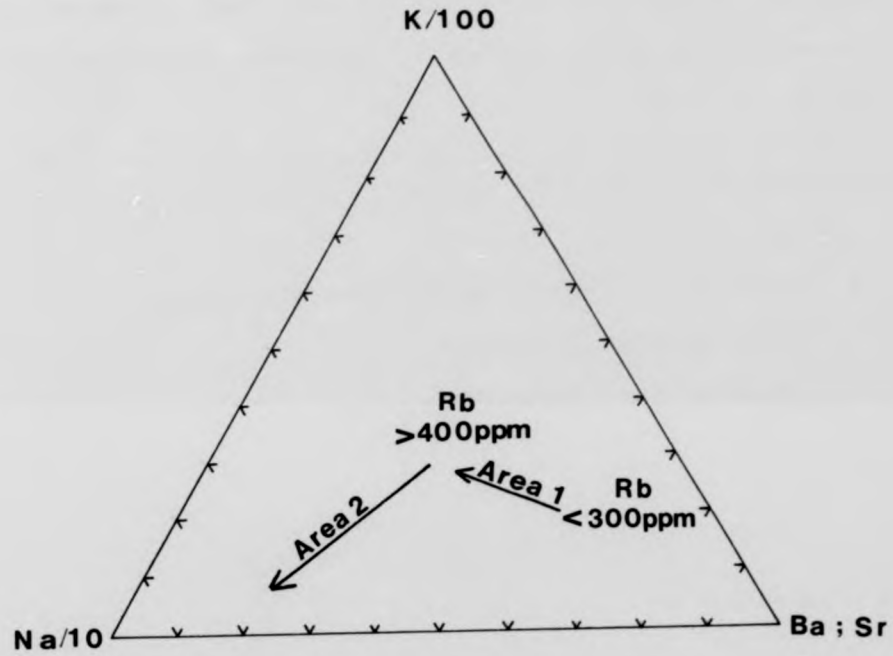

Figure 6.7

Triangular compositional plots for bulk rock alkali feldspars from the Dragsmark granites, together with the fields occupied by megacrysts from the two Areas.

Derivation as for Fig. 6.4

▲ - Bulk rock feldspar (groundmass plus megacrysts)

- Field of Area 1 megacrysts

- Field of Area 2 megacrysts

A : Ba - Rb - Sr

B : K/100 - Rb - Sr x 10

.7

ulk rock alkali feldspars from

h the fields occupied by megacrysts

s plus megacrysts)

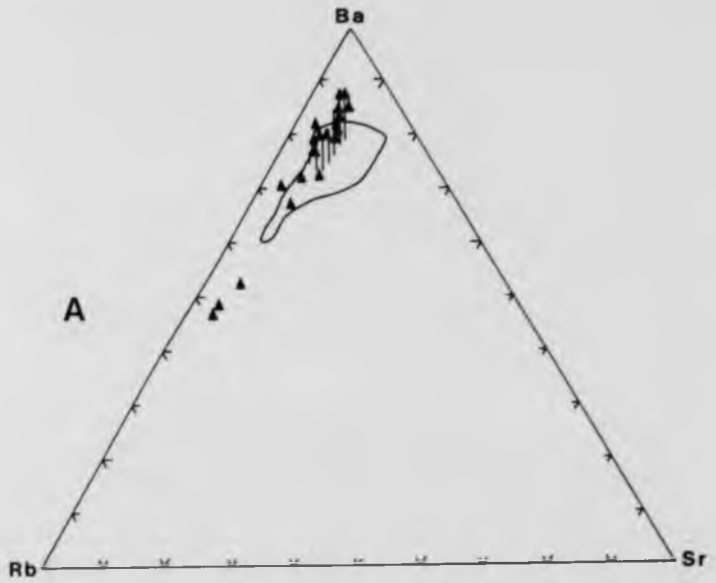

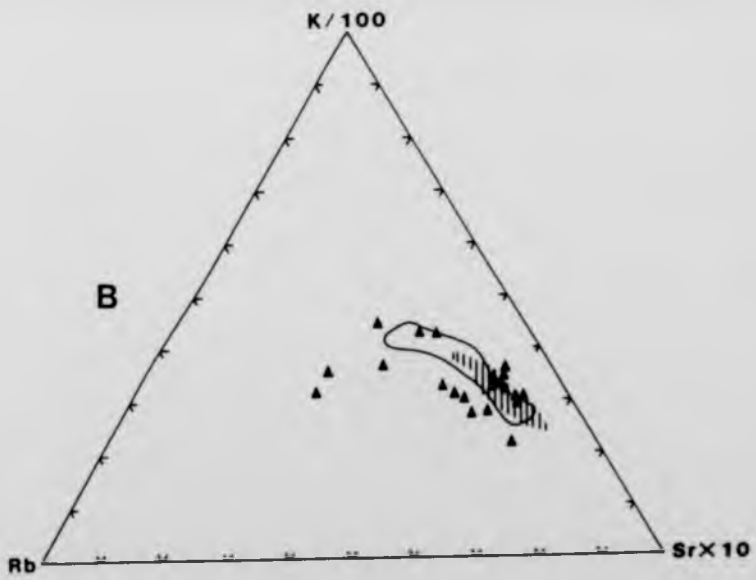

Figure 6.8

Triangular compositional plots for alkali feldspars (bulk rock) from the Dragsmark granites, together with the fields occupied by megacrysts from the two Areas.

Derivation as for Fig. 6.4

▲ - Bulk rock feldspar (groundmass plus megacrysts)

- Field of Area 1 megacrysts

- Field of Area 2 megacrysts

A : K/100 - Na/10 - Ba

B : K/100 - Na/10 - Sr x 10

6.8

alkali feldspars (bulk rock)

er with the fields occupied by

ass plus megacrysts)

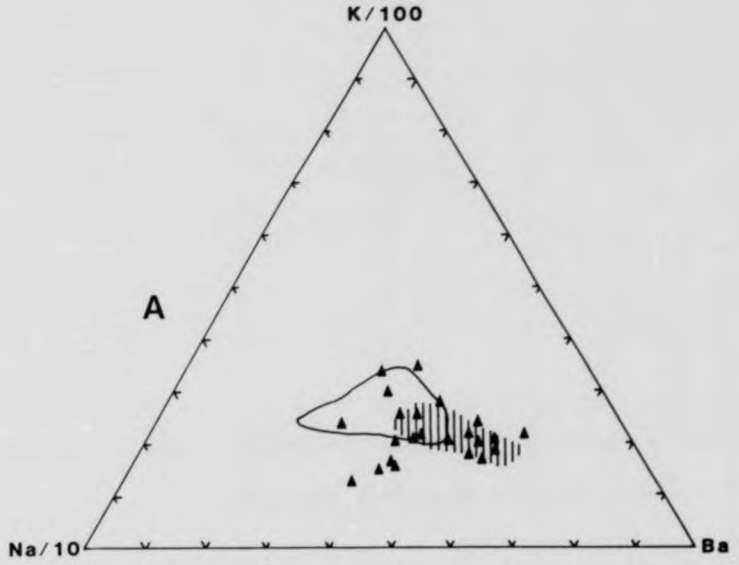

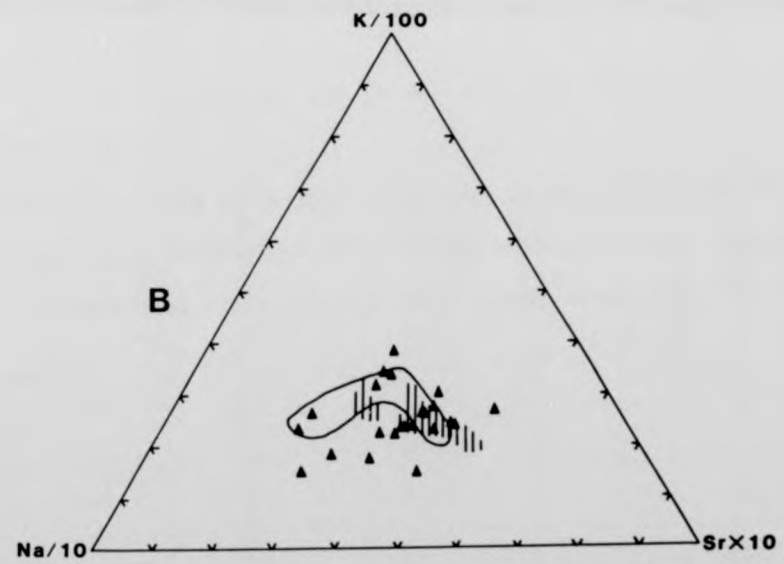

Figure 6.9

Representative electron microprobe wavelength dispersive scans across megacrysts from the Dragsmark granites.

Megacrysts nos. 53 and 818 (top) are from Area 1; megacrysts nos. 888 and 891 (bottom) are from Area 2.

Continuous profiles are given for K, Na, Ba, and Ca.

Very intense peaks can be correlated microscopically with albitic exsolution lamellae; their absence from the samples from Area 2 is consistent with these latter being string/crypto perthites.

Figure 6.9

Representative electron microprobe wavelength dispersive scans across megacrysts from the Dragsmark granites.

Megacrysts nos. 53 and 818 (top) are from Area 1; megacrysts nos. 888 and 891 (bottom) are from Area 2.

Continuous profiles are given for K, Na, Ba, and Ca.

Very intense peaks can be correlated microscopically with albitic exsolution lamellae; their absence from the samples from Area 2 is consistent with these latter being string/crypto perthites.

6.9

wavelength dispersive scans

rk granites.

re from Area 1; megacrysts nos. 888

K, Na, Ba, and Ca.

ed microscopically with albitic

from the samples from Area 2 is

string/crypto perthites.

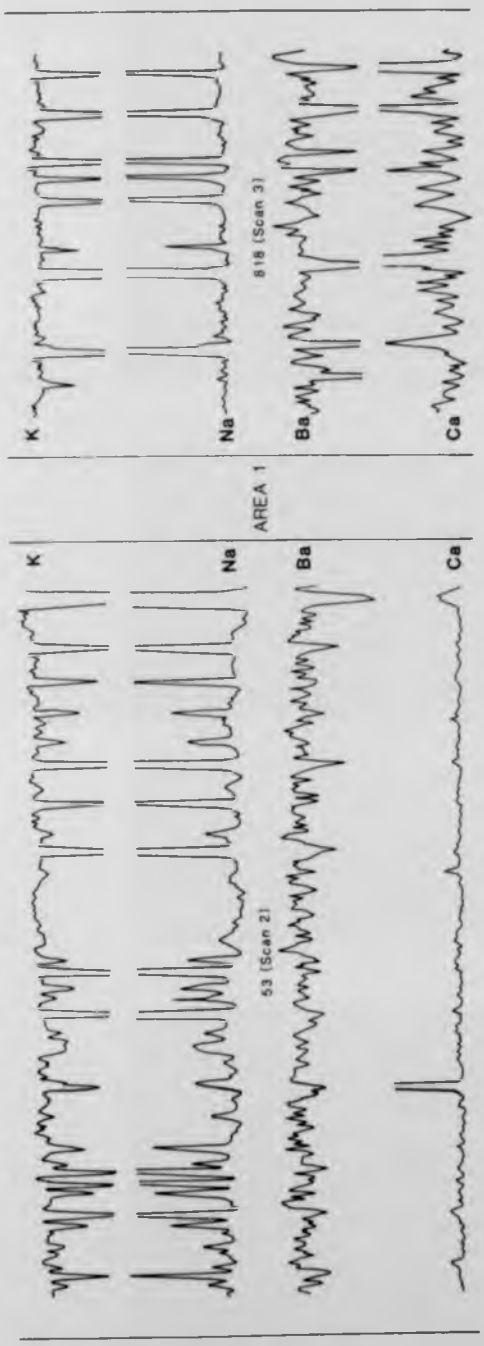

Figure 6.10

Photomicrographs of the alkali feldspar megacrysts from the Dragsmark granite across which electron microprobe scan analyses were carried out.

A : Sample no. 818

B : Sample no. 821

C : Sample no. 823

par megacrysts from the Dragsmark

robe scan analyses were carried out.

par megacrysts from the Dragsmark

robe scan analyses were carried out.

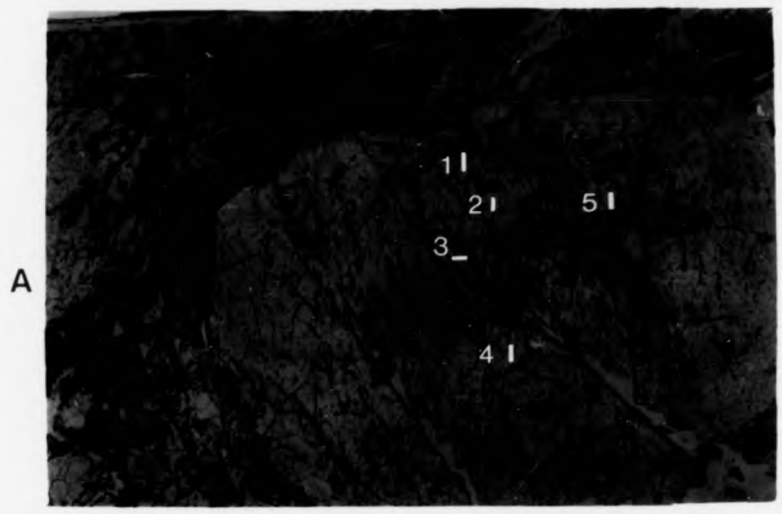

Figure 6.11

K/100 - Na/10 - Ba triangular compositional plot for alkali feldspar megacrysts from the Dragsmark granites.

The compositional trends yielded by electron microprobe scans positioned from core to rim of megacrysts are compared with the fields occupied by megacrysts from the two Areas (analysed by wet chemistry).

The large arrows indicate the sense of the fractionation that can be assumed to have occurred.

● - Megacryst no. 821
▲ - Megacryst no. 823

both from Area 1

6.11

...itional plot for alkali feldspar

...es.

... electron microprobe scans

...rysts are compared with the fields

... Areas (analysed by wet chemistry).

... of the fractionation that can

...th from Area 1

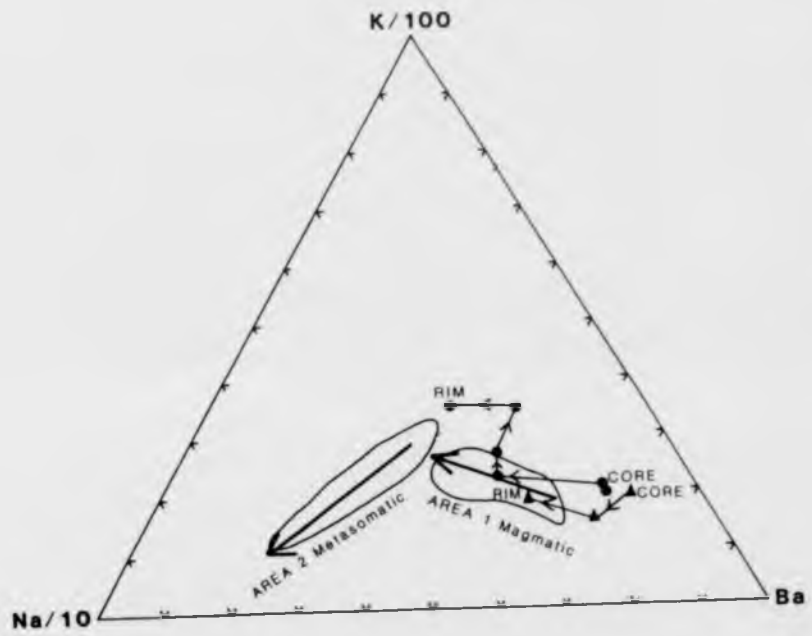

Figure 6.12

Semi-quantitative Ba anomalies revealed by electron microprobe analyses across alkali feldspar megacrysts from the Dragsmark granites (see text p. 69).

The positions of perthitic lamellae are shown, and there is no correlation with Ba anomalies.

Only those megacrysts from Area 1 exhibit oscillatory zonation of the anomalies, with zones ranging in thickness from 40μ to 250μ.

2

d by electron microprobe analyses

the Dragsmark granites (see text

e shown, and there is no

bit oscillatory zonation of the

ness from 40μ to 250μ.

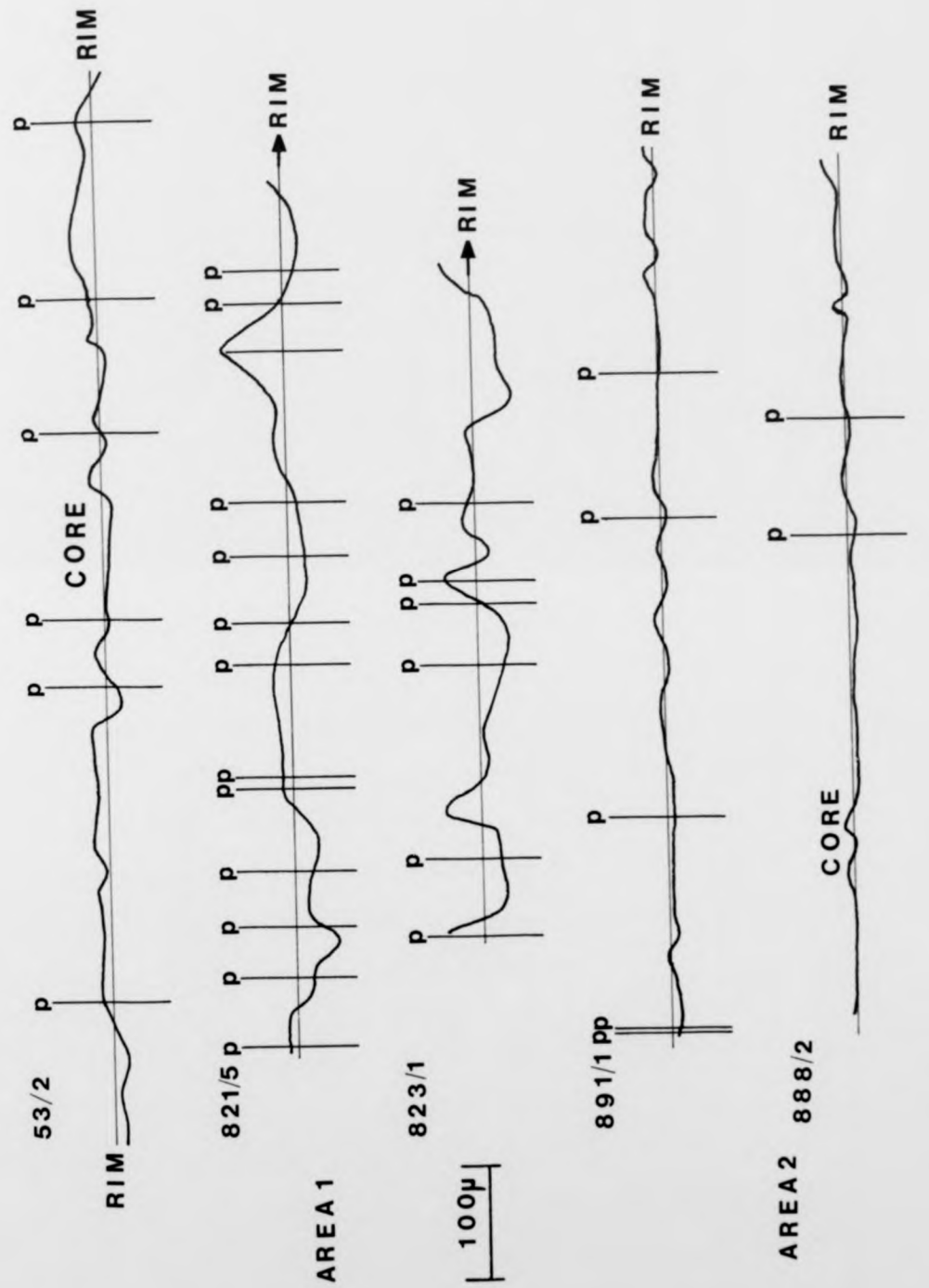

Chapter 7

Conditions of Formation of the Granite

a) Fluid Inclusion Geothermometry

When crystals grow or recrystallize in a fluid medium, growth irregularities at the crystal surface trap small amounts of fluid which become inclusions. In their unaltered state, such inclusions are therefore samples of the fluid which coexisted with the mineral at the time of its growth. This is the fundamental premise of fluid inclusion geothermometry. Its validity will be greatly affected by subsequent modifications to the system, and much effort has been directed towards ascertaining grounds for recognition of unaltered inclusions.

The most prominant feature of fluid inclusions is the presence of a vapour or gas bubble in the liquid. This bubble forms on cooling because the volume co-efficient of thermal expansion of minerals is much less than that of water (and most liquids) and hence the 'container' shrinks much less than the fluid. When the pressure in the inclusion is equal to the relevant vapour pressure, a bubble should nucleate and grow. In the mid-nineteenth century, Sorby (1858) recognized that this process should be reversible by simply heating until homogenization occurred, thus obtaining the temperature of trapping (after applying a pressure correction). Much of the recent work has been published by Roedder and a detailed bibliography is given in Roedder(1979).

The major assumptions involved in the use of homogenization temperatures as a geothermometer are (ibid):

i) The fluid was originally a single homogeneous phase

ii) The effects of pressure on the system are known

iii) The origin of the inclusions (whether primary or secondary) is known.

Heterogeneous systems are rare in nature and readily identified by large variations in phase ratios between inclusions: no significant variation was observed in the samples from Dragsmark. The absence of two immiscible fluids from inclusions at room temperature implies that the CO_2 content is less than 5 mole % (Takenouchi and Kennedy,1964). The presence of dissolved NaCl reduces the solubility of CO_2 in water (ibid) and this is therefore the maximum possible value.

Fisher (1976) presents the volumetric properties of pure water under conditions from 0 - 1,000^{o}C and 1 - 10,000 bars in graphical format. Making the assumption of constant density above the boiling curve, these enable calculation of a line in P-T space for any given homogenization temperature; the conditions of formation of the inclusion must lie on this line. The volumetric properties of the fluid are affected by the concentration of salts (commonly NaCl) in solution. Because of the problems of metastability in small inclusions (Roedder,1979) no freezing point determinations of composition were made in the present study, but the absence of daughter halite crystals places an upper limit of c. 25 % on the NaCl concentration. Most magmatically derived hydrothermal ore deposit fluids fall in the range 0 - 5 wt.% NaCl-equivalent (ibid) and this range is thus used here. Extrapolation of data presented by Potter (1977) for pressures up to 2kb for various salt concentrations shows that the errors thus introduced are minimal (less than 10^{o}C) in the P-T region of interest.

The area of greatest uncertainty, and the probable source of the scatter commonly found in fluid inclusion studies, is the designation of individual inclusions as primary or secondary. Secondary inclusions are those which have resulted from recrystallization, usually along fractures, at some time after the formation of the crystal. Roedder (1979) has presented a table of criteria for distinguishing between the two, but many of these are often not applicable. The most useful criteria are that

primary inclusions are generally larger, isolated and randomly distributed throughout a crystal, whereas secondary inclusions occur in planar groups outlining annealed fractures or cleavages and amy be very thin or show evidence of necking down. In the samples studied, many clearly secondary inclusions were faceted negative crystals, which present the lowest-energy surfaces.

A number of doubly-polished thin slivers suitable for fluid inclusion studies were made from samples of the Dragsmark granites. No inclusions which could be considered primary were observed in feldspars or in quartz crystals from the groundmass, although secondary inclusions were abundant in the quartz. Many of these contained only a single (liquid) phase. These findings are entirely in keeping with the geological setting - recrystallization could have occurred in the post-magmatic stage, during the D2 deformation or during the Sveconorwegian metamorphism. Using the above criteria, two-phase primary inclusions were however observed in rounded quartz inclusions within alkali feldspar megacrysts. Homogenization temperatures of these were determined using the methods outlined in Appendix A; the results are presented graphically in Fig. 7.1 with tabulated data in Table B7.1 .

Most of the phenomena which can affect primary fluid inclusions lower the apparent homogenization temperature. The major cause of scatter is necking down, that is local recrystallization of a large inclusion into several smaller ones. Such an event may also on occasion cause the formation of a two-phase inclusion which homogenizes well above the trapping temperature (Fig. 7.2). The homogenization value that should be taken as the uncorrected trapping temperature is therefore not the mean of the observed values, but the mode i.e. c.330^{o}C in the present study (Fig.7.1).

Using the data of Fisher (1976) and Potter (1977) for salinities of 0% and 5% NaCl respectively, the loci of possible conditions of form-

ation of the inclusions and hence the quartz can be shown on a P-T diagram (Fig. 7.3). The slope of this fluid inclusion line is such that it does not intersect any reasonable geotherm, the pressure correction being 105°C/kb. The possibility of the quartz and inclusions being inherited from an upper amphibolite facies precursor can therefore be discounted, implying that the quartz is of magmatic origin.

The presence of aqueous fluid inclusions thus requires that a free aqueous phase was present in the granite magma and hence the phase relationships for wet granite must be used. At any given pressure, the maximum temperature of formation of magmatic quartz is given by the quartz-in line. Under H_2O over-saturation conditions this lies some 30°C above the granite solidus, which represents the minimum possible temperature. The intersection of the fluid inclusion loci with these curves thus defines a very small area in P-T space within which the granite must have crystallized (Fig. 7.3). It is therefore concluded that the Dragsmark granite formed at a pressure of 3.4 - 3.2 kb and a temperature of 675 - 660°C under water over-saturated conditions.

b) Two-Feldspar Geothermometry/Geobarometry

For two feldspars in equilibrium, the chemical potential of albite in each phase must be equal:

$$\mu_{ab}^{AF} = \mu_{ab}^{PF} \qquad (1)$$

irrespective of the bulk composition or mineralogy of the system. The chemical potential of any component in a phase is related to that at a standard state by the expression:

$$\mu_i^j = \mu_i^o + RT \ln a_i^j \qquad (2)$$

where a_i^j = activity of i in j

Hence, the compositions of co-existing feldspars are governed by the relationship:

$$\Delta\mu_{ab}^o = RT \ln \left[\frac{X_{ab}^{AF} \gamma_{ab}^{AF}}{X_{ab}^{PF} \gamma_{ab}^{PF}} \right] \qquad (3)$$

where γ is the activity co-efficient

The idea of using the distribution of albite between co-existing plagioclase and alkali feldspar was put forward by Barth (1951) and subsequently modified in a series of papers. Because of a lack of thermodynamic data he was forced to make a number of assumptions which can now be shown to be invalid, in particular those concerning the activity-composition relationships of alkali feldspars and the effects of pressure. Stormer (1975) and Whitney and Stormer (1977) have made use of modern determinations of thermodynamic properties to obtain a more accurate two-feldspar geothermometer/geobarometer. Expressions have been derived for sanidine-high albite and maximum microcline-low albite solid solutions; there is insufficient thermodynamic data to formulate analogous equations for intermediate structural states. Both are complex functions of the form:

$$T = f(X_{AF}, X_{pf}, P) \qquad (4)$$

where X_{AF} = mole fraction $NaAlSi_3O_8$ in alkali feldspar

and X_{PF} = mole fraction $NaAlSi_3O_8$ in coexisting plagioclase.

The major sources of error in the method are the use of these end-member structural states and the rather subjective petrographic determination of equilibrium between mineral pairs. Minimum errors are probably $\pm 30^{o}C$.

Whitney and Stormer (1977) used the averages of results obtained from the two calibrations to investigate the crystallization histories of a number of monzogranitic plutons from the Georgia Piedmont. Taking coexisting feldspar pairs which were believed to have equilibrated in a melt, they obtained estimates of the pressures and temperatures of formation by the intersection in P-T space of the two-feldspar equilibrium lines and the granite solidus. They conclude that "feldspar temperatures for coarse grained porphyritic granites ... appear to be consistent and meaningful" (ibid p.63).

Electron microprobe analyses of plagioclase grains in contact with alkali feldspars in samples from the main sheet of Dragsmark granite yield compositions of 28% to 31% An. This is confirmed by Universal stage determinations. As is indicated in Chapter 2, a considerable range of plagioclase compositions may be found within a single thin section, but groundmass grains that are not retrogressed to albite are usually close to An_{30}. Inclusions in megacrysts tend to be more calcic. A mole fraction of albite (X_{PF}) of 0.70 ±2 is therefore used as the composition of the plagioclase.

Because the alkali feldspar is so coarsely perthitic, scans of even 1000μ in length by wavelength-dispersive electron microprobe yield lower sodium contents than atomic absorption analyses. It is thus not practicable to use compositions of adjacent feldspar grains as would be desirable to ensure textural equilibrium. Megacrysts from Area 1 which are believed to be phenocrysts range in composition from 77% to 87wt.% Or

with an average of 82% and a standard deviation of 2%. Twenty bulk rock alkali feldspar analyses exhibit a similar range, with an average of 81 wt.% Or (see Ch.6).

The effects of changes in alkali feldspar composition on temperatures obtained by the two-feldspar method are far greater than those due to changes in plagioclase composition. Using the above compositional range, the equation for maximum microcline yields a pressure range of 1.5kb to 9kb. The imprecision of the potassium feldspar data for the Dragsmark granite thus renders two-feldspar geothermometry/geobarometry valueless when used in isolation, but the following points are worthy of note.

Firstly, substitution of the average feldspar compositions (X_{AF} = 0.19 ±2 and X_{PF} = 0.70 ±2) into the maximum microcline equation yields a P-T box which brackets the intersection of the fluid inclusion curve (p. 73) and the wet granite solidus (Fig. 7.4). This suggests that the feldspars are at least approximately in equilibrium with each other. Secondly, the very high pressures (average 7kb) yielded by use of the equation for sanidine of Stormer(1975) might suggest that the thermodynamic properties of orthoclase are closer to those of microcline than those of sanidine. However, a more recent thermodynamic model for sanidine-high albite by Haselton et al. (1983), yields pressures only 1kb or so higher than the maximum microcline line at any given temperature.

c) Feldspar Solvi

Most of the megacrysts from the Dragsmark granites that have been analysed contain more than 70wt.% Or in their bulk composition and possess very low calcium content (see Ch.6 and Table B6.1); they are consequently of little value as indicators of conditions of formation. A few however have compositions such that their relationships to the feldspar solvi provide constraints on temperature and pressure.

The binary alkali feldspar solvus has been investigated by numerous workers. A critical assessment of published solvi is given by Parsons (1978b),who concludes that complex solvi are not supported by presently available evidence and that the shape of the solvus does not vary significantly with pressure. Several determinations at various pressures are internally consistent to within 2 mole % Or. The solvus of Smith and Parsons (1974) with a critical temperature of 657°C at 1kb is used here, together with their value for dT_{CRIT}/dP of 16°C/kb. Yoder et al. (1957) give a value of 14°C/kb which yields a 1kb T_{CRIT} of 660°C from their 5kb data.

The compositions of a number of megacrysts in terms of orthoclase content (determined by AAS and XRD - see Chapters 5 and 6) are plotted on Fig. 7.5 along with the alkali feldspar solvus. Assuming a maximum temperature of crystallization of c.665°C - the approximate temperature of the K-feldspar -in line at 3.4 - 3.2kb (see p. 74), the maximum possible pressure of formation of any given composition (neglecting the possibility of metastable crystallization) may be calculated using the expression:

$$P_{max} = (T_{max} - T_{solvus}) / dT/dP + 1 \text{ kbar} \quad (1)$$

Hence, using the values given above

$$P_{max} = (665 - T_{solvus}) / 16 + 1 \text{ kbar} \quad (2)$$

This yields pressure estimates of 1.8kb to 4.8kb for a number of

megacrysts from Area 2. With the exception of samples 249/1 and 249/2 (see Table B 6.1), which yield a maximum pressure of 3kb, megacrysts from Area 1 are too potassic to provide useful pressure constraints. These values are in moderate agreement with estimates obtained using fluid inclusion and two-feldspar geothermometry/geobarometry (see Ch.7a and 7b), the data for Area 2 perhaps suggesting a lower pressure for the growth of the porphyroblasts. This approach however ignores the marked effects of calcium on the system, and it is precisely these sodic megacrysts which are also the most calcic (see Table B6.1). For a more realistic assessment, the ternary feldspar system must be examined.

The ternary feldspar solvus resembles a distorted dome with a triangular base. The amount of solid solution between anorthite and orthoclase is limited, but there is a continuous solid solution between anorthite and albite and, under certain conditions, between albite and orthoclase (Fig. 7.6A). At high temperatures or low pressures, sodic feldspars may contain appreciable amounts of both calcium and potassium: such feldspars are termed anorthoclases. At elevated pressures and/or low temperatures, the stability field of anorthoclase is greatly reduced, and a miscibility gap appears between Na-rich and K-rich alkali feldspars. The binary feldspar solvus intersects the wet granite solidus at 2.2kb and 675^{o}C. Above this water vapour pressure, two alkali feldspars may crystallize directly from a silicate melt whereas at lower pressures a melt may be in equilibrium with only one feldspar. Provided the shape of the solvus is known, the occurrence of anorthoclase places constraints on the possible P-T conditions.

Little expermental data is available for pressures in the region of interest (less than 5kb) other than that at 1kb. Iiyama (1966) tentatively proposed a very complex solvus with fields of one, two or three coexisting feldspars at temperatures of 700^{o}C or less. These were

established largely on the basis of variations in the NaCl / NaCl + KCl ratio of a hydrothermal fluid in contact with the feldspars. This complexity is not supported by later experiments using silicate melts but there is moderate agreement between the two methods.

Hamilton (1969) published sections through the solvus at 700°C and 1kb water vapour pressure and 900°C and 0.5kb. Unfortunately he does not consider the effects of pressure on the system and therefore no conclusions can be drawn as to the relative influence of pressure and temperature. Smith (1978) presented T-X sections through the 1kb alkali feldspar solvus with varying percentages of anorthite added to the synthetic mixtures of albite and orthoclase. These enable approximate sections to be constructed through the ternary feldspar solvus. Those for 700°C and 650°C are shown in Fig. 7.6B, together with the 700°C, 1kb solvus of Hamilton (1969), and compositional data for megacrysts from the Dragsmark granites.

It can be seen from Fig. 7.6B that most of the megacrysts plot below (outside) the 1kb solvus as could be anticipated from the estimate of c.3kb derived in Chapter 7a. Three megacrysts from Area 2 (X4, X5, D8) however plot on the 650°C, 1kb section. Either a slight decrease in temperature or an increase in pressure of the order of one kilobar would cause these samples to fall inside the solvus. The conclusion is therefore drawn that these porphyroblasts were formed at c.650°C and under a pressure of c.1kb. It should be noted that these three feldspars are chemically distinct from other Area 2 megacrysts (see p.61) and are furthermore all taken from the margins of granite sheets (see Map 3), D8 being pegmatitic.

The above conclusions imply the removal of 2kb of overburden pressure, equivalent to c.8km of rock, between the solidification of the Dragsmark granites and the development of these particular alkali feldspar

porphyroblasts. As the solidified granite could not have risen such a distance, this implies either that the metasomatism was not related to the intrusion of the granite, or that there were two metasomatic events. One of these would presumably be late-magmatic, with the minor second event occurring after removal of c.2kb of lithostatic pressure. The virtual restriction of porphyroblasts to the upper and western parts of the granite (see Chapters 2 and 3), the overlap of chemistry of phenocrysts and porphyroblasts (see Ch.6) and the likely effects of fluorine release in the post-magmatic stage (see Ch.8) all argue in favour of the latter hypothesis. This is further supported by the occurrence of hypersolvus granitoid veins (see Ch. 2d) throughout the area. Such veins must have formed at a water vapour pressure of less than 2.2kb, and it seems reasonable to postulate that the intrusion of these veins was accompanied by minor metasomatism at the margins of the Dragsmark granites.

d) Origin of Alkali Feldspar Megacrysts

It has been argued in Chapters 5 and 6 that the megacrysts of the Dragsmark granites comprise both phenocrysts and porphyroblasts. The former are dominant in Area 1 (the main sheet) and the latter in Area 2 (the overlying bodies), but examples of both are found throughout the granite. It has also been demonstrated (Chapter 3) that some alkali feldspar megacrysts have been formed by replacement of large plagioclase crystals, presumably through the action of a potassic fluid. The majority however are relatively pure alkali feldspar with a few inclusions of quartz, plagioclase and accessory minerals. Because these megacrysts are such a distinctive and characteristic feature of the Dragsmark granites, it is important to discuss possible reasons for their existence.

Considering first those alkali feldspar megacrysts which are interpreted as phenocrysts, the most likely origin seems to be growth of a few isolated tabular crystals from the magma as a result of the effects of P,T,X etc. on crystal morphology. This may perhaps be followed by recrystallization of and subsequent overgrowth around a cluster of two or more early formed crystals. Fenn(1977) has investigated crystal growth in the system $NaAlSi_3O_8$ - $KAlSi_3O_8$ - H_2O at P = 2.5kb. He finds that the main factors governing the development of textures are P_{H_2O} and the degree of undercooling. Undercooling is defined as the temperature interval between the liquidus and the nucleation and growth steps (the temperature at which the experimental charge was held). Neither the Na/K ratio of the system nor, in water-oversaturated systems, the absolute water content, appear to have any significant effect on crystal kinematics. At undercoolings of less than about $100^{o}C$, the texture is dominated by a few rapidly growing isolated tabular crystals. At higher degrees of undercooling, such as would occur in rhyolites, spherulitic growth is more important, leading ultimately to a large number of small equigranular

crystals.

It is possible that the rhythmic zonal variation in Ba content of phenocrysts both from the Dragsmark granites (see Ch.6c) and from Black Forest granites (Mehnert and Büsch, 1981) is due to rapid growth of the alkali feldspars. At slow growth rates the medium in which a crystal was growing would be effectively homogeneous with respect to those elements forming the mineral, At faster growth rates, both the diffusion rates for the various atomic species and boundary layer interaction effects could influence the local chemical environment of the crystal thereby causing compositional heterogeneities.

Mehrnert and Büsch (1981) present evidence that many alkali feldspar megacrysts from granites from the Black Forest consist of a series of concentric shells formed around a recrystallized core of earlier formed crystals. Although now in crystallographic continuity, such cores are revealed by zonation in Ba content and the presence of thin septa of quartz delineating relict crystal outlines (ibid, Fig.17). Only the latterphenomenon has been observed in megacrysts from the Dragsmark granites, but that does not eliminate this as a possible growth mechanism.

Turning now to the porphyroblastic alkali feldspar megacrysts, some will indubitably have arisen by recrystallization of and/or over-growth on pre-existing large phenocrysts. However, the occurrence of crystals growing across contacts to wall-rock (e.g. Fig.3.2)together with the distinctive structural and chemical properties (see Chapters 5 and 6) suggests that most originated by growth in the solid state from groundmass alkali feldspar. The influx of a fluid into a fine grained rock at slightly sub-solidus temperatures is one of the classic methods of recrys-tallization and grain-coarsening. In this context it should be noted that addition of water to an undersaturated system lowers the effective degree

of undercooling and this could be sufficient to change the stable growth morphology from spherulitic to tabular. Fenn (1977) suggests that spherulites may well recrystallize into single prismatic crystals during subsolidus cooling.

As an illustration of how recrystallization may produce megacrysts, a very simplistic mathematical model of granite has been investigated. An equigranular homogeneous granite can be represented by a tessellation of regular hexagons of which 30% (see modal analyses, Ch.2), randomly distributed, are defined as alkali feldspar. The assumptions are now made of a limited amount of diffusion (over less than one grain diameter) and that alkali feldspar grains in contact or within this limit will recrystallize to single larger crystals.

To allow comparison with the Dragsmark granites, an initial grain size of 0.5mm was used in the model (cf. groundmass grain sizes, p.19). An example of the texture this produced is given in Fig. 7.7A, together with a representative section of a granite from one of the minor sheets of Area 2 (Fig. 7.7B). In reality, the high surface energy of the more irregular megacrysts produced by the model would cause them to further recrystallize to more rational crystal shapes. Examination of Figs. 7.7A and 7.7B shows that both exhibit a large number of small equant alkali feldspars with a few larger, more irregular megacrysts containing inclusions of quartz and plagioclase.

Whilst the ideas put forward in this section are highly speculative, it is believed that it has been shown that the development of both phenocrystic and porphyroblastic alkali feldspar megacrysts can be independently related to the interaction between thermal history and fluid behaviour within a granite body. That porphyroblasts occur mainly in Area 2 at Dragsmark and that different parts of the same intrusion in

south-west England show differing degrees of megacryst development (Store and Austin, 1961) demonstrates that the growth of megacrysts is critically dependent on factors which may show significant local variation.

Figure 7.1

Histogram of homogenization temperature (T_H) of two-phase (fluid plus vapour) fluid inclusions in quartz grains within alkali feldspar megacrysts from the Dragsmark granite.

20 inclusions determined.

The temperature used for further analysis is the upper limit of the modal class -: 330°C.

7.1

ature (T_H) of two-phase (fluid plus
grains within alkali feldspar
ite.

nalysis is the upper limit of the

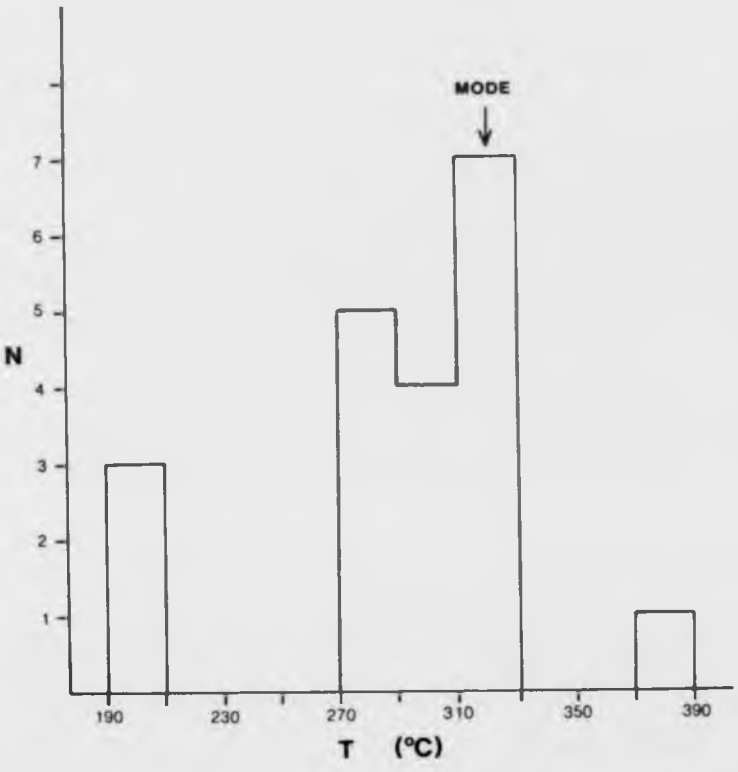

Figure 7.2

Diagram to illustrate the phenomenon of 'necking down', and the consequent production of two-phase fluid inclusions which homogenize at temperatures which are not representative of the true trapping temperature (after Roedder, 1979).

$T_4 > T_3 > T_2 > T_1$

T_4 - True trapping temperature - a single phase fluid inclusion

T_3 - Appearance of a vapour bubble

T_2 - The fluid inclusion necks down to form 2 two-phase inclusions

T_1 - Further necking down leads to 3 fluid inclusions, one of which is single-phase.

Inclusion A will homogenize above T_4

Inclusion B is single-phase

Inclusion C will homogenize between T_2 and T_3

n of 'necking down', and the
fluid inclusions which homogenize
esentative of the true trapping

single phase fluid inclusion

n to form 2 two-phase inclusions
3 fluid inclusions, one of which

4

T_2 and T_3

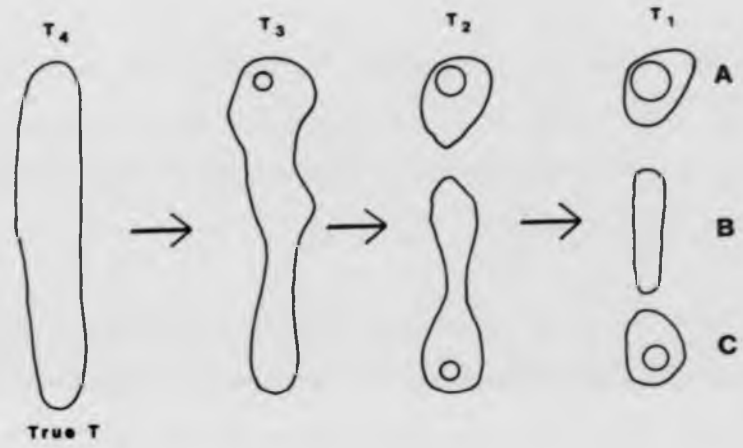

Figure 7.3

Temperature versus P_{H_2O} plot showing the possible P-T space within which the fluid inclusions in the Dragsmark granite could have been trapped. A fluid composition of between 0% and 5% NaCl equivalent is assumed (Roedder, 1979).

The intersection of the above with the wet granite solidus and quartz-in line (first appearance of quartz from a cooling magma) yields an area in P-T space within which the Dragsmark granite must have crystallized.

7.3

the possible P-T space within
agsmark granite could have been
ween 0% and 5% NaCl equivalent

he wet granite solidus and
quartz from a cooling magma)
hich the Dragsmark granite must

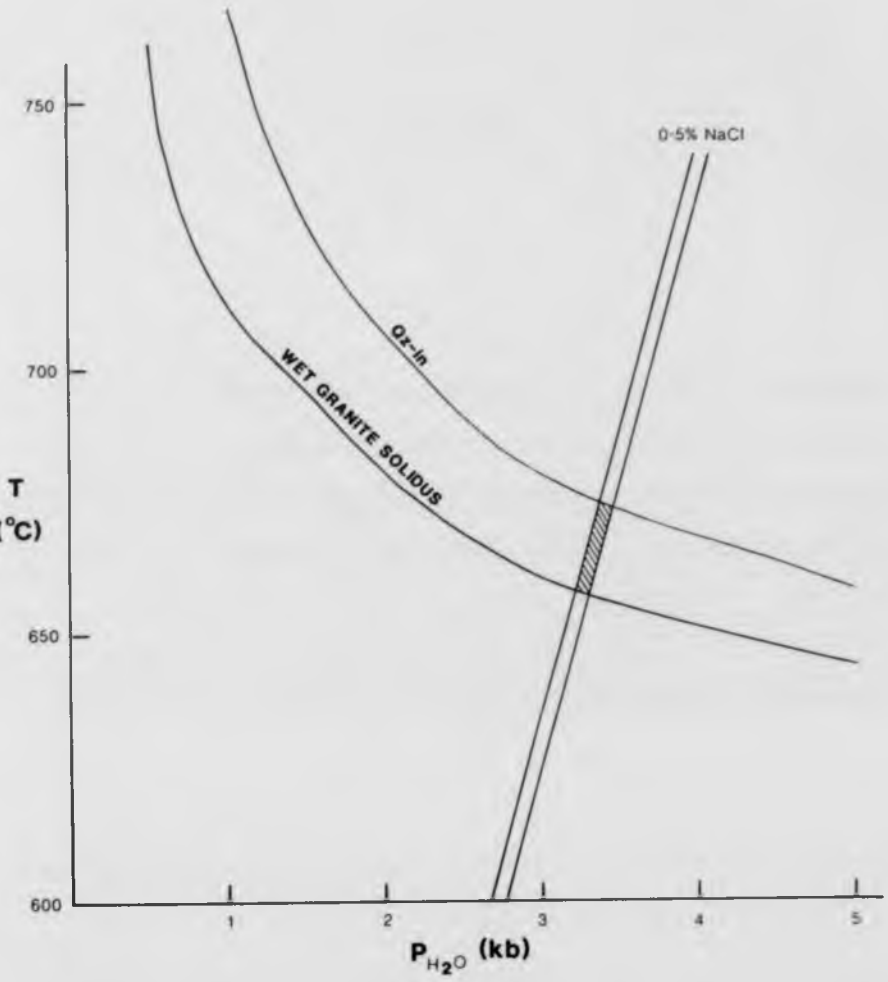

Figure 7.4

Temperature versus P_{H_2O} plot showing the equilibrium P-T curves indicated by two-feldspar geothermometry/geobarometry. The wet granite solidus and the conditions of formation of the Dragsmark granite as indicated by fluid inclusion studies are also shown.

MM - Curve obtained using the maximum microcline - low albite equation of Whitney and Stormer (1977)

SN (H) - Curve obtained using the sanidine - high albite equation of Haselton et al (1983)

SN (S) - As above; equation of Stormer (1975)

81/30 etc. - K-feldspar composition 81 wt% Or; plagioclase An_{30}

e 7.4

ng the equilibrium P-T curves
ometry/geobarometry. The wet
of formation of the Dragsmark
usion studies are also shown.

m microcline - low albite
r (1977)

sanidine - high albite equation

rmer (1975)

n 81 wt% Or; plagioclase An_{30}

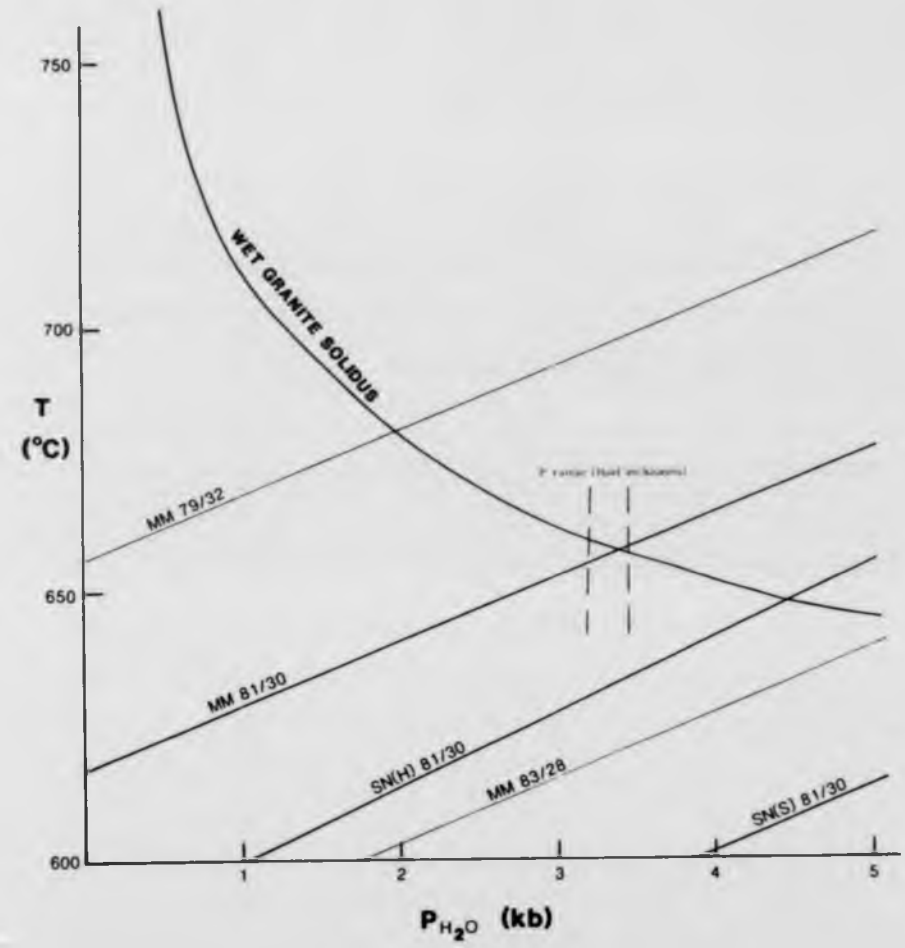

Figure 7.5

The 1 kb. hydrostatic anorthite-free alkali feldspar solvus (Smith and Parsons, 1974), with bulk compositions of alkali feldspar megacrysts from the Dragsmark granites.

A temperature of formation of 665°C is assumed (see text p. 78).

The vertical lines between the solvus and the 665°C isotherm indicate the maximum pressure under which feldspars of the relevant composition may form stably. At this pressure, the relevant portion of the solvus is at 665°C.

o - Area 1 megacrysts

• - Area 2 megacrysts

A maximum pressure of formation of 1.8 to 4.8 kb. is indicated for Area 2 megacrysts.

dspar solvus (Smith

lkali feldspar

(see text p. 78).

65°C isotherm indicate

he relevant composition

t portion of the solvus

. is indicated for

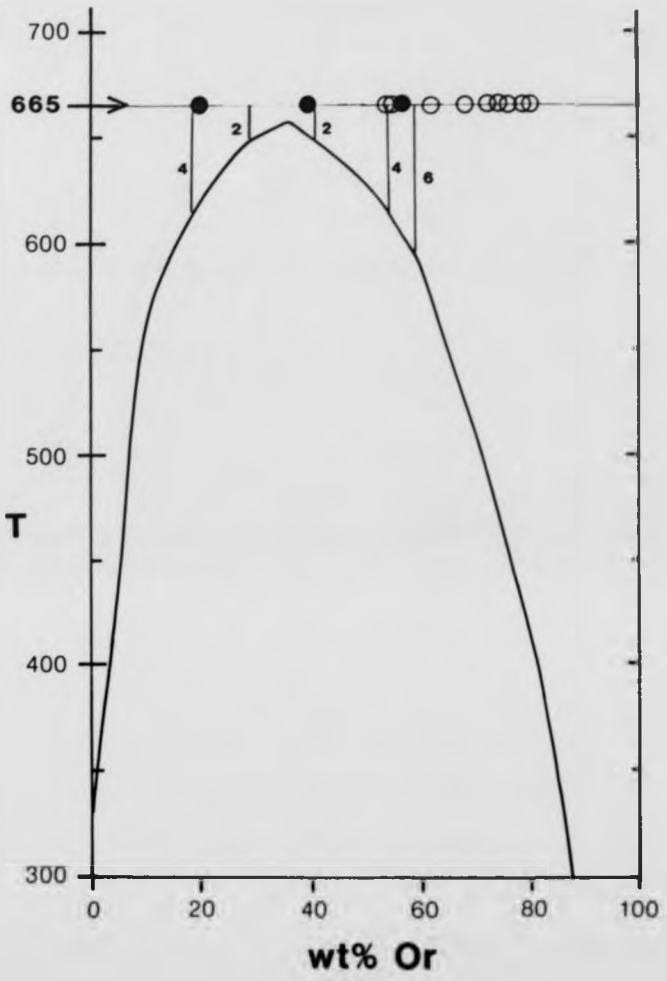

Figure 7.6

A : Nomenclature of the ternary feldspars (after Smith, 1974)

B : Data for alkali feldspar megacrysts from the Dragsmark granites together with various determinations of the ternary feldspar solvus.

—— - Hamilton (1969); 700°C, 1 kb.

– – – - Smith (1978); 700°C, 1 kb.

– · – - Smith (1978); 650°C, 1 kb.

(note the presence of a miscibility gap in the 650°C solvus between Na-rich and K-rich alkali feldspars)

o - Area 1 megacrysts

X4, X5, D8 - three chemically distinct megacrysts from the margins of Area 2 bodies. See text pp. 80-81.

(after Smith, 1974)

from the Dragsmark granites

of the ternary feldspar

n the 650°C solvus between

megacrysts from the margins

ext pp. 80-81.

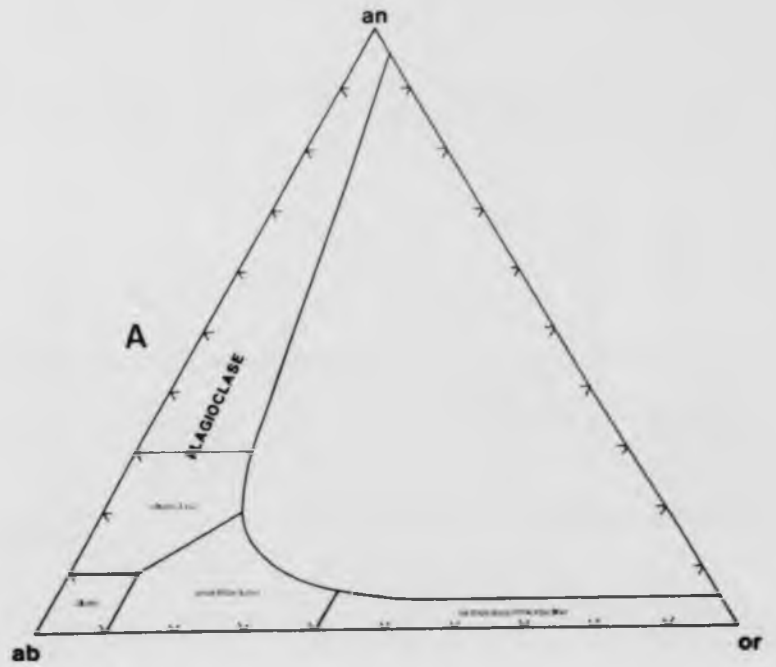

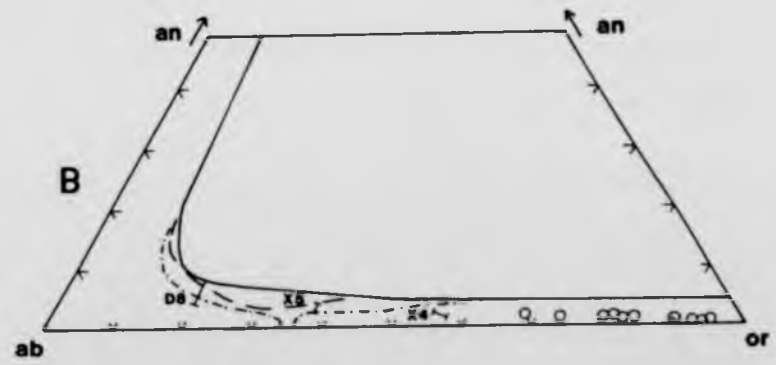

Figure 7.7

Textural relationships of alkali feldspar megacrysts in relation to the mechanism of growth.

\\\ - plagioclase

A : Result of a simple geometrical model of megacryst growth by limited diffusion and recrystallization of an originally homogeneous random distribution of alkali feldspar grains. An example of the original distribution is given in the bottom right corner.

- microcline

∴ - quartz

B : Drawing of a thin section of sample no. 888 from one of the minor sheets in Area 2.

gacrysts in relation to

megacryst growth by

of an originally

li feldspar grains.

is given in the bottom

888 from one of the

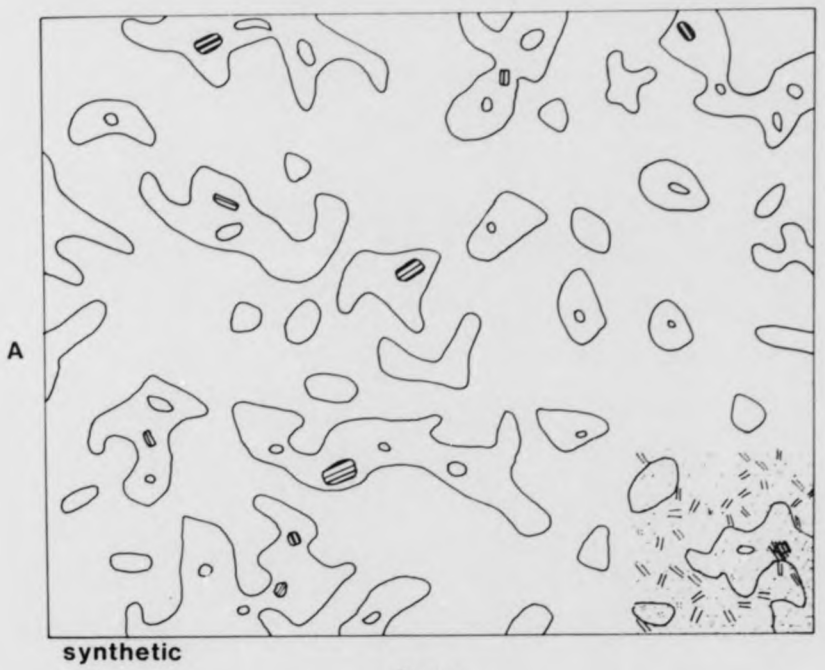

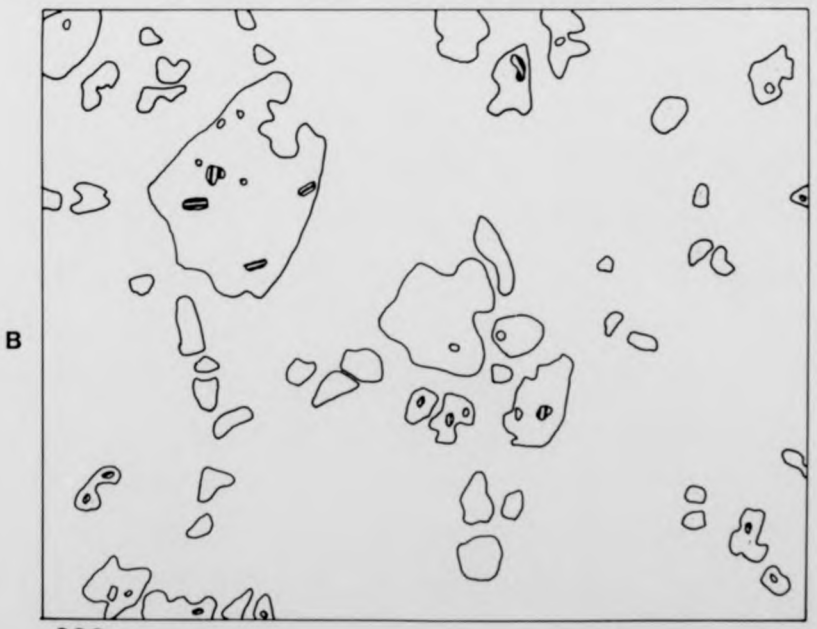

Chapter 8

Whole-Rock Geochemistry

a) Description and Classification

Nineteen samples were analysed for major elements, ferrous iron, loss on ignition, and the trace elements Rb, Sr, Y, Zr and Ba. The standard techniques employed at Keele for sample preparation and analysis by X-ray fluorescence, titration and ignition were used: see Appendix A. Ten of the samples were from the Dragsmark granites, including two from Area 2, one from the older augen granite (Kållviken granite), three from the gneissose granite, three from the Stora Le -Marstrand migmatites and paragneisses and two of veins cutting the Kållviken granite (see Map 3). Nine of the granite samples were analysed for Li by flame emission and for F by selective ion electrode. The fluorine analyses were performed by the University of Exeter. Geochemical data are summarized in Table 8.1 with full analyses in Tables B8.1 and B8.2 .

The three analyses of the country-rock gneisses conform with the fuller work of Daly (1978) and use will be made throughout this chapter of his data for the Stora Le -Marstrand gneisses and the Assmunderöd-Myckleby augen granite. The gneisses range from pelites to quartzites, but are dominatly semipelites (Ch.2) with SiO_2 contents ranging from 65.1% to 78.2% . Neither the gneissose granite nor the one sample from the Kållviken granite can be distinguished chemically from the Dragsmark granites, all having silica contents of between 68% and 75% and low iron and magnesium contents, in keeping with their low modal abundance of mafic minerals (Tables B8.1, Ch.2). The Kållviken granite sample could be grouped with the Assmunderöd-Myckleby granite, which is slightly richer in many trace elements than the Dragsmark granites sensu stricto. One of the two samples (3001) from veins cutting the Kållviken granite is Na-enriched

TABLE 8.1

Summary geochemical data for the Dragsmark granites

	Mean	Range
Major oxides (wt.%)		
SiO_2	71.0	68.5 - 74.9
TiO_2	.45	.25 - .75
Al_2O_3	13.8	12.6 - 15.1
Fe_2O_3	.86	.30 - 1.43
MnO	.04	.02 - .06
MgO	.70	.48 - 1.02
CaO	1.53	.77 - 2.25
Na_2O	2.83	2.41 - 3.52
K_2O	5.23	4.49 - 5.89
P_2O_5	.13	.05 - .25
FeO	2.06	1.30 - 3.55
Trace elements (ppm)		
Rb	160	127 - 273
Sr	130	71 - 177
Y	43	25 - 80
Zr	263	160 - 388
Ba	759	359 - 1083
Li	25	0 - 50
F	2100	1300 - 2900

relative to the granite and may be hypersolvus (see Ch.2), the other (3002) is K-enriched. The position of this latter on ab-Q-or and ab-an-or plots (Fig 8.1) suggests that it may be genetically associated with the Dragsmark granites; this would not conflict with the evidence on their relative ages.

Of the samples analysed from the Dragsmark granites, only two (72 and 418) are from Area 2 (see Map 3). With the exception of no.256, these samples are the most sialic (Table 8.1) and have the lowest K/Rb ratios (see Fig 8.5). Number 256 is chemically anomalous in that its position on discriminant plots relative to the other Area 1 samples is very variable. The Dragsmark granites have a mean silica content of 71.0%, with a mean K_2O/Na_2O ratio of 1.85 and average CaO 1.53% (Table 8.1). These values are consistent with the average mode of 31% quartz, 29% alkali feldspar, 29% plagioclase and 11% mafic minerals: the rock is a monzogranite (see Ch.2). Because the granite has suffered subsequent deformation, metamorphism and possible metasomatism, the mineralogical and chemical variation observed cannot be simply interpreted with confidence.

Figure 8.2 shows the positions of the Dragsmark granite samples on an AFM plot together with data from various granitoid complexes (Brown et al.,1981) for comparison. This diagram can be used to distinguish between granitoid suites of compression zones (e.g. the British Caledonides) and the relatively iron- and alkali-enriched extension zone intrusions (ibid.). Although it is doubtful if such broad tectonic implications should be drawn from the relatively minor granites of this part of south-west Sweden, it is interesting that the Dragsmark granite data, albeit rather limited, clearly show greater affinity with the Fennoscandian rapakivi granites and Nigerian younger granites than those of the British Caledonides. Furthermore Marmo (1971) notes that both the

rapakivi and the Nigerian younger granites contain appreciable amounts of fluorine, not only in biotite and hornblende, but also as fluorite and abundant topaz. Rapakivi contains between 0.05% and 0.47% fluorine, generally 0.20 - 0.40% (Saharra, 1945). The fluorine content of the Dragsmark granite ranges from 0.13% to 0.29% (Table 8.3).

Brown et al. (1981) use Y/Sr and Ba/Rb plots to discriminant between the earlier 'permitted' and later 'forceful' intrusions of the Newer Granites of Scotland. Data for the Dragsmark granites (Fig 8.3) show greatest similarity to the Loch Doon intrusion which is largely granodioritic and is interpreted as being transitional between these two magmatectonic groups.

The field and petrographic evidence of abundant metasedimentary xenoliths, restricted compositional variation, high silica content and xenocrystic garnet and plagioclase all implies a sedimentary origin for the Dragsmark granites. This is borne out by the chemical discriminants between S- and I-types of Chappell and White (1974), although the mineralogical evidence is ambiguous. Thus the granites have less than 3.2% Na_2O and about 5% K_2O (Tables 8.1 and B8.1); most have CIPW normative corundum slightly greater than 1% and the SiO_2 content varies only from 68.7% to 74.9%. The molar $Al_2O_3 / (Na_2O + K_2O + CaO)$ ratio however is not greater than 1.1, the average being 1.05. On balance therefore the chemical evidence is interpreted as supporting an S-type origin. Mineralogically, the presence of sphene is supposed to indicate an I-type source (ibid.) as is the occurence of magnetite rather than ilmenite (Ishihara, 1977). As will be discussed later (Ch.8c) however, the mafic mineralogy is believed to be largely inherited and thus should not be used as an indicator of magma type. The distinction on the basis of the nature of the opaque minerals is founded on the assumption of relatively low oxygen fugacity in S-type magmas reflecting the presence of reducing agents such

as graphitic shales in the source. The nature of the Stora Le -Marstrand metasediments invalidates this criterion.

Further evidence for an S-type origin is provided by the modified ACF plot of White and Chappell (1977), which can also be used as a non-rigorous phase diagram (Fig 8.4). The Dragsmark granites are located well within the S-type field whereas the data points for the gneissose granite straddle the boundary. The composition of garnet marked on Fig 8.4 is taken from microprobe analyses (Table B9.1), as are those of plagioclase and biotite. The latter two cannot be represented as points because of compositional variation and uncertainty as to the oxidation state of iron. The 'tie-lines' drawn are such that only samples containing garnet fall within the plagioclase-garnet-biotite field and the country gneisses plot within the muscovite-accessible field.

In keeping with their higher SiO_2 contents, the samples from Area 2 have lower K/Rb ratios than those from Area 1, indicating a degree of fractionation. Shaw (1968) defines R (the K/Rb ratio) as $\left[\%K / ppm\ Rb \right] \times 10^4$; the 'normal' value for crustal rocks is accepted as 229 with a range of 160 - 300. All the Dragsmark granites lie within this range, samples 418 and 72 having the lowest values of 173 and 214 respectively whilst the range for Area 1 is from 242 to 293, average 265. They therefore lie within the Main trend of Shaw (op.cit.) with the Area 2 samples plotting nearest the Pegmatitic-Hydrothermal trend (Fig 8.5). It is also demonstrated (ibid.) that anatexis of a gneiss, such as the average Stora Le -Marstrand gneiss, with a K/Rb value of 220 (Daly,1978), should lead to the production of a rubidium enriched fluid. Such a fluid would be capable of causing the Rb enrichment of megacrysts from Area 2 relative to those of Area 1, as noted in Ch.6 .

Lambert and Holland (1974) have proposed a standard calc-alkaline

trend on the basis of CaO/Y relationships and explain variations from this trend in terms of crystal fractionation. Data for the Dragsmark granites are shown on Fig. 8.6 together with this standard calc-alkaline trend and the vector effects of the addition of various phases to a minimum melt. Note that since the composition of the melt is similar to that of biotite the addition of this mineral would have very little effect. It can be seen that a residual mixture of garnet, plagioclase and sphene could produce the observed range in granite compositions, which is extremely difficult to produce by magmatic crystal fractionation.

trend on the basis of CaO/Y relationships and explain variations from this trend in terms of crystal fractionation. Data for the Dragsmark granites are shown on Fig. 8.6 together with this standard calc-alkaline trend and the vector effects of the addition of various phases to a minimum melt. Note that since the composition of the melt is similar to that of biotite the addition of this mineral would have very little effect. It can be seen that a residual mixture of garnet, plagioclase and sphene could produce the observed range in granite compositions, which is extremely difficult to produce by magmatic crystal fractionation.

b) The Granite System

As discussed earlier (Ch. 7a) the magma from which the Dragsmark granites crystallized is believed to have contained a free aqueous vapour phase and therefore experimental studies of anatexis with $P_{H_2O} = P_{total}$ are applicable. The results thus obtained should be treated with some caution as the assumption has to be made that the composition of the granite represents the composition of an original silicate melt, and this may be invalid. Several authors (Wyllie,1977; White and Chappell,1977; Winkler,1979) have proposed that, in addition to the accepted refractory minerals such as cordierite and garnet, plagioclase and quartz may also be present in considerable amounts as solid residual phases in granitic magmas. This would clearly imply that the melt was more potassic than the observed bulk composition although evidence for potassium metasomatism provided by the alkali feldspar megacrysts of Area 2 (Map 1) would imply the reverse.

Considering first the likely origin of the granite by partial melting of Stora Le -Marstrand paragneisses, the best experimental work available for comparison is that of Piwinskii(1968) and Stern and Wyllie (1981) on a biotite-granite from the Central Sierra Nevada Batholith. This has a modal composition of 35% quartz, 31% plagioclase (oligoclase), 29% orthoclase and 5% biotite + accessories; the SiO_2 content is 75%. Stern and Wyllie (1981) determined that for pressures up to 20Kb, the solidus for this granite is identical with that of a muscovite-granite and the anorthite-free ternary eutectic composition, and that at less than 5kb it behaves like a eutectic granite except that the melting interval is slightly smaller (35^{o}C). The amount of water did not affect the silicate phase relations, provided it was present in excess. Above 5kb quartz was found to be the liquidus phase but was replaced by plagioclase below 3kb pressure. This is in agreement with the work of Piwinskii (1968) at

pressures up to 3kb, where the crystallization sequence was found to be plagioclase - quartz - biotite - potassium feldspar, with a temperature interval of 25°C at 3kb between the quartz - in line and the solidus.

Winkler (1979) presents data on the melting of a paragneiss with the modal composition 34% plagioclase (An_{28}), 26% quartz, 20% alkali feldspar, 20% biotite at 5kb P_{H_2O}. Here the melting sequence was determined as alkali feldspar - quartz - plagioclase, with the quartz-out line being 20°C above the solidus. Furthermore, it is pointed out that in rocks with low to moderate CaO content, the initial melts in coexistence with all three felsic phases all lie in the central part of the Q - ab - or triangle and consequently the melting of alkali feldspar is accompanied by melting of subequal amounts of quartz and plagioclase. As the cotectic line (Fig. 8.7) slopes only gently with respect to temperature, large amounts of melting take place over narrow temperature intervals. Thus a rock with 20% alkali feldspar will yield about 60% melt within 10°C or so of its solidus, leaving residual plagioclase, quartz and biotite.

Turning to theoretical models of the granite system, the classic work of Tuttle and Bowen (1958) in determining phase relationships in the system $NaAlSi_3O_8$ - $KAlSi_3O_8$ - SiO_2 - H_2o has been expanded by various researchers (James and Hamilton,1969; Winkler,1979) to include $CaAl_2Si_2O_8$. Figure 8.7 illustrates the important features of the system or - ab - an - Q under water-saturated conditions. Points to note concerning Fig. 8.7 are:

i) At pressures greater than 2.2kb the point P is the ternary eutectic in the Ca-free system.

ii) All melts in equilibrium with quartz, plagioclase, alkali feldspar and vapour lie on the line P-E_5 (the cotectic line) and, because the plagioclase in most gneisses is rarely more calcic than An_{40}, are generally restricted to regions near P.

iii) The position and temperature of P is pressure dependant,

moving towards the ab apex with increasing P_{H_2O} (Tuttle and Bowen,1958).

iv) The position and temperature of the cotectic line P-E_5 is also dependant on the composition of the fluid phase, particularly the halide content (Manning,1979), with P again moving towards the ab apex with increasing Cl^- or F^- content.

In general, on melting a rock containing quartz, relatively sodic plagioclase and potassium feldspar, the first melt will lie on the cotectic line near P. The composition of the melt will change relatively little until all of one of the felsic phases (usually K-feldspar) is completely dissolved. At this point, which will be only 10 - 20°C above the solidus, the system will contain 30% - 60% melt of a cotectic composition i.e. a minimum melt of White and Chappell (1977). On further heating the melt composition moves onto one of the three cotectic surfaces (usually the quartz - plagioclase - liquid - vapour surfaces $E_1 - E_2 - E_5 - P$ of Fig. 8.7) until another felsic phase is completely dissolved. The liquid then leaves the cotectic surface and moves into the stability field of the remaining phase. Considerable temperature rises will generally be required to achieve melting of more than two of the phases.

Winkler and Breitbart (1978) present ternary projections of the phase boundaries at 5kb and 7kb with the isotherms on the cotectic surfaces contoured for weight % of the fourth component. CIPW normative ratios for the Dragsmark rocks together with some data on Stora Le -Marstrand gneisses from Daly (1978) are plotted on these diagrams in Figs. 8.8 and 8.9 . The Dragsmark granites can be seen to cluster in the thermal trough, that is the cotectic line, and towards the or apex. Comparison of the values of normative an and Q with those of the contours shows that most of the samples lie in the alkali feldspar space, near the alkali feldspar - quartz cotectic surface ($E_5 - E_3 - P$ on Fig. 8.7). If the bulk compositions as

plotted represent the compositions of the granitic melt, this implies that quartz and plagioclase were completely dissolved, leaving a restite of potassium feldspar and biotite.

This hypothesis is incompatible with the experimental evidence, the observed modal analyses of the country gneisses (p. 9), which would suggest K-feldspar as the first phase to disappear, and the limited textural evidence available concerning restite mineralogy. The implication is that the apparent excess of Or is a result either of potassium metasomatism or of the method of calculation of the norm. The CIPW norm for oversaturated rocks allocates all K_2O to orthoclase whereas in reality a considerable proportion is present in biotite, which would reduce the apparent Or content. For this reason the use of modal analyses is perhaps to be preferred. The average modal analysis, normalized to Q + A + P = 100, of the Dragsmark granite is 35% quartz, 33% plagioclase (An_{30}) and 32% alkali feldspar (Or_{80}), from Chapters 2 and 6. The calculated values in the Q - or - ab - an system are plotted on Figs. 8.8 and 8.9 and it is apparent that the 'new' bulk composition lies in the plagioclase space above the cotectic line. This position is compatible with the granite being a mixture of a near-cotectic melt and restite plagioclase. Applying the lever rule to a plagioclase of composition An_{30}, this bulk composition, and the cotectic line (Fig. 8.9) suggests that the average Dragsmark granite contains approximately 10% - 15% inherited plagioclase.

c) Restite Modelling

White and Chappell (1977) develop a model for the production of granitic bodies by partial melting of the source to produce a mobile mixture of granitoid melt and solid residuum (termed restite). Separation of these two components by whatever means will produce a range of compositions which may be described in terms of proportions of the two end-members: pure melt and pure restite. The source composition will also lie between these two. Moderate degrees of anatexis of a typical gneiss produce a melt of a composition on or near to the cotectic minimum in the granite system (Ch.8b). Such a melt will have an SiO_2 content of c.76% and moreover will contain negligible amounts of components that do not enter the quartz and feldspar lattices e.g. P_2O_5, MnO and TiO_2 (ibid.). Further heating would involve breakdown of minerals such as biotite and apatite resulting in enrichment of the melt in the above components and reduction of the silica content. Both mechanisms produce linear chemical variation diagrams in contrast to the curved patterns typical of fractional crystallization processes (Fig. 8.10).

Plots of P_2O_5, MnO, MgO, TiO_2, Fe_2O_3t and Zr against SiO_2 are presented in Fig. 8.11 for samples from the Dragsmark granites together with an indication of the range of compositions of the less silicic of the Stora Le -Marstrand gneisses analysed by Daly (1978). Variation diagrams for those components which enter a minimum melt i.e. Na_2O, K_2O, CaO and Al_2O_3 are given in Fig. 8.12. These diagrams demonstrate that the Dragsmark granites can be modelled as a mixture of a minimum melt and a restite produced by anatexis of pelitic Stora Le -Marstrand gneisses. This model is compatible with the petrographic and field evidence of xenocrystic and xenolithic marerial, with a dominance of psammitic over pelitic xenoliths. The model can also be applied to the Assmunderöd - Myckleby granite (using the data of Daly, 1978) which is slightly richer

in the "non-minimum melt" elements than the Dragsmark granite. The lower average SiO_2 content (70.1% cf 71.0%) of the former perhaps indicates a lower degree of separation of melt and restite.

The concept of a model restite (Compston and Chappell, 1979) is here applied to S-type granites, with compositional data for xenocrystic minerals being used to calculate a normative restite mineralogy. Many assumptions and approximations are involved, so the results should only be regarded as semi-quantitative. For restite to coexist with a cotectic minimum melt, it must contain quartz and both feldspars: the limiting case is the disappearance of one of these phases. Modelling the restite from production of an I-type granite as a normative quartz-free two-pyroxene granulite, Compston and Chappell (op.cit.) obtain SiO_2 restite contents of c.50% for many case studies. This value is therefore used in this study, and also yields normative quartz-free restites, but the further assumption is made that the restite has no normative alkali feldspar. Strictly, this means that the melt did not lie on the cotectic line, but on or slightly above the quartz-plagioclase cotectic surface, and was thus not a minimum melt. This is consistent with previous conclusions (p.94) and examination of Fig. 8.7 reveals that the difference between the proposed melt composition and a true minimum melt is negligible.

Using the observed mineralogy of the granites (Ch.2) the model restite is taken to consist of plagioclase, biotite, garnet, sphene, apatite and zircon; the biotite and garnet compositions are simplified averages of those obtained by microprobe analysis (see Tables B9.1 and B9.2). The dubious assumption that mineralogy and mineral chemistries remain relatively unchanged during palingenesis is necessary and is justified on the grounds of the small changes in temperature envisaged, the lack of pressure dependence of the system and the internal consistency of the results. Starting from compositional parameters derived by extra-

polation of best-fit linear regression lines to the chemical data, the normative mineralogy of the restite was calculated according to the scheme given in Appendix A. Iterative corrections were then applied until a result was obtained that fulfilled the logical requirements of summation of major oxides to 100% and absence of excess components i.e. all major oxides were assigned to the above minerals. The lines drawn on Figs. 8.11 and 8.12 are the visual best-fit lines that satisfy these requirements.

The major oxide chemistry and normative mineralogy of the model restite thus derived for the Dragsmark granite are given in Table 8.2 . As previously stated the nature of the model is such that the values obtained should be regarded as, at best, semi-quantitative. In particular the relative proportion of biotite to garnet is sensitive to the K_2O content of the restite and Compston and Chappell (1979) have indicated that this is difficult to estimate from observed variations because of the mobility of potassium in geological environments. Increasing the restite SiO_2 content such that normative quartz appears would increase the proportion of biotite, decrease the proportions of garnet and aluminosilicate and make the plagioclase less calcic; the melt would then lie on the quartz-plagioclase cotectic surface.

In summary, despite large uncertainties in extrapolations and assumptions, an internally consistent model restite based on zero or very low normative quartz content can be produced. This restite has mineral proportions which are not out of keeping with those actually observed in the Dragsmark granites and gneisses, the mineralogy being dominated by plagioclase and biotite.

Taking the original gneisses to have had a silica content of 67% (see Fig. 8.11), the melt component to be a minimum melt with 76% SiO_2 (p.95) and the restite to have 50% SiO_2 (Table 8.2, p.96) application

TABLE 8.2

Model Restite Chemistry and Normative Mineralogy

	wt.%	Normative Mineralogy	wt.%
SiO_2	50	Plagioclase (An_{33})	48.8
TiO_2	1.5	Biotite	27
Al_2O_3	20.2	Garnet	16
Fe_2O_3t	12	Aluminosilicate	4
MnO	0.2	Sphene	3
MgO	2	Apatite	1
CaO	6.5	Zircon	0.2
Na_2O	4		
K_2O	3		
P_2O_5	0.5		
Zr (ppm)	1100		

of the lever rule indicates that the magma at source was about 65% melt. Applying the same principle to the samples of Dragsmark granite (Table B8.1), values are obtained ranging from 71% to 95% melt, with an average of 80%. This range is presumably the result of crystal settling and/or separation of melt-enriched magma at source. The estimate thus obtained of 10% restite-derived plagioclase in the average granite agrees with conclusions drawn from consideration of the granite system (p.94).

d) Fluorine

Nine whole rock fluorine analyses were performed by the University of Exeter; methodology is given in Appendix A and results in Table 8.3, together with Li analyses. The association F - Sn - Li is a useful discriminant between granite types, but Sn concentrations were below detection limit by X.R.F.S.; the Dragsmark granites are thus classified as 'normal' as opposed to stanniferous or Li - F granites. A plot of Li against F (Fig. 8.13) shows, with considerable scatter, a positive correlation of lithium with fluorine. Samples 72 and 53, both taken from very near contacts to the country rock (Map 3), have the lowest fluorine contents, in keeping with accepted concepts of marginal degassing (Bailey, 1977).

The average F content of granites is 800ppm with a range from 20 - 7000ppm (ibid.). Higher (greater than 0.1% F) values are usually associated with alkali varieties, late hyperbyssal stocks and autometasomatized granites. The lowest values are obtained from migmatites and ultrametamorphic catazonal granitoids (average 140ppm F). The average fluorine content of the Dragsmark granites is 2100ppm.

Much of the fluorine in granites is held in biotite, with the remainder largely in accessories such as apatite, sphene, topaz and fluorite. The first three are ubiquitous in the granites of Dragsmark, but fluorite has only been observed at locality 30 (Map 3) in the Källviken granite. Kanisawa (1979) demonstrates a crude inverse relationship between d_{005} of biotites and their F content which has been used to obtain values for three samples (Table 8.3). In two of these, two types of biotite appear to be present; those with the lower fluorine content are probably to some extent retrogressed - many biotites are heavily chloritized such that determination of OH^- content was not feasible. Microprobe analyses (Table B9.2) indicate a range in chlorine content of

TABLE 8.3

Lithium and Fluorine analyses of the Dragsmark granite

Sample	Li ppm.	F (wt.%)	F (wt.%) in biotite
53	16	.16	-
72	11	.13	-
249	31	.22	-
256	0	.18	0.3 - 0.7
418	50	.21	-
706	44	.22	-
821	6	.29	0.65 - 0.75 and 0.2 - 0.65
823	43	.23	0.5 - 0.8 and 0.2 - 0.65
Källviken granite			
30	8	.21	-

biotites from below detection limit to 1500ppm, with an average of c.1000ppm. These values for halogen content contrast strongly with averages of 0.38% F and 0.013% Cl in biotites from ferruginous metapelites obtained by Petrov et al. (1972). Unfortunately no data are available on partitioning between biotites and fluids so no conclusions can be drawn concerning the composition of the aqueous fluid coexisting with the magma.

Gavrilin et al. (1972) have studied the behaviour of fluorine in "biotite plagiogneisses" (plagiogneiss is equivalent to trondhjemite (Streckeisen,1975) , so that biotite plagiogneisses are presumably tonalites or granodiorites). These rocks had undergone varying degrees of migmatization and granitization from the development of quartzo-feldspathic glomeroblasts to cross-cutting granitic dykes. They find that, irrespective of both the mechanism of formation and the composition of the granitoid "separates", their F content is 2 - 10 times lower than that of the unaffected gneisses (average values are 200ppm as compared with 700 - 800ppm in the gneisses). Melanosome (biotite) selvedges are of course richer in fluorine (average 2000ppm) and where such are present, mass balance calculations indicate no loss of fluorine from the system.

The conclusion drawn from the above information is that gradual accumulation of the leucosome 'squeezed out' from a region undergoing migmatization cannot be responsible for the formation of relatively fluorine rich granites such as those of Dragsmark.

Various workers have studied the effects of fluorine on the granite solidus and although their results are inconsistent, it is apparent that whilst the nature of the accompanying cation (H^+, Na^+, K^+) has some effect, addition of F^- lowers solidus temperatures and increases the stability field of quartz. Kovalenko (1977) found that at P_{total} = 1 kb, the solidus for a biotite-granite is lowered to c.630^{o}C in the presence of

1 wt% F as HF. At fluorine contents greater than c.0.4wt%, topaz becomes a stable sub-solidus phase. As topaz occurs throughout the Dragsmark granites, this would seem to imply that the present whole-rock fluorine analyses do not represent the original content of the magma, but that volatiles have been lost from the system. Bailey (1977) notes that fluorite deposits and greisen associated with granites are usually at some distance above the roof of the body.

Manning (1979) presents data which conflict with those of Kovalenko (1977), showing that addition of 1 wt% F causes the Ca-free ternary minimum to drop only to 690°C at 1kb. Temperatures as low as 630°C were only attained in the presence of 4 wt% F. This yields a solidus temperature drop of c.80°C at 3 wt% F, which agrees well with a drop of 70°C at 3 wt% HF at 2.75kb given by Wyllie and Tuttle (1961). This suggests that, to a first approximation, the effect of fluorine on the granite system is independent of pressure and that the solidus would be lowered by about 10°C in the presence of 0.4 wt% F. Relatively low concentrations of fluorine in a granitic magma do not therefore have any great effect on the crystallization history except to introduce topaz as a subsolidus phase. On the other hand, the effects of addition of F, for instance as a component of a late phase, are very marked.

If a granite body has just crystallized and is only a few degrees below its solidus temperature, then the addition of only 0.5wt% fluorine would be sufficient to cause considerable remelting or at least extensive recrystallization. It is proposed that such a mechanism could account for the growth of alkali feldspar porphyroblasts in the uppermost parts (i.e. Area 2) of the Dragsmark granite. If this were the case it would mean that the blastesis was intimately associated with the intrusion of the granite. The implications of this hypothesis are discussed further in Chapter 10.

Figure 8.1

Projections in the granite system showing data for two veins cutting the Kållviken granite (3001 and 3002) together with the field occupied by the Dragsmark granites. Isotherms on the $P_{H_2O} = 5$ kb isobaric cotectic surfaces are taken from Winkler and Breitbart (1978).

A : Q - ab - or projection

B : an - ab - or projection

∇ : veins

 : Dragsmark granites

ta for two veins cutting

r with the field

ns on the P_{H_2O} = 5 kb

nkler and Breitbart (1978).

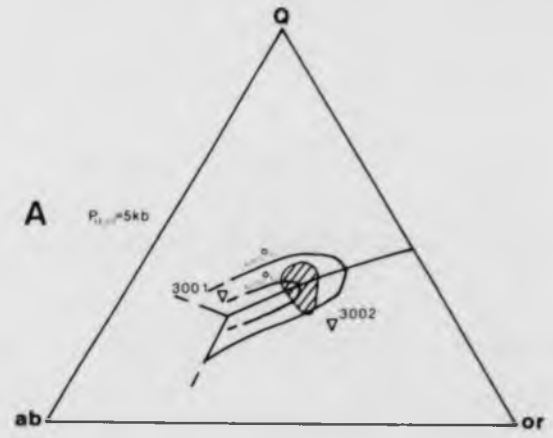

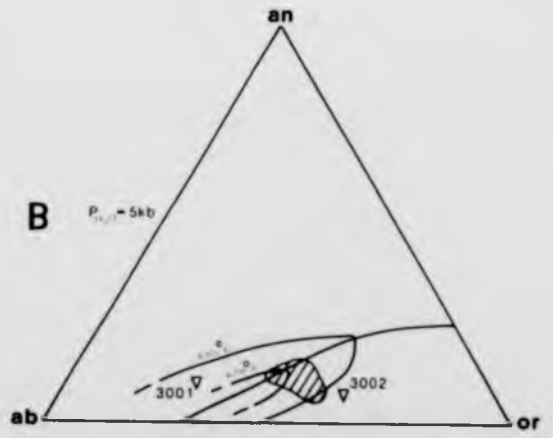

Figure 8.2

AFM diagram for the Dragsmark granites. Total iron as FeO.

o - Area 1 granites

• - Area 2 granites

R,N - field of Rapakivi and Nigerian Younger Granites

BC - field of British Caledonide granites

(From Brown et al, 1981)

iron as FeO.

Granites

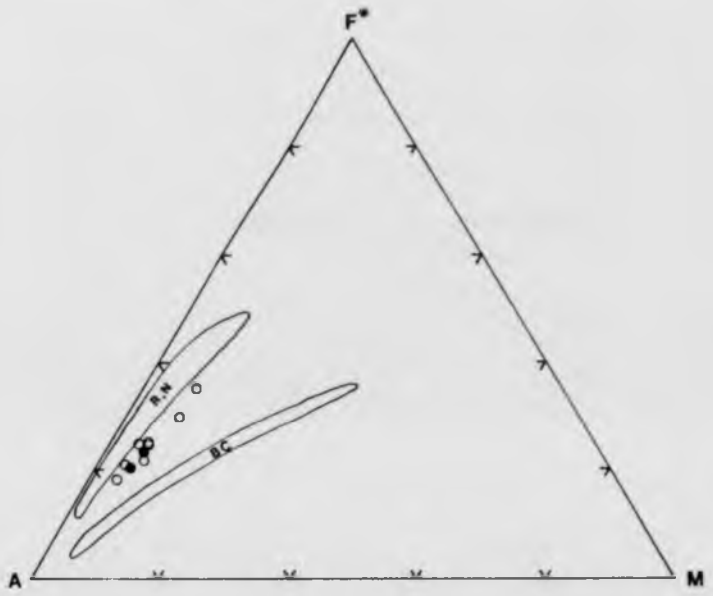

Figure 8.3

Data for the Dragsmark granites plotted on the Y v Sr and Ba v Rb discriminant diagrams of Brown et al. (1981), with various granites from the British Caledonides for comparison.

o - Area 1 granites

• - Area 2 granites

C - Cairngorm

D - Loch Doon

RFS - Rogart, Foyers, Strontian

he Y v Sr and Ba v Rb

), with various granites

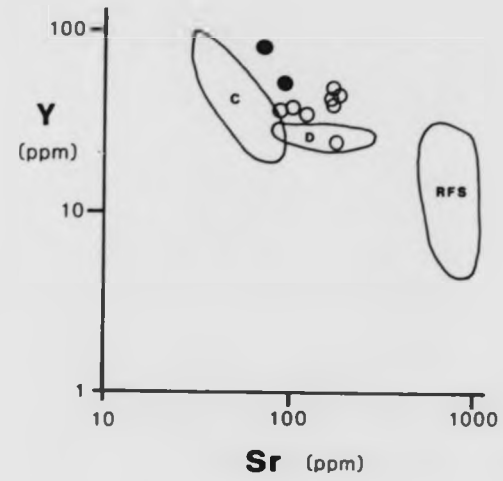

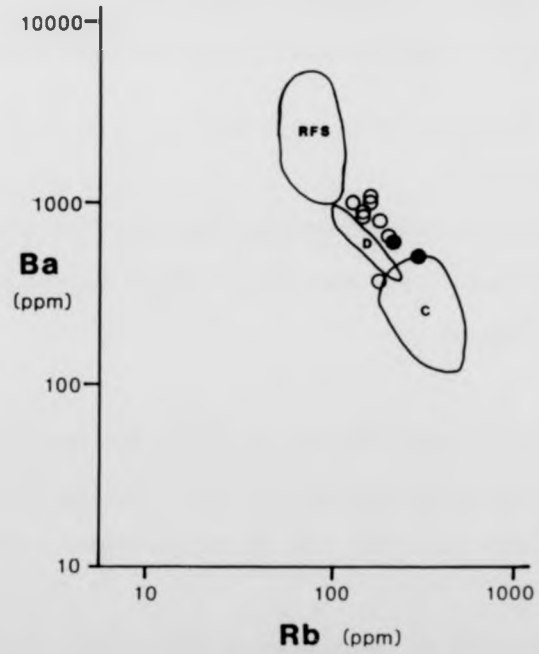

Figure 8.4

Modified A'CF diagram of White and Chappell (1977)

A' - Molecular proportion of Al-Na-K

C - Molecular proportion of Ca

F - Molecular proportion of Fe+Mg

I - Field of I-type granitoids

S - Field of S-type granitoids

♦ - Average mineral compositions from universal stage determinations (plagioclase) and electron microprobe analyses (garnet and biotite)

o - Whole rock analyses of Area 1 Dragsmark granite

• - Whole rock analyses of Area 2 Dragsmark granite

+ - Whole rock analyses of the gneissose granite

For derivation of tie-lines see text p. 89.

(1977)

versal stage determinations

analyses (garnet and

rk granite

rk granite

granite

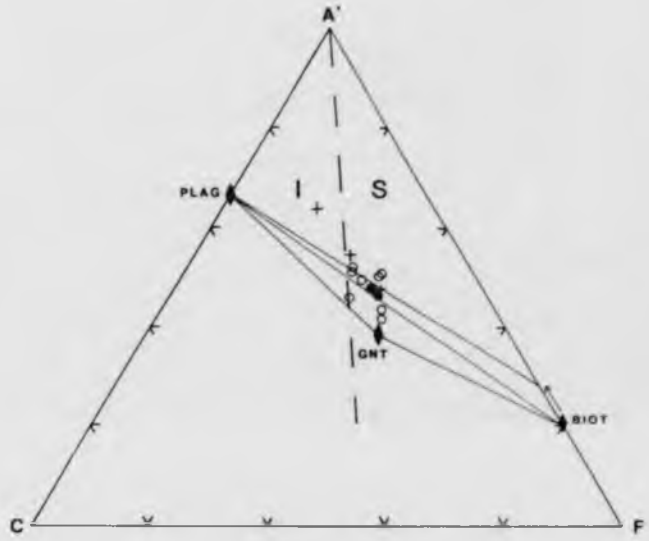

Figure 8.5

K v Rb diagram showing data for the Dragsmark granites together with the fractionation trends of Shaw (1968).

o - Area 1 granites

• - Area 2 granites

MT - Main trend

PH - Pegmatite-Hydrothermal trend

granites together with

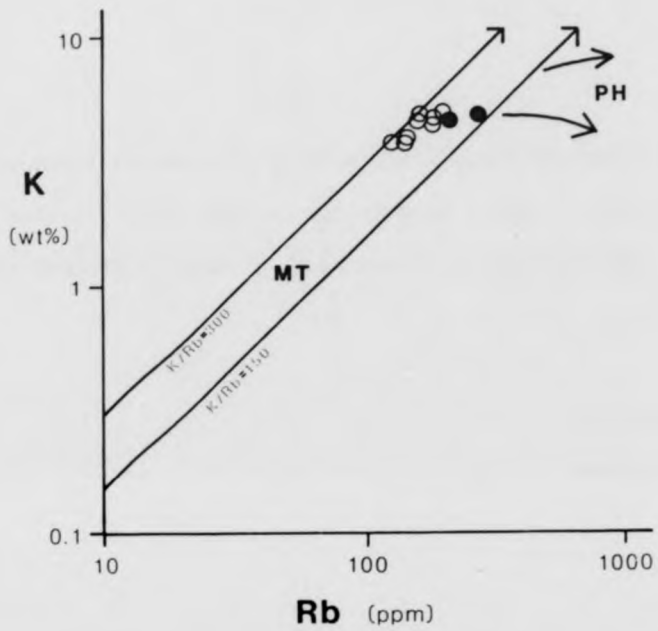

Figure 8.6

Plot of CaO v Y for the Dragsmark granites together with the standard calc-alkaline trend (C-A) of Lambert and Holland (1974). Also shown schematically are the effects of addition of various mineral phases to a granitic melt.

o - Area 1 granites

• - Area 2 granites

gether with the standard
land (1974). Also shown
various mineral phases to

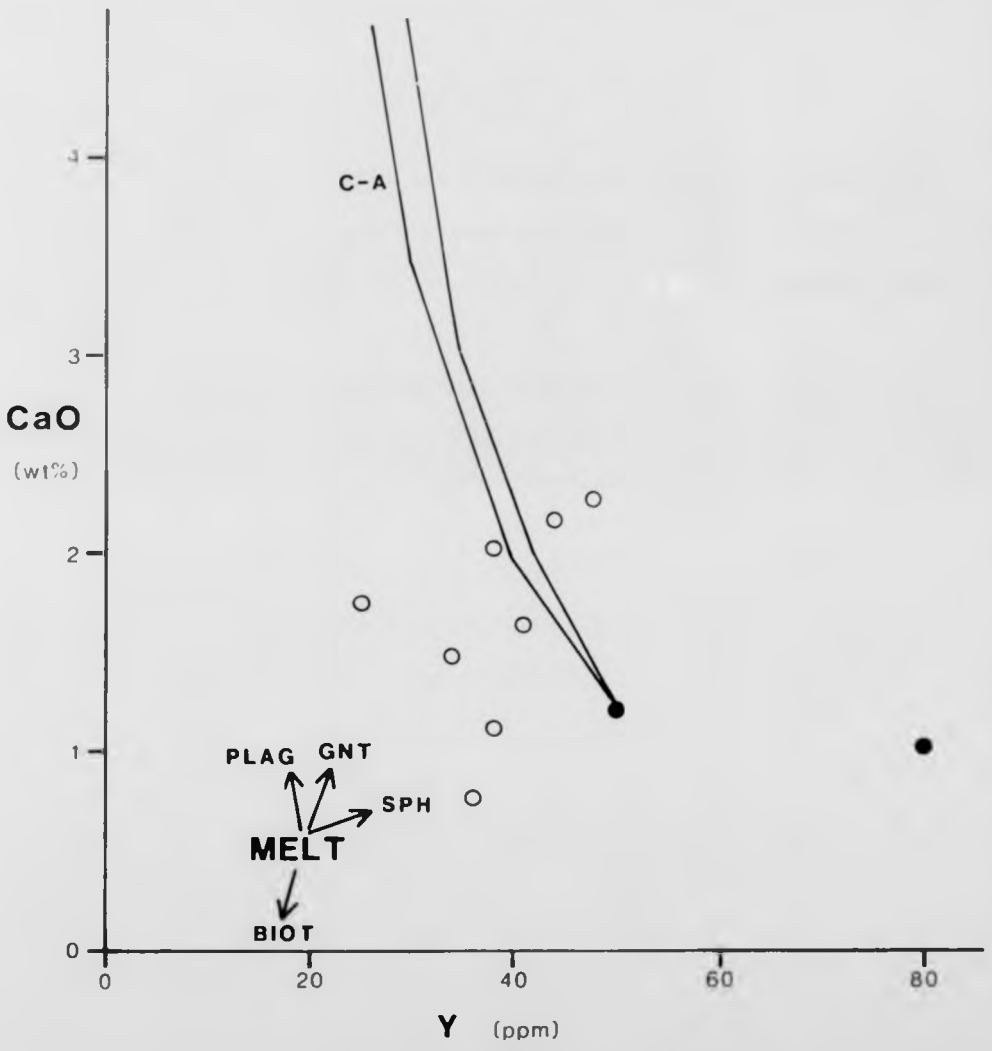

Figure 8.7

The or - ab - an - Q tetrahedron showing the various cotectic and eutectic points, the cotectic surfaces and the cotectic line (after Winkler, 1979).

E_1, E_2, E_3, E_4, E_6 : eutectics in the various binary systems

E_5 : ternary eutectic in the system Q - or - an - H_2O

P : quarternary minimum (eutectic above c. 2.2kb)

$E_1 - E_2 - E_5 - P$: Qtz + Plag + Liquid + vapour cotectic surface

$E_5 - E_3 - P$: Qtz + Ksp + Liquid + vapour cotectic surface

$E_5 - E_6 - E_4 - P$: Ksp + Plag + Liquid + vapour cotectic surface

$P - E_5$: the cotectic line

See text (p.92 and ff.) for further discussion.

rious cotectic and

he cotectic line

us binary systems

an - H_2O

2.2kb)

cotectic surface

tic surface

cotectic surface

ion.

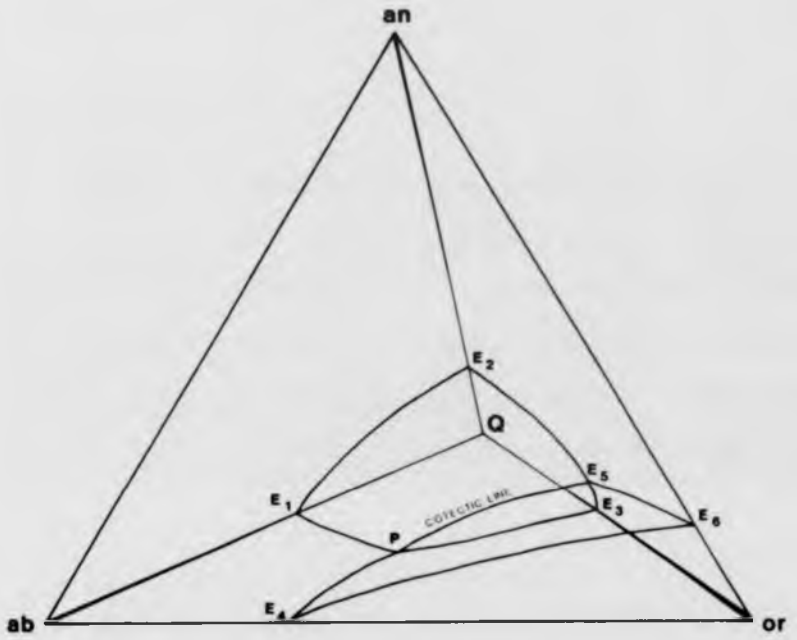

Figure 8.8

Q - ab - or projection showing data for the Dragsmark granites. The heavy lines are the projections of the cotectic lines, the lighter lines are isotherms on the P_{H_2O} = 5 kb isobaric cotectic surfaces. The wt% an on these various curves is given by the larger numbers; the smaller numbers, beside data points, indicate the wt% an for each sample. (After Winkler and Breitbart, 1978).

o - Area 1 granites

• - Area 2 granites

⧫ - average modal analysis of Dragsmark granite

...egsmark granites.

...otectic lines, the

... isobaric cotectic surfaces.

... by the larger numbers; the

... the wt% an for each

...nite

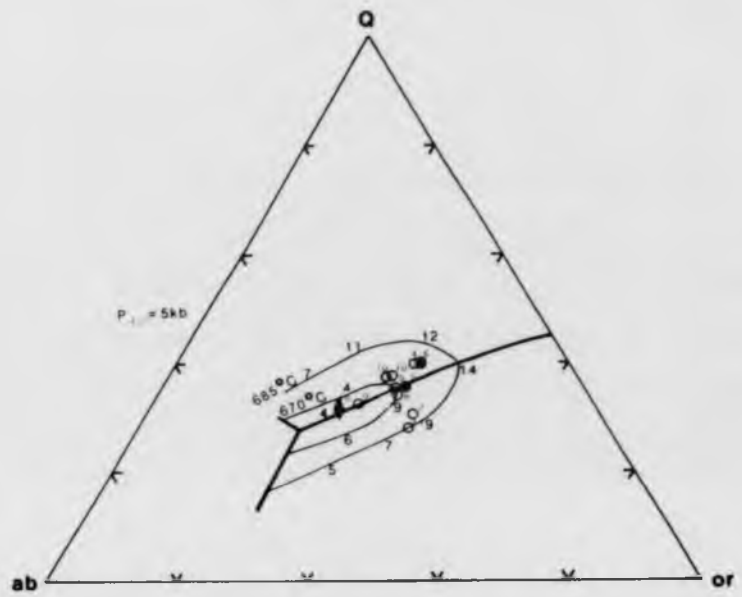

Figure 8.9

an - ab - or projection showing data for the Dragsmark granites. The heavy line is the projection of the cotectic line ($P\text{-}E_5$ of Fig. 8.7), the lighter lines are isotherms on the $P_{H_2O} = 5$ kb cotectic surfaces. The wt% Q on these various curves is given by the larger numbers; the smaller numbers, beside data points, indicate the wt% Q for each sample. (After Winkler and Breitbart, 1978).

Symbols as for Figure 8.8

ngsmark granites. The
line ($P\text{-}E_5$ of Fig. 8.7),
5 kb cotectic surfaces.
the larger numbers; the
the wt% Q for each sample.

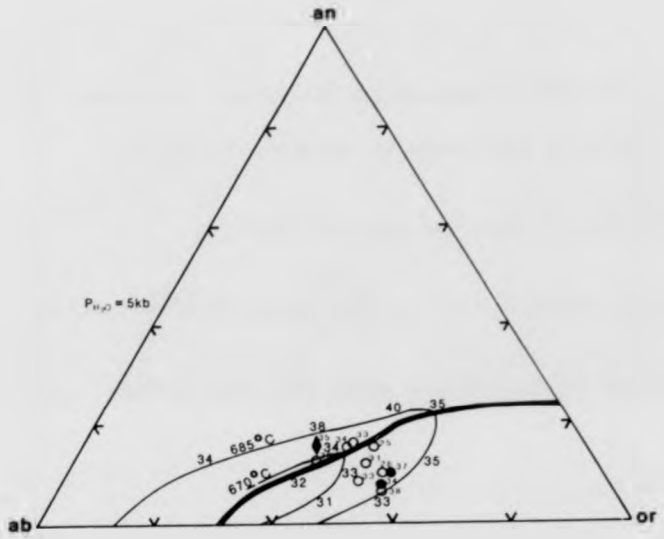

Figure 8.10

P_2O_5 v SiO_2 variation diagram to illustrate the trends caused by different magmatic processes in granitic rocks.

A - Moruya Suite : minimum melt and restite

B - Tuolumne Meadows Suite : fractional crystallization

C - Jindabyne Suite : non-minimum melt and restite

(From White and Chappell, 1976)

the trends caused by

ks.

stallization

restite

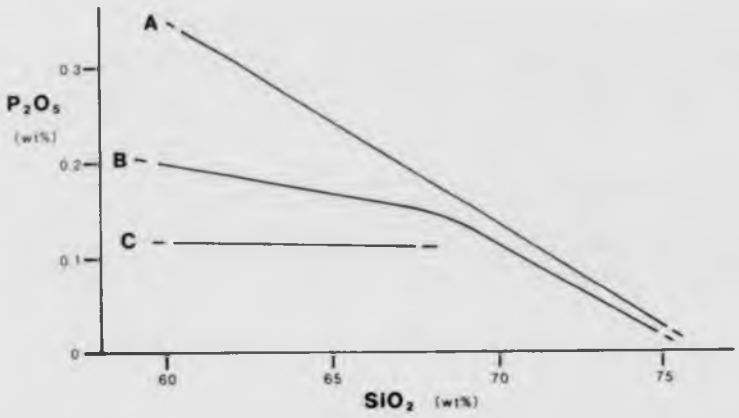

Figure 8.11

Interelement variation diagrams for the Dragsmark granites.

i) Elements not incorporated in a 'minimum melt'.

MgO, Fe_2O_3t, TiO_2, MnO, P_2O_5 and Zr v SiO_2

o - Area 1 granites

• - Area 2 granites

SLM - compositional range of pelitic Stora Le -Marstrand paragneisses (from Daly, 1978).

gsmark granites.

melt'.

O_2

e -Marstrand paragneisses

(from Daly, 1978).

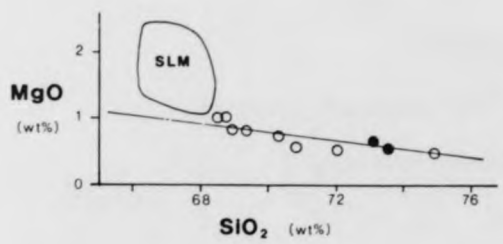

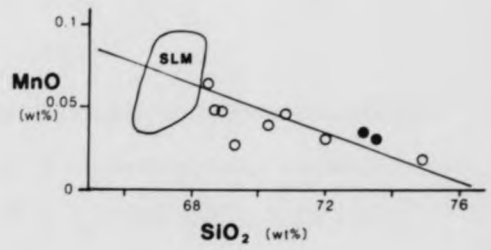

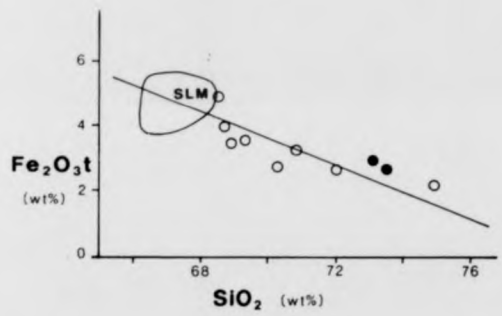

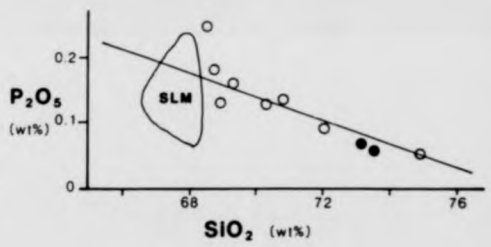

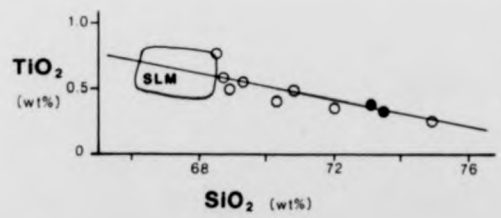

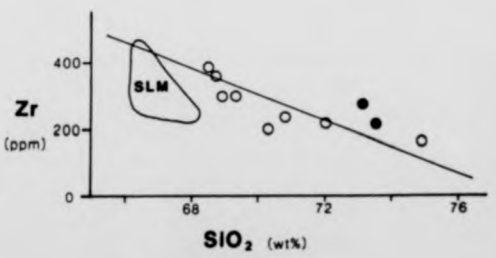

Figure 8.12

Interelement variation diagrams for the Dragsmark granites.

ii) Elements incorporated in a 'minimum melt'.

CaO, Al_2O_3, Na_2O and K_2O v SiO_2

Symbols as for Figure 8.11

smark granites.

t'.

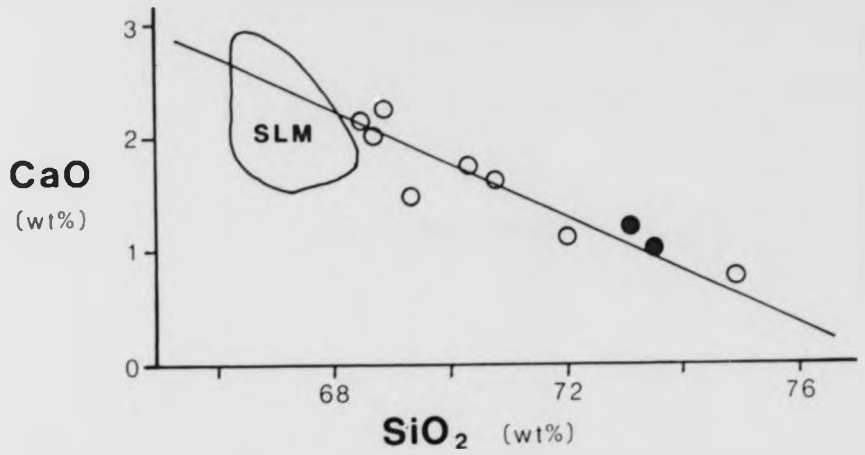

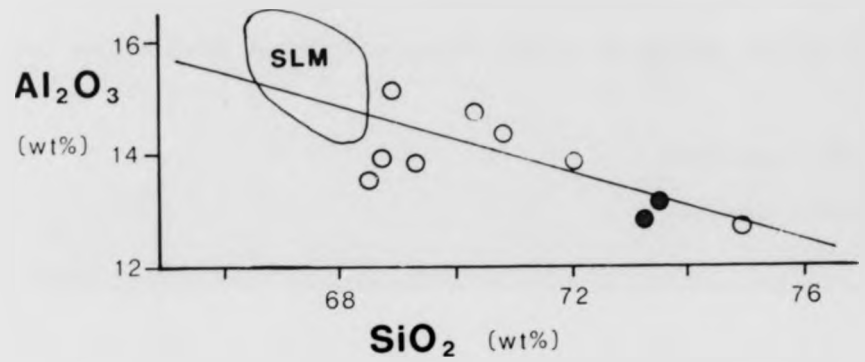

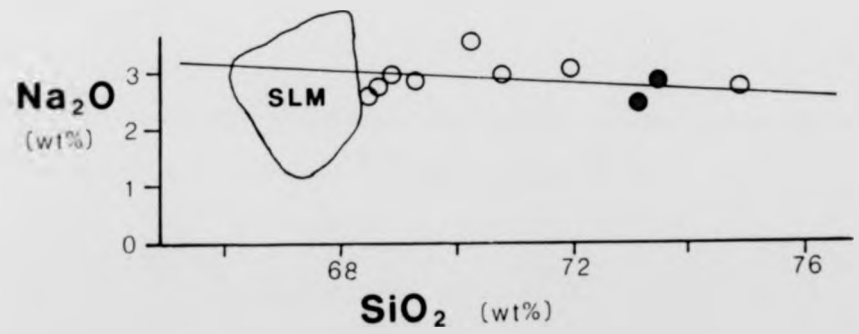

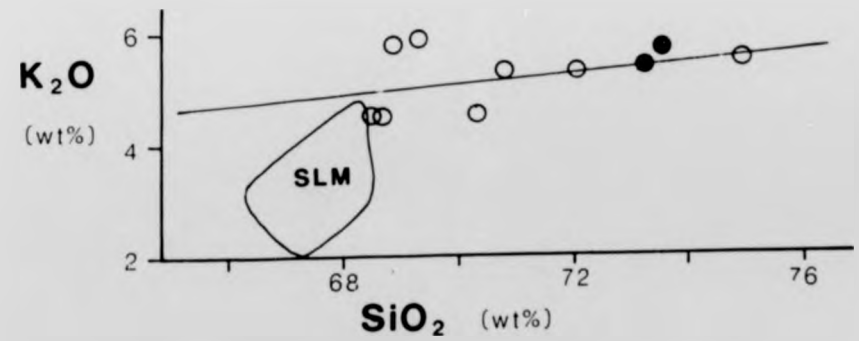

Figure 8.13

Plot of Li v F for the Dragsmark granites. Samples from near contacts (nos.53 and 72) illustrate loss of fluorine from the margins (see text).

o - Area 1 granites

• - Area 2 granites

amples from near contacts

from the margins (see text).

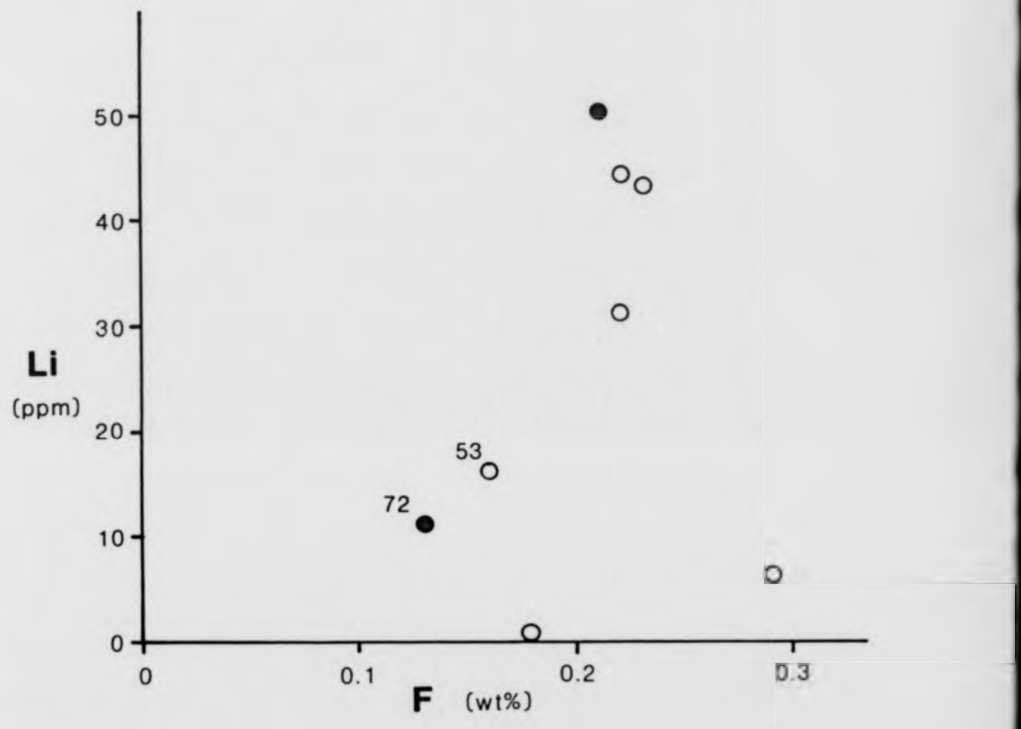

Chapter 9

Garnet-Biotite Geothermometry

a) Thermodynamic Basis

In theory, any reaction involving cation substitution can be used as a geothermometer/geobarometer. In practice, only in reactions for which ΔH (the enthalpy change of reaction) is large are the compositions of the phases involved sufficiently dependent on temperature for the reaction to be usable as a geothermometer. A further constraint is that the standard-state thermodynamic data and activity-composition relationships must be known with reasonable accuracy. For biotite and garnets of essentially almandine-pyrope composition all these criteria are satisfied, but there is still uncertainty regarding the effect of Ca (as grossular) on the activity-composition relationships of garnet. It is in the treatment of factors such as the amount of Ca, Mn, Ti present in the system that most of the published calibrations differ; a number of models are examined here.

The basis of the garnet-biotite geothermometer is the partitioning of iron and magnesium between the various phases in the reaction

$$\underset{\text{almandine}}{Fe_3Al_2Si_3O_{12}} + \underset{\text{phlogopite}}{KMg_3AlSi_3O_{10}(OH)_2} \rightleftharpoons \underset{\text{annite}}{KFe_3AlSi_3O_{10}(OH)_2} + \underset{\text{pyrope}}{Mg_3Al_2Si_3O_{12}}$$

At equilibrium

$$\Delta G^o = -RT \ln \left[\frac{a^G_{Mg} \cdot a^B_{Fe}}{a^G_{Fe} \cdot a^B_{Mg}} \right] = -RT \ln K \qquad (1)$$

where $$a^G_{Mg} = \left[X^G_{Mg} \cdot \gamma^G_{Mg} \right]^3 \quad \text{etc.} \qquad (2)$$

and, taking the standard state to be the pure phase at the pressure and temperature of interest,

$$\Delta G^{o} = \Delta H_{1\ bar,T} - T\Delta S^{o}_{T} + (P-1)\Delta V^{o} \qquad (3)$$

where G = Gibbs free energy

H = enthalpy

S = entropy

a^{G}_{Mg} = activity of pyrope in garnet

X^{G}_{Mg} = cation proportion of magnesium in garnet

γ^{G}_{Mg} = activity coefficient of magnesium in garnet

Substitution of equation (2) into the activity term in equation (1) yields expressions in X and γ. The expression $\frac{X^{G}_{Mg} \cdot X^{B}_{Fe}}{X^{G}_{Fe} \cdot X^{B}_{Mg}}$ is called K_D, the distribution co-efficient. If all solid solutions in the reaction are assumed to be ideal i.e. all $\gamma = 1$ then the condition for equilibrium becomes

$$\Delta G^{o} = -3RT \ln K_D \qquad (4)$$

A knowledge of the standard state thermodynamic properties thus allows calculation of the equilibrium temperature; alternatively, empirical observation of a correlation of $\ln K_D$ with temperature otherwise estimated can be made.

b) Available Models

i) Thompson (1976) presents a graph of $-\ln K_D$ against T, from which the relationship

$$T\ (^{o}K) = (\ln K_D + 3.667) / 0.0033 \qquad (5)$$

may be derived. Temperatures are obtained from consideration of P - T - X phase relations in the system $K_2O - FeO - MgO - Al_2O_3 - SiO_2 - H_2O$ for pelitic rocks. The assumptions are made of ideal mixing in almandine - pyrope solid solutions, low Fe^{3+} in biotite, and implicitly that all minerals in the rock are in equilibrium.

ii) Goldman and Albee (1977) attempt statistically to take account of the effects of Ca, Mn, Ti etc. on the system, deriving a five-parameter and a two-parameter solution from a relatively small number of samples having a mean X^{G}_{Ca} of 0.072, and the assemblage biotite-garnet-quartz-muscovite ± plagioclase ± accessories. The two-parameter solution does not involve compositional parameters (other than K_D). They also assume ideal mixing for garnets, and their calibration is dependent on the attainment of chemical and oxygen isotopic equilibria at the same temperature. In concluding they suggest that the calibration of the quartz-magnetite $^{18}O / ^{16}O$ geothermometer on which the method is based may be incorrect at temperatures greater than $550^{o}C$.

iii) Ferry and Spear (1978) investigated Fe - Mg partitioning between synthetic garnet and biotite experimentally at P = 2.07kb and T = 550 - 800°C. From their results they derived values for the thermodynamic properties of the Fe - Mg garnet-biotite reaction (p.102) of ΔH^{o} = 12,454cal. and ΔS^{o} = 4.662e.u. , together with the relationship

$$\ln K_D = -2109 / T + 0.782 \qquad (6)$$

Combining these and rearranging yields (using equations (3) and (4))

$$T(^{o}K) = 12{,}454 + 0.057\,P(bars) / (4.662 - 3R\,T \ln K_D) \qquad (7)$$

They suggest that this model, which assumes ideal mixing of garnets of composition $alm_{\geq 80}\ py_{\leq 20}$, can be used without correction for systems where $X^{B}_{Ti} + X^{B}_{Al^{VI}} \leq \sim 0.15$ and $X^{G}_{Ca} + X^{G}_{Mn} \leq \sim 0.2$.

All these models (i, ii, iii) have errors of the order of $\pm 50^{o}C$ associated with them.

iv) Hensen et al. (1975) use the symmetrical regular solution model for pyrope-grossular solid solutions to derive the activity - composition relationships from experimental data on garnets with 10 - 12 mole % grossular at temperatures of 1000 - 1300°C and pressures of 15 - 21 kb. Their results indicate the existence of a solvus with a critical temperature of 629 ± 90°C. Combining their data with the work of Cressey et al. (1978) on almandine-grossular solid solutions in the range 850 - 1100°C enables calculation of $\ln\left[\frac{\gamma^{G}_{Mg}}{\gamma^{G}_{Fe}}\right]$ as a function of composition and temperature. Comparison of this with the value of $RT \ln\left[\frac{\gamma^{G}_{Mg}}{\gamma^{G}_{Fe}}\right]$ derived from O'Neill and Wood (1979) (equation 15) yields temperatures for the present study of the order of 1000°C. This is clearly geologically unacceptable, being some 200°C or more above the liquidus for wet granite at pressures greater than 1kb. The most likely sources of error are the values of γ^{G}_{Mg} and the various interaction parameters; both Hensen et al. (1975) and O'Neill and Wood (1979) present data only for Mg-rich compositions at supersolvus temperatures, whereas the present study is concerned with Mg-poor compositions at temperatures where a miscibility gap is present in the pyrope-grossular solid solution series.

c) Discussion of Results

Analysis of garnet-biotite pairs from a variety of lithologies from the Dragsmark area was performed by electron-microprobe. Results are presented in Tables B9.1 and B9.2 with values for the relevant compositional factors in Table B9.3. In most samples it was possible to find grains of garnet and biotite actually in contact with no reaction rims. Such instances were taken as evidence of equilibrium but even then points were analysed a short distance from the edges of the grains to avoid the possibility of reverse zoning in the garnet rims. In no case was the distance between analysed garnets and biotites greater than 1mm.

Because of the pervasive chlorization (probably associated with D4 deformation) along fractures in garnets, no systematic study of zoning was attempted. Several garnets were analysed at both rim and core however, and the results are tabulated in Table B9.1 and represented diagrammatically in Fig. 9.1, together with data for a garnet from an Orust dyke taken from Daly (1978). None of the Orust dykes sampled in Dragsmark contained garnet and biotite in close association.

Fig. 9.1 shows that, within analytical error (Dunham and Wilkinson, 1978), the garnets are essentially homogeneous with respect to MgO and CaO and show decreasing MnO and increasing FeOt from core to rim, with the notable exception of 133 no.4, from an older amphibolite, where CaO increases from core to rim, FeOt decreases, and MnO and MgO are constant. Many garnets from such amphibolites in the Dragsmark area show inclusion-filled cores and inclusion free rims (Fig. 9.2A), indicating two phases of growth. The patterns of zoning in garnets exhibited by the megacryst granites and later Orust dykes however, suggest a simple history of growth with falling temperature or incomplete equilibration to a temperature below that of formation.

As the various methods described in model iv) for estimating the values of the activity coefficients in garnet produce meaningless temperatures, only the first three models, all of which assume ideal mixing, are used. Temperatures for the analysed mineral pairs derived from Thompson (1976) - equation (5), Goldman and Albee (1977) - both solutions, and Ferry and Spear (1978) - equation (7) are given in Table 9.1 , together with data for Orust dykes from Daly (1978). A pressure of 3kb (see Ch.7) is used in equation (7) ; the effects of pressures below c.10kb are negligible.

The variation, both within and between methods, in temperature estimates for all samples of megacryst-bearing granite is less than the associated error ($\pm 50^{o}C$), with the exception of the Goldman and Albee two-parameter solution (Table 9.1, Method c). This close agreement between three methods based on fundamentally different principles argues strongly for the acceptance of the estimated temperature of about $630^{o}C$.

The one sample from the gneissose granite (624) yields very high temperatures, c.$800^{o}C$, although all three methods are still in moderate agreement; the two-parameter solution yields much lower values. Taking the activity-composition relationships of garnet into account (see discussion on p.105), it seems likely that at temperatures above c.$630^{o}C$ the assumption of ideal mixing becomes untenable and hence the temperatures estimated may be invalid.

Considering next the basic rocks, both older amphibolites and Orust dykes, the geothermometers of Thompson (1976) and Ferry and Spear (1978) are still in close agreement. Temperatures estimated using the method of Goldman and Albee (1977) (Table 9.1 , Method b) are, on average, $80^{o}C$ higher. Their method is the only one of those discussed in which the composition of the 'host' rocks is likely to be involved in the cal-

TABLE 9.1

Temperatures calculated by Garnet-Biotite Geothermometry

Method	a)	b)	c)	d)
Sample (gnt,biot)	Temperature (°C)			
Dragsmark granites				
32 3,2	631	613	552	619
32 4,5	680	653	585	683
32 6,7	661	638	571	657
935 3,1	626	612	548	612
53 5,4	634	614	553	622
53 6,3	629	599	550	616
Average	643	612	560	635
Standard Deviation	22	20	15	29
Källviken granite				
30 1,2	632	600	552	620
30 4,3	657	625	569	651

a) Thompson (1976)

b) Goldman and Albee (1977) 5-parameter solution

c) ibid. 2-parameter solution

d) Ferry and Spear (1978)

TABLE 9.1 (cont.)

Sample (gnt,biot)	Method	a)	b)	c)	d)
		Temperature (^{o}C)			
Stora Le -Marstrand gneisses					
6	2,1	623	596	487	609
6	4,3	517	468	547	496
Gneissose granite					
624	2,1	755	770	646	805
624	4,3	779	826	667	849
Older amphibolite					
133	1,2	705	774	604	721
133	4,3	679	711	584	682
133	6,5	647	699	562	639
Orust dykes (data from Daly,1978)					
Average		483	578	478	471
Range		445-546	555-607	454-505	438-529

ibration (see Ch.9b). It is interesting to note that the temperatures derived using this model differ least from those of the others when the bulk rock compositions are closest to those of the samples on which the calibration is based i.e. sialic. Moreover, in their Fig.3 (p.761, op. cit.), the five-parameter solution yields a range in temperatures of 135°C for hornblende-garnet-biotite rocks as opposed to a range of 60°C for the two-parameter solution, which excludes the compositional variables. Temperatures estimated using this two-parameter solution for the Dragsmark samples and the Orust dykes of Daly (1978) are given in Table 9.1 , Method c. As can be seen from the Table, this solution agrees with the other geothermometers for the Orust dykes, but yields lower temperatures for the granites (average 559°C) and especially for the gneissose granites and older amphibolites.

It is concluded that the Ferry and Spear (1978) garnet-biotite geothermometer is the most reliable available at present and that it can be used with confidence in all lithologies and for garnets of X_{Ca}^{G} as high as 0.35 for temperatures of up to c.650°C, above which it probably over-estimates. The Goldman and Albee (1977) five-parameter solution is only applicable to sialic rocks, but their two-parameter solution provides reasonable estimates for all lithologies and is perhaps better than the Ferry and Spear model at higher temperatures.

The model proposed in Chapter 8 of derivation of the Dragsmark granites by anatexis and palingenesis of Stora Le -Marstrand paragneisses to yield a magma of a 'minimum melt' and a restite implies that most of the mafic mineralogy of the granites is inherited. This view is supported by textural evidence (Fig. 9.2B) of deformation of garnets in the Dragsmark granites, the close association of fractured garnets with undeformed alkali feldspar megacrysts (Fig. 9.3), and field observations that garnets do not cut the S2 fabric. In contrast, Daly (1978) notes

that garnets in Orust dykes are syn- to post-D3. Moreover, the preservation of igneous and metasomatic features in the alkali feldspars, together with the lack of evidence for local partial remelting, argues strongly against a post-intrusion metamorphic temperature of 630°C, only slightly below the wet granite solidus. The conclusion is therefore drawn that the garnets in the Dragsmark granite are inherited and have equilibrated in the late-magmatic stage. The blocking temperature may perhaps be related to the departure of fluids from the system, which would severely inhibit ion exchange between minerals.

Figure 9.1

Compositional zoning in garnets from the Dragsmark area, determined by electron microprobe spot analyses.

Plots of FeOt, MgO, CaO, and MnO against qualitative position within the crystal.

▽ - Orust dyke (Daly, 1978; sample no. SBR 25)

o - Dragsmark granite; sample no. 935/3

● - Kallviken granite; sample no. 30/4

△ - Older amphibolite; sample no. 133/4

\+ - Stora le -Marstrand paragneiss; sample no. 6/4

smark area, determined

litative position

25)

no. 6/4

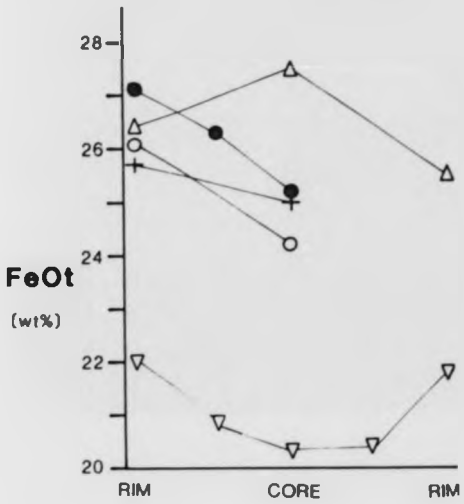

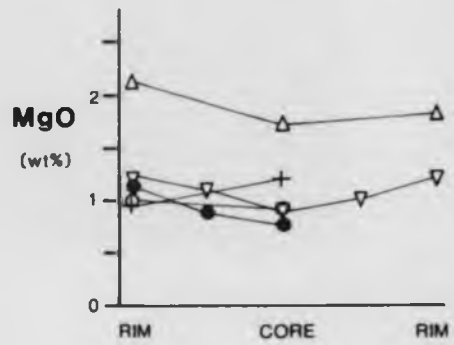

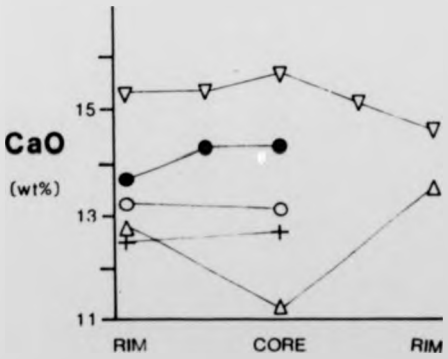

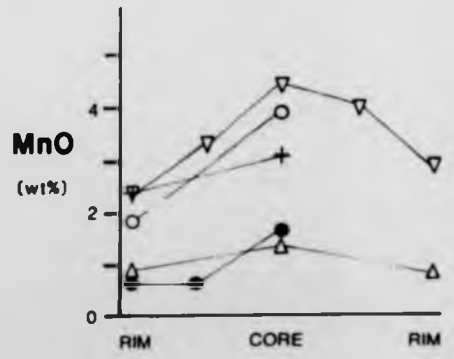

Figure 9.2

A : Photomicrograph of garnets in an older amphibolite showing inclusion (mainly quartz) filled cores and inclusion-free rims.
Sample no. 133.
Plain polarized light.

B : Photomicrograph of a highly deformed garnet in the Dragsmark granite (sample no. 253).
Plain polarized light.

amphibolite showing
and inclusion-free rims.

arnet in the Dragsmark

A

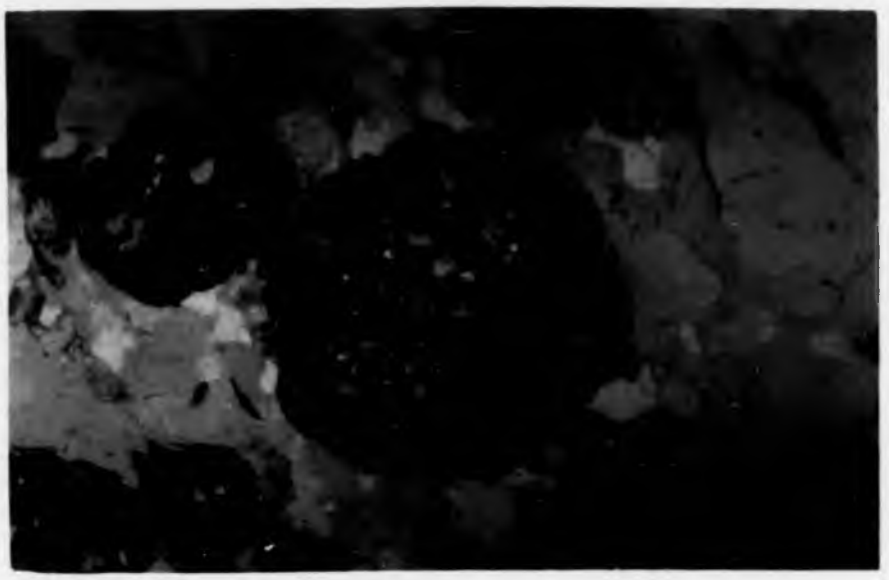

B

A

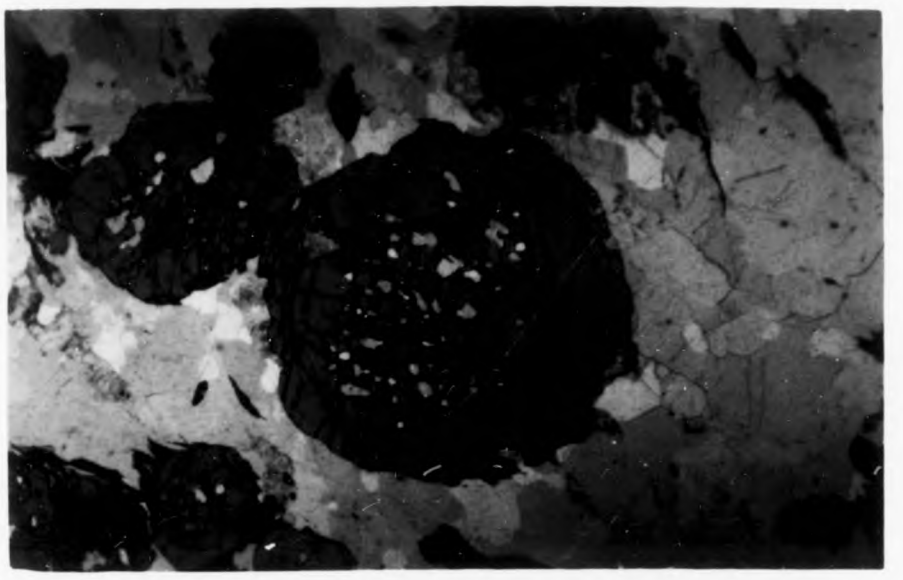

B

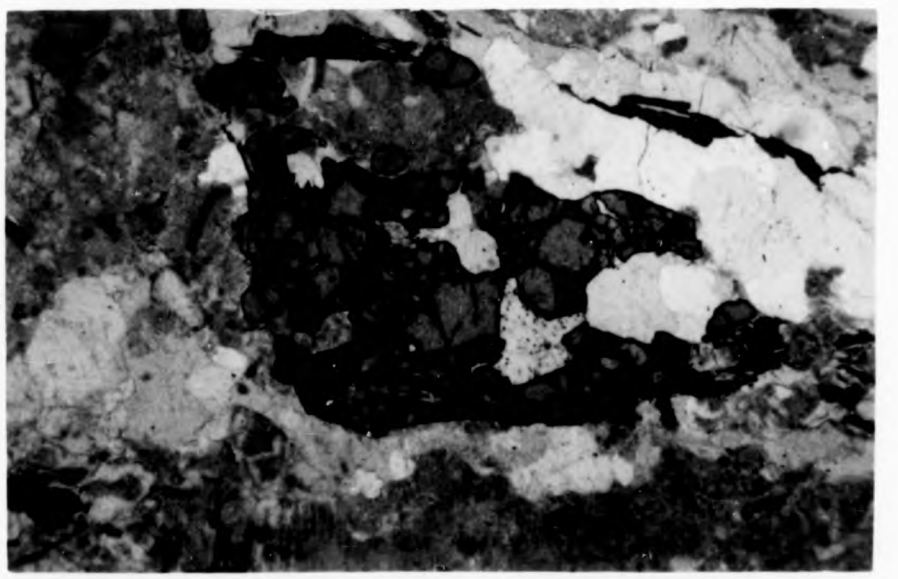

Figure 9.3

Photograph of deformed garnets (G) in close association with relatively undeformed alkali feldspar megacrysts (A) in the Dragsmark granite at loc. 541.

Lenscap measures 5 cm. across.

agsmark

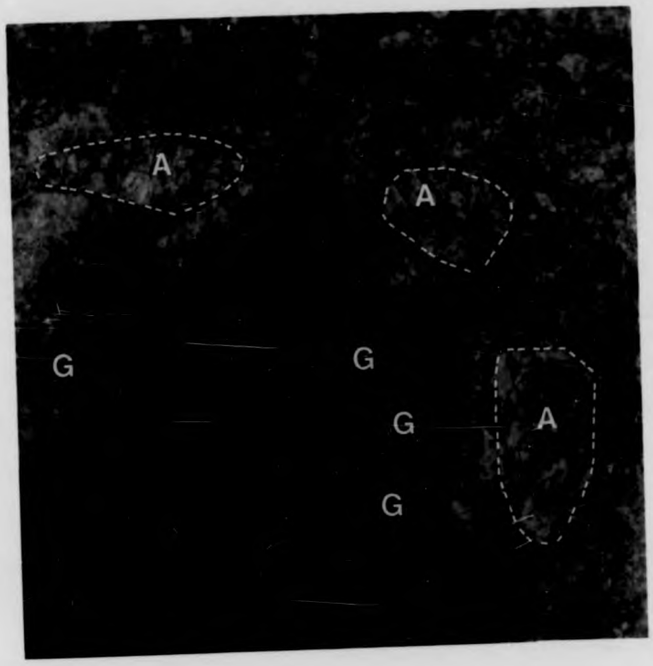
A
A
G
G
G
A
G

Chapter 10

Discussion and Conclusions

a) Introduction

The granites of Dragsmark are pink, medium-grained, extremely megacrystic monzogranites. They have the assemblage:

Quartz - K-feldspar - plagioclase - biotite

with minor garnet, sphene, topaz and accessories. Optically the alkali feldspar megacrysts are perthitic microclines, but X-ray diffraction studies reveal a relict monoclinic phase. These megacrysts exhibit a range of relationships to structural features such as foliation and folding. The Kållviken granite can be distinguished by its much greater degree of deformation.

Chemically, the Dragsmark granites are homogeneous, with a range of silica content of only 68% to 75%. The average SiO_2 content is 71%, with a mean K_2O/Na_2O ratio of 1.85, average CaO of 1.53% and average total ferromagnesian content of 1.6%.

The granites consist of a main lower sheet (termed Area 1), which is split into two wedges above and below the Kållviken granite, and a number of smaller overlying sheets (termed Area 2). The main sheet attains a (pre-deformational) thickness in excess of 600m in the north-east.

The three most important questions concerning the Dragsmark granites are their origin, position in the regional geological chronology (and temporal relationship to the Kållviken granite) and the origin and nature of the alkali feldspar megacrysts. These points are addressed in the following sections.

b) Origin of the Dragsmark Granites

The lack of a ghost stratigraphy and general absence of feldspar porphyroblasts from the wall rocks argues against an origin by in situ metasomatism. Locally, especially near Rödberget, metasomatic effects are observed, but these can readily be related to the expulsion of fluid from the intrusion on its crystallization. There is abundant field evidence, in the form of partially assimilated country rock xenoliths and inhomogeneously distributed broken and corroded mafic phases (garnet and hornblende), for at least a major crustal contribution to the parent magma.

A closure temperature for diffusion of iron and magnesium between garnet and biotite of c.630^{o}C is indicated by three variants of this geothermometer. In the absence of evidence for extensive local remelting and bearing in mind that the post-granite Orust dykes show metamorphic assemblages consistent with the lower amphibolite facies, it is concluded that this temperature represents equilibration in the post-magmatic stage rather than during a later metamorphism. It is therfore inferred that the garnets (and presumably other refractory phases such as sphene and magnetite) are inherited from a crustal precursor.

Limited whole rock geochemical data support the hypothesis of a crustal (metasedimentary) source for the Dragsmark granites. They are classified as S-type on chemical grounds, although the mineralogy seems to indicate an I-type maga - but the mafic mineralogy is thought not to be igneous in origin.

Geochemical modelling of the mixing of a minimum-melting-point granitic magma with 'restite' suggests that the granites were derived by palingenesis of pelitic Stora Le -Marstrand type gneisses. A degree of melting of about 65% of the source is indicated, with the actual magma

that was emplaced being, on average, 80% melt.

The presence of two-phase aqueous fluid inclusions in quartz grains within alkali feldspar megacrysts demonstrates that a free hydrous phase was present when these quartz crystals were formed. An homogenization temperature of 330°C for these fluid inclusions is incompatible with a metamorphic origin, but yields an intersection with the wet granite solidus at 660-675°C and 3.2-3.4 kb pressure, corresponding to a depth of c.12 km. The Dragsmark granites are therefore considered to have crystallized under approximately these conditions from a wet magma.

The only alternative explanation for the above data is large-scale assimilation of a variety of lithologies by the ascending magma. If a granitic (s.l.) melt were to disaggregate a pre-existing granite (such as the Kållviken body), metasediments and minor amphibolites, it could conceivably acquire all the above-mentioned characteristics. No evidence concerning its origin and conditions of emplacement would then be available. This seems somewhat improbable, but could only be convincingly disproved by trace element and isotopic studies which have not been undertaken.

c) Chronological Significance

In general, the Dragsmark granites fit readily into the existing chronological framework for the Stora Le -Marstrand belt. They cut the S1 gneissosity in the country rocks and do not contain either of the two widely developed migmatitic leucosomes. As already noted, cross-cutting Orust dykes occur; these have elsewhere been shown to be affected by D3 and the contemporaneous metamorphism. The granites were therefore intruded after D1 but before D3, and the folds within them may be ascribed to D2 (as may the fabric).

In detail however, this simple interpretation of the chronology breaks down. In the south of the area, large-scale folds of the margins of the granite can be mapped out; the main augen fabric (S2A) is best interpreted as being axial planar to these folds. There is abundant textural evidence of syn-S2A growth of megacrysts. This deformation (D2A) was largely confined to the development of a planar fabric. This fabric is in turn affected by open to tight folds with wavelengths of 10 cm. to hundreds of metres. These folds are designated F2B, although all that can be said with certainty is that they are post-D2A and pre-D4. The minor folds are usually overgrown to a greater or lesser extent by alkali feldspar megacrysts, especially in the Vågerød body.

The fact that magmatic conditions of formation are indicated for fluid inclusions from all parts of the Dragsmark granite suggests that the megacrysts from the overlying sheets (Area 2) are of late- to post-magmatic origin rather than the result of a separate metasomatism. This supports the interpretation that those folds across which megacrysts grow are D2 in age, rather than D3.

Three megacrysts from the margins of granite outcrops have distinctive ternary feldspar chemistry which indicates a pressure of

formation of c. 1 kb. Discounting the possibility that the granite rose approximately 8 km. in the solid state, this suggests a later, minor, metasomatism after the removal of c. 2 kb. of overburden pressure. It is postulated that this event could be associated with the intrusion of hypersolvus (one feldspar) veins which cut the granite. These are of indeterminate age; they may perhaps be allied to the younger granites of Park et al (1979).

The Källviken granite is a highly deformed and migmatized augen granite, being slightly more melanocratic than the Dragsmark granite, although the two cannot be distinguished geochemically on the available evidence. In the field it has a generally more deformed nature with the widespread development of a migmatitic leucosome, locally axial planar to upright isoclinal folds affecting the main gneissosity.

This fabric could be correlated with that in the Dragsmark granite (S2A). This hypothesis cannot be disproved, but would require markedly heterogeneous strain after emplacement (during D2). It would also be difficult to account for the localized migmatization that would need to be invoked.

The alternative hypothesis, which is favoured here, is to correlate the neosome in the Källviken intrusion with the second generation migmatite leucosome in the country rock gneisses. The Koskår dykes, which cut both lithological units, also carry this leucosome but are not strongly foliated (except locally by S3 or S4). As the granite cuts S1 - the compositional banding in the gneisses - a relative chronology can be established. A local fabric-forming event is required after the intrusion of the Källviken granite but before the intrusion of the Koskår dykes, the development of the second generation neosome and the emplacement of the Dragsmark granites. The Källviken body may thus be tentatively correlated with at least parts of the Assmunderöd-Myckleby augen granite.

d) The Alkali Feldspar Megacrysts

The field appearance of theDragsmark granite is dominated by ubiquitous pink-red alkali feldspar megacrysts. These are usually 2 to 4 cm. long, but can be found up to 15cm. in length. The intensity of the colouration, which is due to the presence of sub-microscopic flakes of haematite within feldspar crystals, is qualitatively related to the degree of deformation; the reasons for this are not known. Megacrysts account for about 80% of the alkali feldspar and the Dragsmark granites may thus be described as extremely megacrystic.

The geographical division into Areas 1 and 2, corresponding respectively to the main sheet and smaller overlying sheets in the reconstruction of the primary shapes, is supported by differences in the properties of the megacrysts from the two Areas. These are described in detail in Chapters 3, 5 and 6. The evidence suggests that most megacrysts from Area 1 originated as phenocrysts, whilst Area 2 is dominated by porphyroblasts. It should be borne in mind that this distribution is not exclusive and individual crystals from any part of the intrusion may exhibit properties interpreted as indicative of either origin. Features regarded as diagnostic are summarized below.

Macroscopically, the S2A augen fabric is commonly seen to be overgrown by potassium feldspar megacrysts, with deformed and euhedral crystals occuring in the same hand-specimen. This is interpreted as indicating at least two phases of growth. Conclusive evidence for porphyroblastesis is given by the rare occurrence of megacrysts growing across contacts to wall-rock; this phenomenon is more common in Area 2.

Microscopically, features taken to imply a porphyroblastic origin include: string/crypto perthite, assimilation of groundmass plagioclase,

myrmekite rims, inclusions of, or local concentration of, topaz, and very irregular margins with extensive 'pseudopods'. In addition, crystals with porphyroblast-like features do not exhibit those characteristics indicative of a phenocrystic origin. These latter include: stepped Carlsbad twin planes, concentric zones of oriented plagioclase inclusions, bead perthites, and coarser microcline twinning at the rim. The latter two are taken as evidence of the preservation of superimposed disequilibrium textures. Many phenocrysts also show minor porphyroblastic growth of the rims.

Using the above criteria, 86% of alkali feldspar megacrysts from Area 2 are interpreted as porphyroblasts, contrasted with 50% from Area 1. These figures compare favourably with those derived by examination of feldspar chemistry. Analysis of alkali feldspars for the important cations (i.e. K, Na, Ca, Ba, Rb and Sr) reveals two populations of megacrysts distinguishable by their positions on triangular plots. The Rb, Sr and Ba contents and K/Ba andK/Na ratios are particularly useful in discriminating between the two groups, which are interpreted as corresponding to phenocrysts and porphyroblasts. Using this method, 85% of megacrysts from Area 2 are found to be porphyroblasts, but only about 10% from Area 1. Only approximately 10% of megacrysts cannot be assigned to one of the populations. The cause of the discrepancy in porphyroblast percentage in Area 1 given by the two methods is not known.

Some separation between the two groups is also apparent on plots of various cation concentrations and ratios against orthoclase content, with Area 2 samples tending to fall outside the 'Smith granite field'. This is largely due to their lower than normal Ba and Sr content.

The Rb/K and Ba/K ratios indicate that the Dragsmark granite was more crystalline at the time of growth of megacrysts from the overlying sheets than it was when those from the main sheet grew, supporting the

view of the former as porphyroblasts and the latter as phenocrysts. This is further evidenced by variations in the Ba content of the alkali feldspar. Electron microprobe analyses indicate a decreasing Ba content in phenocrysts from core to rim, which trend is also apparent in plots of bulk megacryst composition. From such diagrams it can be seen that the phenocrysts exhibit roughly constant K/Na ratio, whilst Ba and Sr decrease and Rb increases with fractionation. The groundmass K-feldspar from the main sheet is more fractionated than such megacrysts, as predicted by classical crystallization theories.

This is consistent with buffering of the orthoclase content during crystallization of a granitic magma under approximately constant pressure and temperature. Trace element concentrations would not be buffered and could therefore be expected to show greater variation. Minor fluctuations in the conditions of formation are evidenced by rhythmic variation in the K/Ba ratio of phenocrysts, with a wavelength of 80-500μ. This qualitative zonation has only been detected in samples from Area 1; it is not related to exsolution or twinning effects and is thus considered primary. Megacrysts from Area 2 have roughly constant K/Ba ratios and show no such variations.

Porphyroblasts also exhibit roughly constant bulk K/Ba and K/Sr ratios, whilst the orthoclase content is highly variable. It is postulated that this is explicable in terms of a greatly reduced availability of the constituent elements of alkali feldspar during metasomatism combined with considerable variation in vapour pressure and temperature.

The third source of evidence for a dual origin for the megacrysts of the Dragsmark granite is the study of their Al/Si structural state through X-ray powder diffractometry. All samples, of both megacrysts and

groundmass feldspars, consist of a dominant maximum microcline triclinic phase with exsolved low to intermediate albite lamellae. In about 70% of cases however, a third, monoclinic, phase is present. Such feldspars often show patchily developed cross-hatched twinning, indicating incomplete inversion to a triclinic lattice from a primary monoclinic state. They also commonly exhibit large Δa implying a highly strained lattice in the host potassic phase, again consistent with partial failure to invert.

Consideration of the relationship between the Al/Si order of this monoclinic phase in megacryst and groundmass alkali feldspar reveals a difference between samples from the main sheet and those from the overlying sheets. In the former, megacrysts are more disordered and hence probably crystallized at a higher temperature than the groundmass, whilst the reverse holds true in the latter. The first observation is consistent with a simple magmatic model of rapid growth of phenocrysts (thereby preserving metastable disordered states) followed by crystallization of the groundmass. Due to its finer grain size, slow cooling allowed this to equilibrate to lower temperatures. The preservation of relatively disordered states in the groundmass of the overlying sheets can be interpreted as due to rapid cooling as a result of the much smaller volumes of magma involved; this also accounts for the paucity of phenocrysts. The megacrysts in these bodies do not fit this model, being more ordered than the groundmass, and are best interpreted as porphyroblasts. Their lower degree of Al/Si disorder may be due to growth at lower temperatures and/or at a slower rate.

Three independent lines of enquiry have thus been shown to indicate a dual origin for the megacrysts of the Dragsmark granites. On the basis of the evidence presented, it is concluded that the majority of alkali feldspar megacrysts in the main sheet (Area 1) originated as phenocrysts, whilst those from the overlying sheets (Area 2) were formed by

porphyroblastesis, probably in the immediately post-magmatic stage.

Although inevitably speculative, it is felt appropriate to discuss possible mechanisms by which this dual origin could have arisen. The Rb/K ratios of megacrysts from various traverses through the main sheet indicate that crystals from the southern termination and from the upper part of the northern outcrop are less differentiated than those from the lower part of the northern outcrop (where the granite is thickest). Reconstruction of the original pre-deformational shape of the main sheet shows that it transgressed slightly upwards to the south and west, and it can therefore be postulated (although not proven) that the southern end was also topographically above the base of the northern zone. This is consistent with the earlier crystallization of these areas (i.e. the granite solidified from the roof downwards). This would further imply that most heat loss occurred through the roof zone.

Despite having crystallized earlier, the upper northern and the southern parts of the granite show the highest megacryst densities (number per unit area of outcrop) of the main sheet. The overlying Area 2 bodies exhibit great variation in megacryst density. It is here proposed that these facts, together with the origin by porphyroblastesis for most megacrysts from Area 2, can be accounted for by the autometasomatic effects of the escape of fluids from the cooling granite below.

The present average fluorine content of the Dragsmark granites is 0.21 wt%, but the ubiquitous occurrence of topaz suggests that the F content originally exceeded 0.4 wt%. There is therefore evidence that fluorine has escaped from the intrusions, presumably together with water (fluid inclusions record the original H_2O-oversaturated nature of the magma). Consideration of the effects of fluorine as a late-stage vapour phase within the granite system shows that as little as 0.5 wt% F would

cause considerable remelting or at least extensive remobilization. Such a fluid would naturally migrate upwards and its effects would be most extensive in those parts of an intrusion which received the greatest flux. One likely effect would be the recrystallization of alkali feldspar.

Thus fluid released from the lowest levels could have caused growth of porphyroblastic feldspar in the upper part of the main sheet, and the combined effects of the whole process would be seen in the overlying sheets. Porphyroblastesis is indeed observed to be the dominant megacryst-forming mechanism in the upper parts of the complex. There would of course be considerable variation in the flux through any given volume, thereby accounting for the variability in megacryst density and size in these upper intrusions.

In conclusion, the development of phenocryst and porphyroblast alkali feldspar megacrysts in the Dragsmark granite can be seen to be independently related to the thermal history and fluid behaviour of the cooling intrusive complex.

APPENDIX A

METHODOLOGY

X-ray diffraction

Sample preparation: For analysis of bulk rock alkali feldspar, hand specimens were broken and crushed in a percussion mortar, then ground in a Tema tungsten carbide disc mill. The sample was then passed through test sieves and the -60 +120 fraction retained. After washing and drying overnight, the powder was run through a magnetic separator to remove magnetite, biotite, chlorite and epidote. The remaining impure mixture of quartz, plagioclase and alkali feldspar was then separated in a funnel using a mixture of 1,1,2,2 tetrabromoethane and dimethylformamide of a specific gravity such that quartz and plagioclase sank and alkali feldspar floated ($\rho \approx 2.60$). After vigorous stirring and standing for at least 24hrs, the floats were extracted and copiously washed with acetone. Examination by petrological microscope showed the final product to be c.98% alkali feldspar.

Megacrysts for analysis were cut out of rock slabs 5 - 10mm thick using a hammer and chisel. Thin-sections had previously been made corresponding to one side of the slab thereby enabling the microscopic features of individual megacrysts to be investigated. All the megacrysts were removed from some slabs in order to ascertain the nature of the groundmass alkali feldspar. Such samples were thereafter prepared in the same manner as bulk rock feldspars, as were the megacrysts, except that the latter were sufficiently pure for heavy liquid separation to be omitted. The extracted alkali feldspar samples were then ground in an agate mortar and pestle together with approximately 20 vol % sintered CaF_2 as an internal standard. Smear mounts of this mixture were then made with distilled water.

Analytical techniques: X-ray powder diffraction analysis was performed on a Siemens X.R.D. unit with a Type F goniometer at the University of Keele. The samples were irradiated using a Cu tube operating at 35kV and 20mA with slit widths of 1^{o} and 0.4mm. Three scans were made from 12^{o} to 57^{o} 2θ for each sample at a goniometer speed of $\frac{1}{2}^{o}$/min and a chart recorder speed of ½cm/min with the ratemeter at 4×10^{2}imp/sec and a time constant of 2secs.

The positions of all peaks on the charts were then measured in millimeters from the CaF_2 311 peak (to the nearest ½mm). These values were converted to $^{o}2\theta$ and corrected for deviation from the nominal 1cm ≡ $1^{o}2\theta$ ratio, stretching of the paper, etc. using a computer program written by the author. A two-part linear correction was applied by comparing the distances between the 311 and 220 CaF_2 peaks and the 220 and 111 CaF_2 peaks with the differences between their standard 2θ values (55.77^{o}, 47.0^{o} and 28.28^{o} respectively). This yielded an 'actual' cm/$^{o}2\theta$ ratio for the two regions either side of 47^{o} which was used to calculate the 2θ values for the feldspar peaks. As a check on the validity of this correction procedure, the calculated 2θ values for seven quartz peaks as measured on over 70 charts were compared with the standard values: in no case was the difference greater than two standard deviations.

Calculation of cell parameters: The peaks were indexed using the tables given in Wright and Stewart (1968) for maximum microcline, monoclinic K-feldspar and sodic perthite lamellae. Only those peaks that were unambiguously monoclinic were indexed as such; common peaks were assigned to the dominant triclinic phase. The reflections were then qualitatively ranked following the scheme of Orville (1967) and only the more reliable measurements used for refinement. Computation was carried out in the manner described by Wright and Stewart (op.cit) using a version of the cell refinement program of Evans, Appleman and Handverker (1963). Starting

parameters for the three structural polymorphs are required for the program, and standard values were used as follows:

Microcline a = 8.58A, b = 12.96A, c = 7.21A, $\alpha = 91^{o}$, $\beta = 116^{o}$, $\gamma = 88^{o}$

Orthoclase a = 8.60A, b = 13.00A, c = 7.19A, $\beta = 116^{o}$

Albite a = 8.15A, b = 12.78A, c = 7.15A, $\alpha = 94^{o}$, $\beta = 117^{o}$, $\gamma = 88^{o}$

Final refinements were obtained with a fixed-index cycle and cell parameters derived from the initial variable-indexing refinements.

Composition of perthites: Perthitic feldspars may be homogenized by heating in a Pt container at 1050^{o}C for 48hrs (Orville, 1967). This yields a single $\bar{2}01$ peak on powder diffraction patterns, the position of which is dependent on composition.

The 2θ value of this peak was determined from smear mounts of homogenized feldspars with $KBrO_3$ and quartz as internal standards. Six runs from 21.5^{o} to $19^{o}2\theta$ were made for each sample at a goniometer speed of $\frac{1}{4}^{o}$/min and a chart speed of 1cm/min. A correction factor was applied as for the full refinements using the $KBrO_3$ 101 peak at $20.215^{o}2\theta$ and the α-quartz 100 peak at $20.835^{o}2\theta$ as reference points. The equations given in Wright (1968) and Jones et al. (1969) were used to calculate wt.% Or from the position of the $\bar{2}01$ reflection: the difference between the two methods was less than 1wt.% Or.

Feldspar chemistry

Analysis of alkali feldspars for K, Na, Ca, Ba, Rb, Sr and Mg was performed on a Pye Unicam SP2900 Spectrophotometer by both atomic absorption and flame emission.

Sample preperation: For analysis of bulk rock alkali feldspar, the same preparation procedure was followed as for X-ray diffraction. Relatively fresh megacrysts were collected on traverses across the various granitic sheets and from many of the smaller bodies at Östersidan (see Map 3). These were broken with a hammer and hand-picked. Only pieces with no sign of alteration or iron-staining and with lustrous cleavage planes were selected for analysis. Such pieces were then reduced to less than 1mm in a tungsten carbide ball mill. No attempt was made to remove inclusions of other minerals and consequently the megacryst samples were less pure than those of bulk rock feldspars. This is reflected in the lower totals obtained (range 70.3 - 104.2 wt.%, average 90.4 wt.%, see Table B6.1). Microscopic examination showed most mineral inclusions to be quartz, with plagioclase uncommon and biotite rare (see Ch.3). Whitney and Stormer (1977) also explain low totals from AA analyses of alkali feldspars as resulting from small amounts of included quartz. The amount of chemical, as opposed to physical, contamination is thus negligible and little error is introduced by normalization to 100%. The high coefficient of variation of CaO (Table B6.2) perhaps reflects the presence of inhomogeneously distributed plagioclase inclusions.

Analytical techniques: It was found that the high Ba content of the feldspars caused the formation of a white insoluble precipitate of barium sulphate if a standard $HF/H_2SO_4/HNO_3$ digestion was used. Fortunately, alkali feldspar dissolves readily in HF alone, and thus a modified method was adopted. 0.2500g of sample, dried overnight at 110°C, were

weighed out into a Pt crucible and approximately 12ml 50%HF added. This was evaporated to dryness on a sand bath and the residue dissolved in 20ml warm 1 + 19 HNO_3 before being made up to 50ml with distilled water: this formed the stock solution. Blanks were run with each fresh batch of reagents but no contamination was detected.

1ppm in the stock solution is equivalent to 200ppm in the feldspar and the solution thus contains approximately 600ppm K_2O. This is sufficient to act as an ionization buffer where needed, and Ba, Sr and Rb were therefore determined on the stock solution. For the determination of K_2O and Na_2O, it is necessary to add caesium as an ionization buffer and also to reduce the concentration of the alkali elements. These oxides were determined on a x10 dilution, 10ml of stock solution and 10ml of CsCl solution being made up to 100ml with distilled water. Silicon and aluminium affect the response to calcium and magnesium, but this can be overcome by the addition of 0.2% w/v lanthanum as chloride. A third solution was therefore made with 10ml stock and 5ml 1% La solution made up to 50ml.

Calcium and magnesium were determined by atomic absorption, the other elements by flame emission. Strontium and barium require the use of a nitrous oxide / acetylene flame rather than air / acetylene in order to achieve the higher temperatures necessary to stimulate emission. Machine conditions are given in Table A1.

Standards: The spectrophotometer was calibrated before each batch of unknowns was run using sets of standard solutions. A mid-range standard was run after every 3 - 5 samples in order to check, and correct if necessary, for drift. This was found to be especially necessary when determining barium. Details of the standards used are given in Table A2.

As the response to rubidium is affected by the concentration of aluminium and potassium, a synthetic alkali feldspar solution was added to the Rb standards. This solution was made by dissolving $KAl(SO_4)_2.12H_2O$ and NaCl in distilled water in such proportions as to yield final concentrations of approximately 1000ppm Al_2O_3, 700ppm K_2O and 100ppm Na_2O.

Because of problems of adsorption of ions from standard solutions onto the polyethylene containers, fresh standards of Sr, Rb and Mg (those with low concentrations) were made up each week from 1000ppm stock standards. The more concentrated standards for the other elements were replaced from stock solutions each month. As an illustration of such adsorption, a combined standard solution originally containing 80ppm K_2O and 20ppm Na_2O was redetermined after several months at 63ppm K_2O and 19ppm Na_2O.

Recalculation: The concentrations of the various elements and oxides in the sample were obtained by use of a best-fit linear regression line through the data for the standards. Stoichiometric formulae for hypothetical end-member feldspars (with barium as $BaAl_2Si_2O_8$) were then used in a computer program written by the author to calculate Al_2O_3 and SiO_2 content and hence the total wt.% feldspar in the sample. This is the value given as the original total in Table B6.1 . As explained above, the generally low totals obtained were probably due to quartz inclusions, so the analyses were normalized to 100wt.% and the content of the various components recalculated. These normalized values were used to plot the various Figures.

As the response to rubidium is affected by the concentration of aluminium and potassium, a synthetic alkali feldspar solution was added to the Rb standards. This solution was made by dissolving $KAl(SO_4)_2.12H_2O$ and NaCl in distilled water in such proportions as to yield final concentrations of approximately 1000ppm Al_2O_3, 700ppm K_2O and 100ppm Na_2O.

Because of problems of adsorption of ions from standard solutions onto the polyethylene containers, fresh standards of Sr, Rb and Mg (those with low concentrations) were made up each week from 1000ppm stock standards. The more concentrated standards for the other elements were replaced from stock solutions each month. As an illustration of such adsorption, a combined standard solution originally containing 80ppm K_2O and 20ppm Na_2O was redetermined after several months at 63ppm K_2O and 19ppm Na_2O.

Recalculation: The concentrations of the various elements and oxides in the sample were obtained by use of a best-fit linear regression line through the data for the standards. Stoichiometric formulae for hypothetical end-member feldspars (with barium as $BaAl_2Si_2O_8$) were then used in a computer program written by the author to calculate Al_2O_3 and SiO_2 content and hence the total wt.% feldspar in the sample. This is the value given as the original total in Table B6.1 . As explained above, the generally low totals obtained were probably due to quartz inclusions, so the analyses were normalized to 100wt.% and the content of the various [illegible] recalculated. These normalized values were used to plot the [illegible]res.

As the response to rubidium is affected by the concentration of aluminium and potassium, a synthetic alkali feldspar solution was added to the Rb standards. This solution was made by dissolving $KAl(SO_4)_2.12H_2O$ and NaCl in distilled water in such proportions as to yield final concentrations of approximately 1000ppm Al_2O_3, 700ppm K_2O and 100ppm Na_2O.

Because of problems of adsorption of ions from standard solutions onto the polyethylene containers, fresh standards of Sr, Rb and Mg (those with low concentrations) were made up each week from 1000ppm stock standards. The more concentrated standards for the other elements were replaced from stock solutions each month. As an illustration of such adsorption, a combined standard solution originally containing 80ppm K_2O and 20ppm Na_2O was redetermined after several months at 63ppm K_2O and 19ppm Na_2O.

Recalculation: The concentrations of the various elements and oxides in the sample were obtained by use of a best-fit linear regression line through the data for the standards. Stoichiometric formulae for hypothetical end-member feldspars (with barium as $BaAl_2Si_2O_8$) were then used in a computer program written by the author to calculate Al_2O_3 and SiO_2 content and hence the total wt.% feldspar in the sample. This is the value given as the original total in Table B6.1 . As explained above, the generally low totals obtained were probably due to quartz inclusions, so the analyses were normalized to 100wt.% and the content of the various components recalculated. These normalized values were used to plot the various Figures.

Fluid inclusions

Fluid inclusion geothermometry was carried out using a Linkam Scientific Instruments TH600 Programmer and Heating-Freezing Stage. This was calibrated against a set of eight standard melting point chemicals by recording the melting temperature of a small amount of sample placed on a cover slip. The standards cover the range 0^{o} to 230^{o}C. A heating rate of 90^{o}C/min was used for both standard and samples. In no case was the difference between the observed and expected melting temperatures greater than 5^{o}C; the average difference was -2.5^{o}C (observed lower than standard). The calibration was performed by D.Cronshaw.

0.4mm thick sections of alkali feldspar megacrysts from the Dragsmark granites were polished on both sides and examined for quartz inclusions. Pieces of section containing these were then placed on the heating stage and examined for primary two-phase fluid inclusions using a Leitz x32 Universal Stage (long working distance) objective lens. Such inclusions were then heated until the vapour bubble disappeared, at which point the temperature was recorded, this being the homogenization temperature T_{H}. Temperatures thus obtained were reproducible to within 3^{o}C.

Whole-rock geochemistry

Sample preparation: Sampling for whole-rock geochemical analysis was carried out with particular attention to freshness. Specimens were taken from roadside blastings wherever possible, and outcrops with extensive D4 epidote veining were avoided. Samples of the Dragsmark granites weighed about 5kg, those of the finer-grained country gneisses rather less. After splitting in a Denbigh rock-splitter and removal of weathered material, the whole sample was passed through a Sturtevant jaw crusher. The resulting rock chips (about 5mm across) were homogenized by successive cone and quartering to obtain two batches of 100 - 150gm each. One of these was halved and ground for 15secs in a tungsten carbide Tema disc mill. After homogenization, the resultant powder was used for determination of ferrous iron. The other batch was Temaed for 30secs, rehomogenized and approximately 30gm milled for 20mins in a tungsten carbide ball mill. This sample was used for preparation of fused discs and pressed pellets for X-ray fluorescence analysis.

Analytical techniques: Determination of major and selected trace elements was performed on a Philips PW1212 X-ray fluorescence spectrometer in the Department of Geology, University of Keele. Trace elements and sodium were determined on pressed powder pellets containing 6gm sample and a few drops of Moviol binder. Major elements were determined on fused discs of 0.25gm ignited sample and 2.5gm Spectroflux SP100A (lithium metaborate). Details of the machine conditions used at Keele are given by Daly (1978) and Bevins (1979). Major element corrections were performed by computer using a program written by G.J.Lees. This is a modification for SP100A of the methods of Norrish and Hutton (1969) and Harvey et al. (1973).

Determination of FeO was carried out by dissolving 0.25gm of

sample in 10ml hot 1:1 mixture of HF and conc. H_2SO_4, neutralizing with boric acid and titrating against a standardized potassium dichromate solution.

Lithium was determined on a Pye Unicam SP2900 Atomic Absorption Spectrophotometer in flame emission mode. A standard $HF/H_2SO_4/HNO_3$ digestion of 0.25gm powdered sample was used to obtain a stock solution.

Fluorine analyses were performed by A.Palmer and J.Merefield of the Department of Geology, University of Exeter. The method is a modified version of Troll et al. (1977). Measurement was carried out using a Philips PW9416 selective ion analyser and a Beckman F electrode.

Restite modelling: The normative mineralogy of the model restite was calculated according to the following scheme:

Biotite composition: $K_2Mg_{1.4}Fe_{3.5}Al_3Si_{5.5}O_{22}$ (see Table B9.2)

Garnet composition: $Ca_1Fe_{1.8}Mg_{0.2}Al_2Si_3O_{12}$ (see Table B9.1)

i) All TiO_2 assigned to sphene ($CaTiSiO_5$)

ii) All P_2O_5 assigned to apatite ($Ca_5(PO_4)_3OH$)

iii) All K_2O assigned to biotite (of above composition)

iv) All remaining MgO assigned to garnet (of above composition)

v) All remaining CaO assigned to anorthite ($CaAl_2Si_2O_8$)

vi) All Na_2O assigned to albite ($NaAlSi_3O_8$)

vii) Anorthite and albite combined to yield plagioclase

viii) All remaining Al_2O_3 assigned to aluminosilicate polymorph (Al_2SiO_5)

ix) All Zr assigned to zircon ($ZrSiO_4$)

x) Any remaining SiO_2 assigned to quartz

Table A1

Machine conditions for the analysis of alkali feldspars by AA/FES

Element/Oxide	Mode	Oxidant	Burner	Wavelength (nm)
K_2O	FES	air	Meker	766.5
Na_2O	FES	air	Meker	589.0
CaO	AA	air	10cm slot	422.7
Ba	FES	N_2O	5cm slot	553.5
Rb	FES	air	Meker	780.0
Sr	FES	N_2O	5cm slot	460.8
MgO	AA	air	10cm slot	285.2

AA: atomic absorption

FES: flame emission

Fuel: acetylene

Table A2

Standards used to calibrate the Atomic Absorption Spectrophotometer

Element/Oxide	as	Concentrations (ppm)	Additives
K_2O } combined standard	Cl^-	0, 20, 40, 60, 80	} +30ppm Cs
Na_2O } combined standard	Cl^-	0, 5, 10, 15, 20, 25	} +30ppm Cs
CaO	CO_3^{--}	0, 2, 4, 6, 8, 10	+0.2% w/v La
Ba	Cl^-	0, 5, 10, 15, 20	+0.1% w/v K
Rb	Cl^-	0, 1, 2, 4, 5, 10	+ 10% v/v SAF
Sr	CO_3^{--}	0, 0.5, 1, 1.5, 2	+0.1% w/v K
MgO	Cl^-	0, 1, 3, 5, 10	+0.2% w/v La

SAF: synthetic alkali feldspar solution - see text

References

AUSTIN,W.G.C. (1960) Geology of the Carnmenellis Area, Cornwall. M.Sc. thesis, Univ. Birmingham (unpubl.)

BAILEY,J.C. (1977) Fluorine in granitic rocks and melts: A review. Chem. Geol., 19, 1 - 42

BARTH,T.F.W. (1934) Polymorphic phenomena and crystal structure. Am. J. Sci., 5, 273

BARTH,T.F.W. (1951) The feldspar geologic thermometers. Neues Jb. Miner. Abh., 82, 143 - 154

BERGSTRÖM,L. (1963) Petrology of the Tjörn area in western Sweden. Sver. geol. Unders. C593

BERTHELSEN,A. (1980) Towards a palinspastic tectonic analysis of the Baltic Shield. Int. geol. Congr. (Paris) Colloquium C6, 5 - 21

BERTHELSEN,A. and MURTHY,T.N.N. (1970) Structural relations between supracrustal and granitoid rocks in north-eastern Orust, western-most Sweden. Sver. geol. Unders., C649

BEVINS,R.E. (1979) The geology of the Strumble Head - Fishguard region, Dyfed, Wales. Ph.D thesis, Univ. Keele (unpubl.)

BOETTCHER,A.L., PIWINSKII,A.J. and KNOWLES,C.R. (1967) Zoned potash feldspars from the Rainy Creek complex near Libby, Montana. Earth Planet. Sci. Lett., 3, 8 - 10

BOOTH,B. (1966) Petrogenesis of the Land's End granites. Ph.D thesis Univ. Keele (unpubl.)

BOOTH,B. (1968) Petrogenetic significance of alkali feldspar megacrysts and their inclusions in Cornubian granites. Nature, 217, 1036 - 1038

BROWN,G.C., CASSIDY,J., LOCKE,C.A., PLANT,J.A. and SIMPSON,P.R. (1981) Caledonian Plutonism in Britain: A Summary. J. geophys. Res., 86, B11, 10502 - 10514

BROWN,W.L., BECKER,S.M. and PARSONS,I. (1983) Cryptoperthites and Cooling Rate in a Layered Syenite Pluton: A Chemical and TEM Study. Contr. miner. petrol., 82, 13 - 25

CHAPPELL,B.W. and WHITE,A.J.R. (1974) Two contrasting granite types. Pacific Geol., 8, 173 - 174

COMPSTON,W. and CHAPPELL,B.W. (1979) Sr-Isotope Evolution of Granitoid Source Rocks in The Earth: Its Origin, Structure and Evolution (ed. McElhinny,M.W.) 377 - 426 (Academic, 1979)

CRESSEY,G., SCHMID,R. and WOOD,B.J. (1978) Thermodynamic Properties of Almandine - Grossular Garnet Solid Solutions. Contr. miner. petrol., 67, 397 - 404

DALY,J.S. (1978) Geochemical and geochronological studies in the Stora Le -Marstrand Belt of Orust, S.W. Sweden. Ph.D. thesis, Univ. Keele (unpubl.)

DALY,J.S., PARK,R.G. and CLIFF,R.A. (1979) Rb-Sr ages of intrusive plutonic rocks from the Stora Le -Marstrand belt in Orust, S.W. Sweden. Precambrian Res., 9, 189 - 198

DALY,J.S., PARK,R.G. and CRANE,A. (1982) Age relations of Sveconorwegian granitoid rocks in the Stora Le -Marstrand belt, Orust area, Sweden. Geol. För. Stockh. Förh., 104, 11 - 16

DALY,J.S., PARK,R.G. and CLIFF,R.A. (1983) Rb-Sr isotopic equilibrium during Sveconorwegian (=Grenville) deformation and metamorphism of the Orust dykes, S.W. Sweden. Lithos, 16, (in press)

DICKSON,F.W., SABINE,C. (1967) Barium-zoned large K-feldspars in quartz monzonites of eastern and south eastern California. Progm. geol. Soc. Am. Meeting, Santa Barbara, 33

DUNHAM,A.C. and WILKINSON,F.C.F. (1978) Accuracy, precision and detection limits of energy-dispersive electron microprobe analyses of silicates. X-ray Spectrom., 7, 50 - 56

EVANS,H.T., APPLEMAN,D.E. and HANDVERKER,D.S. (1963) The least squares refinement of crystal unit cells with powder diffraction data by an automatic computer indexing method (abstr). Am. Crystallogr. Ass. Camb., Mass., A. Mtg. Progm., 42 - 43

FENN,P.M. (1977) The nucleation and growth of alkali feldspars from hydrous melts. Can. Miner., 15, 135 - 161

FERRY,J.M. and SPEAR,F.S. (1978) Experimental Calibration of the Partitioning of Fe and Mg Between Biotite and Garnet. Contr. miner. petrol., 66, 113 - 117

FISHER,J.R. (1976) The volumetric properties of H_2O - a graphic portrayal J. Res. U.S. geol. Surv., 4, 189 - 193

FLEUTY,M.J. (1964) The description of folds. Proc. Geol. Ass., 75, 461 - 489

GAVRILIN,R.D., AGAFONNIKOVA,L.S. and SAVINOVA,E.N. (1972) Behaviour of fluorine in the initial stages of granitization. Geochem. Int., 9, 180 - 185 translated from Geokhimiya, 3 (1972)

GOLDMAN D.S. and ALBEE,A.L. (1977) Correlation of Mg/Fe partitioning between garnet and biotite with $^{18}O/^{16}O$ partitioning between quartz and magnetite. Am. J. Sci. 277, 750 - 767

GORBATSCHEV,R. (1971) Aspects and Problems of Precambrian Geology in Western Sweden. Sver. geol. Unders. C650

GORBATSCHEV,R. (1975) Fundamental subdivisions of Precambrian granitoids in the Åmål mega-unit and the evolution of the south-western Baltic Shield, Sweden. Geol. För. Stockh. Förh., 97, 107 - 114

GORBATSCHEV,R. and WELIN,E. (1975) The Rb-Sr age of the Ursand granite on the boundary between the Åmål and "Pregothian" mega-units of south-western Sweden. Geol. För. Stockh. Förh., 97, 379 - 381

GORDIENKO,V.V. and KRIVOVICHEV,V.G. (1978) Can the Ba/Rb ratio in minerals serve as an indicator of the depth of mineral formation. Zap. vses. miner. Obsbch., 107, 481 - 487 (in Russian)

HAGESKOV,B. (1978) On the Precambrian structures of the Sandbukta-Mölen inlier in the Oslo Graben, S.E. Norway. Norsk. geol. Tidsskr., 58, 69 - 80

HAGESKOV,B. and PEDERSEN,S. (1980) Rb-Sr whole rock age determinations from the western part of the Østfold basement complex, S.E. Norway Bull. geol. Soc. Danm., 29, 119 - 128

HAMILTON,D.L. (1969) Solid solution of anorthite in alkali feldspars at 700° and 900°C. Prog. exp. petrol. NERC. 1st. report, 51 - 52

HARRY,W.T. (1951) The migmatite and feldspar-porphyroblast rock of Glen Dessarry, Inverness-shire. Q. J. geol. Soc., 107, 137-156

HARVEY,P.K., TAYLOR,D.M., HENDRY,R.D. and BANCROFT,F. (1973) An accurate fusion method for the analysis of rocks and chemically related materials by X-ray fluorescence spectrometry. X-ray Spectrom., 2, 33-44

HASELTON,H.T.,Jr., HOVIS,G.L., HEMINGWAY,B.S. and ROBIE,R.A. (1983) Calorimetric investigation of the excess entropy of mixing in analbite-sanidine solid solutions: lack of evidence for Na, K short-range order and implications for two-feldspar thermometry Am. Min. 68, 398 - 413

HEIER,K.S. (1957) Phase Relations of Potash Feldspar in Metamorphism J. Geol., 65, 468 - 479

HEIER,K.S. (1962) Trace elements in feldspars - a review. Norsk geol. Tidsskr., 42, 415 - 454

HENSEN,B.J., SCHMID,R., and WOOD,B.J. (1975) Activity-Composition Relationships for Pyrope-Grossular Garnet. Contr. miner. petrol., 51, 161 - 166

HIGGINS,M.W. (1971) Cataclastic rocks. Geol. Surv. prof. Pap., 687, 1-97

HIGGINS,N.C. and KAWACHI,Y. (1977) Microcline megacrysts from the Green Lake granodiorite, Eastern Fiordland, New Zealand. N.Z. J. Geol. Geophys., 20, 273 - 286

HOBBS,B.E., MEANS,W.D. and WILLIAMS,P.F. (1976) An outline of structural geology. (Wiley, 1976)

IIYAMA,J.T. (1966) Contribution à l'étude des équilibres sub-solidus du système ternaire orthose-albite-anorthite à l'aide des réactions d'éxchange d'ions Na-K au contact d'une solution hydrothermale. Bull. Soc. fr. Minér. Cristallogr., 89, 442 - 454

ISHIHARA,S. (1977) The magnetite-series and ilmenite-series granitic rocks. Ming geol., 27, 293 - 305

JAMES,R.S. and HAMILTON,D.L. (1969) Phase Relations in the System $NaAlSi_3O_8$ - $KAlSi_3O_8$ - $CaAl_2Si_2O_8$ - SiO_2 at 1 Kilobar Water Vapour Pressure. Contr. miner. petrol., 21, 111 - 141

JONES,J.B., NESBIT,R.W. and SLADE,P.G. (1969) The determination of the orthoclase content of homogenized alkali feldspars using the $\bar{2}01$ X-ray method. Mineralog. Mag., 37, 489 - 496

KANISAWA,S. (1979) Content and behaviour of fluorine in granitic rocks, Kitakami Mountains, northeast Japan. Chem. Geol., 24, 57 - 67

KOVALENKO,N.I. (1977) The reactions between granite and aqueous hydrofluoric acid in relation to the origin of fluorine-bearing granites Geochem. Int., 14(2), 108 - 118 translated from Geokhimiya, 4, 503 - 515

KÖHLER,A. (1948) Erscheinungen an Feldspaten in ihrer Bedeutung für die Klärung der Gesteinsgenesis (Ein Versuch und eine Anregung). Tschermaks miner. petrogr. Mitt., 3, 1, 51 - 67

KROLL,H. (1971) Determination of Al, Si distribution in alkali feldspars from X-ray powder data. Neues Jb. Miner. Mh., 2, 91 - 94

LAMBERT,R. St.J. and HOLLAND,J.G. (1974) Yttrium geochemistry applied to petrogenesis utilizing calcium-yttrium relationships in minerals and rocks. Geochim. cosmochim. Acta, 38, 1393 - 1414

LARSSON,W. (1956) Beskrivning till kartbladet Vårvik. Berggrunden. Sver. geol. Unders., Aa 187, 10 - 127

LINDSTRÖM,A. (1902) Beskrifning till Kartbladet Uddevalla. Sver. geol. Unders. Ac3

LUNDEGÅRDH,P.H. (1958) Göteborgstraktens berggrund. Sver. geol. Unders. C553

McINTYRE,D.B. and WEISS,L.E. (1956) Construction of Block Diagrams to Scale in Orthographic Projection. Proc. Geol. Ass., 67, 142 - 155

MAGNUSSON,N.H. (1960) Age determinations of Swedish Precambrian rocks. Geol. För. Stockh. Förh., 82, 407 - 432

MAGNUSSON,N.H. (1965) The Pre-Cambrian history of Sweden. Q.J. geol. Soc., 121, 1 -30

MAGNUSSON,N.H., THORSLUND,P., BROTZEN,F., ASKLUND,B. and KULLING,O. (1960) Description to accompany the map of the Pre-Quaternary rocks of Sweden. Sver. geol. Unders., Bal6, 5 - 66

MANNING,D.A.C. (1979) An experimental study of the effect of fluorine, in addition to water, on crystallization in the system Qz-Ab-Or, and its application to Cornish granitic rocks rich in fluorine. Proc. Usser Soc., 4, 380 - 389

MARMO,V. (1971) Granite Petrology and the Granite Problem. (Elsevier, 1971).

MEHNERT,K.R. and BUSCH,W. (1981) The Ba content of K-feldspar megacrysts in granites: a criterion for their formation. Neues Jb. Miner. Ab, 140, 221 - 252

NORRISH,K. and HUTTON,J.T. (1969) An accurate X-ray spectrographic method for the analysis of a wide range of geological samples. Geochim. cosmochim. Acta, 33, 431 - 453

O'NEILL,H.St.C and WOOD,B.J. (1979) An Experimental Study of Fe-Mg Partitioning Between Garnet and Olivine and Its Calibration as a Geothermometer. Contr. miner. petrol., 70, 59 - 70

ORVILLE,P.M. (1967) Unit-cell parameters of the microcline-low albite and the sanidine-high albite solid solution series. Am. Miner., 52, 55 - 86

PARK,R.G., BAILEY,A., CRANE,A., CRESSWELL,D. and STANDLEY,R. (1979) Structure and Geological History of the Stora Le -Marstrand rocks in western Orust, Southwestern Sweden. Sver. geol. Unders., C763

PARSONS,I. (1978)a Feldspars and fluids in cooling plutons. Mineralog. Mag., 42, 1 - 18

PARSONS,I. (1978)b Alkali-feldspars: which solvus? Phys. Chem. Miner., 2,199-213

PARSONS,I. and BOYD,R. (1971) Distribution of potassium feldspar polymorphs in intrusive sequences. Mineralog. Mag.,38, 295-311

PETROV,B.V., RAZVOYZHAYEVA,E.A. and MAKRYCINA,V.A. (1972) The behaviour of volatile components during regional metamorphism of Upper Proterozoic rocks of the Potomsk Uplands. Geochem. Int., 9, 234-240 (translated from Geokhimiya)

PIWINSKII,A.J. (1968) Experimental Studies of Igneous Rock Series Central Sierra Nevada Batholith, California. J. Geol., 76, 548-570

POTTER,R.W.,II (1977) Pressure corrections for fluid-inclusion homogenization temperatures based on the volumetric properties of the system NaCl-H_2O. J. Res. U.S. geol. Surv., 5, 603-607

RAYLAND,P.C. (1969) Composition and structural state of the potassic phase in perthites as related to petrogenesis of a granitic pluton. Lithos, 3, 167-189

ROBIN,P.-Y.F. (1974) Stress and strain in cryptoperthite lamellae and the coherent solvus of alkali feldspars. Am. Miner., 59, 1299-1318

ROEDDER,E. (1979) Fluid Inclusions as Samples of Ore Fluids. in Geochemistry of hydrothermal ore deposits. (ed. Barnes,H.L.) 67-110 (Wiley,1979)

SAHAMA,Th.G. (1945) On the chemistry of the east Fennoscandian rapakivi granites. Bull. Commn. géol. Finl., 136, 15-67

SAMUELSSON,L. (1978) The Pre-Quaternary Geology of the Göteborg region, South-western Sweden. Geologiska Institutionen, Univ. Lund

SHAW,D.M. (1968) A review of K-Rb fractionation trends by covariance analysis. Geochim. cosmochim. Acta, 32, 573-601

SHMAKIN,B.M. and MAKAGON,V.M. (1979) The Ba/Rb ratio in potassic minerals- a reliable indicator of geochemical specialisation and the depth of formation of pegmatites. Zap. vses. miner. Obshch., 108, 631-633 (in russian)

SKIÖLD,T. (1976) The interpretation of the Rb-Sr and K-Ar ages of late Precambrian rocks in southwestern Sweden. Sver. geol. Unders., C. 747

SMITH,J.V. (1974) Feldspar Minerals (2 Vols.), (Springer,1974)

SMITH,P. (1978) The effect of anorthite on the alkali feldspar solvus at P_{H_2O} = 1 kb. Prog. exp. petrol. NERC. 4th. report, 247-248

SMITH,P. and PARSONS,I. (1974) The alkali-feldspar solvus at 1 kilobar water vapour pressure. Mineralog. Mag., 39, 747-767

SORBY,H.C. (1858) On the microscopic structure of crystals, indicating the origin of minerals and rocks. Q. J. geol. Soc., 14, 453-500

STEIGER,R.H. and HART,S.R. (1967) The microcline-orthoclase transition within a contact aureole. Am. Miner., 52, 87-116

STERN,C.R. and WYLLIE,P.J. (1981) Phase Relationships of I-type Granite with H_2O to 35 Kilobars: The Dinkey Lakes Biotite-Granite From the Sierra Nevada Batholith. J. Geophys. Res., 86, B11, 10412-10422

STEWART,D.B. and RIBBE,P.H. (1969) Structural explanation for variations in cell parameters of alkali feldspar with Al/Si ordering. Am. J. Sci., 267A, 444-462

STEWART,D.B. and WRIGHT,T.L. (1974) Al/Si order and symmetry of natural alkali feldspars, and the relationship of strained cell parameters to bulk composition. Bull. Soc. fr. Minér. Cristallogr., 97, 356-377

STONE,M. and AUSTIN,W.G.C. (1961) The Metasomatic Origin of the Potash Feldspar Megacrysts in the Granites of Southeast England. J. Geol., 69, 464-472

STORMER,J.C.Jnr. (1975) A practical two-feldspar geothermometer. Am. Miner., 60, 667-674

STRECKEISEN,A. (1975) To each plutonic rock its proper name. Earth-Sci. Rev., 12, 1-33

SUNDIUS,N. (1952) Kvarts, fältspat och glimmer samt förekomster därav i Sverige. Sver. geol. Unders., C520

TAKENOUCHI,S. and KENNEDY,G.C. (1964) The Binary System H_2O-CO_2 at High Temperatures and Pressures. Am. J. Sci., 262, 1055-1074

TAYLOR,S.R. and HEIER,K.S. (1960) The petrological significance of trace-element variation in alkali feldspars. Report. 21st. int. geol. Congr. Norden (Copenhagen), pt. 14, 47-61

TERTSCH,H. (1936) Beobachtungen an Orthoklas-Zwillingen nach dem Karlsbader Gesetz. Zentbl. Miner. Abt. A, 198-207

THOMPSON,A.B. (1976) Mineral reactions in pelitic rocks: II. Calculations of some P-T-X(Fe-Mg) phase relations. Am. J. Sci., 276, 425-454

TILLING,R.I. (1968) Zonal Distribution of variations in structural state of alkali feldspars within the Rader Creek pluton, Boulder Batholith, Montana. J. Petrol., 9, 331-357

TROLL,G. FARZANEH,A. and CAMMANN,K. (1977) Rapid determination of fluoride in mineral and rock samples using an ion-selective electrode. Chem. Geol., 20, 295-305

TUTTLE,O.F. and BOWEN,N.L. (1958) Origin of granite in the light of experimental studies in the system $NaAlSi_3O_8$-$KAlSi_3O_8$-SiO_2-H_2O. Mem. geol. Soc. Am., 74, 1-153

WELIN,E. and GORBATSCHEV,R. (1976)a A Rb-Sr geochronological study of the older granitoids in the Åmål tectonic mega-unit, south-western Sweden. Geol. För. Stockh. Förh., 98, 374-377

WELIN,E. and GORBATSCHEV,R. (1976)b Rb-Sr age of granitoid gneisses in the "Pregothian" area of south-western Sweden. Geol. För. Stockh. Förh., 98, 378-381

WELIN E. and GORBATSCHEV,R. (1976)c The Rb-Sr age of the Håstefjorden granite and its bearing on the Precambrian evolution of southwestern Sweden. Precambrian Res., 3, 187-195

WELIN,E. and GORBATSCHEV,R. (1978)a Rb-Sr age of the Lane granites in south-western Sweden. Geol. För. Stockh. Förh., 100, 101-102

WELIN,E. and GORBATSCHEV,R. (1978)b Rb-Sr isotopic relations of a tonalitic intrusion on Tjörn Island, south-western Sweden. Geol. För. Stockh. Förh., 100, 228-230

WELIN,E. and GORBATSCHEV,R. (1978)c A Rb-Sr age of the Åmål granite at Åmål, Sweden. Geol. För. Stockh. Förh., 100, 401-403

WHITE A.J.R. and CHAPPELL,B.W. (1977) Ultrametamorphism and granitoid genesis. Tectonophysics, 43, 7-22

WHITNEY,J.A. and STORMER,J.C.Jnr. (1977) Two-Feldspar Geothermometry, Geobarometry in Mesozonal Granitic Intrusions: Three Examples from the Piedmont of Georgia. Contr. miner. petrol., 63, 51-64

WINKLER,H.G.F. (1979) Petrogenesis of metamorphic rocks (5th. edition) (Springer,New York, 1979)

WINKLER,H.G.F. and BREITBART,R. (1978) New aspects of granitic magmas. Neues Jb. Miner. Mh., H10, 463-480

WRIGHT,T.L. (1968) X-ray and optical study of alkali feldspar. II. An x-ray method for determining the composition and structural state from measurements of 2θ for three reflections. Am. Miner., 53, 88-104

WRIGHT,T.L. and STEWART,D.B. (1968) X-ray and optical study of alkali feldspar. I. Determination of composition and structural state from refined unit-cell parameters and 2V. Am. Miner., 53, 38-87

WYLLIE,P.J. (1977) Crustal anatexis: an experimental review. Tectonophysics, 43, 41-71

WYLLIE,P.J. and TUTTLE,O.F. (1961) Experimental investigation of silicate systems containing two volatile components. Part II. The effects of NH_3 and HF, in addition to H_2O on the Melting Temperatures of Albite and Granite. Am. J. Sci., 259, 128-143

YODER,H.S., STEWART,D.B. and SMITH,J.R. (1957) Ternary feldspars. Yb. Carnegie Instn. Wash. (1957), 206-214

APPENDIX B

TABLES

Table B2.1

Mineral Analyses by Electron Microprobe

	Hornblende		Plagioclase		Perthite			
					Albite lamellae		K-feldspar host	
	133		32		819			
	older amphibolite		Dragsmark granite		Dragsmark granite			
SiO_2	37.92	40.12	62.98	62.49	68.41	68.61	64.79	65.27
TiO_2	1.04	1.34	0.10	N.D.	N.D.	N.D.	0.90	0.06
Al_2O_3	13.71	14.19	23.36	23.12	19.01	19.06	17.97	18.23
FeO	22.19	22.02	0.18	0.17	N.D.	N.D.	N.D.	0.05
MnO	0.28	0.39	N.D.	N.D.	N.D.	N.D.	N.D.	N.D.
MgO	6.41	5.94	0.12	0.23	0.24	0.17	0.19	0.21
CaO	10.01	11.53	5.34	5.39	0.17	0.09	0.11	0.13
Na_2O	1.26	1.64	7.47	7.94	10.35	10.62	0.87	0.73
K_2O	1.25	1.47	0.25	0.13	0.17	0.58	16.04	16.03
	Cation Proportions							
	(23 oxygens)		(32 oxygens)		(32 oxygens)		(32 oxygens)	
Si	6.11	6.16	11.14	11.12	12.07	12.07	11.98	11.98
Ti	0.13	0.16	0.01	-	-	-	0.01	0.01
Al	2.60	2.57	4.87	4.85	3.96	3.95	3.92	3.94
Fe	2.99	2.83	0.03	0.03	-	-	-	0.01
Mn	0.04	0.05	-	-	-	-	-	-
Mg	1.54	1.36	0.03	0.06	0.06	0.05	0.05	0.06
Ca	1.73	1.90	1.01	1.03	0.03	0.02	0.02	0.02
Na	0.39	0.49	2.56	2.74	3.54	3.62	0.31	0.26
K	0.26	0.29	0.06	0.03	0.04	0.13	3.79	3.76
			An 29.0	28.3	1.0	0.5	0.6	0.6
			Ab 69.4	70.9	97.9	95.9	7.1	6.1
			Or 1.6	0.8	1.1	3.6	92.3	93.3

N.D. = Not Detected

TABLE B5.1

Refined Cell Parameters of the Triclinic Potassic Phase i) Dragsmark granite Area 1

Sample	a(Å)	b(Å)	c(Å)	α(° ′)	β(° ′)	γ(° ′)	α^*(° ′)	γ^*(° ′)	V(Å^3)
32/1	8.549	12.945	7.211	90 34	115 56	87 47	90 26	92 11	717.06
32/2	8.553	12.954	7.212	90 35	115 59	87 42	90 28	92 17	717.74
32GM	8.541	12.943	7.210	90 35	115 57	87 40	90 29	92 18	716.13
53/1	8.561	12.972	7.220	90 39	115 55	87 40	90 25	92 17	720.63
53/3	8.554	12.934	7.212	90 39	115 55	87 46	90 22	92 10	717.13
53/4	8.595	12.957	7.215	90 25	116 02	87 54	90 33	92 07	721.43
53GM	8.611	12.922	7.210	90 41	116 04	87 49	90 19	92 06	720.11
79WR	8.573	12.961	7.224	90 41	115 56	87 39	90 23	92 17	721.27
145/1	8.563	12.961	7.216	90 40	115 58	87 39	90 24	92 17	719.39
145/2	8.569	12.971	7.220	90 37	115 58	87 41	90 26	92 17	720.78
145/3	8.571	12.931	7.212	90 43	116 02	87 44	90 19	92 11	717.66
145/4	8.554	12.952	7.212	90 37	115 58	87 43	90 26	92 15	717.79
145/5	8.566	12.967	7.221	90 36	115 58	87 46	90 25	92 12	720.59
145GM	8.617	12.940	7.209	90 29	116 02	87 54	90 29	92 06	721.71

TABLE B5.1 (cont.)

Refined Cell Parameters of the Triclinic Potassic Phase i) Dragsmark granite Area 1 (cont.)

Sample	a(Å)	b(Å)	c(Å)	α(° ′)	β(° ′)	γ(° ′)	α^*(° ′)	γ^*(° ′)	V(Å^3)
187/3	8.551	12.956	7.214	90 44	115 54	87 38	90 20	92 17	718.31
187/2	8.565	12.965	7.217	90 36	115 56	87 43	90 27	92 14	720.23
187GM	8.543	12.950	7.214	90 34	115 57	87 45	90 26	92 14	717.06
241/1	8.550	12.972	7.222	90 38	115 56	87 42	90 26	92 15	719.76
241/2	8.548	12.956	7.214	90 35	115 56	87 43	90 28	92 15	717.93
241/3	8.575	12.953	7.218	90 40	115 57	87 45	90 21	92 11	720.33
249/1	8.610	12.934	7.196	90 36	116 10	87 45	90 27	92 13	718.72
249/2	8.607	12.964	7.219	90 38	115 59	87 39	90 27	92 18	723.45
299WR	8.584	12.934	7.205	90 32	115 58	87 43	90 31	92 17	718.64
364/1	8.635	12.936	7.240	90 35	116 22	87 33	90 22	92 21	723.91

TABLE B5.1 (cont.)

Refined Cell Parameters of the Triclinic Potassic Phase ii) Dragsmark granite Area 2

Sample	a(Å)	b(Å)	c(Å)	α(° ′)	β(° ′)	γ(° ′)	α^*(° ′)	γ^*(° ′)	V(Å^3)
65/1	8.551	12.977	7.221	90 40	115 56	87 40	90 24	92 16	719.90
65/2	8.565	12.966	7.220	90 39	116 02	87 43	90 24	92 14	719.90
65GM	8.624	12.953	7.216	90 38	116 04	87 44	90 25	92 13	723.56
70/1	8.547	12.960	7.219	90 40	115 55	87 40	90 24	92 16	718.61
70GM	8.566	12.963	7.221	90 38	115 57	87 37	90 27	92 21	720.34
73/1	8.620	12.957	7.218	90 32	116 10	87 36	90 35	92 24	722.88
73/2	8.595	12.939	7.207	90 33	115 55	87 48	90 27	92 10	720.43
73GM	8.559	12.965	7.221	90 36	115 57	87 42	90 27	92 16	719.90
205/1	8.579	12.969	7.219	90 45	115 53	87 32	90 21	92 22	721.93
205/2	8.534	12.957	7.213	90 33	115 57	87 42	90 30	92 17	716.54
205GM	8.580	12.939	7.209	90 34	116 03	87 50	90 26	92 08	718.49

TABLE B5.1 (cont.)

Refined Cell Parameters of the Triclinic Potassic Phase iii) Other Lithologies

Sample	a(Å)	b(Å)	c(Å)	α(° ′)	β(° ′)	γ(° ′)	α^*(° ′)	γ^*(° ′)	V(Å^3)
Stora Le -Marstrand gneisses									
39WR	8.590	12.934	7.213	90 32	115 58	87 44	90 31	92 16	719.87
197/1	8.540	12.946	7.212	90 38	115 54	87 38	90 26	92 19	716.60
197/2	8.549	12.942	7.208	90 45	115 56	87 39	90 19	92 15	716.59
Leucosome									
286/1	8.575	12.970	7.223	90 35	115 58	87 45	90 26	92 13	721.67
Granodioritic gneiss									
103WR	8.558	12.956	7.219	90 42	115 58	87 41	90 21	92 14	719.05
105WR	8.564	12.955	7.213	90 40	115 58	87 38	90 24	92 18	718.88
107WR	8.557	12.942	7.217	90 34	115 54	87 47	90 27	92 12	718.42
110WR	8.561	12.965	7.220	90 34	115 56	87 43	90 28	92 15	720.14
Källviken granite									
18WR	8.571	12.946	7.215	90 38	115 59	87 42	90 25	92 15	719.00
Standard Errors	0.008	0.006	0.003	04	02	04	03	03	0.60

TABLE B5.2

Refined Cell Parameters of Perthite Lamellae i) Dragsmark granite Area 1

Sample	a(Å)	b(Å)	c(Å)	α(° ′)	β(° ′)	γ(° ′)	α^*(° ′)	γ^*(° ′)	V(Å^3)
32/1	8.141	12.772	7.132	96 02	116 24	86 12	85 08	91 15	660.45
32/2	8.125	12.772	7.149	93 31	116 32	88 59	86 35	89 23	662.43
32GM	N.R.								
53/1	N.R.								
53/3	8.124	12.805	7.147	94 20	116 32	88 18	86 00	89 45	663.24
53/4	8.122	12.748	7.143	94 05	116 41	88 04	86 24	90 07	659.11
53GM	8.117	12.758	7.147	93 54	116 41	88 05	86 36	90 11	659.76
79WR	8.127	12.746	7.154	94 03	116 31	88 03	86 27	90 09	661.40
145/1	8.135	12.756	7.148	94 04	116 36	88 01	86 27	90 11	661.60
145/2	8.132	12.780	7.163	93 53	116 46	88 16	86 32	90 00	663.15
145/3	N.R.								
145/4	N.R.								
145/5	8.109	12.836	7.153	93 30	116 42	88 19	86 55	90 07	663.98
145GM	8.122	12.821	7.122	92 35	116 30	90 15	86 59	88 25	662.83

N.R. = Not Refinable

TABLE B5.2 (cont.)

Refined Cell Parameters of Perthite Lamellae i) Dragsmark granite Area 1 (cont.)

Sample	a(Å)	b(Å)	c(Å)	α(° ′)	β(° ′)	γ(° ′)	α^*(° ′)	γ^*(° ′)	V(Å^3)
187/1	8.129	12.841	7.138	93 46	116 27	89 08	86 13	89 06	665.69
187/2	N.R.								
187GM	8.112	12.865	7.149	93 32	116 55	88 12	86 57	90 14	663.99
241/1	N.R.								
241/2	8.114	12.766	7.151	93 50	116 33	88 15	86 36	90 03	661.08
241/3	8.139	12.770	7.157	94 17	116 34	87 49	86 18	90 18	663.49
249/1	N.R.								
249/2	N.R.								
299WR	8.119	12.756	7.144	94 07	116 34	88 04	86 22	90 06	659.98
364/1	8.129	12.768	7.176	94 20	117 08	87 35	86 22	90 30	660.86

N.R. = Not Refinable

TABLE B5.2 (cont.)

Refined Cell Parameters of Perthite Lamellae ii) Dragsmark granite Area 2

Sample	a(Å)	b(Å)	c(Å)	$\alpha(^\circ\ ')$	$\beta(^\circ\ ')$	$\gamma(^\circ\ ')$	$\alpha^*(^\circ\ ')$	$\gamma^*(^\circ\ ')$	$V(Å^3)$
65/1	8.111	12.763	7.158	93 57	116 37	88 11	86 30	90 04	660.84
65/2	8.118	12.792	7.147	93 15	116 32	89 03	86 50	89 26	662.89
65GM	8.156	12.726	7.167	94 14	116 49	87 57	86 17	90 10	662.09
70/1	8.126	12.792	7.101	93 10	116 08	89 43	86 37	88 46	661.52
70GM	N.R.								
73/1	8.138	12.767	7.138	93 23	116 30	89 18	86 37	89 06	662.44
73/2	8.122	12.772	7.182	94 03	117 06	87 57	86 29	90 14	661.50
73GM	N.R.								
205/1	8.139	12.768	7.160	94 01	116 47	87 56	86 32	90 17	662.62
205/2	N.R.								
205GM	8.119	12.128	7.128	94 59	116 33	87 07	85 52	90 44	658.78

N.R. = Not Refinable

TABLE B5.2 (cont.)

Refined Cell Parameters of Perthite Lamellae iii) Other Lithologies

Sample	a(Å)	b(Å)	c(Å)	$\alpha(^{o}\ ')$	$\beta(^{o}\ ')$	$\gamma(^{o}\ ')$	$\alpha^{*}(^{o}\ ')$	$\gamma^{*}(^{o}\ ')$	$V(Å^3)$
Stora Le -Marstrand gneisses									
39WR	N.R.								
197/1	8.124	12.771	7.139	93 32	116 93	88 43	86 41	89 40	660.74
197/2	8.124	12.845	7.152	94 31	116 42	88 08	85 53	89 50	664.70
leucosome									
286/1	8.139	12.746	7.164	94 02	116 37	87 58	86 31	90 16	662.70
Granodioritic gneiss									
103WR	N.R.								
105WR	8.143	12.744	7.140	93 56	116 28	88 25	86 23	89 48	661.77
107WR	8.119	12.758	7.152	94 19	116 33	87 41	86 19	90 26	660.85
110WR	8.137	12.782	7.136	94 23	116 44	87 35	86 18	90 29	660.84
Kållviken granite									
18WR	N.R.								
Standard Errors	0.007	0.008	0.005	06	04	07	04	05	0.67

N.R. = Not Refinable

TABLE B5.3

Refined Cell Parameters of the Monoclinic Potassic Phase

i) Dragsmark granite Area 1

Sample	a(Å)	b(Å)	c(Å)	β(° ′)	V(Å^3)
* 32/1	N.R.				
32/2	8.564	13.015	7.183	115 54	720.20
32GM	8.565	12.955	7.223	116 18	718.54
53/1	8.601	12.969	7.176	115 40	721.45
* 53/3	TRICLINIC				
53/4	N.R.				
* 53GM	8.565	12.940	7.181	115 53	715.94
79WR	8.603	12.924	7.195	115 45	720.56
145/1	N.R.				
145/2	N.R.				
145/3	8.605	12.925	7.173	115 53	717.82
145/4	N.R.				
145/5	TRICLINIC				
* 145GM	8.542	13.028	7.190	115 56	719.47
187/1	N.R.				
* 187/2	8.579	12.972	7.183	115 44	719.69
187GM	N.R.				
* 241/1	8.588	12.967	7.188	116 08	718.64
241/2	8.587	13.019	7.193	115 57	723.06
* 241/3	8.599	12.932	7.168	115 42	718.21
* 249/1	8.572	13.010	7.176	115 52	720.06
* 249/2	8.595	12.937	7.183	116 02	717.66
* 299WR	TRICLINIC				
364/1	8.358	13.035	7.193	115 42	706.10

N.R. = Not Refinable

Note $\alpha = \gamma = \alpha^* = \gamma^* = 90^o00$ (* = good refinement)

TABLE B5.3 (cont.)

Refined Cell Parameters of the Monoclinic Potassic Phase

ii) Dragsmark granite Area 2

Sample	a(Å)	b(Å)	c(Å)	β(° ′)	V(Å^3)
65/1	8.567	12.974	7.196	116 06	718.22
65/2	NOT DETECTED				
65GM	TRICLINIC				
70/1	8.623	12.932	7.199	116 09	720.60
* 70GM	8.592	13.005	7.172	116 04	719.78
73/1	8.621	12.899	7.190	115 51	719.54
* 73/2	8.572	12.935	7.208	115 44	719.96
* 73GM	8.614	12.920	7.175	115 40	719.75
205/1	N.D.				
205/2	N.R.				
205GM	N.D.				

TABLE B5.3 (cont.)

Refined Cell Parameters of the Monoclinic Potassic Phase

iii) Other Lithologies

Sample	a(Å)	b(Å)	c(Å)	β(° ′)	V(Å^3)
Stora Le -Marstrand gneisses					
39WR	8.572	12.981	7.235	116 18	721.79
* 197/1	8.661	12.950	7.161	116 37	718.08
197/2	8.561	12.986	7.224	116 21	719.67
leucosome					
286/1	N.R.				
Granodioritic gneiss					
103WR	N.R.				
105WR	8.554	13.024	7.201	116 08	720.27
107WR	8.596	13.004	7.174	115 48	722.12
110WR	8.629	12.957	7.192	115 48	723.95
Källviken granite					
18WR	N.R.				
Standard Errors	0.015	0.02	0.02	10	1.50

TABLE B5.4

Refined Cell Parameters of Minor Triclinic Phases

Sample	a(Å)	b(Å)	c(Å)	$\alpha(^{\circ}\ ')$	$\beta(^{\circ}\ ')$	$\gamma(^{\circ}\ ')$	$\alpha^*(^{\circ}\ ')$	$\gamma^*(^{\circ}\ ')$	V(Å^3)
i) Dragsmark granite Area 1									
53/3	8.585	12.952	7.159	89 42	115 52	90 13	90 14	89 54	716.33
145/5	8.543	12.966	7.171	89 16	115 33	90 34	90 32	89 43	716.60
299WR	8.352	12.941	7.187	90 21	115 39	89 28	89 52	90 25	700.22
ii) Dragsmark granite Area 2									
65GM	8.605	12.919	7.144	89 23	115 44	90 20	90 31	89 56	715.35

TABLE B6.1

Alkali Feldspar Analyses i) Megacrysts

	A1	A2	A3	A4	A5	A6	B1	B2	B3	B4	B5	B6
K_2O (%)	13.15	13.54	13.37	14.10	14.34	15.04	12.89	12.76	14.04	13.02	12.92	13.06
Na_2O (%)	1.75	1.81	1.96	1.93	1.58	1.65	1.86	1.93	1.80	1.68	2.14	1.91
CaO (ppm)	420	1679	877	1772	333	773	1971	155	1067	1402	577	630
MgO (ppm)	264	370	476	242	256	219	359	474	1061	517	561	515
Ba (ppm)	3648	2729	1862	3825	3992	2101	1934	2987	2237	2975	2201	2296
Rb (ppm)	363	308	346	294	353	394	415	394	392	404	461	409
Sr (ppm)	226	287	167	275	308	226	214	241	189	206	181	236
Total (%)	94.1	97.4	97.1	102.0	99.8	104.2	93.9	93.0	100.3	93.3	96.0	94.9
	B7	B8	B9	B10	B11	C1	C2	C3	C4	C5	C6	C7
K_2O (%)	14.12	14.35	12.64	12.90	12.45	11.86	13.81	14.26	13.10	14.12	13.35	13.77
Na_2O (%)	1.82	1.87	1.86	1.72	2.19	2.44	1.98	1.88	1.88	1.81	2.11	1.78
CaO (ppm)	809	1239	240	2190	604	1570	262	88	559	0	2182	4548
MgO (ppm)	379	340	383	305	505	357	441	279	449	199	438	273
Ba (ppm)	1747	2779	2374	3040	1737	2163	2361	1857	3085	2759	2088	2554
Rb (ppm)	441	340	317	359	403	367	388	458	333	358	284	311
Sr (ppm)	100	227	216	148	131	207	192	234	235	218	210	243
Total (%)	100.2	102.4	91.7	93.1	93.4	92.6	99.7	101.2	95.0	99.9	98.9	97.8

TABLE B6.1 (cont.)

Alkali Feldspar Analyses i) Megacrysts (cont.)

	C8	C9	C10	C11	C12	D1	D2	D3	D4	D5	D6	D7
K_2O (%)	12.04	13.58	11.64	13.12	13.17	13.79	11.36	11.34	11.95	12.72	12.26	13.03
Na_2O (%)	1.94	1.87	1.75	2.05	1.86	1.60	2.54	2.69	2.65	1.90	2.13	1.78
CaO (ppm)	240	62	78	1346	1941	242	877	96	1504	204	1746	291
MgO (ppm)	494	246	282	1373	409	616	546	418	1185	345	410	482
Ba (ppm)	1714	2652	2158	2938	2185	1124	1109	935	1053	1442	1033	1259
Rb (ppm)	361	367	372	362	409	354	492	511	568	468	589	490
Sr (ppm)	199	216	232	236	220	145	93	81	86	110	101	97
Total (%)	88.7	97.2	84.7	97.5	95.6	96.1	90.0	90.6	95.1	92.2	92.2	93.1

	D8	D9	E1	E2	E3	E4	E5	F1	F2	F3	F4	F5
K_2O	3.01	13.00	12.96	12.47	13.79	14.11	11.88	13.34	12.05	11.83	12.36	9.48
Na_2O	8.22	1.30	1.89	1.94	1.61	2.07	1.99	1.52	1.86	2.32	2.11	2.80
CaO	7306	490	970	696	568	1322	2184	1495	2291	633	1133	3930
MgO	751	232	425	2189	464	247	451	254	436	586	2315	629
Ba	1025	1104	2981	2657	2382	1843	2259	1935	2300	2188	4106	1473
Rb	138	536	362	329	331	326	285	390	289	294	288	295
Sr	142	111	232	226	176	179	234	134	284	145	303	171
Total	91.9	88.8	94.4	92.8	96.6	102.4	89.3	93.3	89.2	91.0	94.3	82.7

TABLE B6.1 (cont.)

Alkali Feldspar Analyses i) Megacrysts (cont.)

	F6	X1	X2	X3	X4	X5	X6	X7	X8	X9	X10
K_2O (%)	10.88	11.84	9.75	10.85	7.03	4.34	12.36	13.52	13.94	11.00	12.85
Na_2O (%)	2.09	1.58	2.39	2.16	3.69	4.76	2.23	1.96	2.08	2.83	1.68
CaO (ppm)	1528	1974	844	68	2732	5798	1668	937	1120	1393	1695
MgO (ppm)	433	318	985	441	953	1486	885	675	317	1179	344
Ba (ppm)	1172	2024	1055	893	1216	1382	2524	1340	1405	1799	1665
Rb (ppm)	408	396	299	419	252	106	318	492	518	344	443
Sr (ppm)	102	191	116	76	142	269	238	111	98	104	137
Total (%)	83.5	85.3	79.4	83.2	75.2	70.3	94.2	98.0	101.4	91.1	91.9

	BS1	BS2	BS3	BS4	OR2	OR3	OR4	OR8	OR10
K_2O	11.31	13.63	13.39	13.76	11.08	13.39	12.10	13.15	12.70
Na_2O	2.52	1.96	1.96	1.64	2.68	2.20	2.09	1.48	1.61
CaO	4477	1932	2067	1525	2039	1156	2717	1889	1526
MgO	324	384	449	503	654	371	244	254	307
Ba	5339	1812	2389	2602	4664	3531	2850	2510	1102
Rb	263	415	406	382	260	424	413	465	532
Sr	229	110	124	149	654	371	244	254	307
Total	92.3	99.1	97.9	97.2	91.0	99.8	91.7	92.3	90.2

TABLE B6.1 (cont.)

Alkali Feldspar Analyses ii) Bulk Rock Feldspar

	30	72	253	256	361	418	551	706	769	772	818	819
K_2O (%)	10.09	13.06	10.05	14.85	13.25	13.06	11.35	12.65	14.35	14.85	14.45	14.60
Na_2O (%)	3.59	1.49	4.38	1.70	2.60	1.96	3.63	2.19	2.55	1.63	1.8	1.93
CaO (ppm)	2528	1282	1080	1220	1350	1336	900	1650	870	1370	870	1160
MgO (ppm)	N.D.	N.D.	N.D.	N.D.	N.D.	N.D.	N.D.	N.D.	N.D.	N.D.	N.D.	N.D.
Ba (ppm)	3316	2375	2390	1140	2266	1603	2472	3167	2411	1913	3287	1393
Rb (ppm)	246	433	259	900	338	579	290	277	331	729	666	408
Sr (ppm)	134	99	151	120	192	76	161	176	205	181	191	118
Total	92.3	91.3	97.8	103.5	101.8	95.1	99.1	95.2	107.7	103.1	102.3	103.8
	820	821	822	823	824	825	888	891	895	906	934	935
K_2O	13.42	13.00	14.50	14.05	14.05	14.25	11.40	11.58	12.85	15.45	15.3	14.14
Na_2O	2.23	2.74	1.93	1.88	2.25	2.05	3.3	3.1	2.75	1.40	1.28	1.97
CaO	2070	1380	900	2500	1090	910	1310	1925	1580	1090	510	1984
MgO	N.D.	N.D.	N.D.	N.D.	N.D.	N.D.	N.D.	N.D.	N.D.	N.D.	N.D.	N.D.
Ba	2710	2122	2925	3480	3707	1911	2527	2341	1320	1359	3524	3151
Rb	622	313	266	608	707	298	296	600	1359	1307	302	271
Sr	195	179	240	241	234	195	199	278	96	103	250	184
Total	100.3	101.5	103.5	101.5	104.0	102.7	96.8	96.6	100.9	104.6	102.7	102.3

N.D. = Not Detected

TABLE B6.2

Results of Replicate Analyses of Östersidan Pegmatite Feldspar

	1	2	3	4	5	6	7	8	9	Mean	σ	C.V. (%)
K_2O (%)	14.14	15.20	14.32	15.21	14.03	13.95	15.16	12.66	13.79	14.27	0.83	5.8
Na_2O (%)	1.31	1.32	1.32	1.36	1.37	1.23	1.32	1.37	1.34	1.33	0.04	3.2
CaO (ppm)	931	1744	858	933	424	1110	392	258	803	820	440	54.0
MgO (ppm)	N.D.	N.D.	N.D.	N.D.	265	326	293	393	225	300	64	21.2
Ba (ppm)	3341	3189	3291	2759	3051	2708	2468	2628	2815	2917	311	10.7
Rb (ppm)	422	427	451	415	422	427	400	433	416	424	14	3.3
Sr (ppm)	196	183	175	221	246	230	242	258	245	222	30	13.6
Total (%)	96.3	103.0	97.4	102.9	96.0	94.6	102.1	87.8	94.4	97.2	4.9	5.1

N.D. = Not Detected C.V. = Coefficient of Variation

Note: The totals given are based on stoichiometric molecular weights for end-member 'feldspars'.

A pegmatitic feldspar was chosen, rather than one of the augen, because this enabled a large (c. 500g) sample to be used thereby reducing possible errors due to inhomogeneities between aliquots.

Table B7.1

Temperatures of homogenization of fluid inclusions in the Dragsmark granite

		T_H (°C)
AREA 1 :	Sample No. 32	295
		297
		283
		299
		296
	No. 53	287
		327
		318
	No. 145	200
		326
		324
	No. 158	207
		209
		322
	No. 253	315
		284
AREA 2	Sample No. 72	272
		280

TABLE B8.1

Major oxide analyses (in wt.%) i) Dragsmark granite

Sample	SiO_2	TiO_2	Al_2O_3	Fe_2O_3	MnO	MgO	CaO	Na_2O	K_2O	P_2O_5	FeO	L.O.I.
53	68.49	.75	13.53	.91	.06	1.02	2.14	2.57	4.49	.25	3.55	1.45
72	73.15	.37	12.75	.99	.03	.65	1.21	2.41	5.42	.07	1.69	.65
249	72.01	.35	13.80	.30	.03	.50	1.11	3.00	5.27	.09	2.02	.79
256	74.88	.25	12.65	.64	.02	.48	.77	2.70	5.45	.05	1.30	.73
275	68.93	.48	15.10	.81	.05	.79	2.25	2.94	5.78	.13	2.32	.73
418	73.46	.32	13.13	.88	.03	.54	1.02	2.78	5.70	.06	1.54	.63
706	70.80	.47	14.32	.91	.05	.51	1.62	2.86	5.32	.14	2.00	.88
710	70.28	.40	14.67	.68	.04	.73	1.73	3.52	4.50	.13	1.83	1.11
821	69.26	.54	13.79	1.09	.03	.79	1.47	2.83	5.89	.16	2.17	1.18
823	68.68	.57	13.91	1.43	.05	1.01	2.01	2.71	4.51	.18	2.14	2.62

TABLE B8.1 (cont.)

Major oxide analyses (in wt.%) ii) Other lithologies

Sample	SiO_2	TiO_2	Al_2O_3	Fe_2O_3	MnO	MgO	CaO	Na_2O	K_2O	P_2O_5	FeO	L.O.I.
gneissose granite												
594	72.83	.22	14.16	.83	.07	.72	1.45	3.56	3.99	.04	1.12	.78
988	68.24	.58	13.91	1.17	.09	1.10	2.10	2.62	4.12	.15	3.08	1.18
989	72.25	.22	13.54	.72	.03	.07	.94	2.90	5.58	.09	.98	.72
Stora Le -Marstrand gneisses												
707	71.91	.70	12.87	.91	.05	1.67	1.65	2.74	3.11	.04	3.59	1.19
709	71.29	.45	13.85	1.28	.09	1.32	1.43	2.73	3.71	.07	2.19	1.00
Källviken granite												
30	68.51	.66	13.55	1.37	.08	.75	1.84	2.58	4.72	.15	3.84	1.57
veins												
3001	69.87	.34	14.01	1.12	.04	1.04	1.28	4.57	2.90	.09	2.63	1.38
3002	69.71	.29	14.37	.90	.04	.59	1.08	2.78	7.21	.08	1.70	.91
granitic migmatite leucosome												
41	73.18	.34	13.18	.95	.07	.41	1.06	2.70	5.06	.09	2.03	.81

TABLE B8.2

Selected Trace Element Analyses (in ppm)

Sample	Rb	Sr	Y	Zr	Ba
Dragsmark granite					
53	127	177	44	388	982
72	210	90	50	272	597
249	181	165	38	218	768
256	180	84	36	160	359
275	164	165	48	295	1083
418	273	71	80	212	485
706	157	161	41	231	992
710	143	173	25	198	820
821	201	116	34	299	640
823	145	99	38	358	865
gneissose granite					
594	153	118	46	85	334
988	164	129	46	247	1026
989	197	113	15	148	773
Stora Le -Marstrand gneisses					
707	145	172	44	353	534
709	150	180	47	245	806
Kållviken granite					
30	127	121	67	534	1069
veins cutting the Kållviken granite					
3001	104	102	18	279	652
3002	225	131	33	245	1204
granitic migmatite leucosome					
41	208	87	161	203	397

TABLE B9.1

Garnet Analyses

	32/3	32/4	32/6	935/3(R)	935/3(C)	53/5	53/6	30/1	30/4(R)	30/4(M)	30/4(C)
SiO_2	37.10	37.24	37.38	37.46	37.20	37.69	37.07	37.34	37.42	37.29	37.47
Al_2O_3	19.90	20.11	20.11	20.50	20.18	20.61	20.05	19.90	19.87	20.00	20.36
FeO	24.92	28.30	28.18	26.10	24.22	26.77	27.50	27.32	27.11	26.32	25.25
MgO	1.09	1.55	1.44	0.96	0.91	1.26	1.29	1.05	1.15	0.88	0.75
CaO	12.15	11.87	11.84	13.20	13.13	12.75	12.18	13.87	13.66	14.27	14.32
MnO	4.05	0.70	0.76	1.78	3.86	0.93	0.51	0.43	0.60	0.56	1.65
	Cation proportions (based on 12 oxygens)										
Si	2.99	2.98	2.99	2.99	2.99	2.99	3.00	2.98	2.99	3.00	2.99
Al	1.89	1.90	1.90	1.93	1.91	1.93	1.91	1.88	1.87	1.90	1.92
Fe	1.68	1.89	1.89	1.74	1.63	1.78	1.86	1.83	1.81	1.77	1.69
Mg	0.13	0.19	0.17	0.11	0.11	0.15	0.16	0.12	0.14	0.11	0.09
Ca	1.05	1.02	1.02	1.13	1.13	1.09	1.06	1.19	1.17	1.23	1.23
Mn	0.28	0.05	0.05	0.12	0.26	0.06	0.04	0.03	0.04	0.04	0.11

R = rim M = midway C = core

TABLE B9.1 (cont.)

Garnet Analyses

	6/2	6/4(R)	6/4(C)	624/2	624/4	133/1	133/4(R)	133/4(C)	133/4(R')
SiO_2	37.32	37.24	37.01	37.62	37.84	37.49	37.57	37.22	37.48
Al_2O_3	20.30	20.14	20.06	19.92	20.43	20.29	20.22	20.32	20.06
FeO	26.58	25.70	25.02	26.15	25.89	25.77	26.42	27.53	25.50
MgO	1.30	0.95	1.22	1.13	1.24	2.05	2.08	1.68	1.77
CaO	12.09	12.49	12.66	14.55	14.22	12.33	12.72	11.16	13.52
MnO	2.01	2.40	3.14	0.52	1.07	2.14	0.93	1.33	0.76
	Cation proportions (based on 12 oxygens)								
Si	3.00	3.01	2.99	3.00	2.99	2.98	2.99	2.99	2.99
Al	1.92	1.92	1.91	1.87	1.90	1.90	1.90	1.93	1.89
Fe	1.79	1.74	1.69	1.74	1.71	1.72	1.76	1.85	1.70
Mg	0.16	0.12	0.15	0.13	0.15	0.24	0.25	0.20	0.21
Ca	1.04	1.08	1.10	1.24	1.20	1.05	1.08	0.96	1.16
Mn	0.14	0.16	0.22	0.04	0.07	0.14	0.06	0.09	0.05

TABLE B9.2

Biotite Analyses

	32/2	32/5	32/7	935/1	53/3	53/4	30/2	30/3
SiO_2	32.72	34.24	34.13	34.87	34.77	34.58	33.78	34.42
TiO_2	2.65	2.57	2.50	2.71	2.90	3.43	2.38	2.93
Al_2O_3	16.24	15.64	16.04	15.84	15.47	15.30	14.47	14.47
FeO	29.16	25.94	25.84	27.38	26.23	25.19	28.08	27.85
MnO	0.64	0.36	0.32	0.36	0.26	0.20	0.29	0.23
MgO	6.21	5.90	5.80	4.99	6.05	5.71	5.24	5.29
CaO	0.88	0.15	0.06	0.08	0.10	0.06	0.10	0.13
Na_2O	0.76	0.54	0.25	0.23	0.27	0.30	0.65	0.38
K_2O	5.69	9.42	9.27	9.37	9.33	9.23	9.00	9.13
Cl	0.07	0.13	0.14	0.04	0.09	0.15	0.10	N.D.
	Cation Proportions (on the basis of 22 oxygens)							
Si	5.23	5.47	5.47	5.53	5.51	5.53	5.51	5.54
Ti	0.32	0.31	0.30	0.32	0.35	0.41	0.29	0.36
Al	3.06	2.95	3.03	2.96	2.89	2.88	2.78	2.75
Fe	3.90	3.47	3.46	3.63	3.47	3.37	3.83	3.75
Mn	0.09	0.05	0.04	0.05	0.04	0.03	0.04	0.03
Mg	1.48	1.41	1.39	1.18	1.43	1.36	1.27	1.27
Ca	0.15	0.03	0.01	0.01	0.02	0.01	0.02	0.02
Na	0.24	0.17	0.08	0.07	0.08	0.09	0.21	0.12
K	1.16	1.92	1.90	1.90	1.89	1.89	1.87	1.88

N.D. = Not Detected

TABLE B9.2 (cont.)

Biotite Analyses

	6/1	6/3	624/1	624/3	133/2	133/3	133/5
SiO_2	30.70	30.41	33.93	34.23	36.37	32.98	35.23
TiO_2	2.42	2.04	2.67	2.12	2.35	2.71	2.69
Al_2O_3	15.30	15.98	15.03	15.21	15.07	15.43	15.82
FeO	27.69	28.14	29.89	30.63	23.86	23.56	23.66
MnO	0.37	0.38	0.32	0.30	0.30	0.21	0.23
MgO	6.74	7.42	4.18	4.39	7.24	7.73	7.59
CaO	0.50	0.11	0.01	0.10	0.05	0.76	0.08
Na_2O	0.29	0.30	0.25	0.34	0.58	0.48	0.42
K_2O	4.96	4.90	9.40	9.28	8.94	7.57	9.15
Cl	0.09	0.09	0.06	0.15	0.15	0.09	0.07
	Cation Proportions (on the basis of 22 oxygens)						
Si	5.21	4.65	5.48	5.48	5.69	5.38	5.53
Ti	0.31	0.23	0.32	0.26	0.28	0.33	0.32
Al	3.06	2.88	2.86	2.87	2.78	2.97	2.93
Fe	3.93	3.60	4.04	4.10	3.12	3.21	3.10
Mn	0.05	0.05	0.04	0.04	0.04	0.03	0.03
Mg	1.71	1.69	1.00	1.05	1.69	1.88	1.78
Ca	0.09	0.02	0.00	0.02	0.01	0.13	0.01
Na	0.10	0.09	0.08	0.11	0.18	0.15	0.13
K	1.07	0.96	1.93	1.89	1.79	1.58	1.83

TABLE B9.3

Garnet - Biotite Pairs

Sample (Gnt, Biot)	X^G_{Fe}	X^G_{Mg}	X^G_{Ca}	X^G_{Mn}	X^B_{Fe}	X^B_{Ti}	$X^B_{Al^{VI}}$
32 3,2	.536	.042	.335	.088	.725	.052	.047
32 4,5	.602	.059	.324	.015	.711	.055	.074
32 6,7	.604	.055	.325	.016	.714	.053	.088
935 3(R),1	.561	.037	.364	.039	.755	.057	.086
53 5,4	.579	.048	.353	.020	.712	.074	.074
53 6,3	.599	.050	.340	.011	.709	.061	.070
30 1,2	.576	.039	.375	.009	.750	.051	.051
30 4(R),3	.574	.043	.370	.013	.747	.062	.051
6 2,1	.573	.050	.334	.044	.697	.049	.043
6 4(R),3	.561	.037	.349	.053	.680	.046	.091
624 2,1	.553	.043	.394	.011	.801	.056	.059
624 4,3	.546	.047	.384	.023	.796	.044	.060
133 1,2	.544	.077	.334	.046	.649	.049	.084
133 4(R),3	.558	.078	.344	.020	.631	.057	.059
133 4(R'),5	.545	.068	.370	.017	.636	.056	.079

X^G_{Fe}, etc. = cation proportion of Fe in garnet, etc.

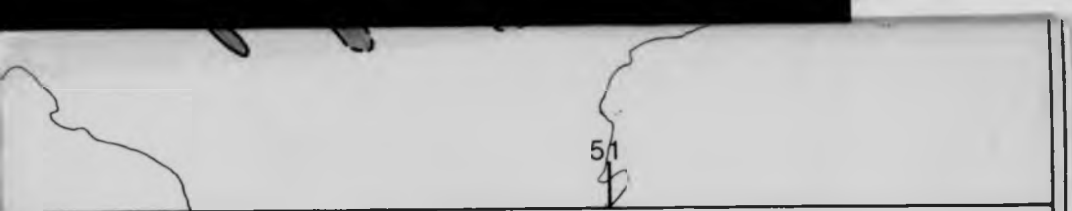

MAP 1

SOLID GEOLOGY

P.R.GAMBLES
1983

GEOLOGY OF

DRAGSMARK & SKAFTÖ,

SOUTH-WEST SWEDEN

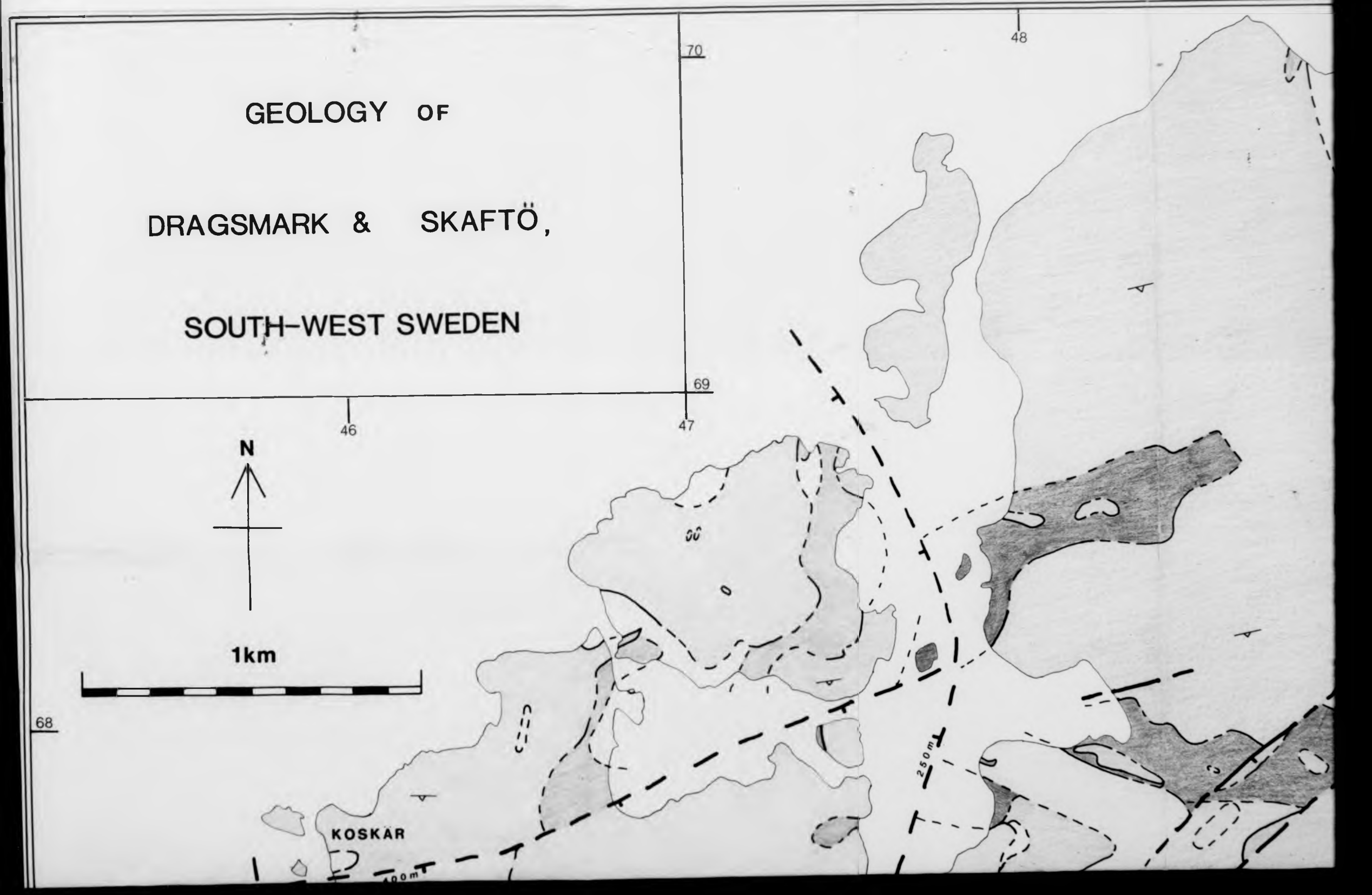

GEOLOGY OF

DRAGSMARK & SKAFTÖ,

SOUTH-WEST SWEDEN

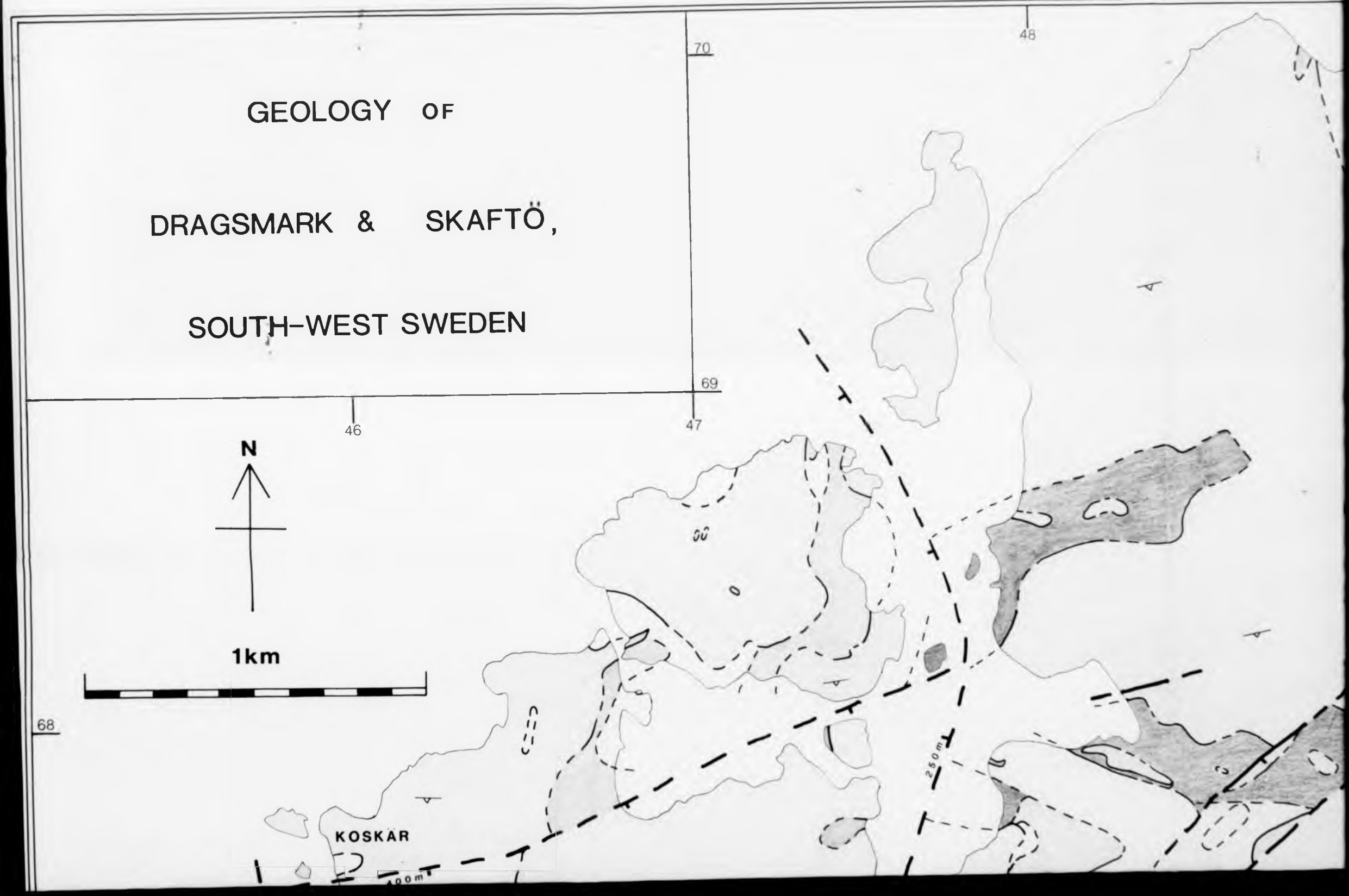

A 2

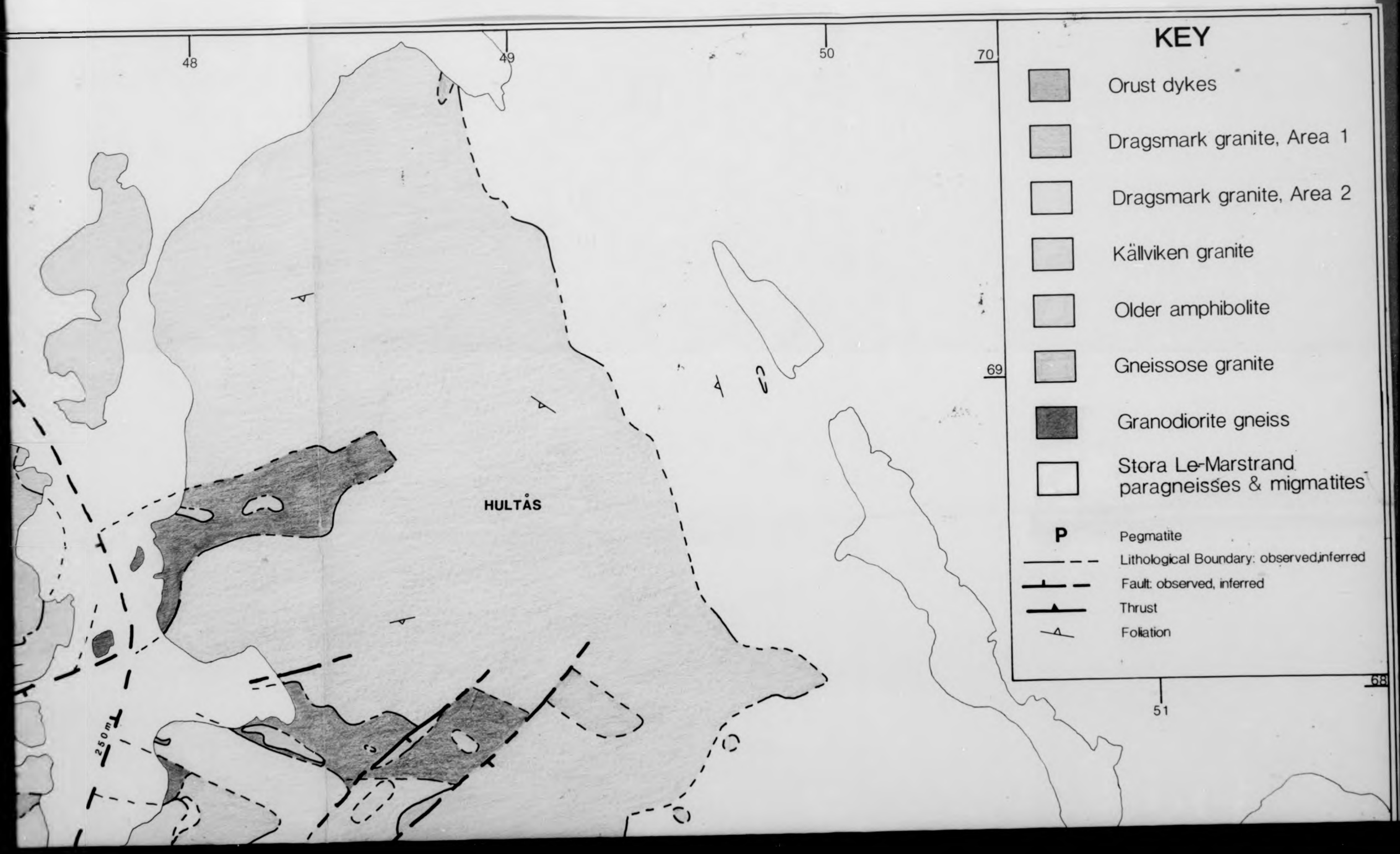
48
49
50
70
69
68
51
HULTÅS
250m
KEY
Orust dykes
Dragsmark granite, Area 1
Dragsmark granite, Area 2
Källviken granite
Older amphibolite
Gneissose granite
Granodiorite gneiss
Stora Le-Marstrand paragneisses & migmatites
P
Pegmatite
Lithological Boundary: observed,inferred
Fault: observed, inferred
Thrust
Foliation

A 2

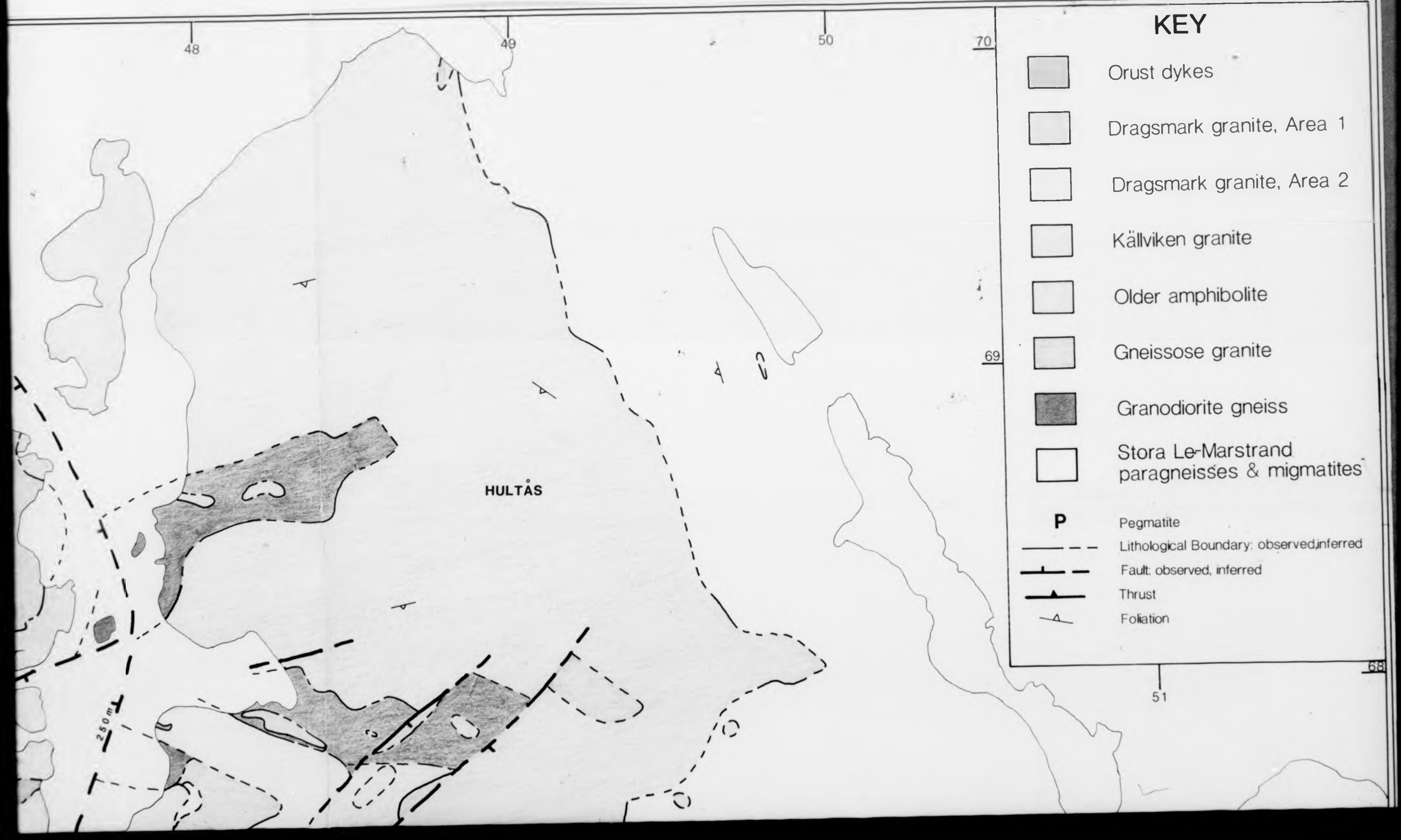
48
49
50
70
69
68
51
HULTÅS
250m
KEY
Orust dykes
Dragsmark granite, Area 1
Dragsmark granite, Area 2
Källviken granite
Older amphibolite
Gneissose granite
Granodiorite gneiss
Stora Le-Marstrand paragneisses & migmatites
P
Pegmatite
Lithological Boundary: observed,inferred
Fault: observed, inferred
Thrust
Foliation

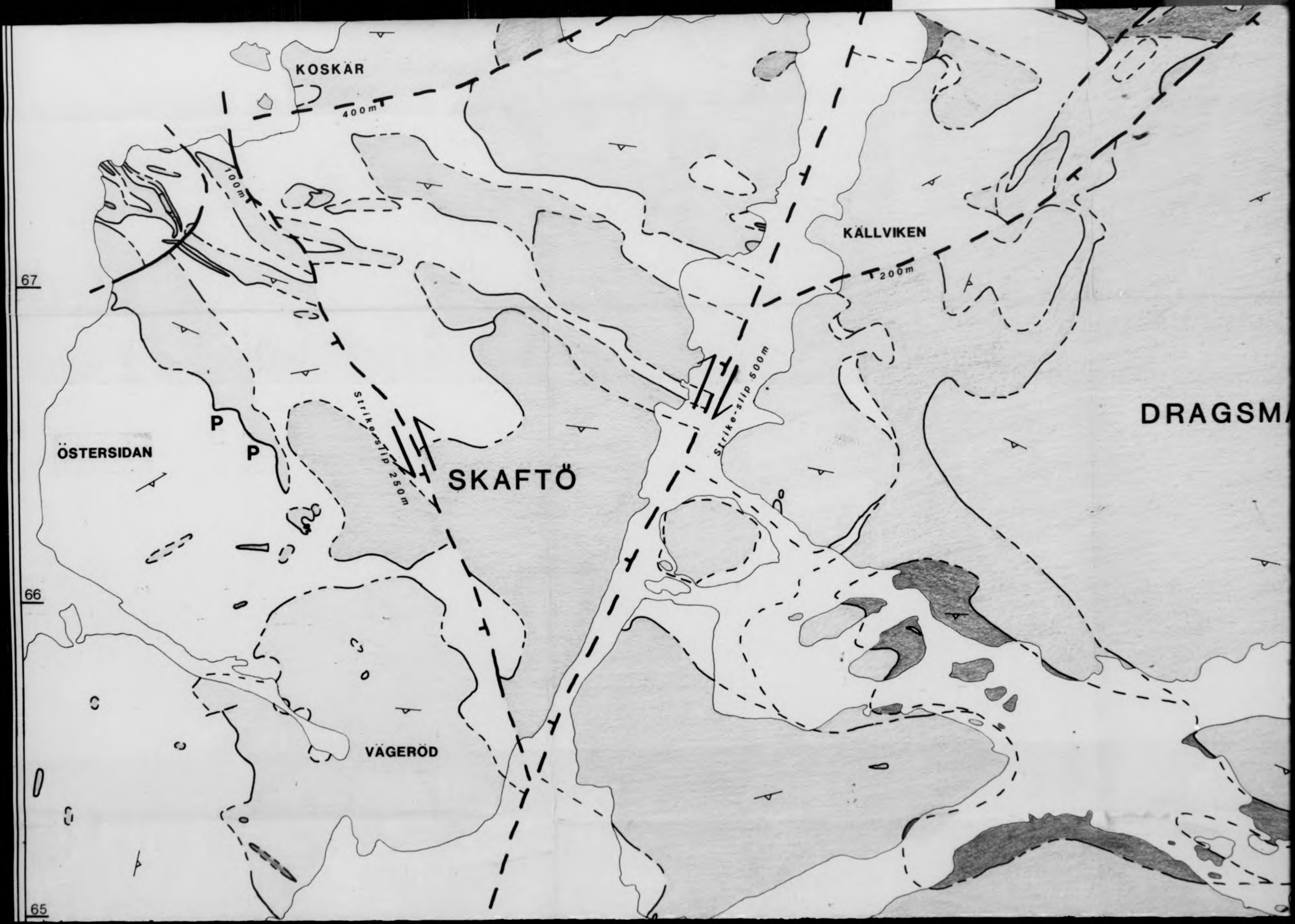
KOSKÄR
400m
100m
KÄLLVIKEN
200m
67
Strike-slip 500m
DRAGSMA
P
P
ÖSTERSIDAN
Strike-slip 250m
SKAFTÖ
66
VÄGERÖD
65

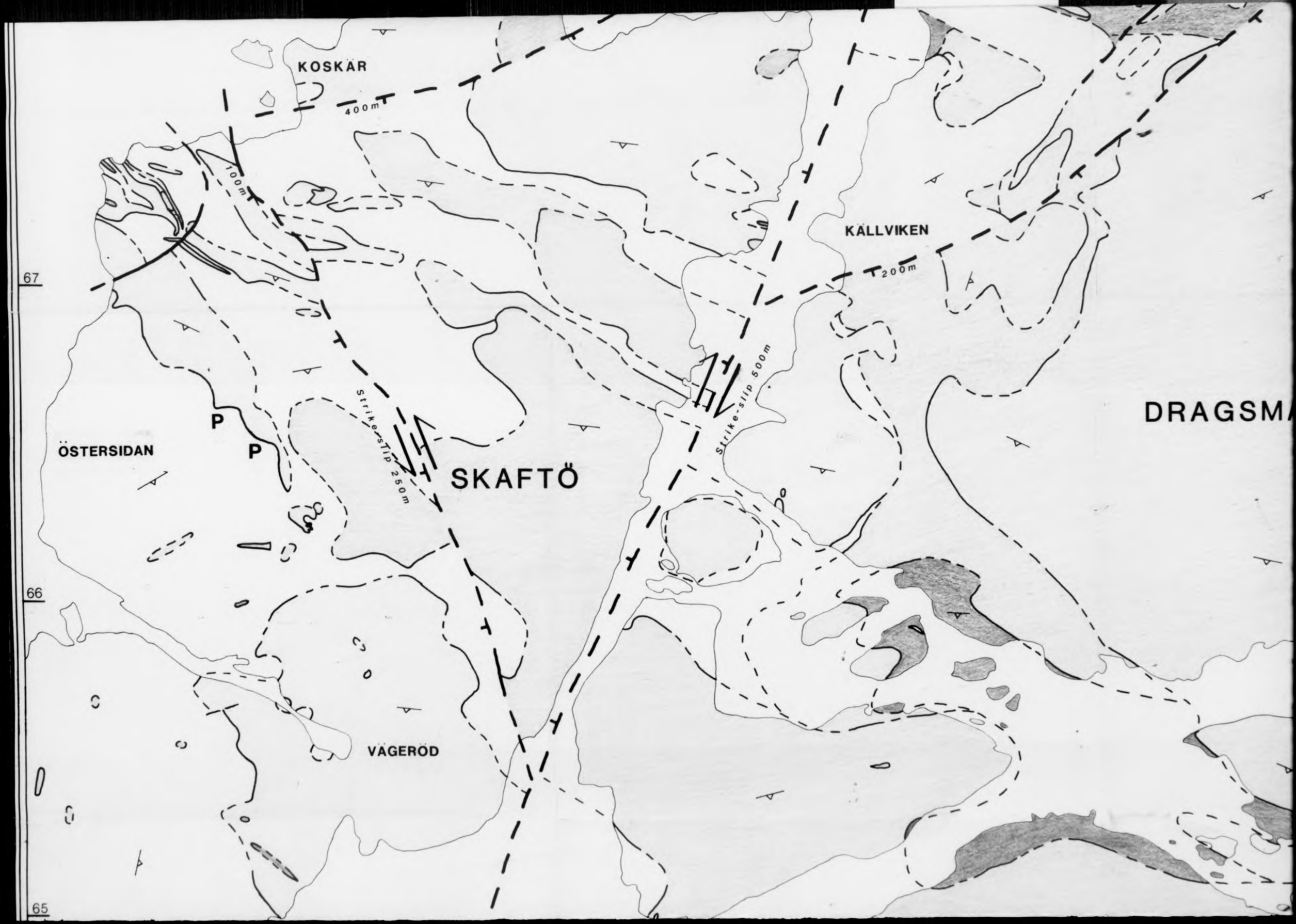
KOSKÄR
400m
100m
KÄLLVIKEN
200m
Strike-slip 500m
DRAGSMA
Strike-slip 250m
SKAFTÖ
P
P
ÖSTERSIDAN
VÄGERÖD
67
66
65

GEOLOGY OF

DRAGSMARK & SKAFTÖ,

SOUTH-WEST SWEDEN

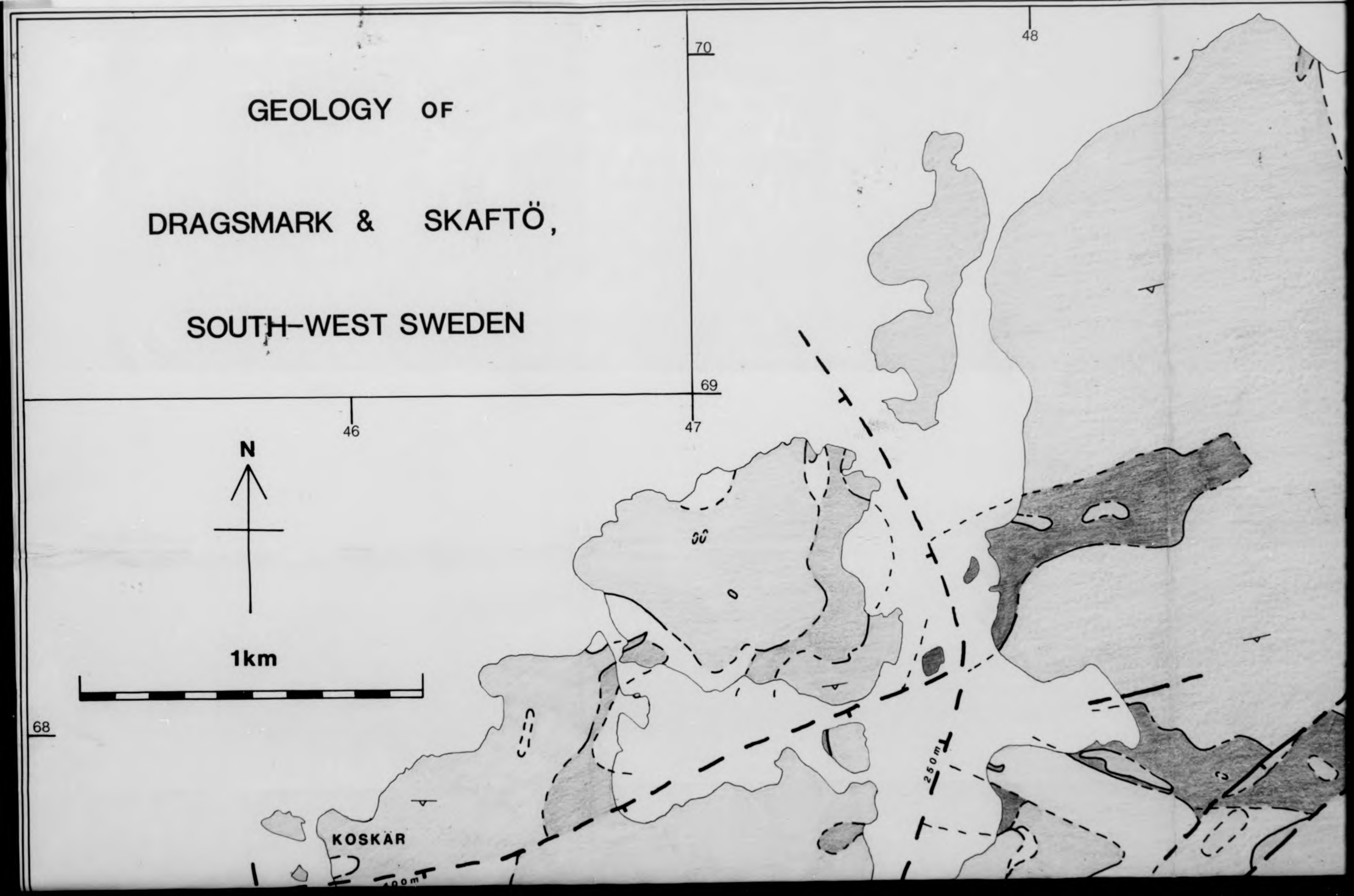

GEOLOGY OF

DRAGSMARK & SKAFTÖ,

SOUTH-WEST SWEDEN

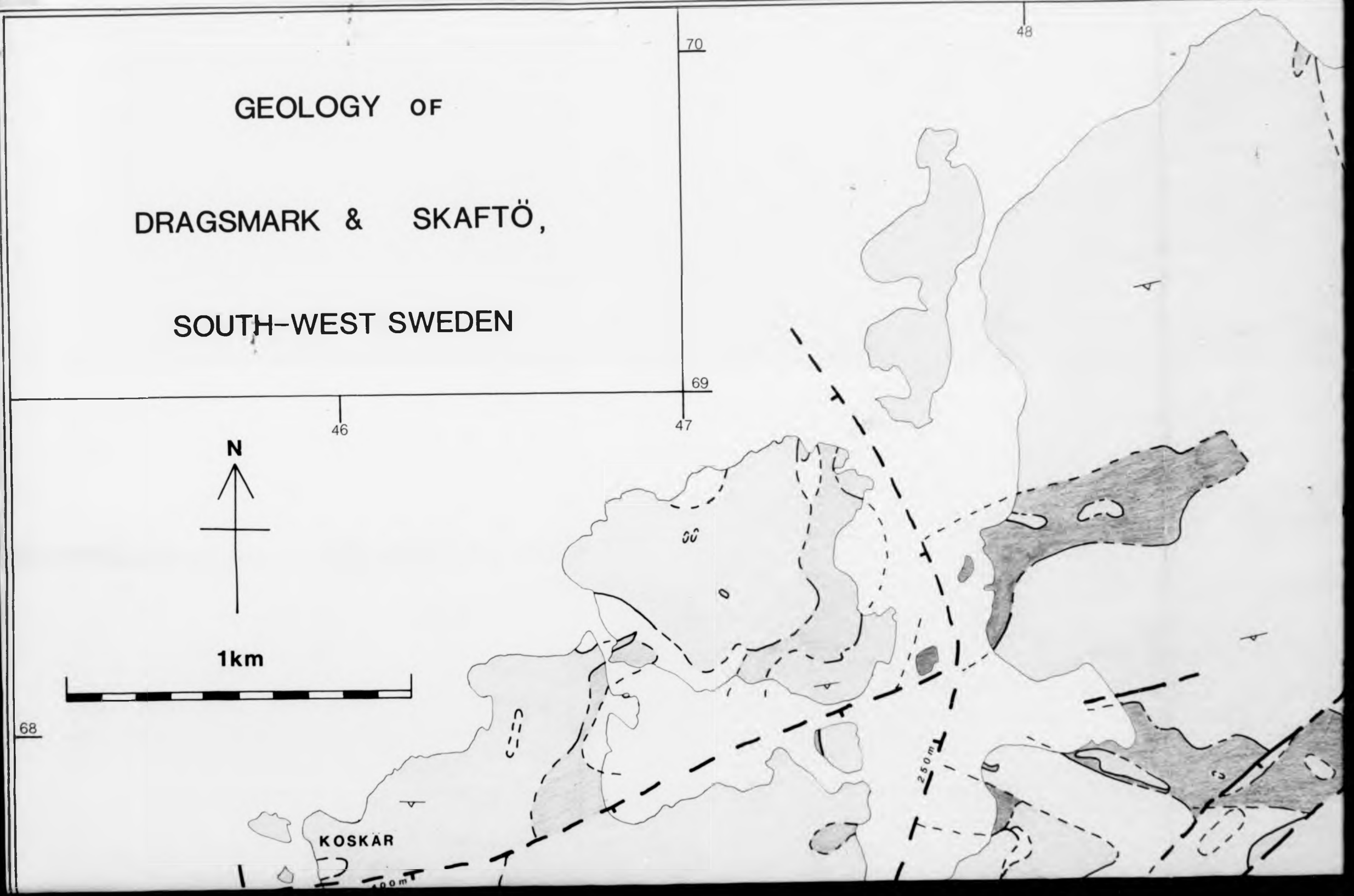

A 2

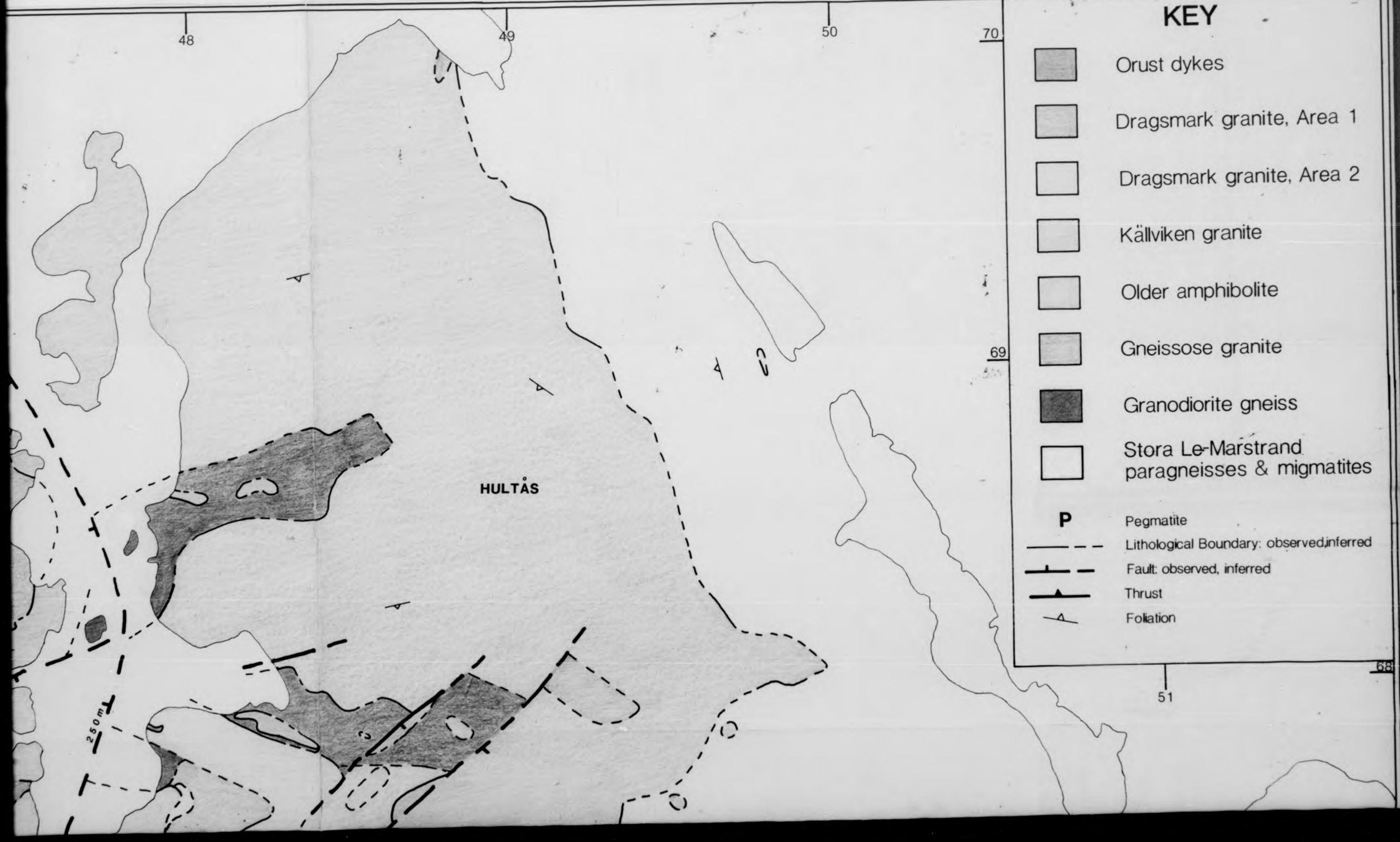
48
49
50
70
69
68
51
HULTÅS
250 m
KEY
Orust dykes
Dragsmark granite, Area 1
Dragsmark granite, Area 2
Källviken granite
Older amphibolite
Gneissose granite
Granodiorite gneiss
Stora Le-Marstrand paragneisses & migmatites
P
Pegmatite
Lithological Boundary: observed,inferred
Fault: observed, inferred
Thrust
Foliation

A 2

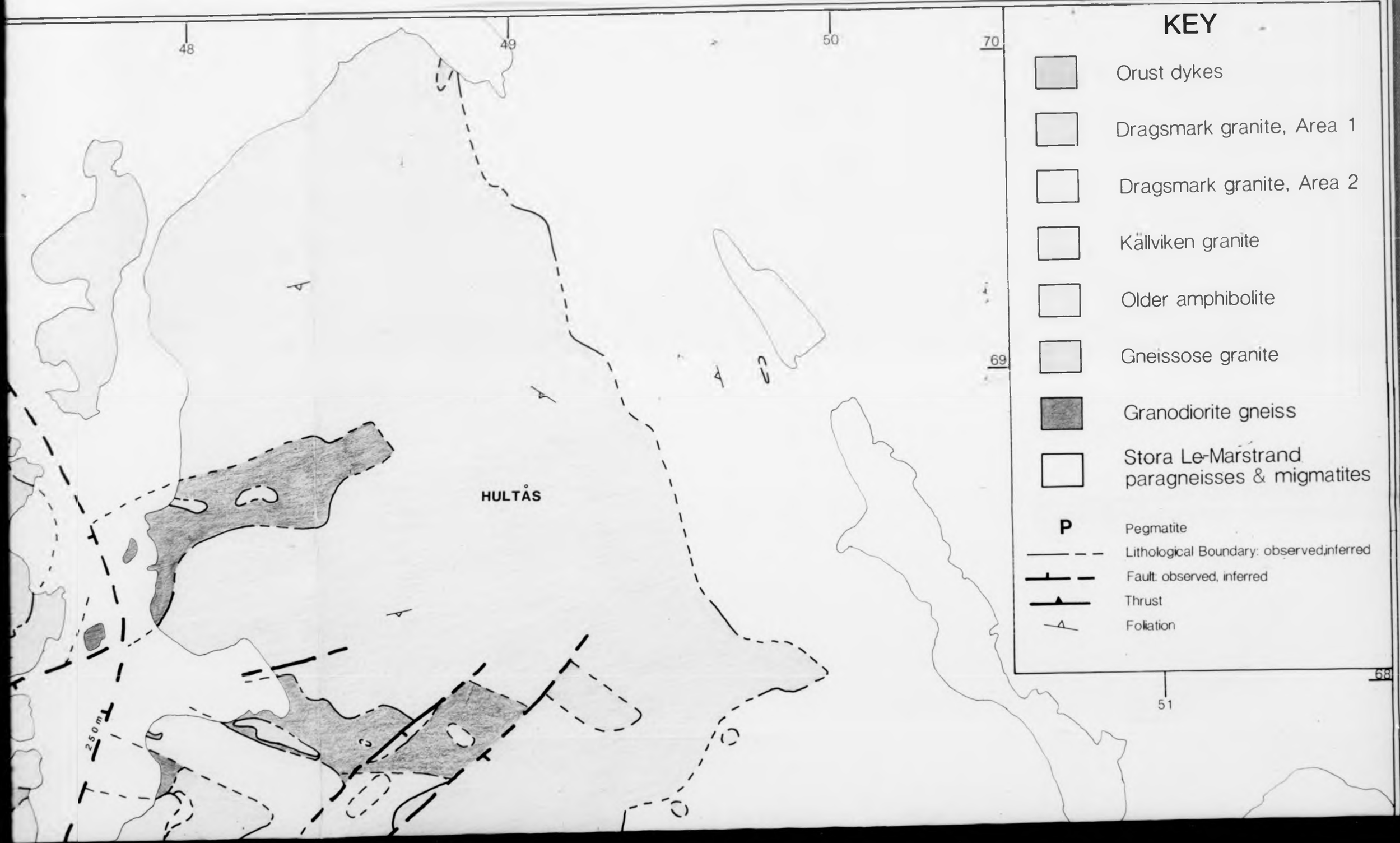
48
49
50
70
69
68
51
HULTÅS
250m
KEY
Orust dykes
Dragsmark granite, Area 1
Dragsmark granite, Area 2
Källviken granite
Older amphibolite
Gneissose granite
Granodiorite gneiss
Stora Le-Marstrand paragneisses & migmatites
P
Pegmatite
Lithological Boundary: observed,inferred
Fault: observed, inferred
Thrust
Foliation

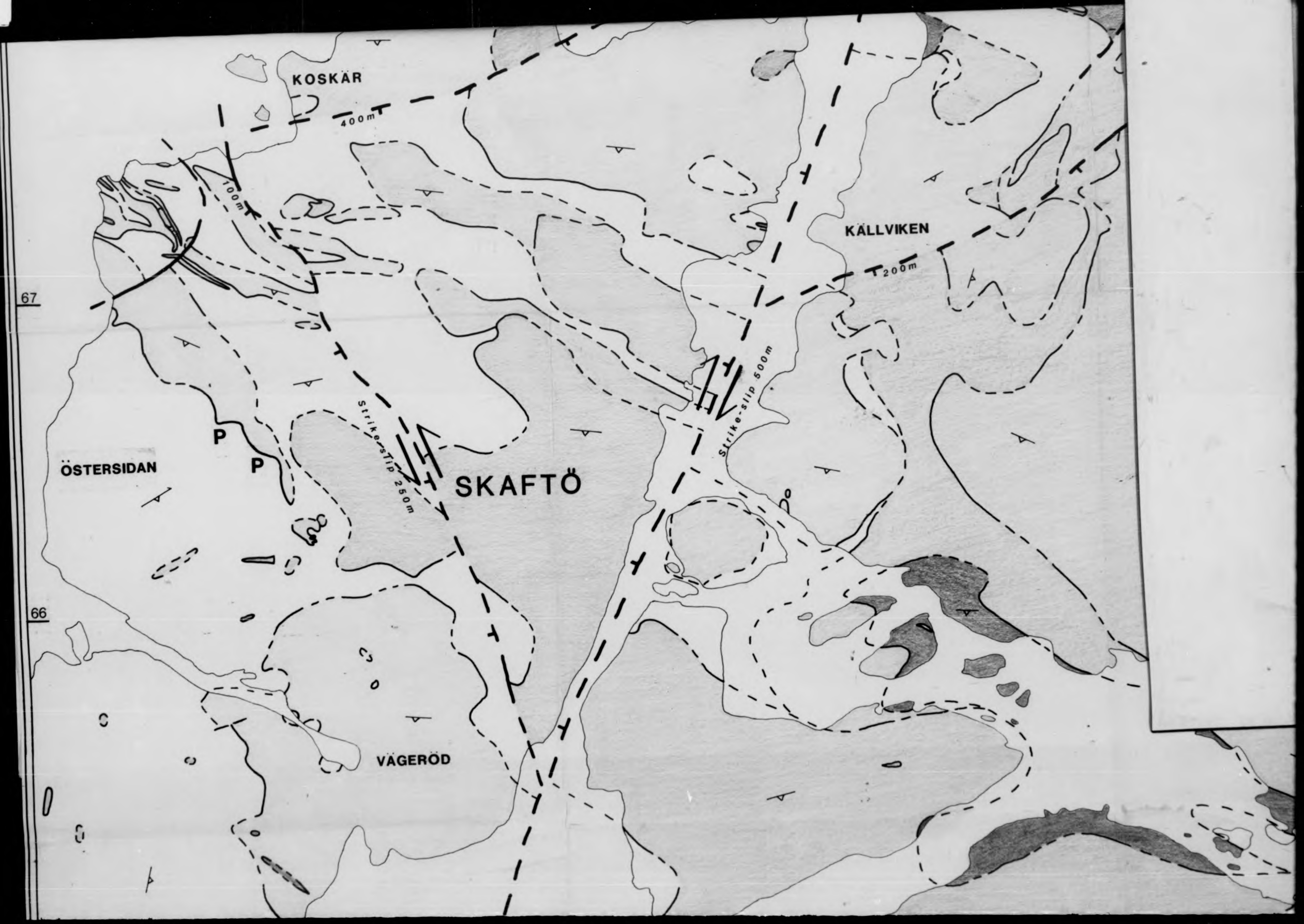
KOSKÄR
400m
100m
KÄLLVIKEN
200m
Strike-slip 500m
Strike-slip 250m
SKAFTÖ
P
P
ÖSTERSIDAN
VÄGERÖD
67
66

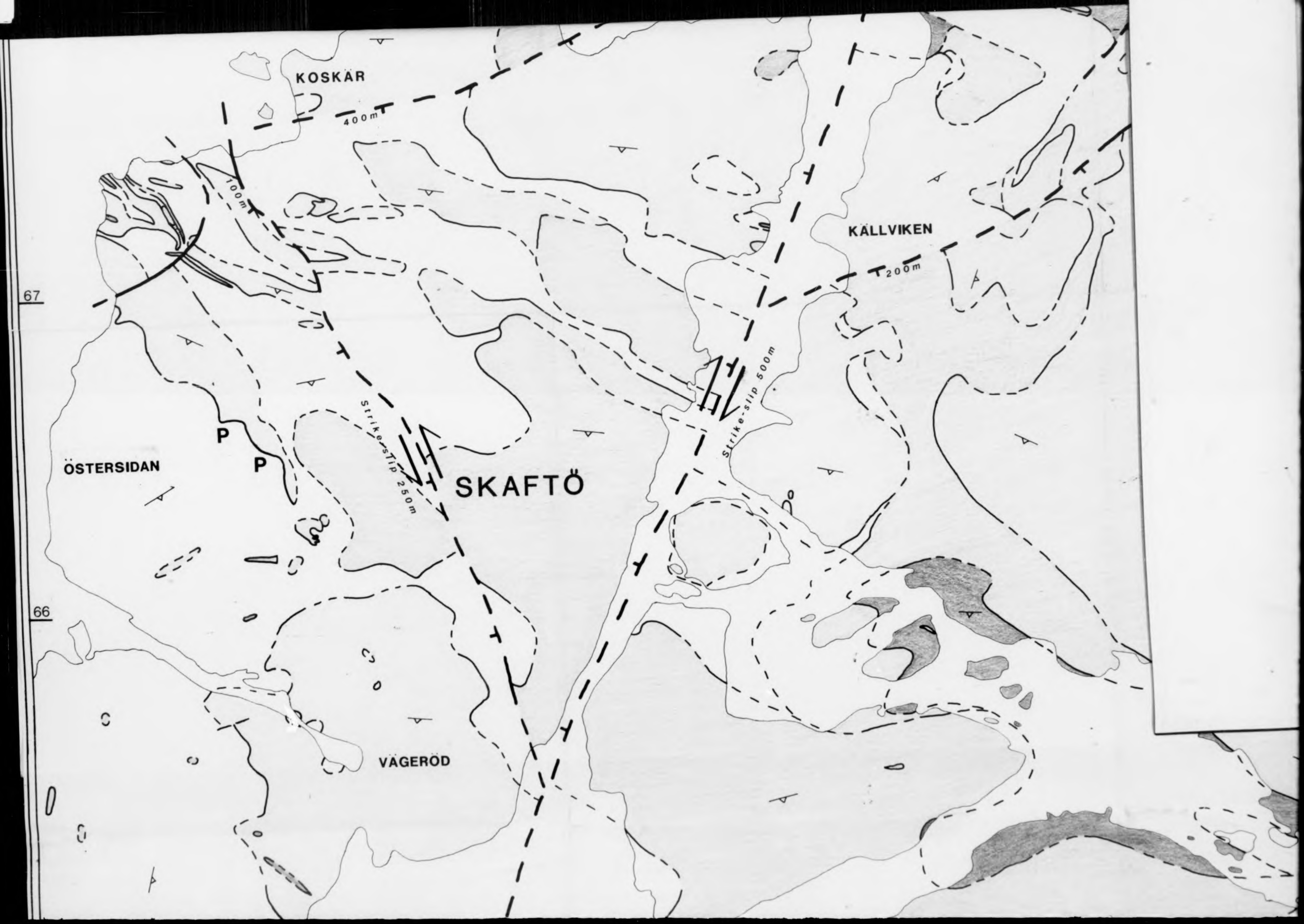
KOSKÄR
400m
100m
KÄLLVIKEN
200m
Strike-slip 500m
Strike-slip 250m
SKAFTÖ
P
P
ÖSTERSIDAN
VÄGERÖD
67
66

B2

KÄLLVIKEN

T 200m

DRAGSMARK

KLOSTERGÅRD

P

P

67

66

50

51

65

B2

KÄLLVIKEN

200m

DRAGSMARK

KLOSTERGÅRD

P

P

67

66

50

51

65

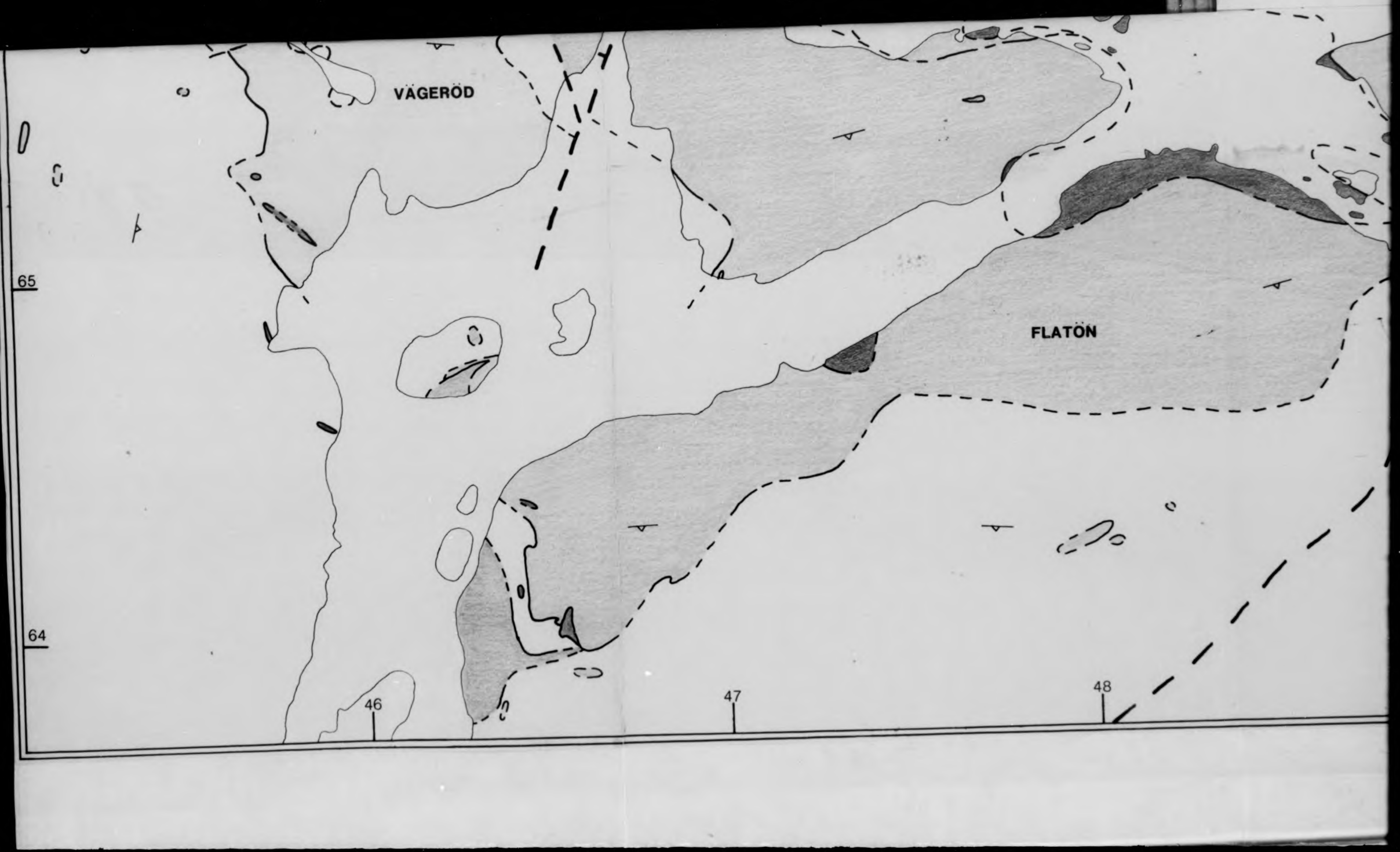
VÄGERÖD
FLATÖN
65
64
46
47
48


VÄGERÖD
FLATÖN
65
64
46
47
48

C2

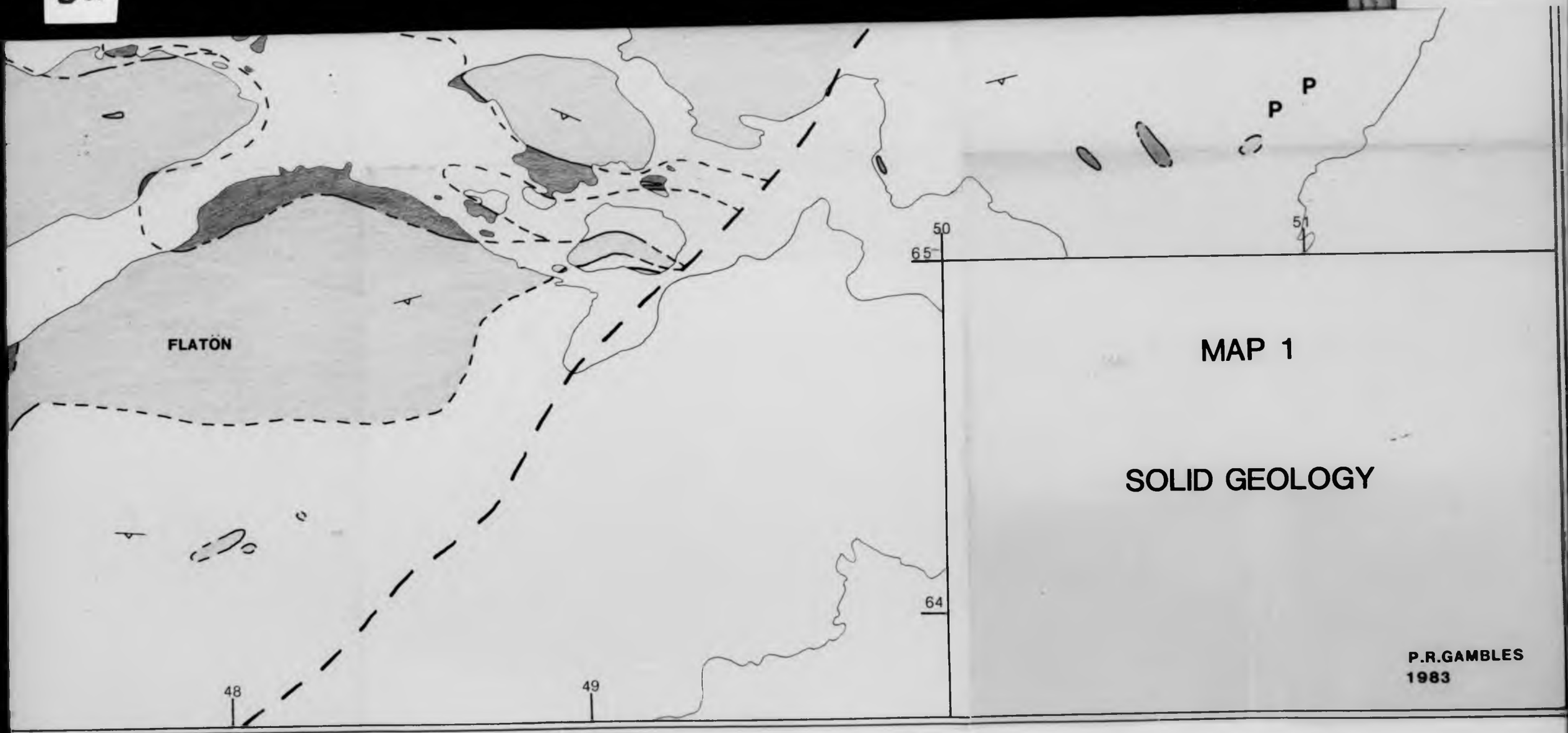

MAP 1

SOLID GEOLOGY

P.R.GAMBLES
1983

C2

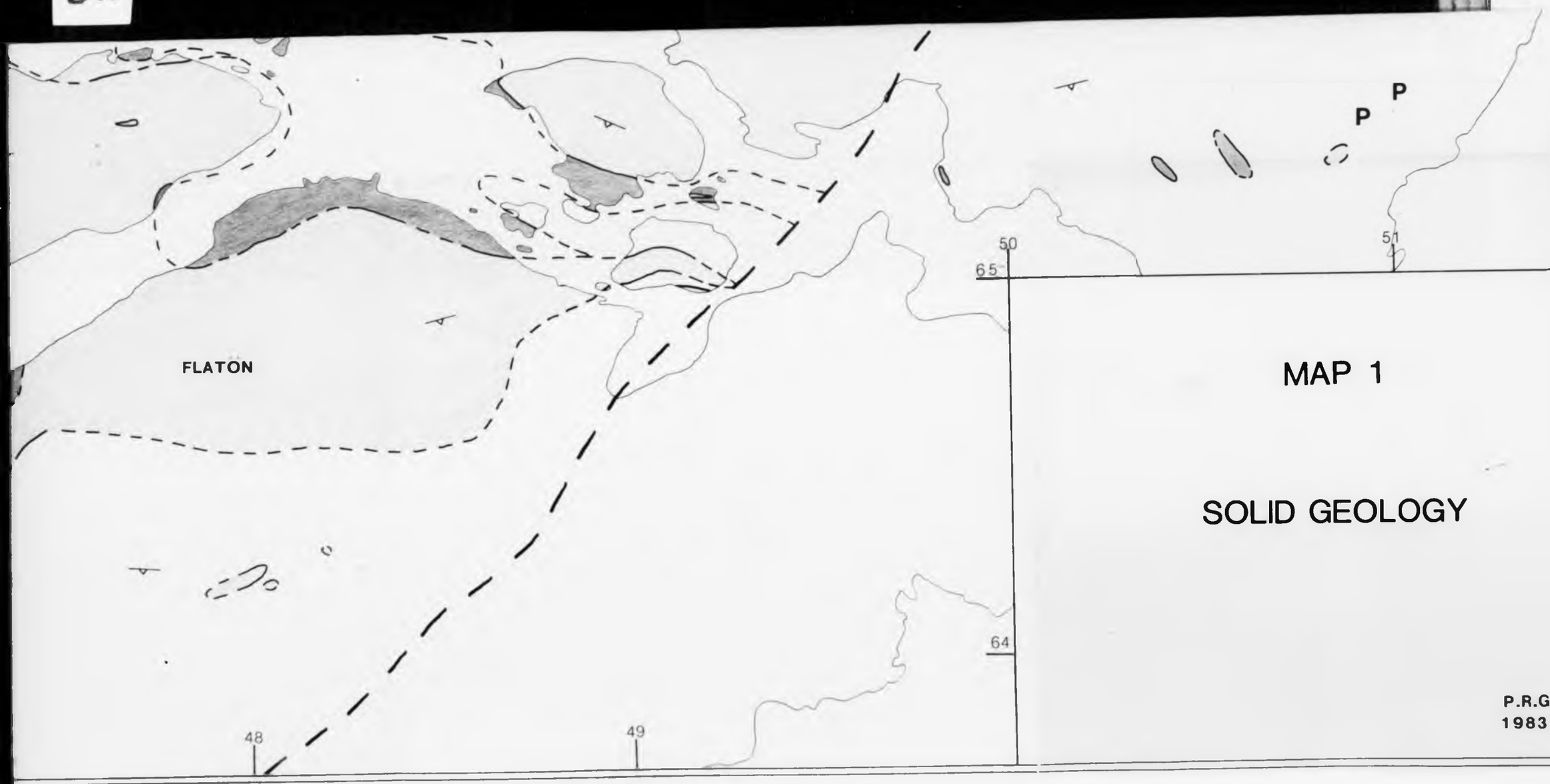

MAP 1

SOLID GEOLOGY

P.R.GAMBLES
1983

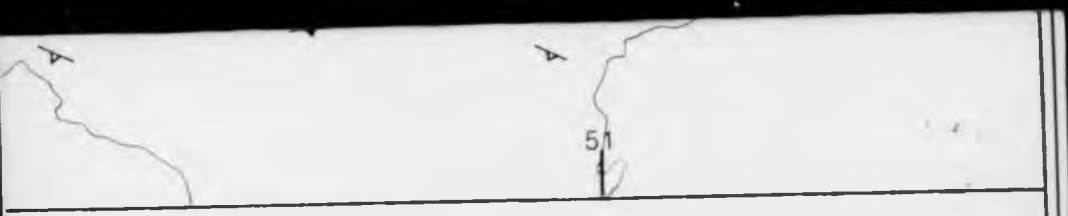

MAP 2

STRUCTURE

P.R.GAMBLES
1983

GEOLOGY OF

DRAGSMARK & SKAFTÖ ,

SOUTH-WEST SWEDEN

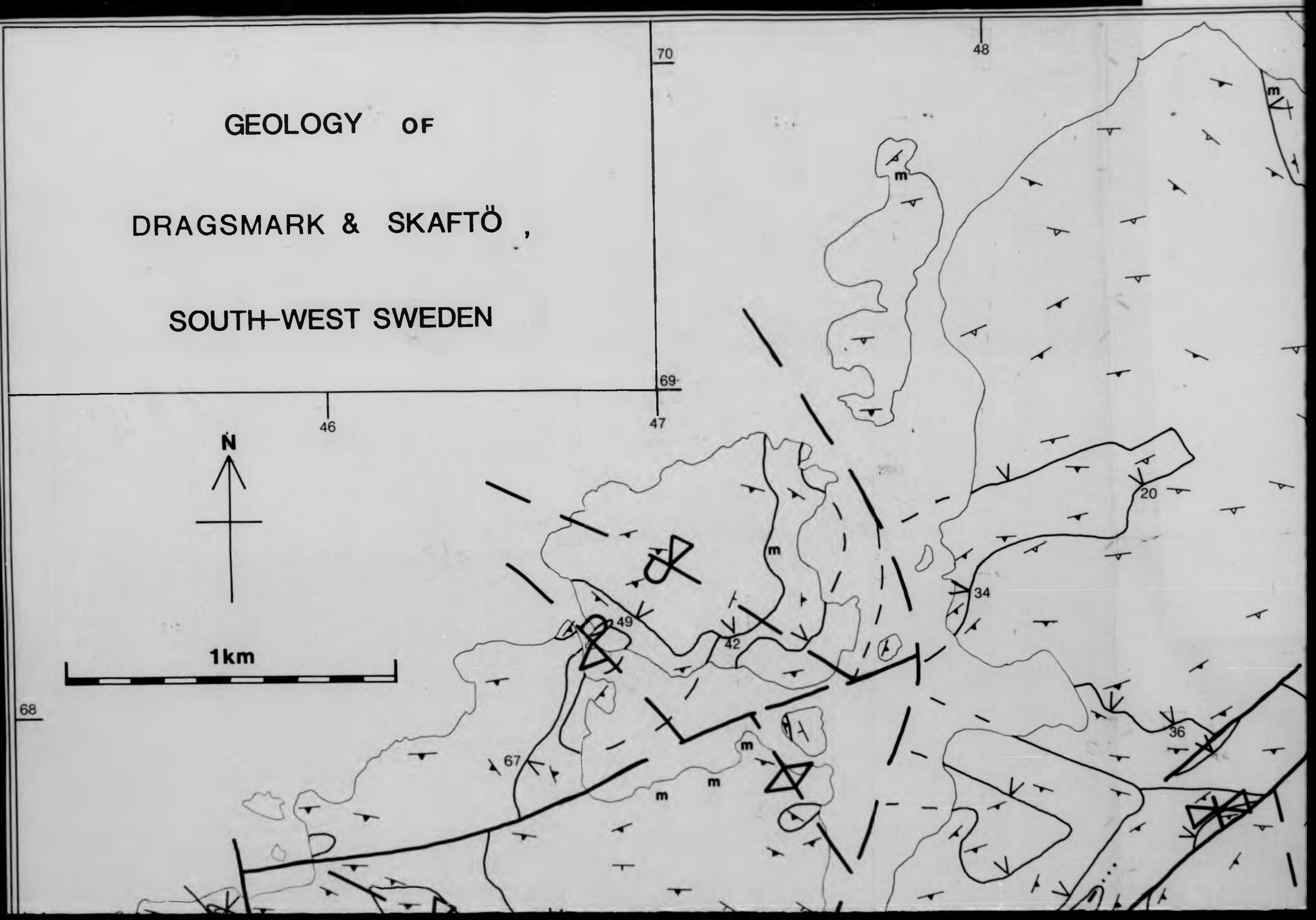

A 2

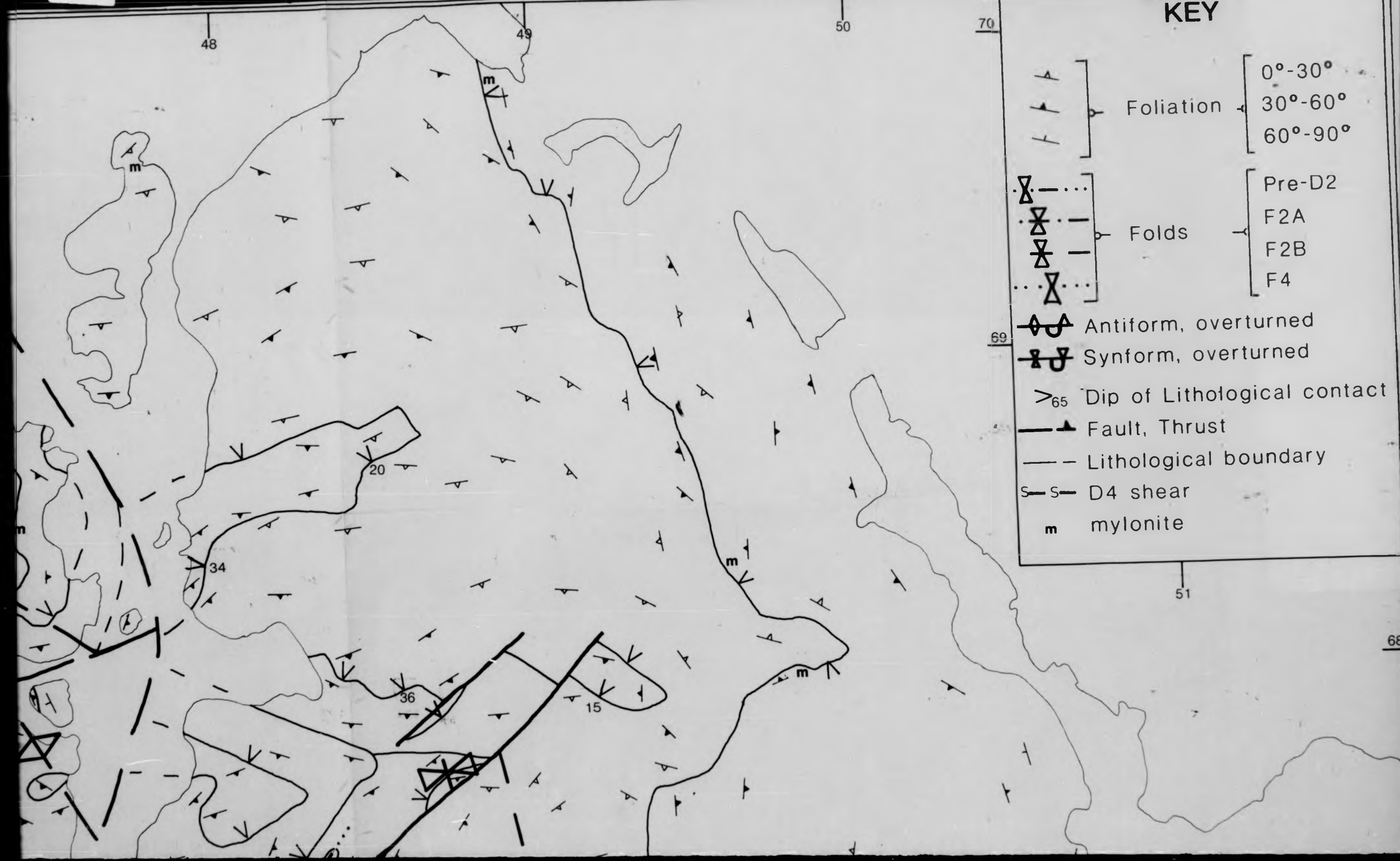
48
49
50
70
69
68
51
m
20
34
36
15
KEY
Foliation
0°-30°
30°-60°
60°-90°
Folds
Pre-D2
F2A
F2B
F4
Antiform, overturned
Synform, overturned
>65 Dip of Lithological contact
Fault, Thrust
Lithological boundary
S— S— D4 shear
m mylonite

B1

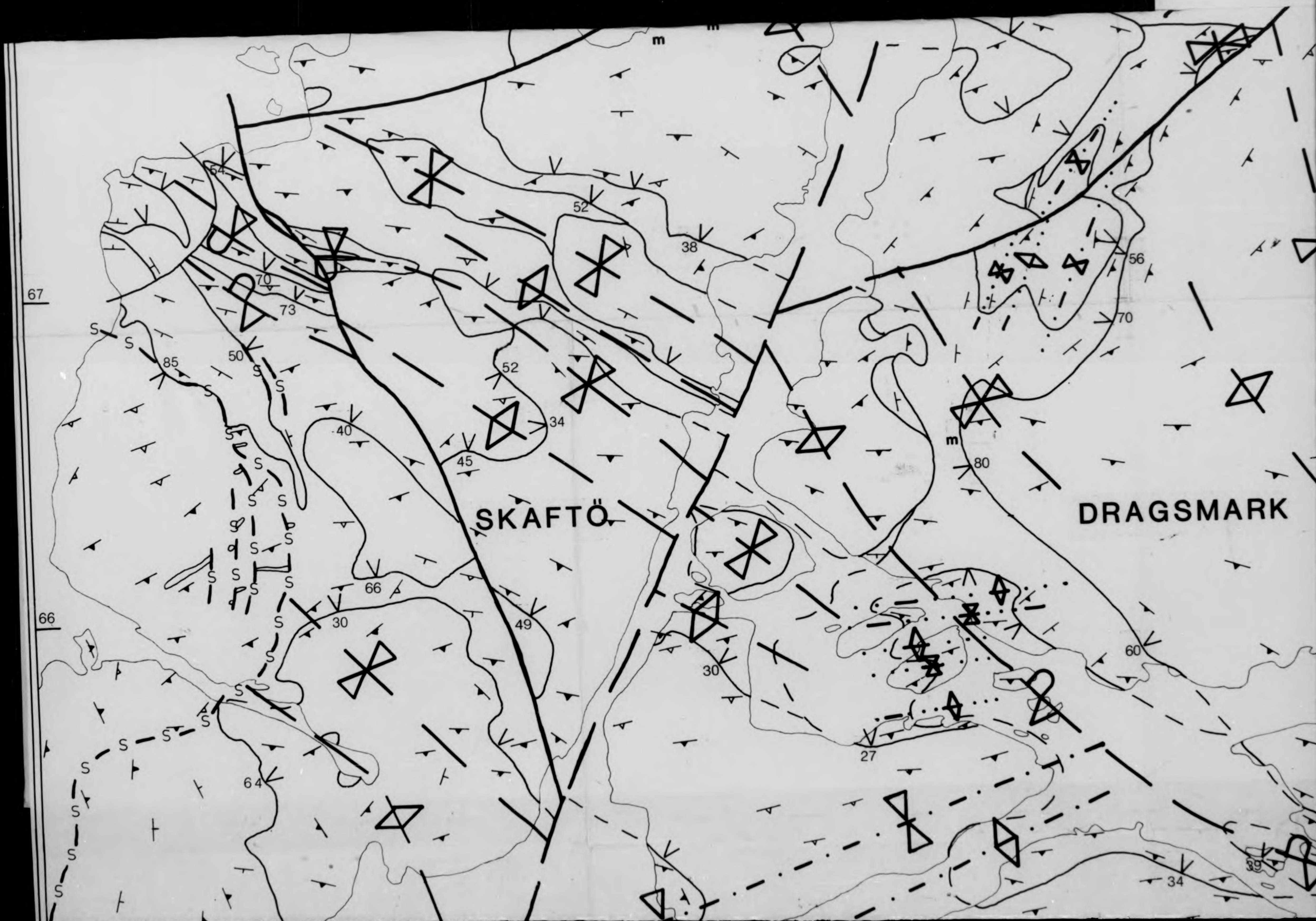

B 2

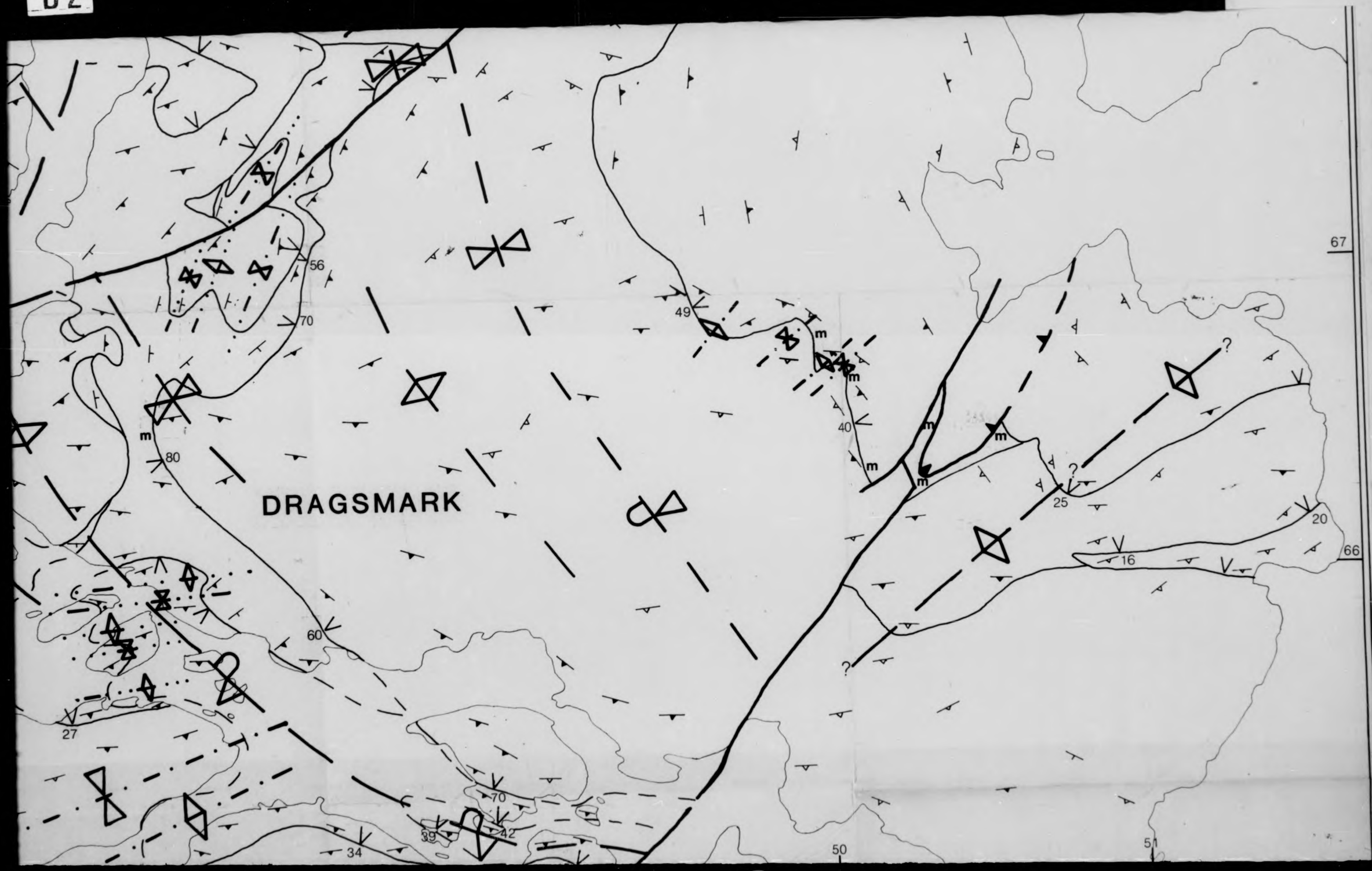

C1

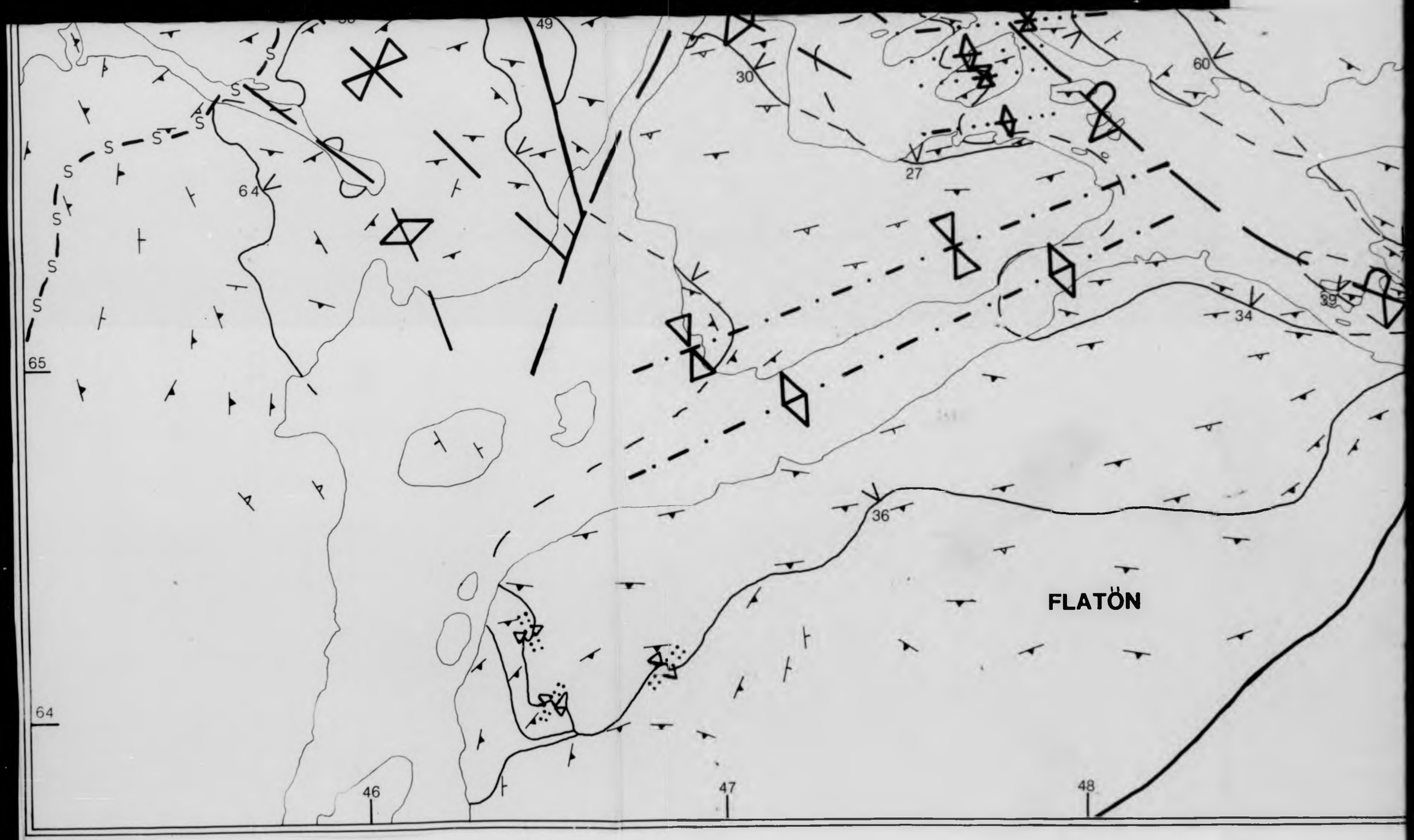

c2

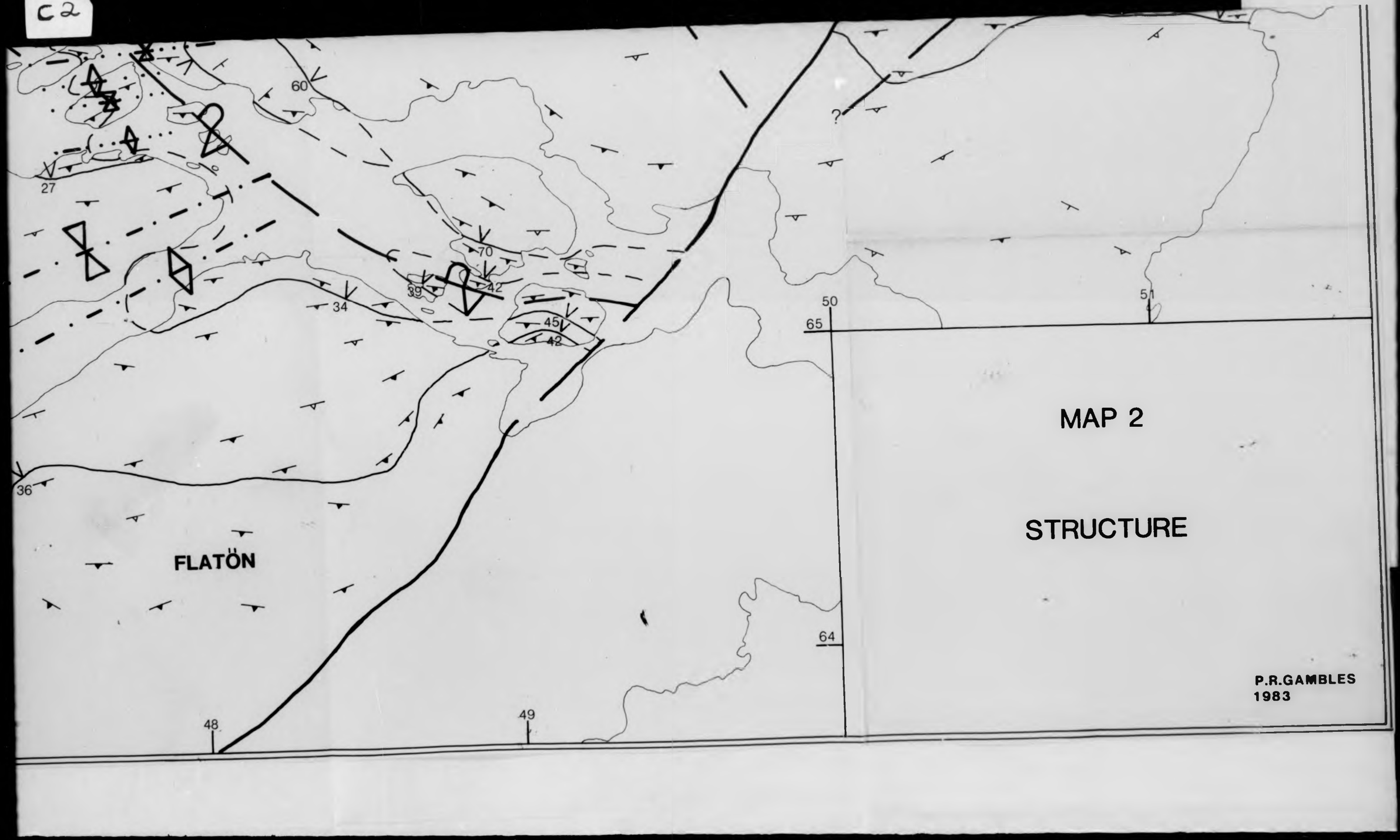

MAP 2

STRUCTURE

P.R.GAMBLES
1983


MAP 3
SAMPLE LOCALITIES
P.R.GAMBLES
1983

GEOLOGY OF

DRAGSMARK & SKAFTÖ,

SOUTH-WEST SWEDEN

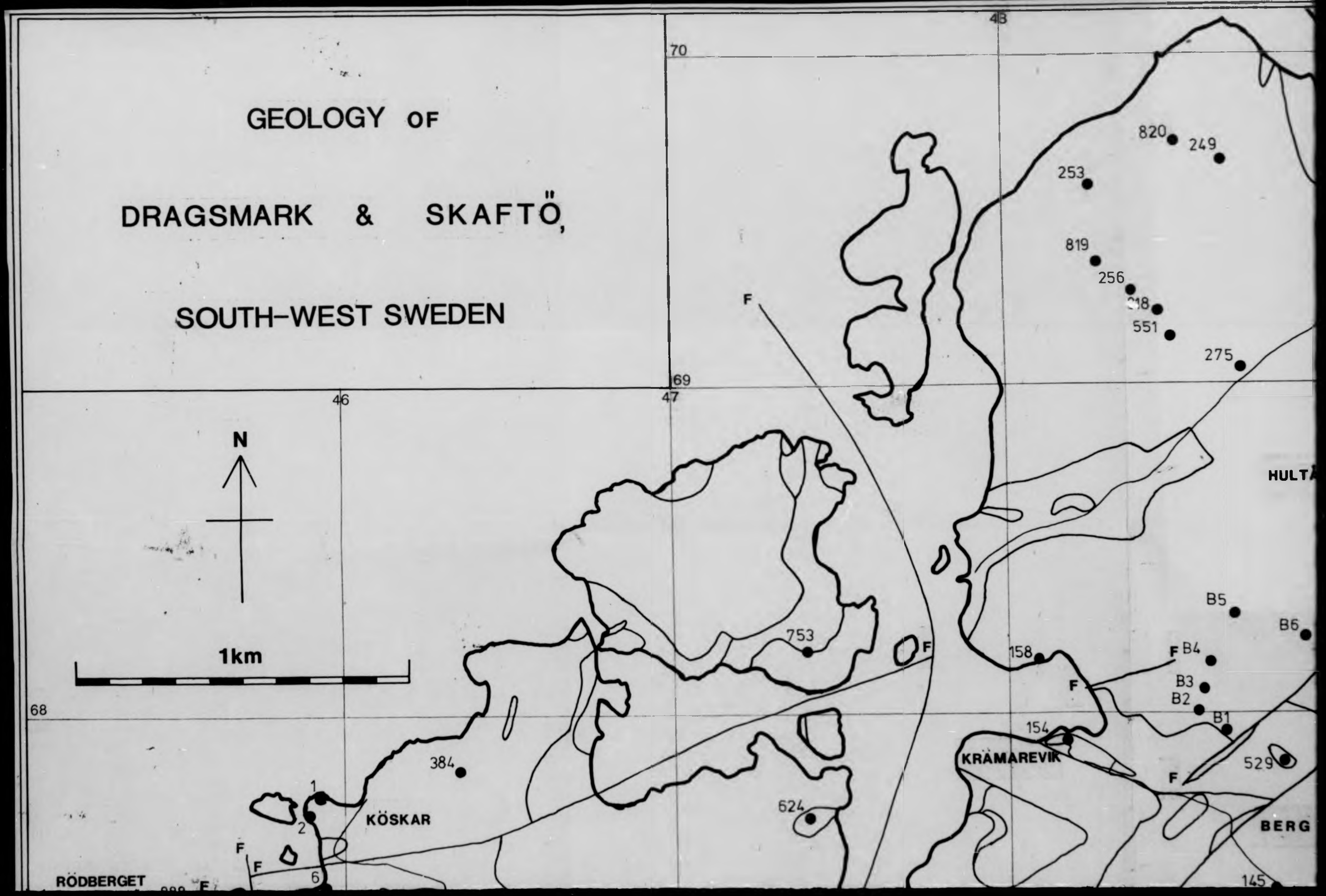

A 2

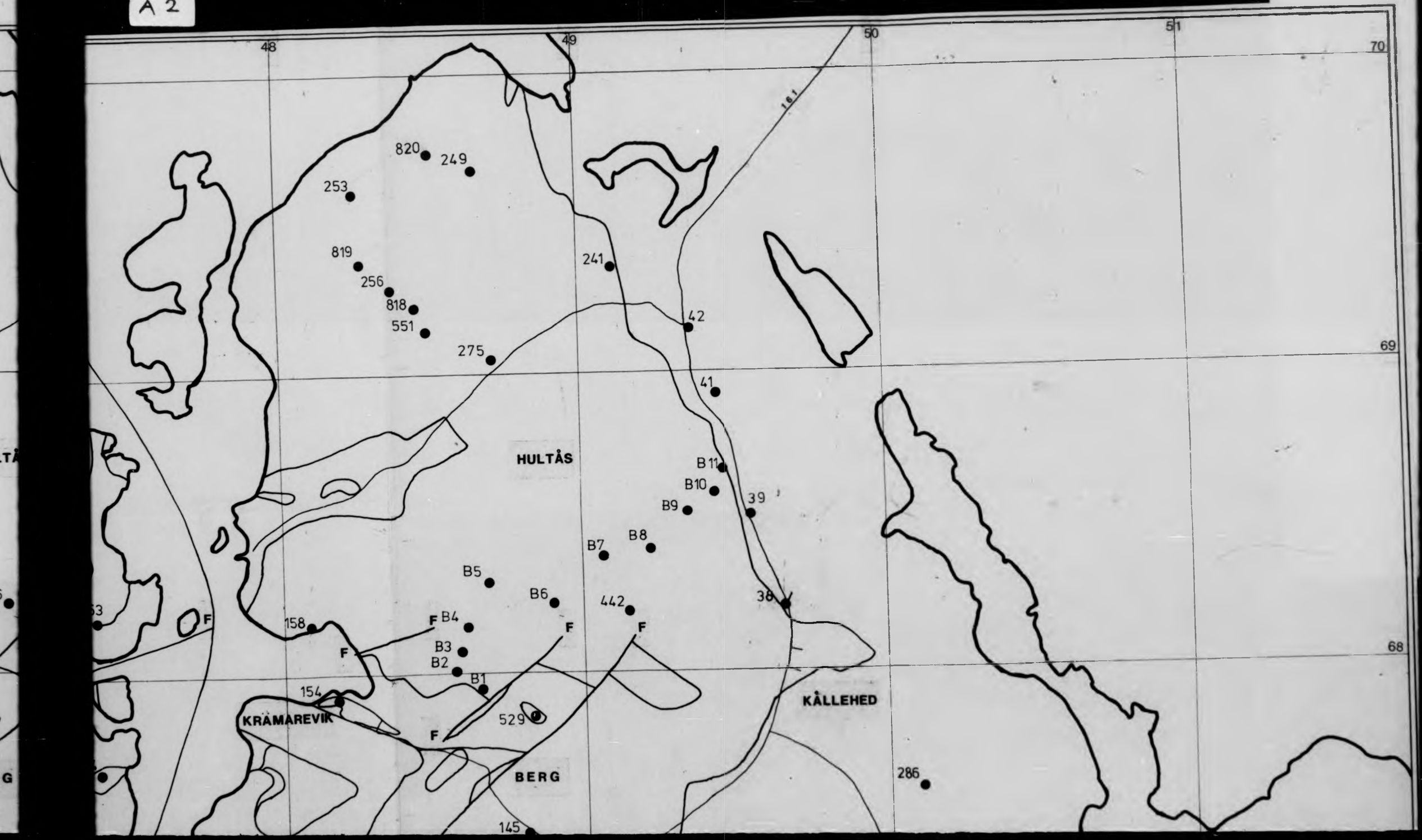
48
49
50
51
70
69
68
161
820
249
253
819
256
818
551
275
241
42
41
HULTÅS
B11
B10
B9
39
B8
B7
B5
B6
442
38
B4
B3
B2
B1
158
154
529
KRÅMAREVIK
BERG
KÅLLEHED
286
145
F

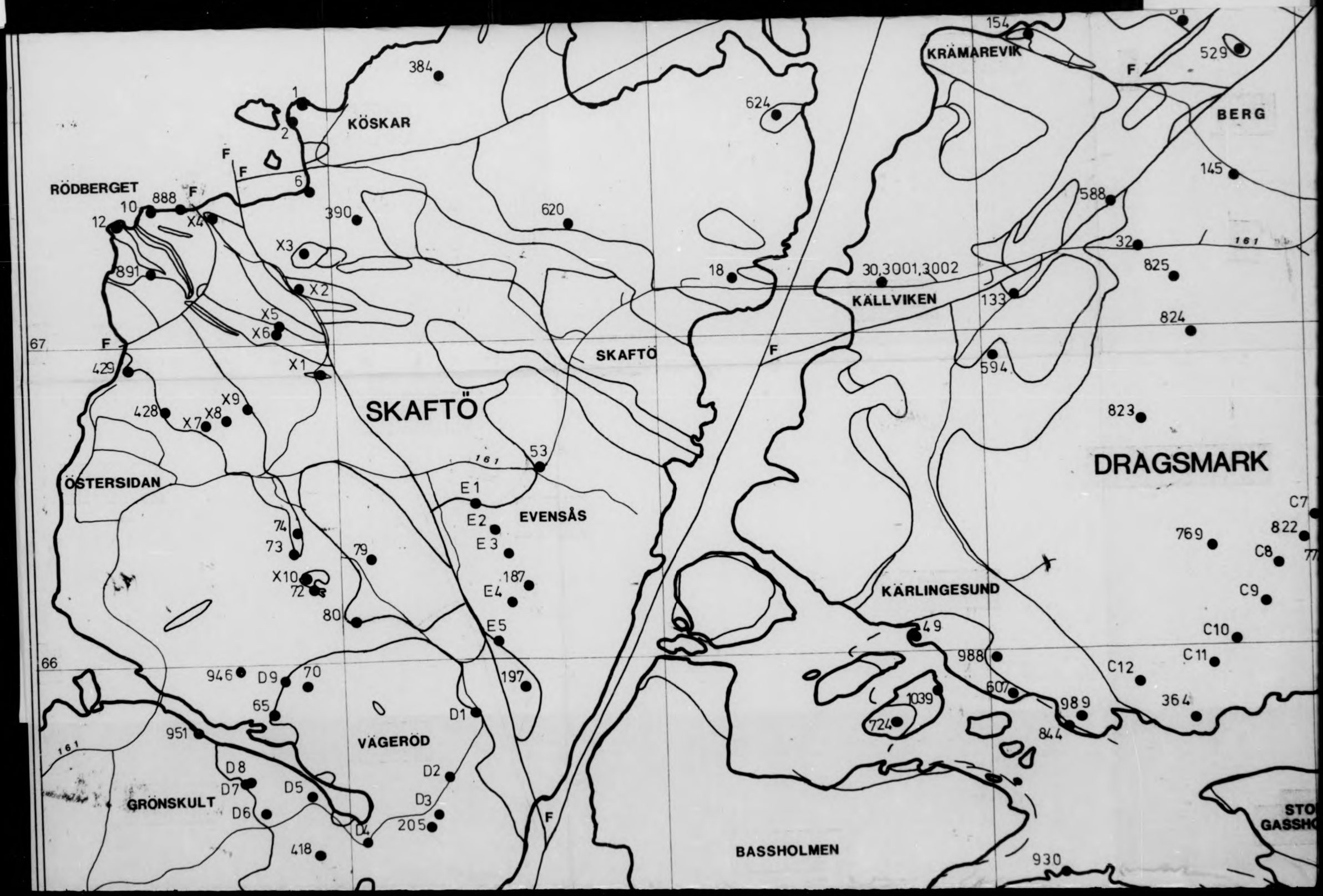
KÖSKAR
RÖDBERGET
SKAFTÖ
ÖSTERSIDAN
EVENSÅS
VÄGERÖD
GRÖNSKULT
KÄLLVIKEN
KRÄMAREVIK
BERG
DRAGSMARK
KÄRLINGESUND
BASSHOLMEN
384
624
620
390
888
891
429
428
X1
X2
X3
X4
X5
X6
X7
X8
X9
X10
1
2
6
10
12
18
53
74
73
72
79
80
E1
E2
E3
E4
E5
187
197
946
D9
70
65
951
D8
D7
D6
D5
D4
D3
D2
D1
205
418
30,3001,3002
133
154
529
145
588
32
825
824
823
594
769
822
C7
C8
C9
C10
C11
C12
49
988
607
1039
724
989
364
844
930
67
66
161

B2

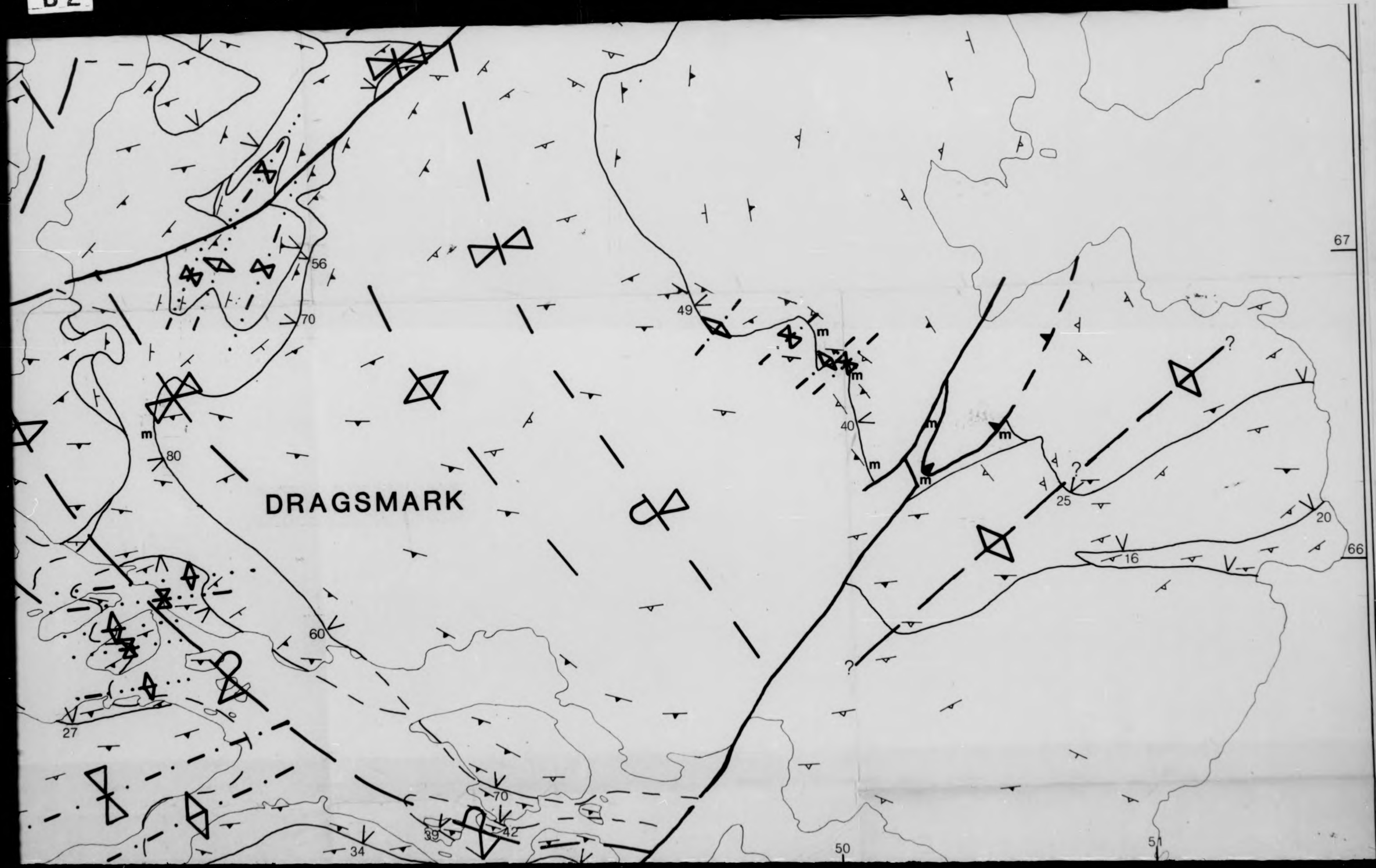

C1

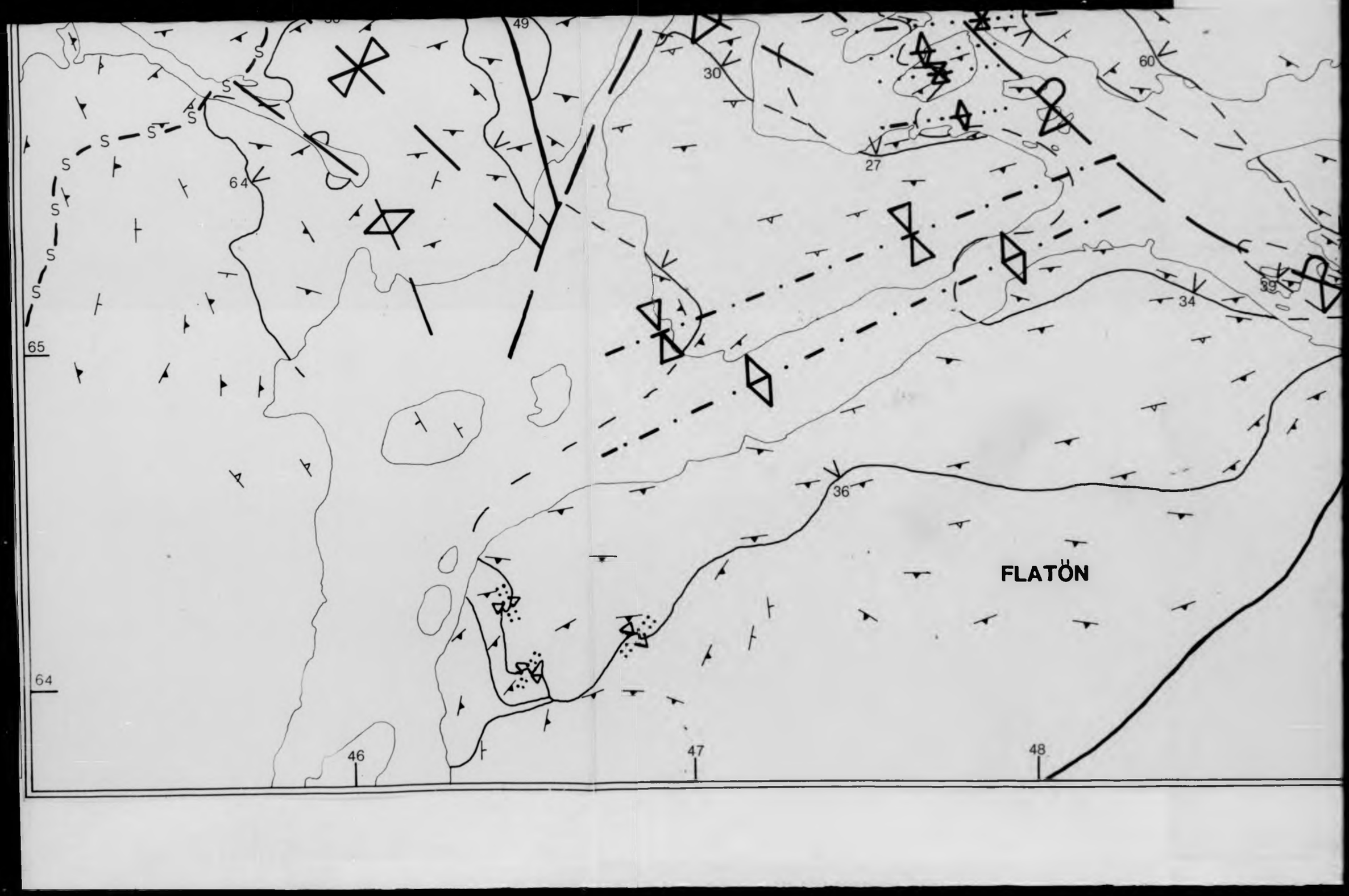

C2

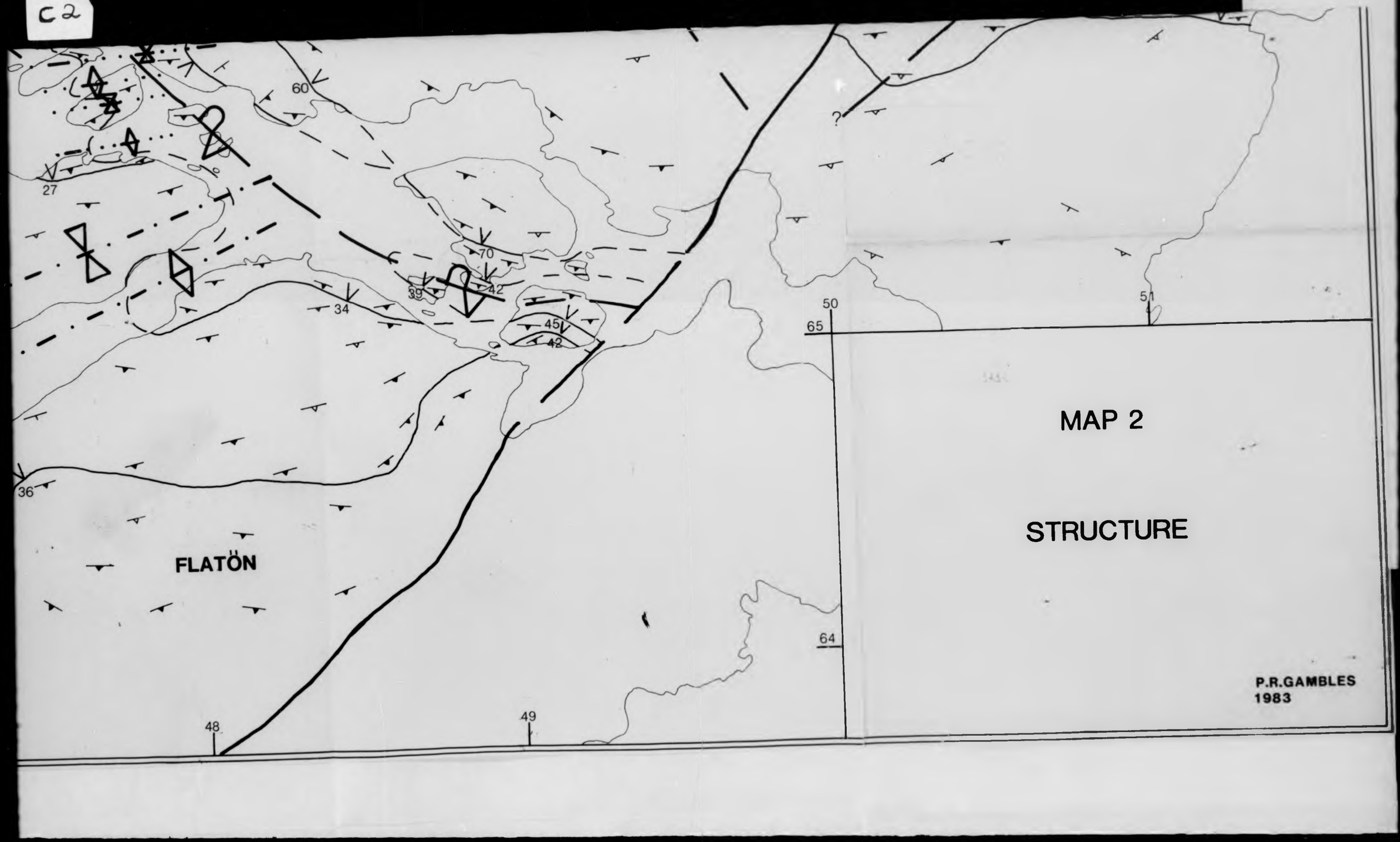

MAP 2

STRUCTURE

P.R.GAMBLES
1983

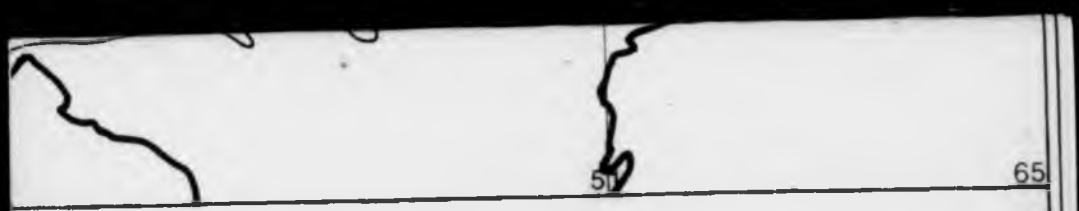

MAP 3

SAMPLE LOCALITIES

P.R.GAMBLES
1983

GEOLOGY OF

DRAGSMARK & SKAFTÖ,

SOUTH-WEST SWEDEN

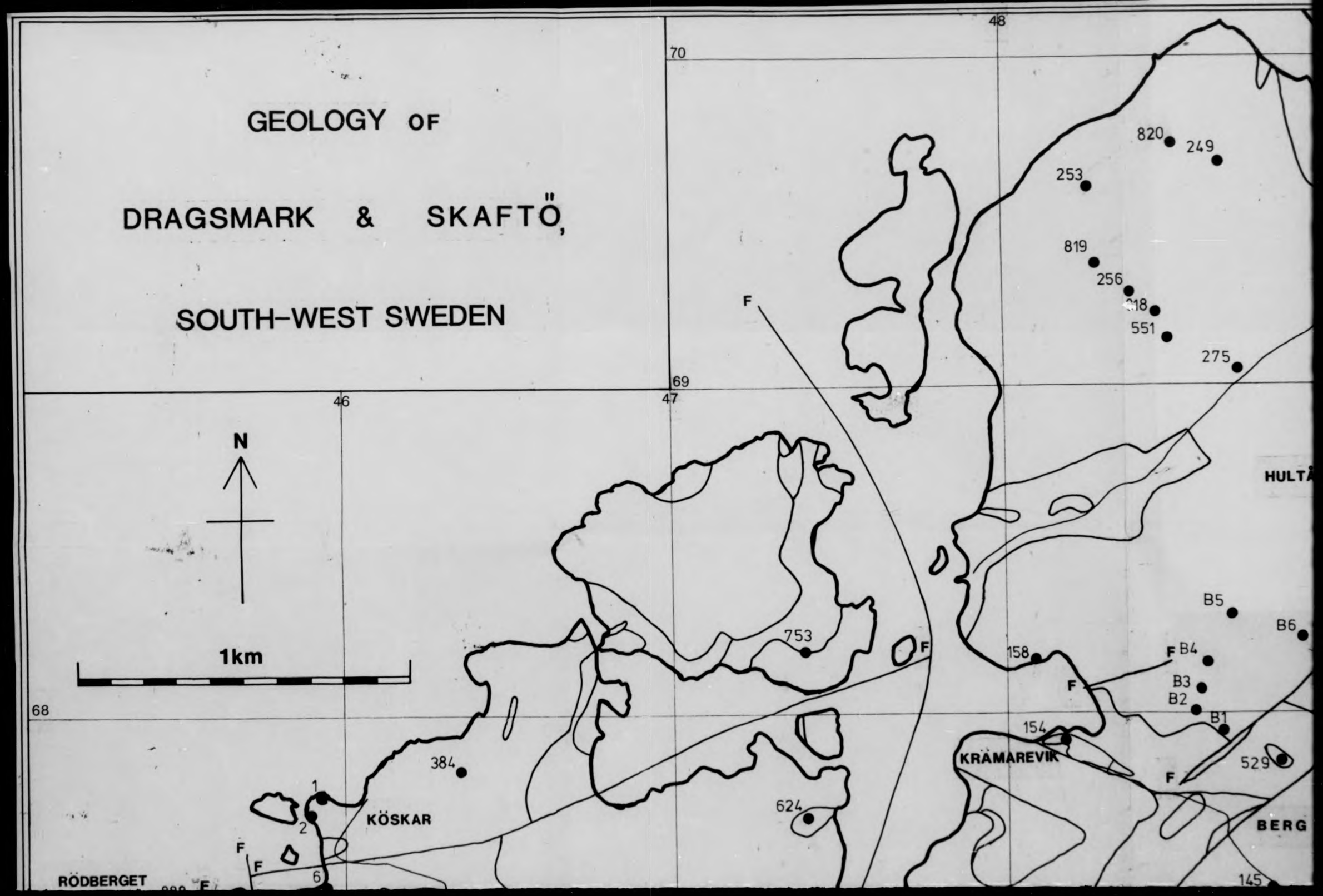

A 2

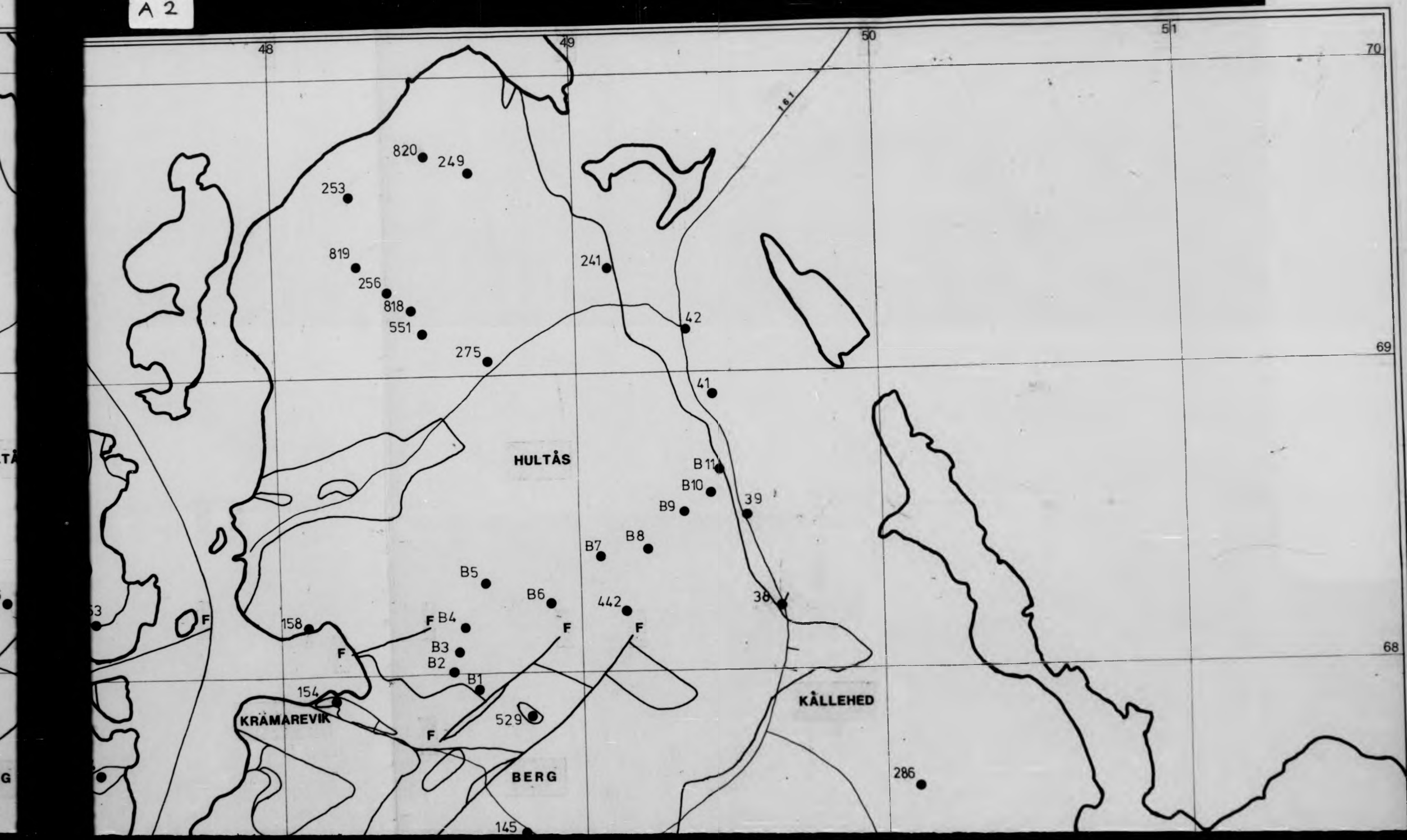
48
49
50
51
70
69
68
161
820
249
253
819
256
818
551
275
241
42
41
HULTÅS
B11
B10
B9
39
B8
B7
B5
B6
442
38
B4
B3
B2
B1
158
154
529
KRÅMAREVIK
KÅLLEHED
BERG
286
145
F

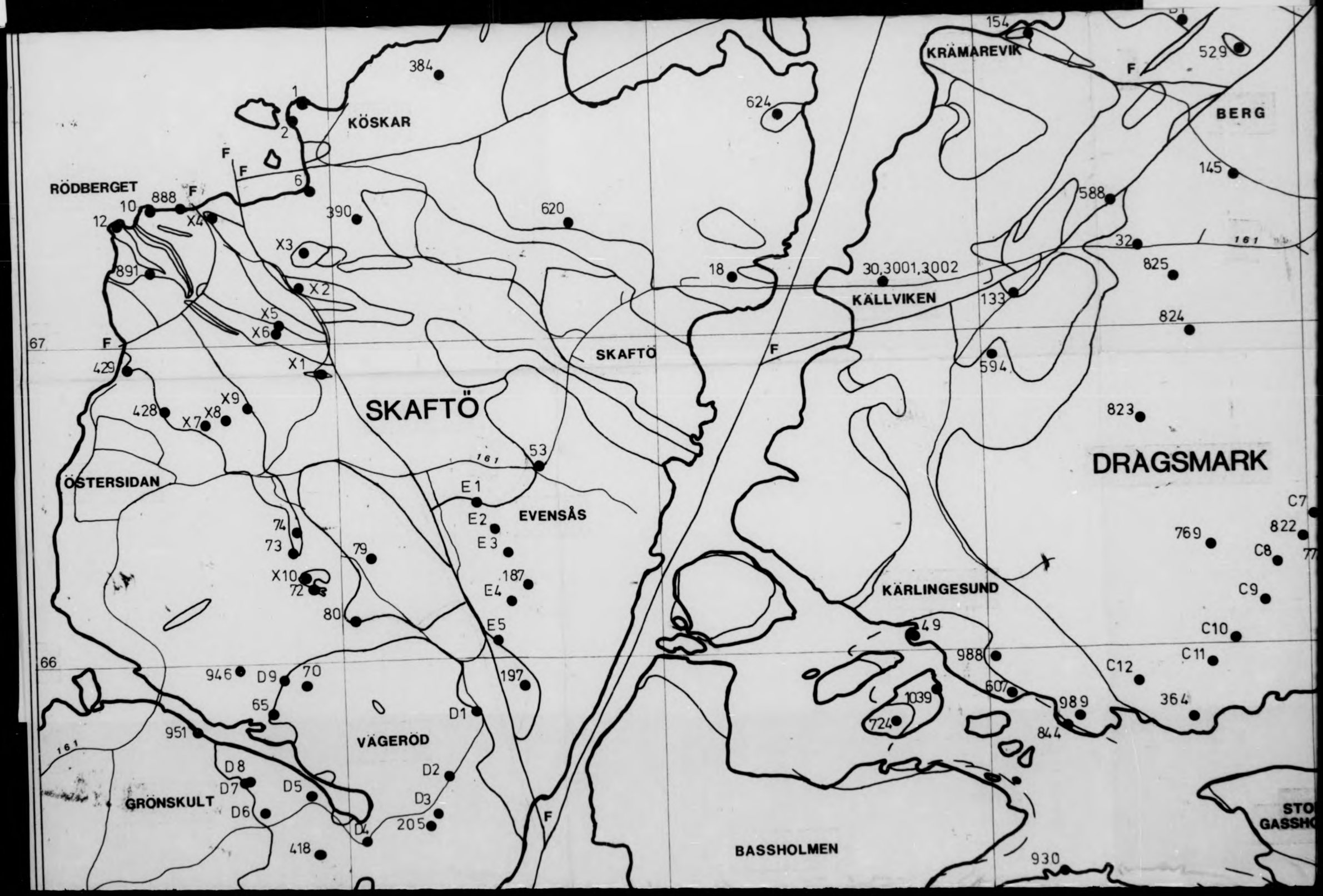
KRÄMAREVIK
BERG
KÖSKAR
RÖDBERGET
SKAFTÖ
KÄLLVIKEN
ÖSTERSIDAN
EVENSÅS
DRAGSMARK
KÄRLINGESUND
VÄGERÖD
GRÖNSKULT
BASSHOLMEN
384
624
154
529
145
588
620
390
888
891
429
428
X1
X2
X3
X4
X5
X6
X7
X8
X9
X10
1
2
6
10
12
18
30,3001,3002
133
32
825
824
594
823
53
E1
E2
E3
E4
E5
74
73
72
79
80
187
197
946
D9
70
65
D1
D2
D3
D4
D5
D6
D7
D8
951
205
418
769
822
C7
C8
C9
C10
C11
C12
364
49
988
607
1039
724
989
844
930
161
67
66
F

B2

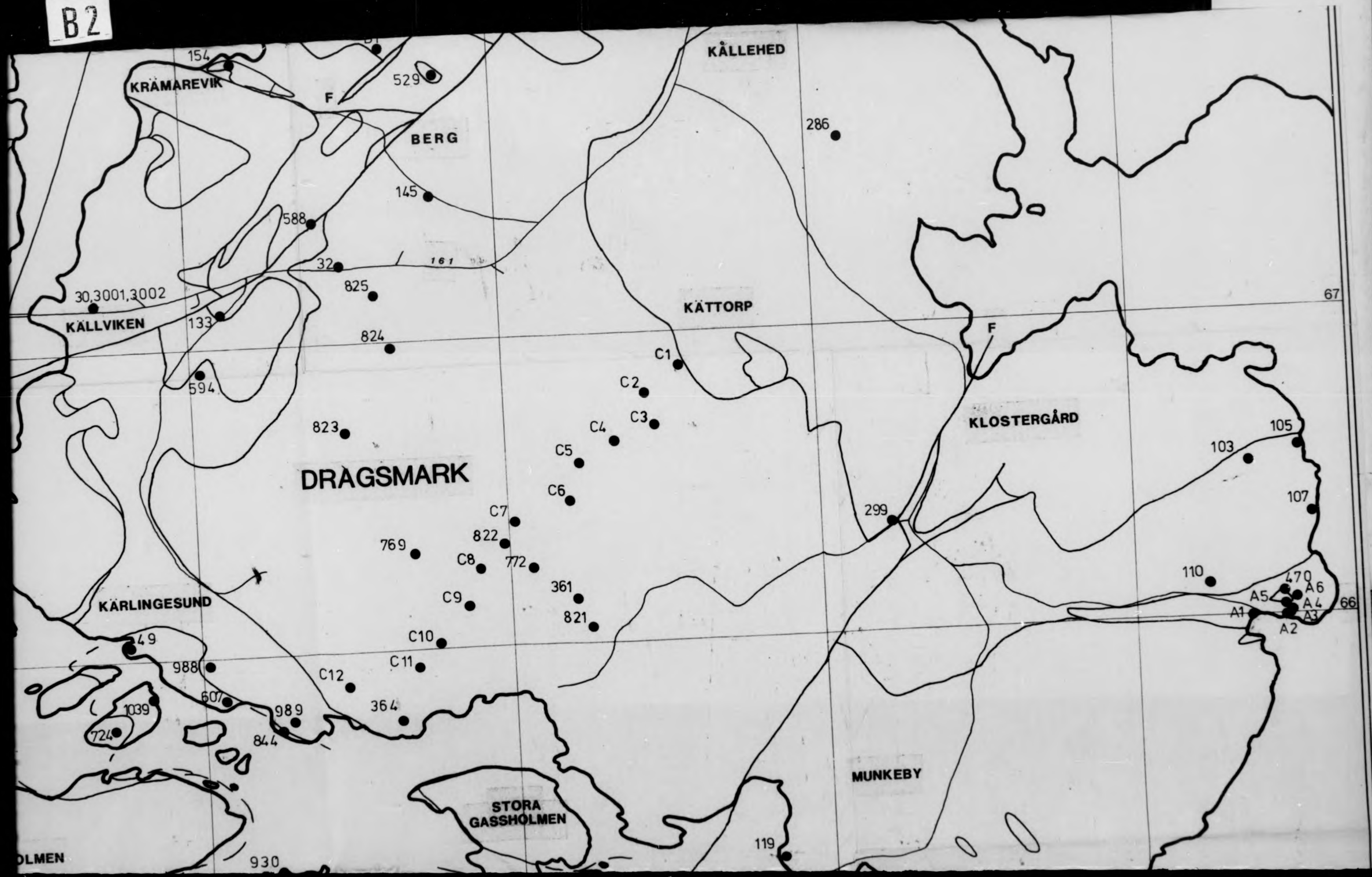
KRÄMAREVIK
154
529
F
BERG
145
588
32
161
825
824
594
823
DRÄGSMARK
KÄLLVIKEN
30,3001,3002
133
KÄTTORP
KÅLLEHED
286
C1
C2
C3
C4
C5
C6
C7
822
769
C8
772
C9
361
821
C10
C11
C12
364
KÄRLINGESUND
49
988
607
989
1039
724
844
930
STORA GASSHOLMEN
MUNKEBY
119
299
KLOSTERGÅRD
105
103
107
110
470
A6
A5
A4
A1
A3
A2
66
67

C1

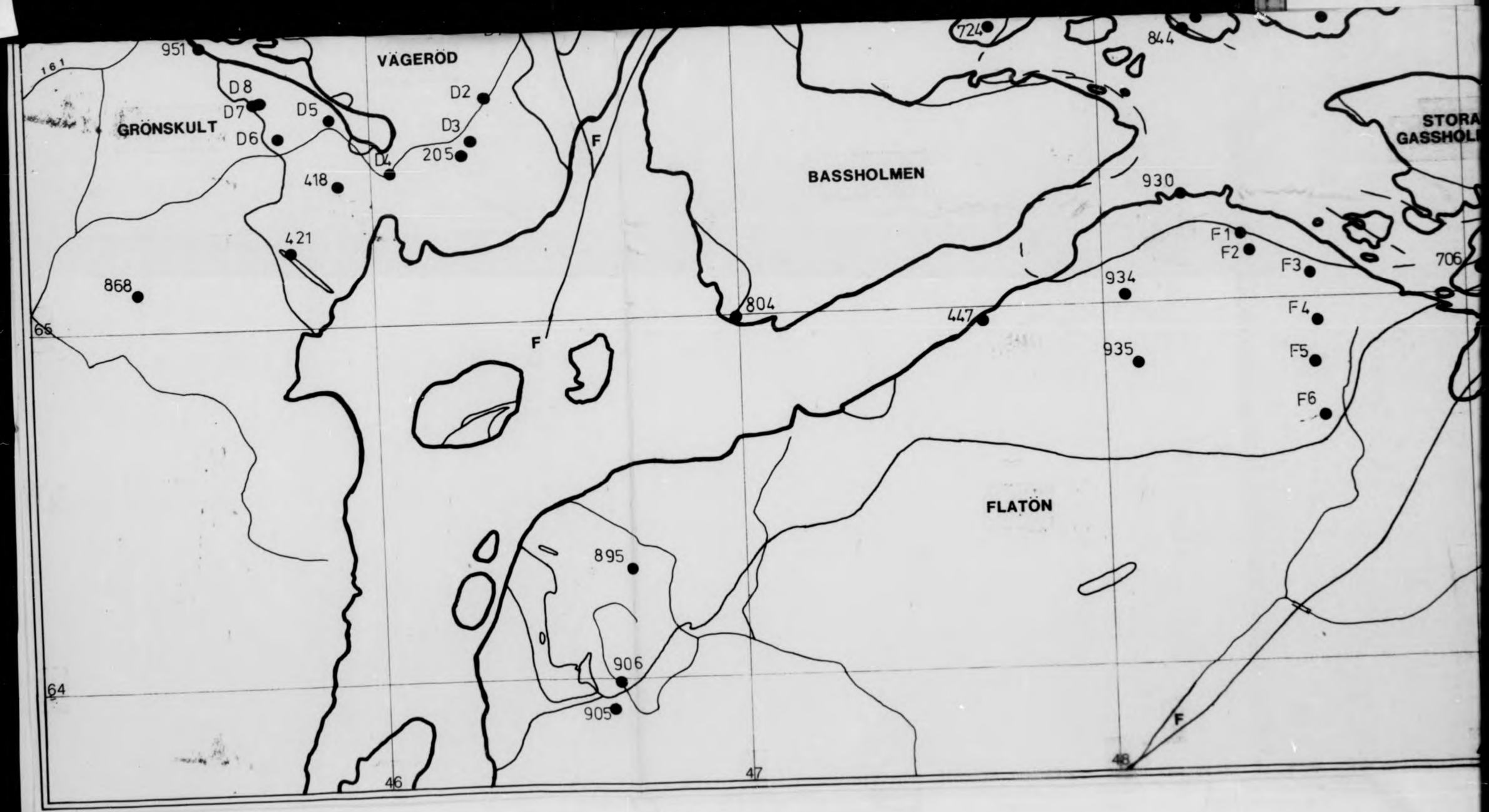
951
161
VÄGERÖD
D8
D7
D5
D2
D3
D6
D4
205
GRÖNSKULT
418
421
868
F
724
844
BASSHOLMEN
930
F1
F2
F3
706
934
804
447
F4
935
F5
F6
FLATÖN
895
906
905
64
65
46
47
48

C2

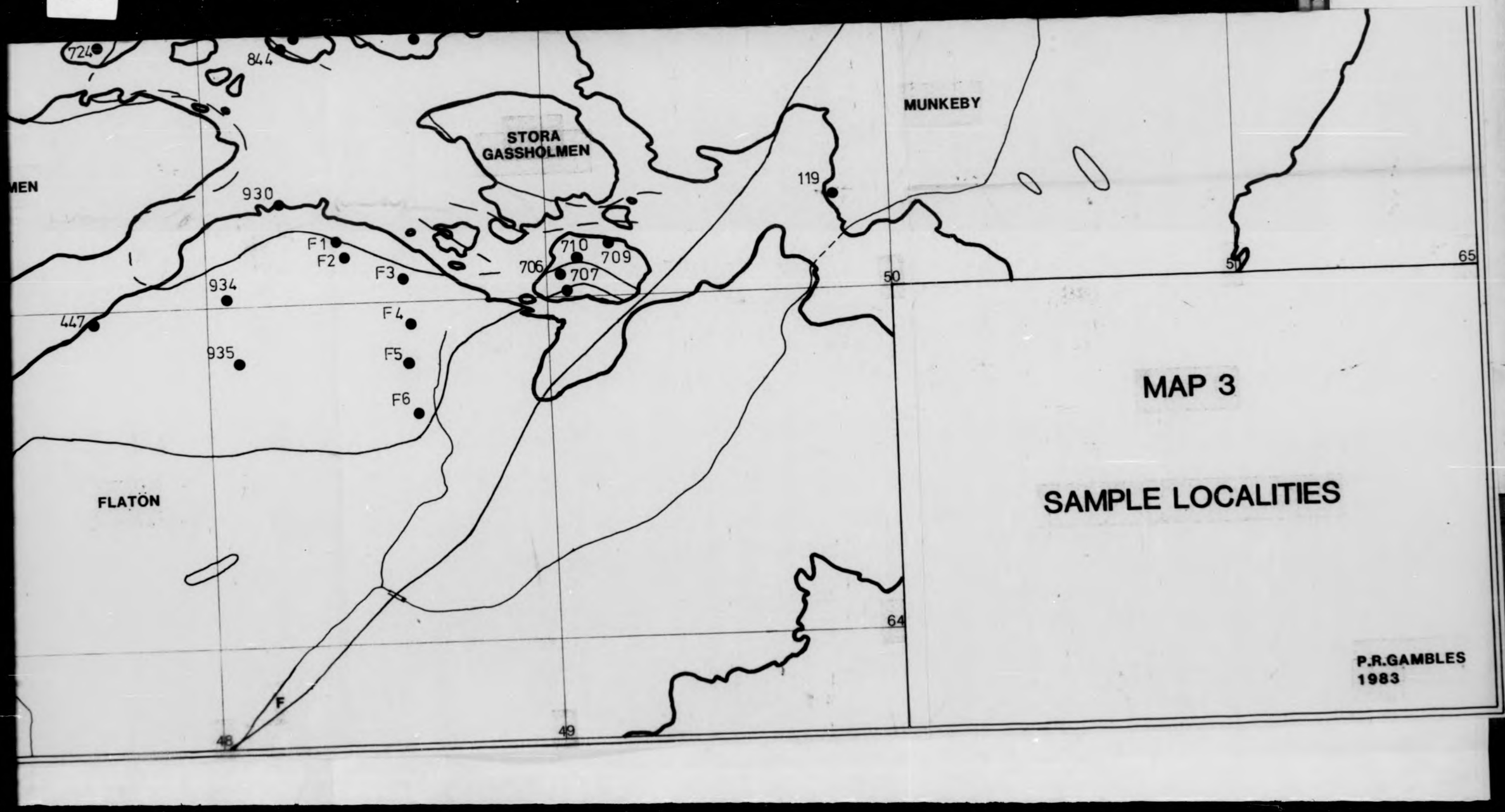
724
844
STORA
GASSHOLMEN
MUNKEBY
119
930
F1
F2
F3
710
709
706
707
934
F4
447
935
F5
F6
FLATÖN
F
48
49
64
50
51
65
MAP 3
SAMPLE LOCALITIES
P.R.GAMBLES
1983

II